THE
PHYSICAL REVIEW
A journal of experimental and theoretical physics established by E. L. Nichols in 1893

SECOND SERIES, VOL. 70, NOS. 7 AND 8 OCTOBER 1 AND 15, 1946

Reaction of Radiation on Electron Scattering and Heitler's Theory of Radiation Damping

H. A. BETHE
Cornell University, Ithaca, New York

AND

J. ROBERT OPPENHEIMER
University of California, Berkeley, California

(Received June 26, 1946)

The reaction of radiation on the scattering of electrons is treated on the basis of Heitler's theory of radiation damping. Because in this theory no account is taken of virtual processes, the infra-red catastrophe reappears, and the theory gives a total cross section for scattering, which depends critically on the longest wave-length radiation that can be emitted, and which does not agree with the correspondence principle. It seems probable that only by a modification of present theories specific to the domain of high energies and small distances will a satisfactory solution of this simple problem be found.

1. THE INFRA-RED CATASTROPHE IN THE ORDINARY THEORY

AMONG the many problems involving radiation damping there is one which has been the subject of much study and to which no satisfactory answer has yet been obtained. This is the reaction of radiation on the scattering of an electron.

If we consider the scattering of an electron in a fixed potential field, which we may for convenience assume to be weak, then the scattering cross section of the electron is given by

$$d\sigma=\left(\frac{m}{2\pi\hbar^2}V_{kp}\right)^2 d\omega, \tag{1}$$

where $\mathbf{k}$ and $\mathbf{p}$ are initial and final momenta,

$$V_{kp}=\int d\tau V e^{i(\mathbf{k}-\mathbf{p})\cdot\mathbf{r}/\hbar}, \tag{1a}$$

$d\mathbf{p}=p^2dpd\omega$, m is the mass, V the scattering potential. One would expect that the reaction of radiation emitted in the collision might not affect the probability of scattering for low velocity of the electron because the recoil of the emitted radiation should be negligible. But as the velocity of the electron is increased, corrections of order $(v/c)^4$ should appear in the formula for scattering, which are proportional to the square of the electron's charge.

It is clear that these corrections, while presumably small, are in principle subject to direct experimental study. The theory of the interaction of radiation with matter should make it possible to compute them. As is well known, if one applies the accepted principles of quantum electrodynamics to this problem, one does not obtain a reasonable or a finite answer. We should like to discuss the status of this problem from a somewhat new point of view in order that we can

see how to apply to it the proposals which have been put forward by Heitler[1] for eliminating the divergence difficulties of the present theory. In fact, it seems not unreasonable to apply all proposed modifications of electrodynamics to this simple problem as a sort of criterion of their adequacy. Judged by this criterion, the proposals put forth by Heitler must be regarded as unsatisfactory.

The difficulties of this problem first appeared in the form of the so-called infra-red catastrophe. In fact, if one computes by perturbation methods the probability that an electron will be scattered with the emission of a quantum of frequency q one obtains the cross section

$$\delta_q d\sigma = \frac{2e^2}{3\pi\hbar c}\frac{(\mathbf{p}-\mathbf{k})^2}{m^2c^2}\frac{dq}{q}\cdot d\sigma, \qquad (2)$$

whose integral will diverge logarithmically for small q. This problem has been analyzed in detail by Bloch and Nordsieck.[2] These authors showed that it is in fact unlikely that a scattering process will take place with the emission of 0, 1, or, in fact, any finite number of quanta. Specifically by a rigorous but non-relativistic solution of the problem for low frequencies, they showed that the increase in probability of scattering with the emission of a large number of quanta is quantitatively compensated by the decrease in the probability of elastic scattering or scattering with the emission of a smaller number of quanta. Thus, they obtained for the total probability of scattering the result (1), as one would indeed expect.

The situation is, however, not as satisfactory as this, because Bloch and Nordsieck neglected the fact that only quanta which are energetically capable of emission, i.e., below the high frequency limit given by the electron's kinetic energy, can in fact be emitted.

Taking this circumstance into account but still calculating non-relativistically, Pauli and Fierz[3] showed that the total cross section for scattering is not unchanged but would in fact vanish because the reaction on the probability of elastic scattering is not adequately compensated by an increased probability for scattering with the emission of high frequency quanta. The divergences at high frequencies which appear in this treatment are again logarithmic.

This subject was further clarified by Dancoff[4] who considered what effect relativistic corrections would have on the high frequency terms of Pauli and Fierz. In doing this he necessarily confined his attention to terms of the second order in the electron's charge. His result was that these terms do not in general converge and that relativistic corrections could not be counted on to alter qualitatively the Pauli-Fierz result. The details of Dancoff's result further suggest that the theory made no sense at all. Thus the precise character of the infinite terms depends on whether the scattering potential is a four-vector or a world scalar and whether the spin of the scattered particle is 0 or $\frac{1}{2}$. It is not possible to believe that in a problem involving only charges moving with low velocity these deductions can have any relation to reality.

If we wish to consider this problem from the point of view proposed by Heitler and, at the same time, wish to be able to take relativistic effects into account, it will be necessary to analyze it in terms of the perturbation theory based on the smallness of the electron's charge. If for a moment we introduce a lowest frequency $\bar{q}$, then it is easy to see the part played by the arguments of Bloch and Nordsieck, Pauli and Fierz, and Dancoff in determining the radiative corrections. This frequency $\bar{q}$ can, in fact, be fantastically low, and this situation may be realized by considering the collision problem as it would be if the electron and the scatterer were both enclosed in a conducting box of enormous dimensions.

When we carry out this calculation we can at first neglect the contribution of processes in which more than one quantum is involved, or which involve a higher order of the electron's charge than the second. We then see that as long as the frequency q is smaller than the upper limit of the spectrum and the velocity of the electron is small compared to the velocity of light, two corrections to the scattering formula

[1] W. Heitler, Proc. Camb. Phil. Soc. **37**, 291 (1941); W. Heitler and H. W. Peng, Proc. Camb. Phil. Soc. **38**, 296 (1942).
[2] F. Bloch and A. Nordsieck, Phys. Rev. **52**, 54 (1937).
[3] W. Pauli and M. Fierz, Nuovo Cimento **15**, 167 (1938).
[4] S. M. Dancoff, Phys. Rev. **55**, 959 (1939).

cancel. One of these is the positive correction which comes from the probability of emitting a quantum of frequency q

$$\delta_1 d\sigma = \frac{e^2}{4\pi^2 \hbar m^2 c^3} \int_{\bar{q}} \frac{dq}{q^5} [\mathbf{p}\times\mathbf{q}-\mathbf{k}\times\mathbf{q}]^2 \cdot d\sigma = \frac{2e^2}{3\pi\hbar c} \frac{(\mathbf{p}-\mathbf{k})^2}{m^2c^2} \frac{dq}{q} \cdot d\sigma. \tag{3}$$

The second is a negative correction to the probability of scattering without emitting a quantum of frequency q,

$$\delta_2 d\sigma = -\delta_1 d\sigma. \tag{4}$$

This second correction may be formally obtained in either of two ways. (a) It may be regarded as caused by the virtual emission and reabsorption of a quantum of frequency q during the scattering process; or (b) it may be regarded as a renormalization of the probability that the incident electron and the scattered electron will in fact have no quanta associated with them. These are, of course, equivalent descriptions. The finite result of Bloch and Nordsieck follows from an expansion of this simple argument to processes involving the multiple emission of quanta. The conclusion which appears above is maintained throughout but, of course, as $\bar{q}$ is made smaller and smaller, the neglect of processes involving more than one quantum finally becomes inadmissible. The argument of Pauli and Fierz is then simply this: The probability of scattering with emission of radiation has no terms for frequency $q > mv^2/2\hbar$. On the other hand, the corrections to the probability of radiationless scattering continue for infinitely high q and lead to a logarithmic divergence. What Dancoff has done is to show that a consistent relativistic calculation for these latter terms does not give generally finite results.

We, therefore, see that the terms involving the virtual emission of quanta as a correction to the probability of radiationless scattering, and which may alternatively be derived as a sort of renormalization of the probability that electrons will be unaccompanied by quanta, have a dual rôle. For low frequencies they are needed to cancel the change in scattering probability caused by the emission of a quantum, a change which, as $\bar{q}$ goes to 0, becomes logarithmically infinite. For high frequencies these terms themselves have nothing left to cancel and give rise to a new logarithmic divergence. Thus, no proposal which is as simple as either including or excluding these terms can give a finite result or a sensible one. This is the essential reason why Heitler's proposals give an unsatisfactory answer when applied to this simple problem.

2. HEITLER'S THEORY: QUALITATIVE CONSIDERATIONS

In the theory of radiation damping developed by Heitler and his collaborators, the transition probability from an initial state, A, to a final state, B, is determined by certain matrix elements U_{AB} which are related to the matrix element H_{AB} of the Hamiltonian by the equation

$$U_{AB} = H_{AB} + i\pi \sum_C \rho_C H_{AC} U_{CB}. \tag{5}$$

The sum goes over all states, C, of the same energy as the initial and final state; ρ_C is the density of states of the type C per unit energy.

The cross section of a process leading from state A to B is given in Heitler's theory by

$$\sigma_{AB} = \frac{2\pi}{\hbar v_A} \rho_B |U_{AB}|^2, \tag{6}$$

where v_A is the velocity of the incident particle, and ρ_B is the density of states of type B per unit energy. Equation (6) is entirely analogous to the usual formula for the cross section except that the matrix element of the Hamiltonian is replaced by that of U.

The last term in Eq. (5) represents the radiation damping. Its function is to keep the transition matrix elements U finite even if the matrix elements of the Hamiltonian or the number of possible final states become very large. Heitler and his collaborators have proved in many papers on the meson theory that all cross sections actually remain finite at high energies while they would increase indefinitely without radiation damping. Also in our case, the result for the cross section is finite under all conditions, but we shall show that the result does not agree with physical expectations as discussed in Section 1.

The matrix elements of the Hamiltonian relevant for our problem are of two types. The first type is the matrix element for simple scattering which is simply the Fourier component of the potential as given in Eq. (1a),

$$(\mathbf{k}|H|\mathbf{p}) = V_{kp}. \tag{7}$$

The other relevant matrix elements correspond to the emission of a quantum $\mathbf{q}$ together with the scattering of the electron from its initial momentum $\mathbf{k}$ to the final momentum $\mathbf{p}$. These matrix elements are

$$(\mathbf{k}|H|\mathbf{pq}) = Cq^{-\frac{1}{2}}(\mathbf{p}-\mathbf{k})\cdot\mathbf{u}\,V_{kp}, \tag{8}$$

where

$$C = e/2\pi\hbar^{\frac{1}{2}}mc^{\frac{1}{2}} \tag{8a}$$

is a constant and $\mathbf{u}$ is a unit vector in the direction of polarization of the quantum. The matrix element (8) is normalized in such a way that the number of states of the quantum can be simply taken equal to the volume in q-space, $d\mathbf{q} = 4\pi q^2 dq$. It is easily seen that (8) agrees with Eq. (3) of the first section.

We shall now estimate the order of magnitude of the cross section for scattering with emission of radiation in first approximation; i.e., with the assumption that radiation is small. We shall also estimate the reaction of radiation on the radiationless scattering, represented by the radiation damping term in (5). We shall find that in contrast to the theory outlined in Section 1, these two effects do not cancel, and we shall show that this lack of cancellation makes Heitler's theory unacceptable.

In first approximation we may put $U=H$ for transitions involving radiation. According to (6) and (8), the cross section for transitions with radiation will then be proportional to V^2C^2 (apart from other factors), which is of the order C^2 times the cross section for scattering without radiation.

We now consider the correction which radiation makes to the cross section for radiationless transitions by applying Eq. (5) to such transitions. The radiation reaction is given by the contribution of states C containing a quantum, to the last term of (5). If we make again the approximation $U_{CB}=H_{CB}$ for such states C, their contribution to the last term of (5) will be of the order V^2C^2. Since H_{AB} is of order V, the relative magnitude of the radiation reaction term in (5) is of order VC^2. This is smaller than the relative probability of collisions *with* radiation by a factor of the order V, which can be made arbitrarily small by a suitable choice of the scatterer.

Actually, the effect of radiation reaction on the *cross section* σ_{AB} is even smaller. This is because the damping term in (5) is imaginary in our present approximation while H_{AB} is real. The effect of the damping term on the cross section σ_{kp} is only of the relative order of V^2C^4 which is extremely small because C contains the (small) electron charge as a factor. Actually, closer examination shows that the leading term in the radiation reaction is not given by inserting for U_{CB} its first approximation, H_{CB}. In the next approximation, an imaginary term appears in U_{CB} which is of the relative order V compared with H_{CB}, and this term gives a *real* contribution to the radiation damping term in Eq. (5). The effect of this, both on U_{AB} and on the cross section σ_{AB}, is of the relative order V^2C^2, whereas the cross section for emission of radiation was shown to be of the relative order C^2. Therefore we see that the transitions with emission of radiation are not compensated by a corresponding reduction of the cross section for scattering without radiation.

This failure of compensation is especially serious because the total probability of emission of radiation diverges logarithmically for small frequencies q as was shown after Eq. (2). The total cross section for scattering with and without emission of radiation will, therefore, depend on the lower limit for the frequency, $\bar{q}$, and thereby on the size of the imaginary box in which the radiator is considered to be enclosed. It is clear that such a dependence has no physical meaning. The Heitler theory of radiation damping in its present form therefore does not solve the problem of the infra-red catastrophe. Moreover, the red end of the spectrum does not appear to involve a profound problem which would require going beyond the scope of present quantum mechanics, so that the failure of Heitler's theory must be considered the more serious.

Heitler's theory forbids, in fact, the customary solution of the infra-red problem as outlined in

Section 1. Heitler's prescription is to calculate the matrix element of each phenomenon only in the first approximation in which such a matrix element appears. This prescription serves to eliminate the usual divergences at high frequencies. However, it also eliminates in our case the perturbation by virtual quanta of low frequencies which gave the result (4), and thereby eliminated the infra-red catastrophe. In Heitler's theory this perturbation must be left out and there is, therefore, no adequate compensation for the scattering which takes place with emission of radiation.

3. HEITLER'S THEORY: QUANTITATIVE CALCULATION

For a quantitative discussion of Eq. (5) we shall make the simplifying assumption that the matrix elements of the scattering potential V_{kp} do not depend on the direction of the vectors $\mathbf{k}$ and $\mathbf{p}$. This amounts to assuming an interaction potential of range very short compared to the electron's wave-length. In addition we shall neglect the higher order effects such as the emission of two quanta or the scattering of quanta. We shall, however, make no restrictions on the magnitude of the electronic charge e and thereby of the constant C, nor any restrictions on the magnitude of the matrix element $V_{kp}=V$.

We shall first write down Eq. (5) explicitly for transitions with and without radiation. Using Dirac's notation for the matrix element, we have for transitions without radiation

$$(\mathbf{p}'|U|\mathbf{p})=(\mathbf{p}'|H|\mathbf{p})+i\pi\frac{4\pi mp}{(2\pi h)^3}\int\frac{d\omega''}{4\pi}(\mathbf{p}'|H|\mathbf{p}'')(\mathbf{p}''|U|\mathbf{p})+i\pi\frac{4\pi mp}{(2\pi h)^3}\int\frac{d\omega''}{4\pi}d\mathbf{q}(\mathbf{p}'|H|\mathbf{p}''\mathbf{q})(\mathbf{p}''\mathbf{q}|U|\mathbf{p}). \quad (9)$$

For scattering with emission of radiation, we have the Heitler equation

$$(\mathbf{p}'\mathbf{q}|U|\mathbf{p})=(\mathbf{p}'\mathbf{q}|H|\mathbf{p})+i\pi\frac{4\pi mp}{(2\pi h)^3}\int\frac{d\omega''}{4\pi}\times[(\mathbf{p}'\mathbf{q}|H|\mathbf{p}''\mathbf{q})(\mathbf{p}''\mathbf{q}|U|\mathbf{p})+(\mathbf{p}'\mathbf{q}|H|\mathbf{p}'')(\mathbf{p}''|U|\mathbf{p})]. \quad (10)$$

In any matrix element, $\mathbf{q}$ means that a quantum exists in the respective state of the system; $\mathbf{p}$ or $\mathbf{p}'$ or $\mathbf{p}''$ denote the momentum of the electron, p the absolute value of the momentum which is the same for all states, the integral $d\omega''$ is over all directions of $\mathbf{p}''$ and the integral $d\mathbf{q}$ is over magnitude, direction and polarization of the light quantum.

These equations are to be solved with expressions (7) and (8) for the matrix elements of the Hamiltonian. It is reasonable to assume, and it will in fact be shown to be true, that the solution will have the form

$$\begin{aligned}(\mathbf{p}'|U|\mathbf{p})&=A_1+A_2\mathbf{p}\cdot\mathbf{p}'/p^2,\\ (\mathbf{p}'\mathbf{q}|U|\mathbf{p})&=q^{-\frac{1}{2}}(B_1\mathbf{p}'\cdot\mathbf{u}+B_2\mathbf{p}\cdot\mathbf{u}).\end{aligned} \quad (11)$$

Inserting (11) into (10) we obtain

$$B_1\mathbf{p}'\cdot\mathbf{u}+B_2\mathbf{p}\cdot\mathbf{u}=VC(\mathbf{p}'-\mathbf{p})\cdot\mathbf{u}+\frac{imp}{2\pi h^3}\int\frac{d\omega''}{4\pi}[V(B_1\mathbf{p}''\cdot\mathbf{u}+B_2\mathbf{p}\cdot\mathbf{u})+VC(\mathbf{p}'-\mathbf{p}'')\cdot\mathbf{u}(A_1+A_2\mathbf{p}''\cdot\mathbf{p}/p^2)]. \quad (12)$$

The integration over $d\omega''$ is elementary. The terms containing only one factor involving $\mathbf{p}''$ vanish upon integration, whereas the average of a term of the form $\mathbf{p}''\cdot\mathbf{a}\ \mathbf{p}''\cdot\mathbf{b}$ gives the result $\mathbf{a}\cdot\mathbf{b}/3$ upon averaging. If we also introduce the abbreviation

$$W=(mp/2\pi h^3)V, \quad (13)$$

and then compare terms with $\mathbf{p}\cdot\mathbf{u}$ and terms with $\mathbf{p}'\cdot\mathbf{u}$ on both sides of the equation, we find:

$$\begin{aligned}B_1&=VC+iCWA_1,\\ B_2&=-VC+iWB_2-iWCA_2/3.\end{aligned} \quad (14)$$

In a similar way we obtain by inserting (11) into (9) and using the abbreviation (13)

$$A_1+A_2(\mathbf{p}'\cdot\mathbf{p}/p^2)=V+i\int(d\omega''/4\pi)\times\Big[W(A_1+A_2\mathbf{p}''\cdot\mathbf{p}/p^2)+\int d\mathbf{q}q^{-3}\times CW(\mathbf{p}''-\mathbf{p}')\cdot\mathbf{u}(B_1\mathbf{p}''\cdot\mathbf{u}+B_2\mathbf{p}\cdot\mathbf{u})\Big]. \quad (15)$$

Evaluation gives

$$A_1+A_2(\mathbf{p}'\cdot\mathbf{p}/p^2)=V+iWA_1 +iWCp^2\frac{8\pi}{3}\left(B_1-B_2\frac{\mathbf{p}'\cdot\mathbf{p}}{p^2}\right)\ln\frac{q_{\max}}{\bar{q}}. \quad (16)$$

In this equation $q_{\max}$ is the Duane-Hunt high frequency limit, $q_{\max}=mv^2/2\hbar$. On the other hand, $\bar{q}$ is determined by the size of the box in which the system is considered to be enclosed. As this box becomes larger, the logarithm in the last term of Eq. (16) increases indefinitely.

Combining Eq. (14) and (16) and using the abbreviation

$$R=(8\pi/3)C^2p^2\ln(q_{\max}/\bar{q}) =\frac{2}{3\pi}\frac{e^2}{\hbar c}\left(\frac{v}{c}\right)^2\ln\frac{mv^2}{2\hbar\bar{q}}, \quad (17)$$

we find the following solutions for the amplitudes:

$$A_1=V\frac{1+iWR}{1-iW+W^2R},\quad A_2=V\frac{iWR}{1-iW+W^2R/3},\quad B_1=\frac{VC}{1-iW+W^2R},\quad B_2=\frac{-VC}{1-iW+W^2R/3}. \quad (18)$$

The quantity R contains the dependence on the size of the box and becomes infinite for infinite size; however, for any reasonable size, R is quite small.

It will be noted that the amplitudes A_1, etc. all remain finite when R goes to infinity. This shows that in this case as in others the theory of radiation damping gives finite results. It will also be noted that for $R=\infty$ (strong coupling with radiation) the coefficients B_1 and B_2 become vanishingly small, so that in this limit the scattering process paradoxically will take place without the emission of radiation. (This result is not changed by integration over all frequencies q which can be emitted.)

The result for the cross sections becomes quite complicated in the general case. For instance, the result for the cross section without emission of radiation takes the form

$$d\sigma=\lambda\!\!\!^{-2}d\omega W^2\times\left|\frac{1+iWR}{1-iW+W^2R}+\frac{iWR\cos\alpha}{1-iW+W^2R/3}\right|^2 \quad (19)$$

where $\lambda\!\!\!^{-}=\hbar/p$ is the de Broglie wave-length of the particle, divided by 2π. The further evaluation simplifies in the limit of very large R in which case the result is

$$d\sigma=\lambda\!\!\!^{-2}d\omega(1+3\cos\alpha)^2. \quad (20)$$

The cross section thus becomes of the order $\lambda\!\!\!^{-2}$ which is reasonable. Generally it is clear that $d\sigma$ is a quadratic function of $\cos\alpha$, the angular dependence being due to the interaction with radiation.

We shall now discuss the result in more detail in the limit of small R and thereby substantiate the qualitative considerations of the last section. If we neglect all terms of higher relative order than W^2R^2, the cross section for scattering without radiation (19) reduces to

$$d\sigma=\lambda\!\!\!^{-2}d\omega W^2[1-W^2-4W^2R+W^2R^2(1+\cos\alpha)^2+\cdots] \quad (21)$$

where α is the scattering angle (angle between $\mathbf{p}$ and $\mathbf{k}$). Similarly, if we neglect terms of relative order W^2R, we find from (18)

$$B_1=-B_2=VC(1+iW+\cdots) \quad (22)$$

and the cross section for scattering with emission of radiation of frequency q becomes (cf. (11))

$$\delta_r d\sigma=\lambda\!\!\!^{-2}d\omega\frac{W^2}{1+W^2}C^2\frac{d\mathbf{q}}{q^3}2p^2(1-\cos\alpha)\sin^2\beta, \quad (23)$$

where β is the angle between $\mathbf{u}$ and $\mathbf{p}-\mathbf{p}'$; or, if we integrate over all frequencies and directions for the emitted radiation:

$$\sigma_r=2\lambda\!\!\!^{-2}d\omega RW^2/(1+W^2). \quad (24)$$

Therefore, the ratio of the scattering with radiation to the scattering without radiation is of the order R. On the other hand, the first correction which the radiation reaction makes to the cross section for radiationless scattering is of the relative order W^2R. This correction,

therefore, does not compensate the cross section with emission of radiation and the total scattering will therefore depend on R, and thus on the minimum frequency which can be emitted.

4. REMARK ON THE SCATTERING BY A POTENTIAL IN HEITLER'S THEORY

If we disregard radiation and simply consider the scattering by a concentrated potential, the cross section becomes

$$d\sigma = \lambda\!\!\!^{-2} d\omega W^2/(1+W^2), \tag{25}$$

which follows from (19) by neglecting R. The expression (25) is obviously correct for small W in which case it is identical with the Born approximation. For strong potentials (large W) the cross section remains finite and attains the limiting value $4\pi\lambda\!\!\!^{-2}$ which is the correct upper limit if only spherically symmetrical scattering is considered. However, this limit will be attained regardless of the sign of the potential. Actually the result $4\pi\lambda\!\!\!^{-2}$ is reasonable only for an attractive potential (and even in this case there should be fluctuations corresponding to resonance) while in the case of a repulsive potential the cross section can never become greater than $4\pi a^2$ where a is the radius of the region in which the repulsive potential exists. This limit holds even for infinitely strong repulsion and is smaller than $4\pi\lambda\!\!\!^{-2}$, because the assumption that the matrix elements for the scattering V_{kp} are independent of the direction of $\mathbf{k}$ and $\mathbf{p}$, is equivalent to assuming $a \ll \lambda\!\!\!^{-}$.

Moreover, Eq. (25) does not correctly describe the deviations from the Born approximation when this approximation first begins to fail. According to (25) the deviations should be of the relative order W^2; whereas the actual theory gives a deviation of the order $W(\lambda\!\!\!^{-}/a)$ which is much larger.

We do not regard this failure of Heitler's theory as significant because the theory was not intended to describe higher approximations for an arbitrary interaction such as the deviations from the Born approximation for an arbitrary potential. Heitler's theory was actually intended to apply to problems of radiation, and the matrix elements of the Hamiltonian should be taken from the fundamental theory of the interaction of particles with radiation. For this reason we consider the failure of the theory in the problem of the infra-red catastrophe as much more significant than its failure in the scattering problem.

5. CONCLUSIONS

The theory of radiation damping developed by Heitler and his collaborators gives, in all applications that have so far been made, a finite result for all cross sections even in the case of very large interactions. However, the application of the theory to the problem of the reaction of radiation on the scattering of electrons does not give a physically sensible result. The effect of radiation damping on the scattering without radiation is extremely small compared with the cross section for scattering with emission of radiation. The total scattering probability is therefore essentially the sum of the uncorrected scattering with and without radiation. The latter is subject to the infra-red catastrophe and depends on the lower limit q of the frequencies which can be emitted, becoming infinite as q goes to zero. It is evident that such a dependence can have no physical reality and that the probability of electron scattering should not depend on its ability to emit radio waves of extremely long wave-length.

In the customary theory as outlined in Section 1, the infra-red catastrophe does not occur because the scattering with emission of radiation is compensated by an equal decrease of the scattering without radiation. This decrease is brought about by the consideration of the influence of virtual quanta with long wave-length on the scattering without radiation. This amounts to the inclusion in the theory of matrix elements which are of higher order than is necessary to obtain a non-vanishing transition probability. The inclusion of such matrix elements is forbidden in Heitler's theory. It is seen that these matrix elements play an important role in avoiding the infra-red catastrophe.

It is well known that the inclusion of the perturbation by the virtual quanta leads to divergent results due to the quanta of *high* frequency. This ultraviolet catastrophe is inherent in the customary theory and avoided in Heitler's theory of radiation damping. What we

have shown in this paper is that it is not possible to obtain a satisfactory answer either by including the effects of virtual quanta as they are given by present theory or by excluding them entirely. They must be retained for long wave-lengths. They must be eliminated or modified for short wave-lengths.

This implies the existence of a critical wave-length. There are at least three possibilities. There is (1) the wave-length corresponding to the Duane-Hunt limit, (2) that corresponding to the electron's Compton wave-length, or (3) a new length characteristic of a future theory and presumably smaller.

The first of these possibilities, which might for instance amount to some method of systematic elimination of all virtual processes except those involving the creation of particles which in the actual problem are energetically capable of being created, would clearly involve a major and not correspondence theoretic change in the formalism of quantum mechanics. In particular, it would mean giving up the existence of a Hamiltonian and a wave function calculable from it. It does not seem likely that this will prove to be the correct path.

The results of Dancoff show that at least in present relativistic theory the Compton wave-length of the electron does not provide a suitable critical wave-length for the problem in question. It therefore seems most probable to us that a new length will be involved in a correct solution, above which the present quantum theory will have a kind of validity and below which new phenomena will have to be taken into account. It would seem likely that only in this way can the correspondence principle be satisfied. It is not satisfied by Heitler's proposals, and that in the last analysis is why they are unsatisfactory. In any case, we believe that the simple problem here considered may afford a useful test of future theories of radiation.

PHYSICAL REVIEW VOLUME 70, NUMBERS 7 AND 8 OCTOBER 1 AND 15, 1946

Scattering of Fast Neutrons by Boron

H. H. BARSCHALL,* M. E. BATTAT,** AND W. C. BRIGHT
Los Alamos Laboratory, Los Alamos, New Mexico

(Received July 1, 1946)

The cross section of boron for the scattering of fast neutrons through angles greater than 30° was measured at neutron energies between 0.2 and 3 Mev.

THE scattering of monoenergetic fast neutrons by boron has been investigated by Kikuchi and Aoki[1,2] for $d-d$ neutrons and by Leipunsky[3] for photo-neutrons of 130-, 220-, and 850-kev energy. In the present experiments the scattering of neutrons of energies from 0.2 to 3 Mev was investigated for the two boron isotopes.

The enriched material available was boron powder containing 53 percent B^{10}. The powder was placed in a cylindrical brass container, $2\frac{15}{16}$" i.d. The density of the powder was increased by shaking it on a vibrating table. 194 grams of the powder formed a layer $1\frac{1}{2}$" thick, containing 0.255×10^{24} atoms/cm². A sample of normal boron powder was prepared in the same way. The normal sample contained 200 grams of powder and had the same number of atoms per cm² as the enriched sample.

The experiments at neutron energies up to 1500 kev were carried out using neutrons obtained by bombarding Li with protons accelerated by the University of Wisconsin's electrostatic generator. For the experiments at 3 Mev the neutrons were produced by bombarding D_2O ice with 200-kev deuterons obtained by means of a Cockcroft-Walton set.

The cross section for the scattering of neutrons through angles greater than 30° was measured.

* Now at the University of Wisconsin.
** Now at Washington University.
[1] S. Kikuchi and H. Aoki, Proc. Phys. Math. Soc. Japan 21, 75 (1939).
[2] H. Aoki, Proc. Phys. Math. Soc. Japan 21, 232 (1939).
[3] A. I. Leipunsky, J. Phys. U.S.S.R. 3, 231 (1940).

The sample was equidistant from the source and the detector. The geometry was chosen such that a neutron scattered at the edge of the disk through an angle of 30° would reach the center of the detector. The line passing through the center of the target, the center of the disk, and the center of the detector was identical with that defined by the incident proton or deuteron beam.

For the experiments at the electrostatic generator a foil of fissionable material surrounded by Cd served as a detector. The foil was contained in a cylindrical volume 1″ high and 1″ in diameter. At the $d-d$ source the detector consisted of a circular thick layer of paraffin, 1″ in diameter, in a cylindrical proportional counter.

The measurements were carried out by placing into the neutron beam successively an empty container, the normal sample and the enriched sample. The primary neutron flux was monitored by a current integrator for the protons in the case of the Li(p, n) reaction. At the $d-d$ source the protons from the accompanying D(d, p)H^3 reaction were used for monitoring the neutron flux.

Cross sections were computed under the assumption that the neutron intensity in the sample decreased according to an exponential law.

The results are summarized in Table I. The second and third columns show the results obtained for the two samples. The contributions of the individual isotopes were then computed assuming that the cross sections are additive. In order to obtain the scattering cross section of B^{10} the absorption cross section is subtracted using the data obtained by Hanson.[4] The accuracy of the measurements as deduced from the consistency of the individual runs is about five percent. In computing the cross section for the isotopes separately the error is multiplied by two in the case of B^{11}, and four in the case of B^{10}.

In order to compare the present results for scattering through angles larger than 30° with the total cross sections quoted by other authors, seven percent should be added to the values given in Table I if one assumes spherical symmetry of the scattering. The result for normal boron at 3 Mev is in agreement with the value of 1.65×10^{-24} cm^2 obtained by Kikuchi and Aoki[1]

TABLE I. Scattering cross sections for neutrons on boron.

Neutron energy (Mev)	Cross section in 10^{-24} cm^2 for 30° geometry: Normal sample	Sample containing 53% B^{10}	B^{11}	B^{10} (total)	B^{10} (30° scattering)
0.2	3.5	3.8	3.4	4.1	1.6
0.6	2.4	2.9	2.2	3.5	2.5
0.8	1.8	2.1	1.6	2.6	2.0
1.0	1.6	1.9	1.4	2.3	1.8
1.2	2.0	1.8	2.2	1.5	1.0
1.5	1.9	1.9	1.9	1.8	1.2
3	1.6	1.6	1.6	1.7	1.1

for the total cross section of boron for 2.5-Mev $d-d$ neutrons, but somewhat lower than Aoki's[2] values for $d-d$ neutrons. Leipunsky[3] found for neutron energies of 130, 220, and 850 kev cross sections of 3.8, 4.2, and 2.9×10^{-24} cm^2, respectively. Although Leipunsky's and the present experiments were carried out at somewhat different energies and for a different geometry, the results of the two experiments do not appear compatible, particularly for 850-kev neutrons.

The authors wish to thank Dr. J. H. Manley for his interest in these experiments, Dr. J. H. Williams for permission to use the electrostatic generator, and the operating crew of the electrostatic generator for their cooperation.

This work was carried out under contract between the University of California and the Manhattan District, Corps of Engineers, War Department.

[4] A. O. Hanson, Private communication.

PHYSICAL REVIEW VOLUME 70, NUMBERS 7 AND 8 OCTOBER 1 AND 15, 1946

Nuclear Induction

F. BLOCH
Stanford University, California

(Received July 19, 1946)

The magnetic moments of nuclei in normal matter will result in a nuclear paramagnetic polarization upon establishment of equilibrium in a constant magnetic field. It is shown that a radiofrequency field at right angles to the constant field causes a forced precession of the total polarization around the constant field with decreasing latitude as the Larmor frequency approaches adiabatically the frequency of the r-f field. Thus there results a component of the nuclear polarization at right angles to both the constant and the r-f field and it is shown that under normal laboratory conditions this component can induce observable voltages. In Section 3 we discuss this nuclear induction, considering the effect of external fields only, while in Section 4 those modifications are described which originate from internal fields and finite relaxation times.

1. INTRODUCTION

THE method of magnetic resonance[1] has been successfully applied to measure the magnetic moment of the neutron[2] and of various nuclei.[3] The principal feature of this method is the observation of transitions, caused by resonance of an applied radiofrequency field with the Larmor precession of the moments around a constant magnetic field. In its application to nuclear moments the deflection of molecular beams in an inhomogeneous field was used as a means of detecting the occurrence of nuclear transitions. This method of detection has proven to be very fruitful but it was clear, at the same time, that the connection between molecular beams and magnetic resonance was not of basic character. The question arose, in particular, whether nuclear transitions could not be detected by far simpler electromagnetic methods, applied to matter of ordinary density.[4]

An attempt in this direction was undertaken by Gorter and Broer[5] whose arrangement was designed to indicate magnetic resonance absorption by a slight change in frequency of an electric oscillator. The experiment was based upon considerations which apply strictly to radiofrequency fields which are so small that they cause only a slight disturbance of the spin orientation; it was carried out with LiCl and KF at low temperatures and it was suggested that the failure to find an effect was caused by the fact that the nuclei had not found the orientation, corresponding to thermal equilibrium.

The first successful experiments to detect magnetic resonance by electromagnetic effects have been carried out recently and independently in the physics laboratories of Harvard[6] and Stanford[7] Universities. The experiment of Purcell and his collaborators is very closely connected to that of Gorter and Broer, the main difference being that resonance absorption manifests itself in the change of Q of an electric oscillator rather than in a change of frequency, and it presupposes, likewise, the necessity of only slightly perturbing r-f fields.

The considerations upon which our work was based have several features in common with the two experiments, previously mentioned, but differ rather essentially in others. In the first place, the radiofrequency field is deliberately chosen large enough so as to cause at resonance a considerable change of orientation of the nuclear moments. In the second place, this change is not observed by its relatively small reaction upon the driving circuit, but by directly observing the induced electromotive force in a coil, due to the precession of the nuclear moments around the constant field and in a direction

[1] I. I. Rabi, Phys. Rev. **51**, 652 (1937).
[2] L. W. Alvarez and F. Bloch, Phys. Rev. **57**, 111 (1940).
[3] I. I. Rabi, S. Millman, P. Kusch, and J. R. Zacharias, Phys. Rev. **53**, 318 (1938); **55**, 526 (1939).
[4] The first purely magnetic experiment to find an effect due to nuclear moments by measuring the susceptibility of liquid hydrogen was published by B. G. Lasarew and L. W. Schubnikow, Sov. Phys. 11, 445 (1937).
[5] C. J. Gorter and L. J. F. Broer, Physica 9, 591 (1942).
[6] E. U. Purcell, H. C. Torrey, and R. V. Pound, Phys. Rev. 69, 37 (1946).
[7] F. Bloch, W. W. Hansen, and Martin Packard, Phys. Rev. 69, 127 (1946).

perpendicular both to this field and the applied r-f field. This appearance of a magnetic induction at right angles to the r-f field is an effect which is of specifically nuclear origin and it is the main characteristic feature of our experiment. In essence, it is similar to the Faraday effect of rotation of the plane of polarization of light around a magnetic field, with the r-f field taking the place of the field vectors in a light wave and the observed perpendicular nuclear induction indicating a rotation of the total oscillating field around the constant magnetic field.

This effect is, of course, most outspoken at resonance (just as the Faraday effect becomes greatest in the neighborhood of a resonant frequency) and, in practice, is noticed by its sudden strong appearance under resonance conditions. It is worth while, however, to point out that the observation of nuclear induction should be possible even without any use of the magnetic resonance. Not only a weak r-f field, acting at resonance over very many Larmor periods, can produce an appreciable nuclear change of orientation, but also a strong field pulse, acting over only a few periods. Once the nuclear moments have been turned into an angle with the constant field, they will continue to precess around it and likewise cause a nuclear induction to occur at an instant when the driving pulse has already disappeared. It seems perfectly feasible to receive thus an induced nuclear signal of radiofrequency well above the thermal noise of a narrow band receiver. It is true that, due to the broadening of the Larmor frequency by internuclear fields or other causes, this signal can last only a comparatively short time, but for normal fields it will still contain many Larmor periods, i.e., it will be essentially monochromatic. The main difference between this proposed experiment and the one which we have actually carried out lies in the fact that it would observe by induction the free nuclear precession while we have studied the forced precession impressed upon the nuclei by the applied r-f field.

2. NUCLEAR PARAMAGNETISM

The existence of a resultant macroscopic moment of the nuclei within the sample under investigation is a common prerequisite for all electromagnetic experiments with nuclear moments. It is in fact a change of orientation of this macroscopic moment which causes the observed effects, and irrespective of the changes of orientation of the individual nuclei which might be induced by a r-f field, their moments would always cancel each other, if they did so initially, and thus escape observation. In the experiments with molecular beams of Stern and Rabi this necessity is avoided by separation in the beam of nuclei with different orientation.

Even in the absence of any orientation by an external magnetic field one can expect in a sample with N nuclei of magnetic moment μ to find a resultant moment of the order $(N)^{\frac{1}{2}}\mu$ because of statistically incomplete cancellation. This moment, however, would naturally be very small and in samples of normal size will be greatly increased as soon as the nuclei have found their equilibrium distribution in a field of a few thousand Gauss which, at the same time, will bring their Larmor precession into the convenient radiofrequency range.

In contrast to the familiar atomic paramagnetism which establishes itself almost immediately upon application of the polarizing field, there is no assurance for the same thing being true in the nuclear case. The time of establishment or "relaxation time" can be expected to vary anywhere between fractions of a second and many hours, depending in the most delicate manner upon the nuclear moments, the electronic structure of the atoms in the sample, their distance, and their motion. To study experimentally and theoretically this interesting relationship between nuclear relaxation time and atomic features seems to us, in fact, to be one of the fruitful fields of investigation which have now opened.[8]

It must be pointed out here that, in cases where the natural relaxation time should turn out inconveniently long, the establishment of thermal equilibrium can often be greatly accelerated by use of paramagnetic catalysts. The problem is similar to that of the conversion of

[8] A good deal of the theory of the paramagnetic relaxation time by I. Waller, Zeits. f. Physik **79**, 370 (1932), R. deL. Kronig, Physica **6**, 33, 1939. J. H. van Vleck, Phys. Rev. **57**, 426 (1940), can readily be adopted to hold also for nuclear paramagnetism. For nuclear paramagnetism and its bearing on reaching low temperatures see E. Teller and W. Heitler, Proc. Roy. Soc. **155**, 629 (1936).

ortho- and parahydrogen which was found, for example to be accelerated by paramagnetic ions in solutions and by admixture of oxygen in the gas phase.

As to the nuclear induction effect, there exists the interesting possibility of first establishing the equilibrium in a strong magnetic field under conditions of relatively short relaxation time (by evaporation into an oxygen atmosphere, addition of a paramagnetic catalyst, heating, etc.), thereupon considerably lengthening the relaxation time (by recondensation, removal of the catalyst, cooling, etc.), and thus preserving the high field polarization for a considerable time, even when the sample is removed from the high field. A subsequent nuclear induction experiment, carried out under suitable conditions, can then exhibit either a moment, pertaining to the field in which it was originally established, or indicate that the relaxation time was comparable or short, compared to the time which has elapsed since removal. We shall come back later to some more considerations of the important role of the relaxation time, which are directly connected with our experiments.

For the following purposes we shall assume that the thermal equilibrium between the nuclear moments and their surrounding atoms has been actually established in an external magnetic field of strength H. Let T be the equilibrium temperature and n the number of nuclei per unit volume, each having a magnetic moment μ and an angular momentum $jh/2\pi$. We shall write

$$M=\chi H, \tag{1}$$

where M is the resultant nuclear moment per cc in the field direction and where χ is the nuclear paramagnetic susceptibility. It is given by the familiar Curie formula

$$\chi=[(j+1)/3j](n\mu^2/kT), \tag{2}$$

in which it is assumed that $H\mu \ll kT$. This condition will always be very well satisfied, except for extraordinarily strong fields or exceedingly low temperatures.

For a numerical example we shall take the protons in water at room temperature ($T=291°$). We have here $j=\frac{1}{2}$, i.e., $(j+1)/3j=1$, and with $\mu=1.4\times10^{-23}$ c.g.s., $n=6.9\times10^{22}$ cm^{-3}, we obtain from (2) for the nuclear susceptibility

$$\chi=3.4\times10^{-10} \tag{3}$$

and with a field $H=10{,}000G$ from (1)

$$M=3.4\times10^{-6}\text{ gauss} \tag{4}$$

for the nuclear polarization.

While this value is small and would be difficult to observe directly, it is actually not M but the rate of change of the rapidly varying nuclear induction $B=4\pi M$, which is observed in our experiment and which we will show to be easily detectable.

3. PRINCIPLE OF THE NUCLEAR INDUCTION

We shall investigate the behavior of the great number of nuclei contained in a macroscopic sample of matter and acted upon by two external fields: a strong constant field and at right angles to it, a comparatively weak radio-frequency field. In order to simplify the explanation of the principle we shall, for the moment, omit some of the actually present complicating factors, and we shall assume:

(1) That the changes of orientation of each nucleus are solely due to the presence of the external fields;
(2) That the external fields are uniform throughout the sample.

The second assumption will evidently be justified with sufficient perfection of the experimental arrangement. It is the first assumption which is more serious; normally it will be far from being justified, and rather essential corrections will have to be introduced later to account for the actual conditions. The following conditions should be satisfied for its acceptance:

(1a) The atomic electrons do not cause appreciable fields to act upon the nuclei.
(1b) The interaction between neighboring nuclei can be neglected.
(1c) The thermal agitation does not essentially affect the nuclei, i.e., the relaxation time is long compared to the considered time intervals.

We shall come back to these three points in Section 4; accepting in this section the above assumptions, the discussion becomes comparatively simple: Let the z-direction be that of the constant field with strength H_0 and the x-direction that of the r-f field with circular frequency ω

and amplitude $2H_1$, so that the total external field vector $\mathbf{H}$ has the components

$$H_x=2H_1\cos\omega t;\quad H_y=0;\quad H_z=H_0. \tag{5}$$

We shall further denote by $\mathbf{M}$ the vector, representing the nuclear polarization, i.e., the resultant nuclear moment per unit volume; it is the variation with time of this vector in which we are primarily interested.

To obtain this variation does not require the solution of the Schroedinger equation. It is enough to remember the general fact that the quantum-mechanical expectation value of any quantity follows in its time dependence exactly the classical equations of motion and that the magnetic and angular momenta of each nucleus are parallel to each other.

The resultant angular momentum vector $\mathbf{A}$ of all the nuclei, contained in a unit volume will, therefore, satisfy the classical equation

$$d\mathbf{A}/dt=\mathbf{T}, \tag{6}$$

where $\mathbf{T}$ is the total torque, acting upon the nuclei and it is

$$\mathbf{T}=[\mathbf{M}\times\mathbf{H}], \tag{7}$$

where the vector $\mathbf{M}$ represents the resultant nuclear magnetic moment per unit volume. The parallelity between the magnetic moment $\boldsymbol{\mu}$ and the angular momentum $\mathbf{a}$ for each nucleus implies

$$\boldsymbol{\mu}=\gamma\mathbf{a} \tag{8}$$

with the gyromagnetic ratio

$$\gamma=\mu/a \tag{9}$$

and we have, therefore, also for the resultant quantities $\mathbf{M}$ and $\mathbf{A}$

$$\mathbf{M}=\gamma\mathbf{A}, \tag{10}$$

with γ likewise given by (9).[9]

Combining Eqs. (6), (7), and (10), we have, therefore, for the variation of the polarization vector $\mathbf{M}$

$$d\mathbf{M}/dt=\gamma[\mathbf{M}\times\mathbf{H}]. \tag{11}$$

For our purposes we are interested in a special solution of this equation which can be obtained if, for the fields H_0 and H_1 of Eq. (5) we have $H_1\ll H_0$, and if both are positive and constant. We shall further assume that the circular frequency ω of the r-f field is in the neighborhood of the resonance frequency ω_0, given by

$$\omega_0=\gamma H_0 \tag{12}$$

i.e., that we have

$$|\omega-\omega_0|\ll\omega_0. \tag{13}$$

The actual oscillating field in the x-direction can then be effectively replaced[10] by a field

$$H_x=H_1\cos\omega t;\quad H_y=\mp H_1\sin\omega t \tag{14}$$

rotating around the z-direction with the sign of H_y and, therefore, the sense of rotation being negative or positive, depending upon whether the sign of γ is positive or negative.

It follows immediately from (11) that the magnitude M of the polarization is constant. Besides, there is a special solution for which its z-component M_z is likewise constant. Introducing the polar angle θ and writing

$$M_x=M\sin\theta\cos\omega t;\quad M_y=\mp M\sin\theta\sin\omega t;\quad M_z=M\cos\theta, \tag{15}$$

one can indeed verify immediately that (11) is satisfied if θ is a constant and chosen such that

$$tg\theta=\gamma H_1/(\gamma H_0\mp\omega), \tag{16}$$

with the minus or plus sign before ω, depending upon whether γ is positive or negative. If we let

$$H^*=\omega/|\gamma| \tag{17}$$

denote the "resonance field at frequency ω" i.e., that field H for which the Larmor frequency $\omega_L=\gamma H$ is equal to the frequency ω of the oscillating field, we can write (16) in the form

$$tg\theta=H_1/(H_0-H^*). \tag{18}$$

Equations (15) represent a solution for which the polarization rotates around the z-direction, i.e., around the strong field H_0 and in such a way that it lies at any instant in the common plane of this field and the effective rotating field (14).

The angle θ between H_0 and the polarization follows from (18) to be small, as long as H_0 is appreciably larger than the resonant field H^*.

[9] Our treatment includes evidently both cases of $\boldsymbol{\mu}$ and $\mathbf{a}$ being parallel (i.e., having the same relative orientation as for a positive rotating charge) and opposite. Both are taken into account by assigning to the quantity γ of Eq. (9) a positive or negative value respectively. We shall see below that the actual sign of γ reveals itself in the phase of the induced voltage signal.

[10] F. Bloch and A. Siegert, Phys. Rev. **57**, 522 (1940).

The direction of the polarization starts to deviate noticeably from the z-direction as the difference H_0-H^* becomes comparable or small compared to the magnitude H_1 of the effective rotating field. It is perpendicular to the z-direction for $H_0=H^*$ and for still further decreasing values of H_0 turns toward the negative z-direction, finally pointing in a direction opposite to H_0 for $H^*-H_0 \ll H_1$.

Formulas (15) and (18) can be conveniently rewritten by introducing the difference

$$\delta=(H_0-H^*)/H_1=\operatorname{cotg}\theta \tag{19}$$

between the actual z-field H_0 and its resonance value H^* in units of the magnitude H_1 of the effective rotating field (14) or the half amplitude of the actual oscillating field (5) in the x-direction. We have then

$$M_x=M\frac{\cos\omega t}{(1+\delta^2)^{\frac{1}{2}}};\quad M_y=\mp M\frac{\sin\omega t}{(1+\delta^2)^{\frac{1}{2}}};\qquad M_z=M\frac{\delta}{(1+\delta^2)^{\frac{1}{2}}}. \tag{20}$$

These formulas show clearly the increase of the rotating component of **M** upon approach to resonance.

The solution (20) differs essentially from those previously[1,2] considered, where the nuclear moment can be assumed to be originally in one of the stationary states in which its angle with the z-direction is given by $\cos\theta=m/j(m=-j\cdots+j)$ and where it becomes suddenly subjected to the action of an oscillating field, thereby undergoing transitions in which θ changes through a change of m by ±1. The solution (20) corresponds, in the language of quantum mechanics, not to a single stationary state, but to a "mixture" or linear combination of all stationary states with different values of m and with their amplitudes and phases so adjusted that the expectation values of the components of the angular or magnetic moment are proportional to the values (20). Particularly the z-component is not quantized, but has an expectation value which varies continuously with variation of δ. In order to obtain a persistent rotating component of the expectation value of **M**, as expressed by (20), it is essential, from this point of view, that we are dealing with a "coherent mixture" of states, i.e., that the relative phases of the wave functions, corresponding to the different states, do not undergo any changes. It can be expected, and will be shown later, that any cause which tends to destroy the phase relation, such as the interaction between neighboring nuclei, will diminish the actual observable value of the rotating component.

Our special interest in the particular solution (20) is based upon the fact that, while it has been derived under the assumption that ω, H_0, and therefore, δ are constant, it can be shown to be equally valid, provided that these quantities vary adiabatically, i.e., slowly enough so that

$$|d\delta/dt| \ll |\gamma H_1|. \tag{21}$$

For constant H_1, i.e., for constant amplitude of the oscillating field, this variation of δ and, thereby, of the components (20) of the polarization can, according to (19), take place through two different procedures. Either the field H_0 in the z-direction is kept constant and the frequency ω of the oscillating field is slowly varied, thereby slowly varying the value H^* of the resonance field, given by (17); or ω and therefore H^* are kept constant and H_0 is varied slowly. Both procedures are recommendable in practice, depending upon the circumstances; we shall here assume that the latter procedure is chosen, i.e., that H_0 varies adiabatically with constant ω.

Whether a variation dH_0/dt of H_0 can be considered as adiabatic or not, depends, according to (19) and (21) upon the half amplitude H_1 of the r-f field, any given variation being the more adiabatic, the larger H_1. The condition (21) for adiabatic variation can also be expressed by stating that the z-field H_0 has to pass through an interval, comparable to the "resonance width" H_1 during a time which is long compared to

$$t_1=1/|\gamma H_1|. \tag{22}$$

As a numerical example, we shall again consider protons with $\gamma=2.66\times10^4$ c.g.s.[11] Choosing an amplitude $2H_1$ of 10 gauss, for the r-f field, i.e., with $H_1=5$ gauss, we have

$$t_1=7.5\times10^{-6}\text{ sec.}, \tag{23}$$

[11] J. M. B. Kellogg, I. I. Rabi, N. F. Ramsey, Jr., and J. R. Zacharias, Phys. Rev. **56**, 728 (1939).

i.e., the variation is adiabatic, if H_0 varies by an amount comparable to the "resonance width" of 5 gauss in a time long compared to 7.5 microseconds. It is clear that with the assumed value of H_1, normal variations of H_0 can be considered as perfectly adiabatic and that H_1 has to be chosen very much smaller before this condition is violated.

We shall now make use of the preceding considerations in order to introduce the nuclear induction effect, i.e., the essential features of an experimental arrangement by which a rotating component of the nuclear polarization can be observed through an induced voltage signal.

A sample, containing among others the nuclei under consideration, shall occupy a relatively small volume between the poles of a magnet so that the field H_0 of the magnet can be considered homogeneous over the extension of the sample, its direction being chosen as the z-direction of a right-handed Cartesian coordinate system. An oscillating field with amplitude $2H_1$ and circular frequency ω shall be produced by an r-f current, passing through a wire which is wound such that the r-f field has an essentially constant amplitude over the sample region and oscillates in the x-direction. Immediately surrounding the sample there shall finally be wound a coil with its axis parallel to the y-axis, so that an r-f flux in the y-direction will manifest itself by an induced r-f voltage signal across its terminals. It is such a signal, produced by the rotating component of the nuclear polarization, in which we are primarily interested, and we shall show that one can expect it to be of easily detectable magnitude, with moderate sizes of the sample and under normal laboratory conditions.

In order to estimate the induced r-f voltage we have to consider the expression for M_y of Eq. (20). The corresponding value of the induction is

$$B_y = 4\pi M_y, \tag{24}$$

and if N turns of the receiver coil surround a cross-sectional area A of the sample, we obtain for the effective flux through the coil

$$F = 4\pi NA M_y = \mp 4\pi NA M \frac{\sin \omega t}{(1+\delta^2)^{\frac{1}{2}}}, \tag{25}$$

and for the induced voltage $\mp V$ across the terminals of the coil

$$V = -\frac{1}{c}\frac{dF}{dt} = \pm \frac{4\pi}{c} NA M \omega \frac{\cos \omega t}{(1+\delta^2)^{\frac{1}{2}}}, \tag{26}$$

where the variation of δ has been considered slow enough so that its time derivative can be neglected compared to that of $\cos \omega t$.

The amplitude of the signal voltage V reaches evidently a maximum at resonance, i.e., for $\delta = 0$, so that here the z-field H_0 has, according to (17) and (19), the value $H_0 = \omega/|\gamma| = H^*$. We shall now assume that the sample has been for a sufficiently long time in a field $H_0 = H > H^*$, so that M has reached its thermal equilibrium value, corresponding to that field, and is given by (1) to be $M = \chi H$. If now H_0 starts to decrease and if our previous assumptions, and particularly that of the constancy of M, remain valid, we can substitute this value into (26), thus obtaining

$$V = \pm \frac{4\pi}{c} NA \chi H \omega \frac{\cos \omega t}{(1+\delta^2)^{\frac{1}{2}}}. \tag{27}$$

It has to be observed that it is sufficient for the "equilibrium field" H to be larger than the resonance field H^* only by a small percentage, i.e., by several times the relatively weak field H_1, in order that thermal equilibrium can be established under non-resonant conditions. If we assume this to be actually the case, we can substitute in (27) for H the resonance value $H^* = \omega/|\gamma|$. We shall further rewrite the formula (2) for the nuclear susceptibility, using (9) and writing $a = jh/2\pi$ for the angular momentum, so that

$$\chi = n \frac{j(j+1)}{3kT} \left(\frac{\gamma h}{2\pi}\right)^2,$$

and finally

$$V = \frac{1}{\pi c} NA n \frac{j(j+1)}{3kT} h^2 \gamma \omega^2 \frac{\cos \omega t}{(1+\delta^2)^{\frac{1}{2}}}. \tag{28}$$

The plus or minus sign in (27), referring to positive or negative γ-values, respectively, does not appear any more in this formula, provided that γ is here taken algebraically, i.e., positive or negative, depending upon the nuclei under consideration.

We shall now compute from (27) the voltage amplitude $a_v = (4\pi/c) NA \chi H \omega$ at resonance (i.e.,

for $\delta=0$) of the signal voltage for protons in water, using the same conditions ($H=10{,}000G$, $T=291°$), which led to the value (4) for $\chi H=M=3.4\times10^{-6}G$. The corresponding circular frequency is given by $\omega=|\gamma|H=2.66\times10^{4}\times10{,}000=2.66\times10^{8}$ sec.$^{-1}$. ($\nu=42$ megacycles.) Assuming the cross-sectional area A of the sample to be 1 cm^2 and the number of turns on the receiver coil $N=10$, we obtain the resonance amplitude in volts

$$a_r=10^{-8}\times4\pi\times10\times3.4\times10^{-6}\times2.66\times10^{-8}=1.1\times10^{-3}\text{ volt.}$$

We see thus that even under the moderate conditions, here assumed, with linear dimensions of the sample of the order of 1 cm, one can expect from these considerations an r-f signal voltage of the order of a full millivolt, giving a considerable margin in the limits of observation.

Such a margin is desirable, not only because it allows a convenient reduction in the applied values of H and ω, but also because the voltage, given by (27) or (28) represents actually an overestimate. These formulas omit the influence of internuclear and thermal interaction, and we shall see later that they can cause an appreciable reduction from the above estimate.

Not only the magnitude of the induced voltage signal is of interest, but also its sign, i.e., its relative phase with respect to the "driving field" H_x of Eq. (5). It is evident that the sign is partly determined by that of γ, but its determination in Eq. (28) depends also upon the special assumptions under which it was derived, particularly the one expressed in formula (20), that M_z has the positive value M for large positive values of δ, i.e., according to (19) for z-fields H_0 appreciably *above* the resonance field H^*. This assumption is of course justified, if thermal equilibrium has been established, previous to the passage through resonance, in fields *higher* than the resonance field. If, on the other hand, the thermal equilibrium was previously established in fields *below* the resonance field, one must obviously demand that the opposite initial condition is fulfilled, i.e., that M_z is positive for negative values of δ. This requires changes in the considerations, leading to Eq. (20), which can immediately be derived from the starting Eq. (11). This equation is linear and homogeneous in the components of the polarization vector **M** so that a change of sign of all components leads necessarily from one solution to another solution. In order to satisfy the condition for positive M_z below resonance, it is therefore only necessary to change the sign in the formula (20). The subsequent considerations will all remain valid, except for a change of sign of M_y and V, leading thus, instead of (28), to the more general formula

$$V=\pm NAn\frac{j(j+1)}{3kT}\hbar^2\gamma\omega^2\frac{\cos\omega t}{(1+\delta^2)^{\frac{1}{2}}},\qquad(29)$$

with the $\pm$ sign referring to the case of the polarization parallel to the z-field far above or below resonance, respectively. In using the phase of the induced voltage signal with respect to the driving field for a determination of the sign of γ, or of the nuclear moment, it is therefore necessary to keep also the relative magnitude of equilibrium field and resonance field in mind, since it likewise affects the phase.

The fact that our formulas express an "indefinite memory" of the nuclear polarization, as to the conditions under which it was created, rests of course upon the initial simplifying assumptions of this section, and particularly upon assumption (1c), that thermal agitation does not affect the nuclei during the time of observation. It is clear from the previous considerations that finite, although possibly rather long, relaxation times will play an important role in the actual behavior of the observable phenomena, and they will be discussed in the following section.

4. INFLUENCE OF THERMAL AGITATION AND INTERNUCLEAR ACTION

The considerations of the preceding section can be regarded only as qualitative, since they are based upon the assumption (1) that all changes of nuclear orientation are due to the external fields. It implies the omission of three major internal actions, mentioned under (1a), (1b), and (1c), of Section 3, which are likewise responsible for changes of orientation.

The first action is that of atomic moments upon the nuclei. Its importance depends evidently upon the substance under consideration,

i.e., upon whether such moments are actually present or not. There are indeed many substances (e.g., water) where it is safe to assume their absence, i.e., where the electronic spin moments will be paired off and where orbital moments which may be present in the free atoms or molecules are quenched because of intermolecular action. While assumption (1a) is justified under these circumstances, one has to introduce major changes in the presence of permanent atomic moments. The fields due to these moments and acting upon the nuclei will generally be considerably stronger than the external fields, and we do not have to deal in first approximation with independent nuclei, but with nuclear moments which are strongly coupled to the atomic frame. The situation is analogous to that investigated by Rabi and his collaborators[12] for free molecules, where the r-f field causes transitions between hyperfine structure levels. Except for a broadening of these levels, due to interatomic forces, similar phenomena can be expected in liquids and solids (e.g., in the salts of the rare earths), but we shall not enter here upon their discussion and shall restrict ourselves to the case where permanent atomic moments are absent.

There remain then the internal fields due to thermal agitation and internuclear action which have to be considered. Although both these fields are usually considerably weaker than the external applied fields, they are of importance because of their cumulative effects over longer periods of time. We shall not attempt here to give a rigorous quantum-mechanical theory of these effects; an excellent start for such a theory has been made in the papers mentioned in reference 8. Instead, we shall restrict ourselves to a semi-macroscopic description, trying to introduce into Eq. (11) for the macroscopic polarization such modifications as are necessary to account for the principal features of these effects.

To arrive at these modifications we shall consider a finite polarization **M** to exist at a certain moment and shall separately investigate the changes which it will undergo due to thermal agitation and internuclear action. Although there is a certain similarity insofar as both represent random actions upon the individual nuclei, there is this essential difference, that only thermal perturbations can change the energy of the total spin system, while internuclear interactions leave this energy unchanged.

The dominant part of the total spin energy E is caused by the strong field H_0 in the z-direction and can be written in the form

$$E=-H_0M_z. \tag{30}$$

Major changes of the total energy are therefore necessarily due to a change of the z-component of the polarization and it will be the thermal perturbations which will be responsible for these changes. The equilibrium value which M_z will approach under the influence of thermal perturbations is given by

$$M_0=\chi H_0. \tag{31}$$

If at any time $M_z\neq M_0$, it will approach this value exponentially with a characteristic time constant T_1, which we shall call the "thermal" or "longitudinal" relaxation time, and we can describe the rate of change of M_z, due to thermal perturbations alone, by the differential equation

$$\dot{M}_z=-(M_z-M_0)/T_1 \tag{32}$$

with the stationary solution $M_z=M_0$.

The actual value of T_1 is very difficult to predict for a given substance; it depends delicately, not only upon the thermal motion of the atoms which is quite different in gases, liquids, and solids, but also upon their electronic structure and its modification, due to interatomic forces. Rough estimates can easily lead to relaxation times of many seconds or even hours. We shall see below that such long relaxation times can be inconvenient for the observation of the induction effect. It is recommendable, in this case, to add to the substance a certain percentage of paramagnetic atoms or molecules. They will essentially act as catalysts, with the relatively strong fields of their permanent moments greatly shortening the relaxation time T_1, even if they are present in a small percentage and do not otherwise affect the nuclei under consideration.

The fields which are due to neighboring nuclei, also contribute to the establishment of the equilibrium because of their thermal agitation. These fields are so small that they alone would normally lead to extraordinarily long thermal relaxation

times with their influence upon the actual value T_1 being negligible. Internuclear actions can, however, be of importance for the changes of the other two components M_x and M_y of the polarization in which we are equally interested. The fact that the nuclei with their moments participate in the thermal agitation is indeed of minor importance and represents only a small correction in their effect upon these components, since changes of M_x and M_y do not affect the energy (30) of the total spin system in the field. These changes can, therefore, take place without the necessity of transferring part of the spin energy E into kinetic energy of the atoms and it is permissible, in this respect, to consider the nuclei at rest and to neglect their comparatively slow motion.

Processes in which the total energy of the spin system does not change and which therefore affect only the components of the polarization which are transversal to the field are not necessarily due to internuclear forces alone. Small and irregular inhomogeneities of the z-field H_0 and the presence of other moments, such as those of paramagnetic ions in solution, will cause similar effects. It will in fact be permissible, for a qualitative discussion, to describe all these effects, including internuclear actions, by an "effective irregularity" of the z-field of order H' and through this field by a "transversal relaxation time"

$$T_2 = 1/|\gamma| H', \tag{33}$$

which it takes for M_x and M_y to be appreciably affected.

The magnitude of T_2 can be easily estimated if H' is due to neighboring nuclei whose motion can be neglected. With μ being the magnetic moment of a neighboring nucleus and r being its distance one will expect

$$H' \cong \mu/r^3. \tag{34}$$

Choosing $\mu = 10^{-23}$ c.g.s. and $r = 2 \times 10^{-8}$ cm this leads to

$$H' = 1 \text{ gauss} \tag{35}$$

and with $\gamma = 10^4$ c.g.s. through (33) to

$$T_2 = 10^{-4} \text{ sec.} \tag{36}$$

To give a reliable estimate of T_2 in more general cases requires a more detailed investigation of the mechanisms involved and will not be attempted here. The special case leading to (36) will merely be considered as an illustration for the fact that the transversal relaxation time T_2 can be many orders of magnitude smaller than the longitudinal time T_1 and that serious errors may be committed by assuming $T_1 = T_2$. There are, on the other hand, also cases where this equality is justified, particularly those where both relaxation times are due to impacts which last during a time short compared to the Larmor period, so that the distinction between collisions which change the spin energy and those which leave it unaltered becomes immaterial.

In order to obtain a qualitative description of the total change of the nuclear polarization **M** with time we shall now introduce such terms for its rate of change which contain the essential features of a longitudinal and transversal relaxation time and which, at the same time, are chosen so as to complicate the analysis as little as possible. For this purpose we shall assume that in analogy to the change (32) of the longitudinal component, the change of M_x and M_y will likewise be of an exponential character, governed by the equations

$$\dot{M}_x = -(1/T_2) M_x, \qquad \dot{M}_y = -(1/T_2) M_y \tag{37}$$

and that the total rate of change of **M** is obtained by adding to the expression (11), which takes into account the action of external fields only, the changes (32) and (37) of its components due to internal actions. The appearance of the same time constant T_2 in both Eqs. (37) is justified if one considers the substance to be isotropic. We obtain then the following differential equations for the three components of **M**:

$$\dot{M}_x - \gamma(M_y H_z - M_z H_y) + \frac{1}{T_2} M_x = 0, \tag{38a}$$

$$\dot{M}_y - \gamma(M_z H_x - M_x H_z) + \frac{1}{T_2} M_y = 0, \tag{38b}$$

$$\dot{M}_z - \gamma(M_x H_y - M_y H_x) + \frac{1}{T_1} M_z = \frac{1}{T_1} M_0. \tag{38c}$$

The components of the external field are given by Eq. (5) and we shall replace, as in Section 3, the actual oscillating x-component by the ef-

fective rotating component (14), so that we have

$$H_x=H_1\cos\omega t;\quad H_y=\mp H_1\sin\omega t;\quad H_z=H_0 \tag{39}$$

with the two signs of H_y referring to positive and negative values of γ, respectively.

It is convenient to introduce instead of M_x and M_y two new variables u and v through

$$M_x=u\cos\omega t-v\sin\omega t, \tag{40a}$$

$$M_y=\mp(u\sin\omega t+v\cos\omega t). \tag{40b}$$

We shall further choose the time scale in units of $1/|\gamma|H_1$ by introducing the dimensionless quantities:

$$\tau=|\gamma|H_1t;\quad \alpha=\frac{1}{|\gamma|H_1T_1};\quad \beta=\frac{1}{|\gamma|H_1T_2};\quad \delta=\frac{|\gamma|H_0-\omega}{|\gamma|H_1} \tag{41}$$

where $|\gamma|$ is the absolute value of γ. Using (39)–(41), one can then write the Eqs. (38) in the form:

$$du/d\tau+\beta u+\delta v=0, \tag{42a}$$

$$dv/d\tau+\beta v-\delta u+M_z=0, \tag{42b}$$

$$dM_z/d\tau+\alpha M_z-v=\alpha M_0. \tag{42c}$$

The Eqs. (38) differ from the three component Eqs. (11) of Section 3, insofar as they contain on their left sides the "damping terms" inversely proportional to T_1 and T_2 and that on the right side of (38c) there appears an inhomogeneous term, proportional to the equilibrium polarization $M_0=\chi H_0$. Their solution offers no difficulty, especially if δ is a slowly varying quantity so that they appear in the form (42) as a system of linear differential equations with almost constant coefficients; a more detailed discussion will be reserved for a later occasion. We shall here give directly a particular solution which is of special interest for our present purposes; its validity can be verified, provided that the variation of δ is adiabatic in the sense of Section 3 and that both quantities α and β of (41) are assumed to be small compared to unity. The first condition implies $|d\delta/d\tau|\ll 1$; it is identical with Eq. (21) and will be the more closely satisfied for any given variation with time of δ, the larger the amplitude of the oscillating field. In order to have $\alpha\ll 1$, $\beta\ll 1$, it is necessary, according to (41), that either the relaxation times T_1 and T_2 are sufficiently large or that the amplitude $2H_1$ of the oscillating field is sufficiently large.

One can normally expect the transverse relaxation time T_2 to be smaller than the longitudinal T_1 or $\alpha<\beta$. The assumption of "large amplitudes" implies then, according to (41), that

$$H_1\gg\frac{1}{|\gamma|T_2}$$

or, according to (33),

$$H_1\gg H'. \tag{43}$$

Using for a numerical example the value (35) of 1 gauss for H', we see therefore that an amplitude of $2H_1=10$ gauss can already be considered as "large" although it will normally be still very small compared to the strong field H_0 (of the order of several thousand gauss) in the z-direction. It is in this case $\beta=0.2$ and no serious errors are committed in neglecting correction terms in α and β.

With the three quantities $|d\delta/d\tau|$, α and β small compared to unity our particular solution of (38) can be written in the convenient form

$$M_x=\frac{M}{(1+\delta^2)^{\frac{1}{2}}}\cos\omega t, \tag{44a}$$

$$M_y=\mp\frac{M}{(1+\delta^2)^{\frac{1}{2}}}\sin\omega t, \tag{44b}$$

$$M_z=\frac{M\delta}{(1+\delta^2)^{\frac{1}{2}}}, \tag{44c}$$

with

$$\delta=\delta(t)=\frac{H_0(t)-H^*}{H_1};\quad H^*=\frac{\omega}{|\gamma|}, \tag{45}$$

$$M=M(t)=\frac{1}{T_1}\times\int_{-\infty}^{t}\frac{\delta(t')\exp\{-[\theta(t)-\theta(t')]\}M_0(t')}{[1+\delta^2(t')]^{\frac{1}{2}}}dt', \tag{46}$$

$$M_0(t')=\chi H_0(t'), \tag{47}$$

$$\theta(t)-\theta(t')=\frac{1}{T_1}\int_{t'}^{t}\frac{\delta^2(t'')+T_1/T_2}{1+\delta^2(t'')}dt''. \tag{48}$$

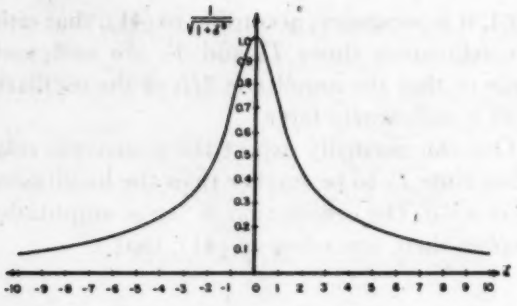

FIG. 1. Schematic representation of the voltage amplitude in the case of rapid passage. The abscissa δ is the deviation of the actual field from the resonance field in units of the half-amplitude of the oscillating field. The ordinate is proportional to the amplitude of the induced voltage and the y-component of the nuclear polarization.

The general solution of (38) is of course obtained by adding to (44) arbitrary multiples of the homogeneous solutions, their factors being determined by the initial conditions. These solutions can be seen to decrease exponentially with time so that it is permissible to omit them after a sufficient time has elapsed. In practice it is only the solution (44) which has to be considered, since it corresponds to the situation where the equilibrium polarization M_0 was zero before a sufficient time in the past, i.e., where the actual conditions have been obtained by adiabatic change, starting from an originally unpolarized sample.

The Eqs. (44) have the same form as the Eqs. (20) of Section 3, with the difference that M is not an arbitrary constant but is generally a function of time, given by (46). It has to be observed that while its absolute value $|M|$ still represents the instantaneous magnitude of the polarization, the quantity M itself is not necessarily positive but can have both signs, depending upon the positive or negative values which δ in the integrand of (46) has assumed in the past. We are primarily interested in the behavior of the polarization near resonance and it is interesting to observe that M may here be considered as essentially constant or appreciably variable, depending upon the speed of variation of δ, i.e., of either H_0 or ω in comparison to the relaxation times.

Formula (46) shows in fact that the value of M at any time is determined by the past history and that the more remote a past is of importance, the slower the decrease of the exponential. The functional dependence of M upon time and particularly its behavior near resonance will be primarily determined by the relative change of δ and of the exponential in the integrand of (46).

We shall speak of the limiting case of "rapid passage" if δ varies near resonance by an amount of order unity during a time short compared to the variation of the exponential. This case is the more approximately realized the more rapid the change of δ or, according to (48), the longer the relaxation times T_1 and T_2. It can be easily seen with the use of Eqs. (41) that because of the assumed smallness of α and β such a relatively rapid change of δ is compatible with the adiabatic condition $|d\delta/dt| \ll 1$. In the neighborhood of resonance M can be considered in this case to be essentially constant, its actual value depending mostly upon the values which M_0 and δ have assumed an appreciable time before approach of resonance conditions.

The amplitude of M_y is then proportional to $1/(1+\delta^2)^{\frac{1}{2}}$ and is schematically represented in Fig. 1. The simplified situation, considered in Section 3, is in fact a special case of "rapid passage" or long relaxation time. It is assumed here that H_0 has been held fixed for a long time at a value H, far from resonance, so that $|\delta| \gg 1$ with a subsequent establishment of resonance conditions during a time, very short compared to T_1. The main contribution to (46) arises then from past times t', where M_0 had the constant value χH and δ^2 had a value large compared to unity. If we assume, besides, for this value $\delta^2 \gg T_1/T_2$ or if we assume, irrespective of δ that $T_1 = T_2$ we obtain from (48)

$$\theta(t) - \theta(t') = \frac{t-t'}{T_1}$$

and from (46)

$$M = \pm \frac{\chi H}{T_1} \int_{-\infty}^{t} \exp\{-(t-t')/T_1\} dt' = \pm \chi H. \quad (49)$$

The magnitude of M corresponds thus, as was to be expected, to the field H, to which the sample was sufficiently long subjected. The plus or minus sign in (49) has to be taken, depending on whether this field was stronger or weaker than the resonance field, i.e., whether during action of this field, far from resonance, we had $\delta/(1+\delta^2)^{\frac{1}{2}} = +1$

or $\delta/(1+\delta^2)^{\frac{1}{2}}=-1$. This duplicity of the resulting sign of M_y upon approach of resonance from "above" or "below" was discussed in Section 3 and must not be confused with the other duplicity, expressed in (44b) and depending upon the sign of γ.

The opposite limiting case, to be considered, is that of "slow passage" through resonance of short relaxation times, where the main variation in the integrand of (46) is caused by the exponential. It can be treated by writing

$$\frac{\partial}{\partial t'}\exp -[\theta(t)-\theta(t')]=\frac{\partial\theta(t')}{\partial t'}\exp -[\theta(t)-\theta(t')]$$

or using (48)

$$\exp -[\theta(t)-\theta(t')]$$
$$=T_1\frac{1+\delta^2(t')}{\delta^2(t')+(T_1/T_2)}\frac{\partial}{\partial t'}\exp -[\theta(t)-\theta(t')]$$

so that by partial integration, we obtain from (48)

$$M(t)=\frac{1+\delta^2(t)}{\delta^2(t)+(T_1/T_2)}\frac{\delta(t)M_0(t)}{[1+\delta^2(t)]^{\frac{1}{2}}}$$
$$-\int_{-\infty}^{t}\exp -[\theta(t)-\theta(t')]\frac{d}{dt'}$$
$$\times\left[\frac{1+\delta^2(t')}{\delta^2(t')+(T_1/T_2)}\frac{\delta(t')M_0(t')}{[1+\delta^2(t')]^{\frac{1}{2}}}\right]dt'. \quad (50)$$

The last integral becomes evidently negligible if the variation of δ and M_0 with time is sufficiently slow. Keeping only the dominant first term in (50) and substituting into (44), we find thus:

$$M_x(t)=\frac{M_0(t)\delta(t)}{\delta^2(t)+T_1/T_2}\cos\omega t, \quad (51a)$$

$$M_y(t)=\mp\frac{M_0(t)\delta(t)}{\delta^2(t)+T_1/T_2}\sin\omega t, \quad (51b)$$

$$M_z(t)=\frac{M_0(t)\delta^2(t)}{\delta^2(t)+T_1/T_2}. \quad (51c)$$

In contrast to the case of rapid passage, where M can be considered essentially constant and where the amplitudes of M_x and M_y reach, according to (44) their maximum at resonance, i.e., for $\delta=0$, it is seen from (51) that in the case of slow passage all three components of the polarization vanish at resonance. Since M_0 varies only little in the neighborhood of resonance, it is permissible to replace it by the equilibrium polarization M^* at the resonance field H^*, i.e., to write

$$M_0=M^*=\chi H^*=\chi\frac{\omega}{|\gamma|}.$$

The amplitudes of M_x and M_y are then given by

$$a_{x,y}=\chi\frac{\omega}{|\gamma|}f(\delta) \quad (52)$$

where

$$f(\delta)=\frac{\delta}{\delta^2+T_1/T_2}. \quad (53)$$

We have plotted this function in Fig. 2. It assumes its extremum values

$$f(\delta)=\pm\tfrac{1}{2}(T_2/T_1)^{\frac{1}{2}} \quad (54)$$

for

$$\delta=\pm(T_1/T_2)^{\frac{1}{2}} \quad (55)$$

and shows qualitatively different behavior from the simple maximum, to be expected in the case of rapid passage and represented in Fig. 1.

The case of "slow passage" can also be treated directly without the restriction $\alpha\ll1$, $\beta\ll1$ which led to the solution (44) and (51). With δ and M_0 so slowly varying that they can be considered as practically constant one can in this case obtain a solution of the Eqs. (42) by assuming u, v, and M_z likewise as practically constant, i.e., by neglecting their derivatives. With $du/d\tau=dv/d\tau$

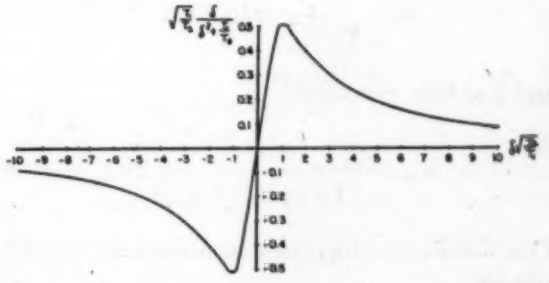

FIG. 2. Schematic representation of the voltage amplitude in the case of slow passage. T_1 and T_2 are the longitudinal and transversal relaxation times, respectively, and the scale is chosen such as to make the plot independent of their values. The significance of abscissa and ordinate is otherwise the same as in Fig. 1.

$=dM_z/d\tau=0$ one obtains directly from the Eqs. (42)

$$u=\frac{\delta}{\beta^2+\delta^2+\beta/\alpha}M_0, \tag{56a}$$

$$v=-\frac{\beta}{\beta^2+\delta^2+\beta/\alpha}M_0, \tag{56b}$$

$$M_z=\frac{\beta^2+\delta^2}{\beta^2+\delta^2+\beta/\alpha}M_0. \tag{56c}$$

Using $\beta/\alpha=T_1/T_2$ and neglecting for small values of β, v and the term β^2 in the numerators this is through (40) identical with the solution (51).

It is interesting, however, to investigate more closely this solution for arbitrary β, particularly since it allows in the case of slow passage a direct comparison between the condition, favorable for nuclear induction on one side and resonance absorption on the other. Using the Eqs. (41) and writing $|\gamma|H_0-\omega=\Delta\omega$ for the deviation of the resonance frequency from ω we can also write

$$u=\frac{|\gamma|H_1T_2^2\Delta\omega}{1+(T_2\Delta\omega)^2+(\gamma H_1)^2T_1T_2}M_0, \tag{57a}$$

$$v=-\frac{|\gamma|H_1T_2}{1+(T_2\Delta\omega)^2+(\gamma H_1)^2T_1T_2}M_0, \tag{57b}$$

$$M_z=\frac{1+(T_2\Delta\omega)^2}{1+(T_2\Delta\omega)^2+(\gamma H_1)^2T_1T_2}M_0. \tag{57c}$$

For nuclear induction it is evidently recommendable to have u as large as possible. Its maximum is obtained for

$$\Delta\omega=\frac{1}{T_2}[1+(\gamma H_1)^2T_1T_2]^{\frac{1}{2}} \tag{58}$$

and has here the value

$$u_{\max}=\frac{|\gamma|H_1T_2}{[1+(\gamma H_1)^2T_1T_2]^{\frac{1}{2}}}M_0. \tag{59}$$

This value again increases monotonically with H_1 and for

$$H_1\gg\frac{1}{|\gamma|(T_1T_2)^{\frac{1}{2}}}$$

becomes

$$u_{\max\,\max}=(T_2/T_1)^{\frac{1}{2}}M_0. \tag{60}$$

The condition that the r-f field amplitude H_1 is large enough to obtain the highest possible u is according to (41) equivalent with $\alpha\beta\ll1$ and also actually assumed in the derivation of (51) since it is valid only for $\alpha\ll1$, $\beta\ll1$.

To obtain maximum absorption, it is on the other hand necessary to make v as large as possible, since it is this quantity which, through (40a) determines the out of phase part of M_x. v has its maximum

$$v_{\max}=-\frac{|\gamma|H_1T_2}{1+(\gamma H_1)^2T_1T_2}M_0 \tag{61}$$

for $\Delta\omega=0$. Unlike $u_{\max}$ this quantity does not increase monotonically for increasing H_1, but decreases for large values of H_1. As observed by Purcell, Torrey, and Pound[6] it is therefore not advisable for absorption experiments to use too intensive r-f fields. The best possible choice is

$$H_1=\frac{1}{|\gamma|(T_1T_2)^{\frac{1}{2}}} \tag{62}$$

and yields

$$v_{\max\,\max}=(T_2/T_1)^{\frac{1}{2}}M_0. \tag{63}$$

It seems satisfactory that the maximum values (60) and (63) of the two decisive quantities u and v is thus the same, although to obtain the one, necessary for induction, requires the r-f field amplitude to be large compared to the "critical amplitude" $1/|\gamma|(T_1T_2)^{\frac{1}{2}}$ whereas the other, necessary for absorption requires it to be equal to this quantity.

It is evident from (44b) and (46) that the magnitude of the signal, induced by the component M_y of the nuclear polarization, depends not only upon the susceptibility χ but also, in a rather complicated way, upon the relaxation times and upon the magnitude and speed of variation of δ. The expression (28) for the induced voltage which was derived in Section 3 under simplifying assumptions will usually not correspond to the observed values but represents merely an estimate to be approached under favorable conditions. The special case of "rapid" passage, considered before and leading to the expression (49) of M represents such a favorable condition, and it is only in this limiting case that

(28) represents the actually observable value of the induced voltage.

The maximum value of M and thereby of the induced voltage signal at resonance must be expected normally to be smaller than (49) and in fact becomes the smaller for given T_2, and under otherwise equal conditions, the longer the relaxation time T_1. In the limit of very large T_1 one obtains from (48)

$$\theta(t)-\theta(t')=\frac{1}{T_2}\int_{t'}^{t}\frac{dt''}{1+\delta^2(t'')}, \qquad (64)$$

which is independent of T_1, so that, according to (46) M becomes inversely proportional to T_1. One may say, in this sense, that too long relaxation times T_1 are unfavorable for the observation of the effect unless the variation of δ with time is changed so as to re-establish favorable conditions. It is otherwise recommendable to use samples in which T_1 is as short as possible, possibly by adding paramagnetic catalysts as previously mentioned. As T_1 becomes sufficiently short, one will approach the case of "slow passage" mentioned above and represented in Fig. 2. While it will not be possible to have actually $T_1 \ll T_2$ it is seen from (54) that the maximum signal will still increase with decreasing T_1, the optimum being reached for $T_1=T_2$.

5. CONCLUSIONS

While the methods of molecular beams and of nuclear induction have a common ground of investigation it is evident that neither one makes the other superfluous. There remains a large complex of interesting nuclear experiments to be done, for which molecular beams are essential, particularly those which call for matter of extremely low density and the least possible interference of neighboring atoms or molecules. There are, on the other hand, many problems which become accessible or which can be more conveniently solved through nuclear induction and some of these will be mentioned here:

(1) The exact comparison of the magnetic moments of the neutron, the proton, and the deuteron is at present one of the most interesting problems, concerning nuclear forces. The main difficulty in this comparison was until now the sufficiently accurate calibration of the resonance field. It can be completely avoided by repeating the experiment of Alvarez and Bloch[2] for neutrons and by observing through nuclear induction simultaneously and in the same field the resonances of protons and deuterons. The problem of comparison of their magnetic moments is thus reduced to that of their respective resonance frequencies and can be solved with high accuracy. It was indeed with this experiment in mind, and while searching for a suitable method of comparison, that the author was led to the thought of nuclear induction, and preparations are now under way at Stanford to carry out the measurement in the near future.

(2) One of the difficulties in the determination of the gyromagnetic ratios of many nuclei by molecular beams is that of finding suitable detectors. The method of nuclear induction is free from this obstacle and should be soon applied to all elements for which this determination is of interest.

(3) While even in its very initial stage, nuclear induction was observed with a sample of 100 milligrams, there are good reasons to believe that the sensitivity can still be greatly increased. This offers the possibility to observe the effect not only in liquids and solids but also in gases under no excessive pressure. With only small amounts of matter necessary for its performance, the experiment offers a convenient way of isotope analysis and particularly also for its application to radioactive nuclei.

(4) It was shown in Section 4 that the induced signals to be expected depend not only upon the nuclear susceptibility but also upon the relaxation times. By suitable choice of the variation with time of resonant field or frequency, it is thus possible to measure these quantities separately. The study of nuclear relaxation times is of interest not only as an experimental method to investigate the establishment of thermal equilibrium, but also because of its importance for reaching extremely low temperatures through the nuclear magnetocaloric effect. While even the information gained at room temperature is valuable, it is clear that it can be greatly enlarged by studying the temperature dependence of the effect and particularly its behavior at low temperatures. It is in this same respect that the effect of paramagnetic catalysts, mentioned in Sections 1 and 4, seems of considerable interest.

(5) As in comparing the moments of neutron, proton, and deuteron, nuclear induction can well be developed as a simple and practical method to calibrate and measure high magnetic fields with great accuracy, and to apply it, for example, in the construction of cyclotrons and mass spectrographs.

There are unquestionably more problems which will become tangible in further development of the new electromagnetic effects. The fact that they are simple to obtain and require only very modest equipment should make it possible for many investigators to enter this field of research.

PHYSICAL REVIEW VOLUME 70, NUMBERS 7 AND 8 OCTOBER 1 AND 15, 1946

The Nuclear Induction Experiment

F. BLOCH, W. W. HANSEN, AND M. PACKARD
Stanford University, California

(Received July 19, 1946)

The phenomenon of nuclear induction has been studied experimentally. The apparatus used is described, both as to principle and detail. Experiments have been carried out in which the signals from protons contained in a variety of substances were observed. The results show the role played by the relaxation time, which was found to vary between about 10^{-5} second and many seconds

INTRODUCTION

IN this paper we aim to describe certain experiments designed to study the phenomenon of nuclear induction, the theory of which is described in the preceding paper. While it will be assumed that this paper, hereafter referred to as I, is familiar to the reader, we will not hesitate to repeat those few formulae which are of immediate importance for the present paper. We start, then, by giving the reasons for the selection of the general methods used and follow this by a brief description of specific apparatus. Finally, the results are described in detail.

METHOD

If matter be placed in a magnetic field H_0, in the z direction, the nuclear magnetic moments will tend to orient themselves parallel to the field. In matter of normal density, thermal equilibrium may be established, in which case there will be a paramagnetic polarization in the z direction

$$M_0=\chi H_0. \tag{1}$$

If now we superimpose an oscillating magnetic field in the x direction

$$H_x=2H_1\cos\omega t, \tag{2}$$

we can expect the polarization vector to deviate appreciably from the z direction if the z field H_0 approaches the resonance value H^* given by

$$|\gamma|H^*=\omega, \tag{3}$$

where γ, the gyromagnetic ratio, is the ratio of nuclear moment to angular momentum characteristic of the nuclei under consideration. Quantitatively, the result of this deviation may be described by a macroscopic polarization vector **M** with components given by Eq. (44) of I,

$$M_x=\frac{M}{(1+\delta^2)^{\frac{1}{2}}}\cos\omega t, \tag{4a}$$

$$M_y=\mp\frac{M}{(1+\delta^2)^{\frac{1}{2}}}\sin\omega t, \tag{4b}$$

$$M_z=\frac{M\delta}{(1+\delta^2)^{\frac{1}{2}}}, \tag{4c}$$

where

$$\delta=(H_0-H^*)/H_1$$

is the deviation of z field H_0 from its resonance value H^* in units of the half-amplitude H_1 of the oscillating x field. The ambiguous sign in (4b) is to allow for the possibility of either positive or negative values of γ. The quantity M depends in

a rather involved manner on the nuclear relaxation times and we will only say that, under favorable conditions, it may be expected to be of the order of the equilibrium polarization M_0; a precise expression is given in I, Eq. (46).

It is this precessing vector **M** which we wish to observe and either to design or discuss a suitable experimental arrangement for this purpose we need some estimate both of the magnitude of **M** and of the field H_1 needed to produce the precession of **M**. These quantities have the same dimensions and so may be compared directly.

For this purpose we may use numbers taken from the experiments as actually performed, a typical case being the use of protons in water and with a field $H_0 = 1826$ gauss. With known values of μ and j one finds a saturation magnetic moment density of 0.6×10^{-6} gauss. If now we consider a spherical sample with given moment density, we easily find that the flux linkage through an equatorial circle is equal to that caused by a magnetic field of magnitude $(8\pi/3)$ times the moment density. Or, in the present case, we can say that the flux linkage through a single equatorial turn about the sphere will be the same as that caused by a uniform field of 5.1×10^{-6} gauss.

In considering possible methods of detecting an oscillating field of this general magnitude, we must not only consider the relative magnitudes of thermal noise power and the power that may be generated by such an oscillating field, but also must compare the magnitude of the field caused by the nuclear moments with the field H_1.

As remarked in I, the field H_1 should be notably larger than the internuclear fields, which are of order one gauss. Thus, a value of five gauss for H_1 will perhaps be suitable. This specifies the magnitude. As to the phase, we note that, by (2) and (4), the driving field, which is in the x direction, is in time quadrature with the y component of the moment to be observed.

Broadly speaking, then, the problem is the detection and measurement of an oscillating field of, say, 5×10^{-6} gauss or less in the presence of a field of the same frequency and of magnitude about 10 gauss, or at least 2×10^6 times larger.

To accomplish this we have used an apparatus which may be described with the aid of Fig. 1. This shows a section in the yz plane, the center

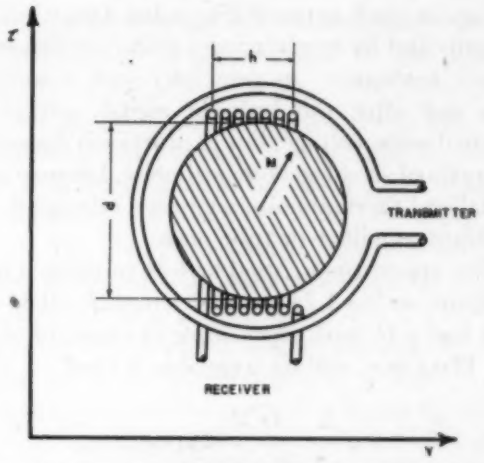

FIG. 1. Schematic diagram of coil arrangement used. A section in the yz plane shows the spherical sample (cross hatched) surrounded by a receiver coil sensitive to variations in flux in the y direction and outside this a transmitter coil producing flux in the x direction. A static field in the z direction is produced by a magnet not shown.

shaded circle representing the equatorial section of a spherical sample of volume Ω containing the nuclei whose total moment $M\Omega$ is to be observed. A static magnetic field H_0 in the z direction is produced by an electromagnet (not shown). An oscillating field of peak value $2H_1$ in the x direction is produced by current flowing through a "transmitter coil." This coil, though shown as a single turn, in actuality consists of a plurality of turns. In consequence of the oscillating field $2H_1$ and the static field H_0, the moment $M\Omega$ will precess: as a result a variable flux links the "receiver coil," whose axis is in the y direction, and the resultant voltage which appears at the terminals is led off to a receiver to be measured.

We now return to the problem of the detection of a field of magnitude 5×10^{-6} gauss oscillation at approximately the Larmor frequency, which turns out to be 7.76×10^6 cycles/sec., for protons in a field of 1826 gauss. We may consider the problem in two stages: first, how would one measure such a field in the absence of the driving field, and second, what effect does the presence of the driving field have.

As to the first, the obvious procedure is to amplify the voltage induced in the pick-up coil by a suitable amount, whereupon the voltage may be measured by various means—provided it is larger than any spurious voltages that may be present. Practically, it is desirable to increase the

voltage as much as possible by using a multiplicity of turns and by introducing a shunt condenser to induce resonance. In principle, such resonance does not alter the ratio of signal voltage to thermal noise voltage, but in practice it does alter the ratio of signal to observed noise, because both signal and thermal noise are raised relative to the constant amplifier or tube noise.

The apparatus we used had 24 turns on a form of diameter $d=1.74$ cm and length $h=0.84$ cm, and had a Q, with the sample in place, of about 80. The r.m.s. voltage available is then

$$V=\frac{1}{\sqrt{2}}\frac{4\pi M}{(d^2+h^2)^{\frac{1}{2}}}NQ\times 10^{-8}$$

and, with a sample of volume 1.46 cc this comes out to be 3.7×10^{-3} volt, so that large amounts of amplification are not needed. Also, this may be compared with the thermal noise voltage which, for this coil, is about 0.7×10^{-6} volt in a 3000-cycle-per-sec. band. Thus, an enormous ratio of signal over noise is potentially available. This ratio is independent of the number of turns on the coil, but could be increased for the same sample and coil size by increasing Q or decreasing the band width.

Two further points must be noted, however.

First, in order to know that the observed amplifier output is caused by the nuclear moments and not by some unknown cause, it is essential that the voltage due to the nuclear moments be varied, or modulated, in some known and controllable manner in which case outputs are real or spurious according as they do or do not correspond to the known modulation.

Second, the magnitude of any spurious signals or "noise" will depend on the frequency band accepted by the resonant pick-up coil and the amplifier which follows. If the noise is of random type, its amplitude will vary with the square root of the band width; if it is of impulse type, the amplitude will vary directly with band width. In any case, it is desirable to reduce the band width as much as possible or convenient, for doing so reduces noise while leaving the signal unaltered.

The straightforward method of reducing the band width is, of course, to increase the sharpness of resonance by reducing the losses as far as may be. Possibilities in this direction are, however, quite limited. For example, if one attains a Q of 100, which is quite good for such small coils in the presence of poor dielectric, the band width at 7 mc is 1.1×10^5 cycles/sec., or much larger than the minimum set by the requirement that the response time be not inconveniently large. While somewhat larger Q values may be possible, it is plain that no attainable value will make the band as small as one might desire.

Some improvement might be obtained by making the modulation cyclic, and following the rectifying device which converts the 7-mc signal to a unidirectional one with a filter, or amplifier, sharply tuned to the modulation frequency. The effectiveness of this scheme may be measured by the effective band width, which is of the order $(\Delta\nu_1\Delta\nu_2)^{\frac{1}{2}}$ where $\Delta\nu_1$ and $\Delta\nu_2$ are the band widths of the circuits before and after the rectifier. Thus reducing $\Delta\nu_2$ reduces the noise, but not as much as one might hope, since the response time goes with $1/\Delta\nu_2$.

The proper way to reduce the band width is by heterodyning the signal down to some lower frequency where a given percentage band width becomes a small absolute band width. This may be done with a detector, and following filter with narrow pass band, if one introduces into the detector an additional signal of constant frequency, usually called the local oscillator signal, and with magnitude large compared to either signal or noise. Then the beats between local oscillator and signal or noise components dominate those between noise components, or between signal and noise components, and the output noise then depends only on $\Delta\nu_2$, being quite independent of $\Delta\nu_1$. In this way the band width may be reduced by any desired amount, the only limit being set by the response time $1/\Delta\nu_2$.

We come now to the question of the effects of the large field H_1 which, it will be remembered, is at least 10^6 larger than the field to be detected.

This large background has two effects. First, if even a moderate fraction appears in the receiver, any amplifiers that may be used will saturate long before the signal is of suitable size. Second, and more fundamental, any fluctuation in the background is indistinguishable from a signal and, with such a large ratio of background to signal, such variations can be serious, though they could be, if necessary, controlled.

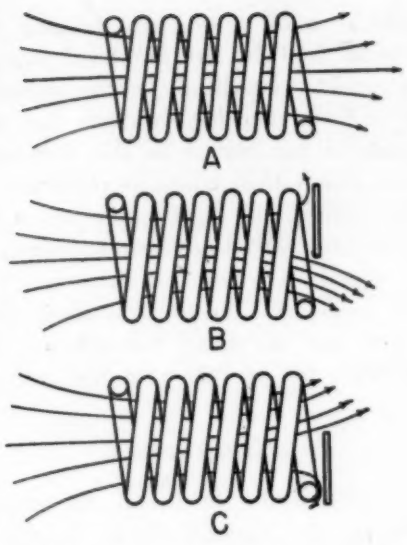

FIG. 2. The drawing (A) shows the flux threading the transmitter coil, while (B) and (C) show how this flux may be "steered" by means of a semicircular copper paddle, so as to link the receiver coil in either the positive or the negative sense.

For these two reasons, we have used a receiver coil which is nearly at right angles to the transmitter coil, so reducing the effect of H_1, which we call leakage, by a factor $\sin \epsilon \cong \epsilon$, where ϵ is the deviation of the angle between transmitter and receiver coils from $\pi/2$. In this way the leakage of H_1 into the receiver coil may easily be reduced by a factor of 10^4 or thereabouts. But a reduction of 10^6 or more, while possible, would be difficult, as it would involve adjustment of an angle to 10^{-6} radian, or 0.2″.

In fact, it is not desirable to try for such extreme reduction, since once the leakage has been reduced to a point where it is only, say, 10^3 times the signal, it may actually be made to serve an important and useful purpose.

Specifically, we have already pointed out the desirability, from a band width point of view, of heterodyning to some lower frequency, and there is no reason for not choosing this frequency to be zero, in which case the leakage signal, slightly modified, is an ideal source of local oscillator voltage.

The modification needed is in the phase for, as we have seen, the leakage and the signal are $\pi/2$ out of phase so that, if one adds the leakage to an amount of signal which is varied by the modulation the result, while having nodes that are not evenly spaced (phase modulation) has a practically constant amplitude, and so, on passage through an ordinary detector, the modulation will not be reproduced. One must, therefore, shift the phase of the leakage by some amount, preferably $\pi/2$, whereupon the variable signal will lead to amplitude modulation which is easily detected. The above ideas may also be expressed by means of vector diagrams, in which representation the leakage is a large vector and the signal a small vector at right angles thereto, so that variations in the signal make variations in the vector sum which are quadratic in the signal. If, on the other hand, the phase of the leakage is shifted by $\pi/2$ so that the vectors are collinear, variations of signal amplitude appear linearly as variations in resultant.

This desired phase shift may be achieved by a device which also serves the purpose of regulating the magnitude of the leakage. More precisely, the device to be described regulates the quadrature component of the leakage: when this is reduced to zero, what remains must be in phase with the signal.

Referring now to Fig. 2A, there is shown, in cross section, the transmitter coil, the receiver coil and the sample being omitted. The flux through the coil will be roughly parallel to the axis or, more exactly, will have symmetry about the axis and will not link any coil whose plane passes through this axis. If now we place a semicircular sheet of conductor across one end of the coil as in Fig. 2B, the currents induced therein will prevent the flux from passing through the sheet. If the lines are going from left to right they would then pass through a plane, at right angles to the paper and containing the axis, in the upward direction. Likewise, if this sheet of conductor, which we call a paddle, be placed as in Fig. 2C the linkage of a coil in the axial plane will be reversed. The change from Fig. 2B to Fig. 2C may be made continuously by mounting the paddle on an axial shaft and rotating same. Thus, by rotating such a shaft either positive or negative flux linkage may be obtained and, by continuity, the desired value of zero must be possible. Any desired sensitivity of adjustment may be had by suitable choice of paddle size.

In this way the quadrature component may be adjusted at will. One might fear that it would be

found that there would be no in-phase component of leakage. Actually this is not found to be true, the reason being that the currents which flow in the paddle are not π out of phase with the currents in the transmitter coil, because of losses in the paddle, and so have a component in phase with the signal.

It remains only to describe the methods of modulation and presentation.

To cause the signal to vary in strength one might vary either the z magnetic field H_0 or the frequency. The former seemed the easier and was adopted for the experiments here described, the field H_0 being varied cyclically about a value H_{dc}. The modulation frequency of 60 cycles/sec. was chosen as being low enough to avoid excessive band width and high enough for the persistence of vision needed for the cathode-ray tube presentation used. Within limits set by these factors a considerable range of frequencies is possible: of these 60 cycles/sec. has the additional advantage that any spurious hum pick-up appears as a recognizable distortion of the final pattern rather than as a blurring.

Presentation was on a cathode-ray tube with horizontal plates giving a deflection proportional to the variation in H_0 and the vertical plates giving a deflection proportional to the signal which in turn depends on the y component of the nuclear magnetic moment. Thus one observes on the screen a plot of M_y *vs.* H_0, the center of the screen corresponding to the field H_{dc}.

We may summarize by giving, in Fig. 3, a block diagram of the complete apparatus. Here the spherical sample is immersed in a field $H_{dc}+H_{ac}\cos 377t$ produced by a magnet, not shown. The nuclear moments oriented by this field are caused to precess by a driving field H_x produced by current from the box labeled transmitter. The precessing moments induce voltages in the receiver coil. These voltages, which vary in amplitude at a 60 c/sec. rate because of the variations in field H_0, are amplified along with stronger constant amplitude leakage signals. The leakage and the varying voltages due to precessing nuclei are mixed in the detector, the output of which then contains pulsating unidirectional current, the steady component due to leakage and the variations corresponding to the desired signal. The d.c. is removed by the blocking condensers in the following amplifier which increases the signal voltages to a magnitude suitable for operation of the cathode-ray tube.

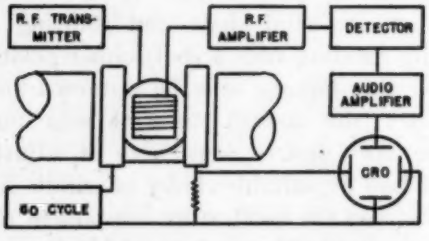

FIG. 3. Block diagram of apparatus.

APPARATUS

We now describe in detail the equipment constituting the various blocks in the above diagram.

The steady magnetic field H_{dc} is supplied by a lecture-demonstration magnet which easily produces the necessary fields of a few thousand gauss. The poles are 3 inches in diameter and these are provided with laminated extensions of transformer sheet which are $3\frac{1}{2}$ inches$\times 3\frac{1}{2}$ inches and 1 inch thick. The spacing between these laminated extensions is $1\frac{1}{2}$ inches and within the central volume of 2 cc, occupied by the sample, the field was found, by flip coil measurements, to be uniform to within 2 gauss. Since variations in field of order $H_1=5$ gauss could be tolerated without undue broadening of the resonance peak, this uniformity is satisfactory.

The 60 c/sec. modulation of the field is provided by current flowing through two coils of about Helmholtz proportions, placed between the laminated pole faces and carrying 60 c/sec. current. The magnitude of this current can be regulated by means of a variac to give values of H_{ac} between zero and 50 gauss. The same current which passes through the coils passes also through a resistor, and the resulting voltage drop actuates the horizontal sweep of the oscilloscope.

As to the transmitter, the main requirement in addition to ability to deliver enough power to maintain the field H_1, is a very high order of output amplitude stability. This requirement arises because variations in leakage are indistinguishable from signal and because even the smallest leakage is large compared to the signal. For example, if the nuclear moment per unit

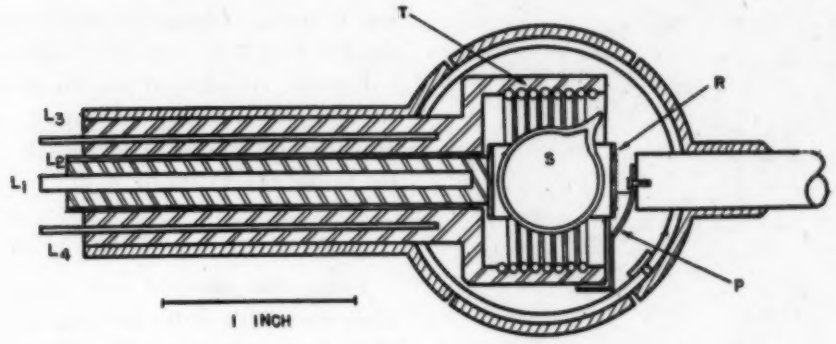

FIG. 4. Scale drawing of an xy section of the r-f head. The spherical sample S is surrounded by a receiver coil R, which is in turn surrounded by a transmitter coil T, the whole being encased in a shield. A rotably mounted paddle P is used to steer the transmitter flux. Leads to the receiver coil are the coaxial leads L_1L_2 while the transmitter leads are L_3 and L_4. The outer shield is split to avoid 60-cycle eddy currents.

volume is 10^{-7} times H_1, as it might be in a typical case, then even if the leakage is reduced to, say, 10^{-3} of H_1, a variation in transmitter output by a part in 10^4 will cause a fluctuation equal to the signal.

The power required to maintain the field H_1 is of the order 1 watt and this, together with considerable excess to allow for imperfect impedance matching, etc., is easily supplied by an 815. The stability is achieved by deriving both filament and plate power from batteries. Magnetic regulators in the primary of an ordinary supply were tried and found worthless because of slow response. A carefully engineered and tested vacuum-tube regulator might do, but batteries were adopted as quicker and absolutely reliable.

The transmitter and receiver coils are best described by the drawing of Fig. 4, which shows the coils and surrounding shield which we may call the r-f head. The transmitter coil consists of seven turns of mean diameter $\frac{7}{8}''$ and length $\frac{1}{2}''$, wound inside a threaded polystyrene shell. Inside the transmitter coil is placed the receiver coil of 24 turns, $\frac{9}{16}''$ in diameter and $\frac{5}{16}''$ long, wound on the outside of a thin threaded polystyrene form. Inside this, in turn, is the sample, contained in a glass bulb $\frac{1}{2}$ in. in diameter. The design aims at the greatest mechanical rigidity and damping possible, in an effort to avoid vibrations which, by varying the coupling between transmitter and receiver, vary the leakage and so introduce microphonics. Such microphonics constitute the biggest experimental difficulty with the equipment here described.

Transmission lines a few inches long lead to a brass box about 4 inches by 8 inches by $8\frac{1}{2}$ inches, which is divided in two by a horizontal partition. The lower portion contains tuning condensers to resonate the transmitter coil; the upper contains a similar condenser for the receiver and also the detector and first audio stage of the receiver, together with suitable batteries for same.

The receiver differs from the block diagram in that the r-f amplifier there shown is omitted, the receiver coil working directly into a diode detector. This has the disadvantage of a very considerable loss in potential signal/noise ratio, but in view of the large signal available from protons it was decided to sacrifice this in the interests of simplicity. This simplicity appears in two ways: First, one replaces an r-f amplifier by a simpler audio stage, and second, whereas a volt or less might saturate an r-f stage, the diode will not saturate. This point is very important in tuning up, for at the start the leakage voltage is usually 100 volts, or more, and it is only after considerable adjustment that this can be reduced to about 0.1 volt which is usually used in operation. The diode detector is conventional as is the first audio stage which acts mainly as an inverter and impedance changer, giving push-pull output at low impedance level. This low impedance output is carried to the main amplifier by a few feet of cable.

The requirements on this amplifier are that it have a gain of a few thousand and pass all significant signal components without appreciable amplitude or phase distortion. The fre-

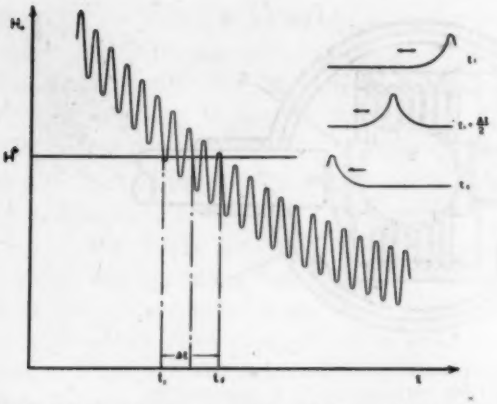

FIG. 5. Schematic representation of the modulated z component H_0 of the magnetic field in its dependence upon time. As the magnet current decreases, the resonance field H^* is first reached at the initial time t_i and last at the final time t_f. During the interval Δt a positive signal is observed to travel across the oscillograph screen as indicated by the arrows on the traces, sketched for three different times at the beginning, the middle, and the end of Δt.

quencies involved are the modulation frequency of 60 c.p.s. and various harmonics thereof. With $2H_1$ of, say, 10 gauss and ΔH of 100 gauss, the first ten harmonics will be of about equal strength and from there on up the strengths will decrease rapidly. About fifty harmonics should then be ample and the amplifier must then pass frequencies between 60 and 3000 cycles/sec. Actually the amplitude response must be practically flat to a considerably lower frequency, say, 6 cycles/sec., if phase shifts in the lower harmonics are not to cause undesirable pedestal effects.

These requirements were met by a three-stage amplifier, using push-pull twin triodes (7F7) throughout. The use of push-pull amplification eliminates cathode bypass condensers and, more important, cancels the otherwise very annoying disturbances due to power supply variation. Likewise, screen by-passes are not needed and the Miller effect is not bothersome because of the rather low value of high frequency cut-off. The amplifier was tested on 60 c/sec. square waves, which it passes without distortion.

Although frequency response, as specified above, is needed to give a completely undistorted pattern on the oscilloscope, it is found in practice that the amount of pedestal effect introduced by raising the low frequency cut-off to 60 or 120 cycles is not objectionable, and the reduction in low frequency disturbances obtained by raising the low frequency cut-off is often a convenience.

Finally, the output of this amplifier actuates the vertical sweep of a Dumont 208 oscillograph and thereby traces a curve of M_y *vs.* H_0 suitable for visual observation.

RESULTS

Using the method and apparatus described above, we have so far investigated nuclear induction of protons only. The advantage of working with protons is twofold. In the first place they have of all known nuclei the highest gyromagnetic ratio γ so that moderate fields are sufficient to bring the resonance frequency into the convenient frequency range of a few megacycles. In the second place there is a great choice of compounds and solutions containing hydrogen which facilitates variation of the conditions of observation, particularly with respect to the relaxation times.

Our first experiments were carried out with water contained in small spherical glass bulbs which could be sealed off. The very first signal was observed with a sample of only 100 milligrams, but in all later experiments the amount was increased to about 1 gram, the glass bulbs being increased to a volume of about 1 cc. These samples were placed into the receiver coil and, after mounting the shields and the a.c. coils, providing the field modulation, were moved into the center of the magnet gap. With proper tuning and adjustment of the apparatus we could then observe the proton signal on the oscillograph screen as the current in the magnet was set to a

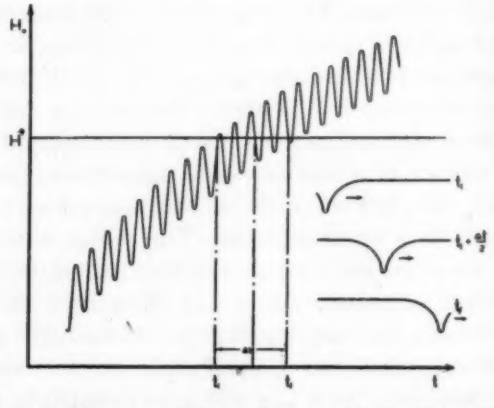

FIG. 6. Time dependence of H_0 as the magnet current increases. A negative signal travels across the screen as indicated by the arrows on the three sketched traces.

value such that the resonance field was contained within the limits of variation determined by the amplitude of the modulating field.

The behavior of the observed signal is determined by various factors, particularly the ratio of the relaxation time to three other time constants which enter into our experiment. The smallest is the time taken to pass through the resonance width which is usually a small fraction of 1/120 sec. The next time of importance is the time between successive transits through resonance, of the order of 1/120 sec. Finally there is the time during which H_{dc} is varied by an amount comparable to H_{ac}; this time can be chosen at will to be anywhere between the time constant of the magnet of the order of one second and many minutes. The following experiments cover various orders of magnitude of the relaxation time relative to the above-mentioned times.

The easiest and most striking visual observation of the protons in water was obtained by first raising the current in the magnet considerably above the value necessary for resonance conditions and then turning it off. This causes the field of the magnet to decrease exponentially with an appreciable time constant, the resonance field entering and leaving the modulation range during a time Δt of about half a second. The variation of the z component H_0 of the field with time is schematically plotted in Fig. 5. The signal was

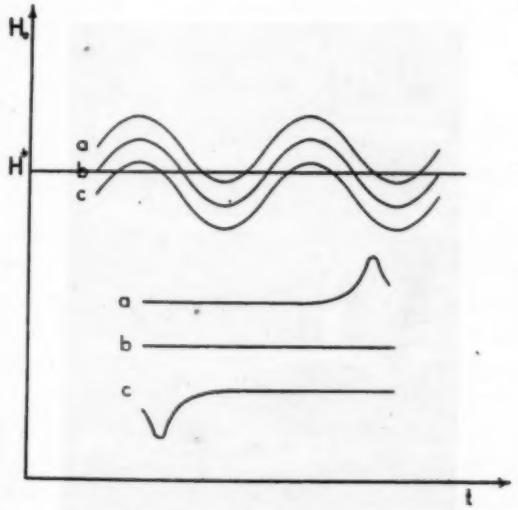

FIG. 7. Time dependence of H_0 with constant magnet current. The a.c. modulation is superimposed upon a d.c. value which in case *a* is above, in case *b* at, and in case *c* below the resonant field H^*. The three sketched traces represent the corresponding oscillograms.

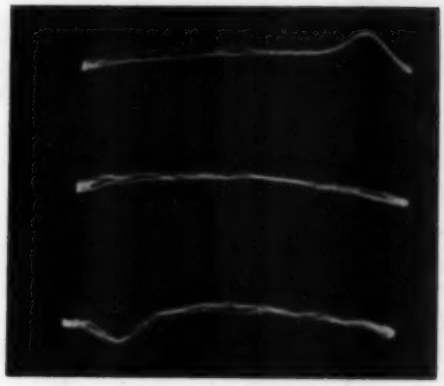

FIG. 8. Photographic record of the proton signal from water. The three traces from top to bottom correspond to the situation *a*, *b*, *c* of Fig. 7.

here observed to appear on the right side of the oscillogram at the initial time t_i, travel across the screen during the time Δt, and to disappear on the left side at the final time t_f as indicated on Fig. 5. The time dependence of H_0 and the corresponding observed oscillograms in the inverse process of turning the magnet current on are schematically indicated in Fig. 6.

The most interesting feature to be observed lies in the fact that in the case of Fig. 5, where the field is decreasing, the observed signal voltage is positive while it is negative in the case of Fig. 6 with increasing field. This remarkable "memory" of the proton induction is in perfect agreement with the formulae (4) and with the expression for M, given in I, Eq. (46). It indicates that the relaxation time T_1 is long compared to the duration Δt of the observation; the sign of M is determined by the sign of δ in the past, which is predominantly positive for decreasing and negative for increasing fields.

It must be noted that, strictly speaking, one cannot directly deduce from the sign of the observed voltage the sign of the signal which, as was pointed out in I, depends also upon the sign of the proton moment. All that can be concluded is that an inversion of the observed (rectified) signal means a reversal of the actual (radiofrequency) signal with respect to the in-phase leakage voltage. To ascertain the sign of the proton moment would require a determination of the sign of the in-phase leakage voltage which we have not carried out in view of the fact that the proton moment is already known to be positive.

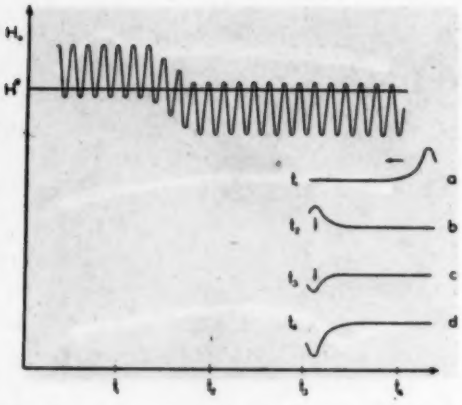

FIG. 9. Time dependence of H_0 with a d.c. value of the field being above the resonant field H^* for $t<t_1$, decreasing between t_1 and t_2 and being below H^* for $t>t_2$. The sketched traces *a*, *b*, *c*, *d* represent oscillograms at four different times, the arrows indicating the initial shift and subsequent reversal of the signal.

Another method of observing the proton signal in water is indicated in Fig. 7. The current in the magnet, and so H_{dc}, is here kept constant. With the relaxation time T_1 long compared to 1/60 second, the signal voltage is, according to I, Eq. (46), essentially determined by the time average of δ which is positive in case *a*, zero in case *b*, and negative in case *c*. A photographic record of the three oscillograms is shown on Fig. 8.

The methods of observation, indicated in Figs. 5–7, allow only a conclusion as to the lower limit of the relaxation time. Thus the behavior of the signal under the conditions of Fig. 7 merely indicates that the relaxation time is long compared to 1/60 second; the fact that with decreasing or increasing current, as in Figs. 5 and 6, the signal does not reverse its sign while traveling across the oscillograph screen during about ½ second sets the lower limit of the relaxation time higher, namely to a value large compared to ½ second. It was observed, on the other hand, that if the current was first decreased, as in Fig. 5, and then made to increase so that resonance conditions, as in Fig. 6, were again reached after about one minute, there was no "memory" retained of the previous decrease. This allows at least the conclusion that the relaxation time is short compared to a minute, and in order to establish its actual value, to be expected somewhere between ½ second and one minute, the method of observation, indicated in Fig. 9 was chosen: Starting at a time t_1, with H_{dc} held for a considerable previous time above the resonance field H^* a positive signal was observed on the right side of the oscillogram, similar to the case *a* of Fig. 7 and as presented on trace *a* of Fig. 8. Thereupon the field was quickly (i.e., during about one second) lowered to a value sufficiently below resonance to make the signal appear on the left side of the oscillogram and then was held fixed at this new value. As was to be expected from the analogous situation of Fig. 5, the signal was originally still positive. However, during the following few seconds it was observed to decrease in magnitude, then to disappear and thereupon to grow again with negative values until after several seconds it had reached its full negative value, corresponding to the case *c* of Fig. 7 and as presented on trace *c* of Fig. 8.

This extraordinary reversal of the signal under fixed external conditions represents actually a direct visual observation of the gradual adjustment of the proton spin-orientation to the changed situation caused by the previous change of the magnet current. The fact that it takes place during a time interval of several seconds evidently indicates the relaxation time, likewise, to be of the order of a few seconds. A photographic record of the process is reproduced on Fig. 10. The top trace *a* is taken at an instant (and with an exposure of slightly over 1/60 second), corresponding to the time t_1 of Fig. 9.

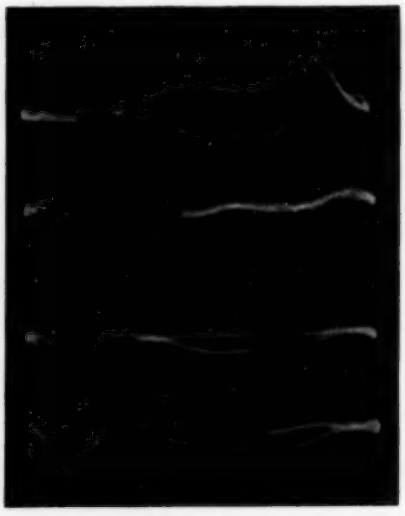

FIG. 10. Photographic record of the proton signal in water. The four traces from top to bottom correspond to the times t_1, t_2, t_3, t_4 of Fig. 9. In the text they are referred to as *a*, *b*, *c*, *d*, respectively.

The following three traces represent snapshots taken during the next 15 seconds at regular 5-second intervals and clearly show on trace *b* the decrease and on traces *c* and *d* the reversal of the signal. The fact that on traces *a*, *b*, *c*, and (slightly) also on trace *d* there appear two separated signals on top of each other is caused by stray 60-cycle pick-up which has the same frequency as the modulation and, appearing on top of the actual proton signal manifests itself in a separation of the forth- and back-sweep, recorded during the exposure of the camera.

It was most surprising thus to establish the proton relaxation time in water to be of the order of a few seconds, although it must be admitted that it is difficult, as pointed out in I, to give a reliable theoretical estimate. Whereas such an estimate can be given for a gas and, to some extent, also, for a crystal, there is not enough known about the molecular motion in liquids to predict more than a crude order of magnitude. Treating the liquid either as a highly compressed gas or as a crystal with thermal amplitudes of the molecules, comparable to the lattice constants one would expect the relaxation time to be of the order of a few hours rather than of a few seconds.

We must point out here that the "relaxation time," as observed in our experiments, does not necessarily represent the usual (and in I, referred to as the "longitudinal") paramagnetic relaxation time T_1 but that it represents rather an "effective" relaxation time, which can be influenced by the possibly different transversal relaxation time T_2, introduced in I. It will require a good deal more experimentation and observation under various conditions to separate clearly the effects of T_1 and T_2 and, with the use of Eq. (46) of I, to ascertain their values separately. This point, however, relates to the quantitative rather than to the qualitative interpretation of our results and is by no means sufficient to explain the extraordinary difference in magnitude between the observed effective and the theoretically expected paramagnetic relaxation time.

We suspected the origin of this discrepancy to be caused by slight impurities and particularly to oxygen dissolved in water. Because of the magnetic moment of the oxygen molecules, acting as catalysts, it would actually take only one molecule of O_2 in about a thousand molecules of H_2O to explain relaxation times of the order of a few seconds. In order to verify this hypothesis we had one of our water samples purified by distillation in a vacuum* with a final partial pressure of oxygen of probably no more than 10^{-4} mm. While with the previous unpurified samples the reversal of the proton signal was essentially completed after 4 to 5 seconds, it took with the purified sample about 15 seconds for completion of the reversal. There is thus a noticeable effect of shortened relaxation times by impurities but it is by no means sufficient to explain their abnormal shortness. We can, of course, not discard the possibility that even after distillation there remained impurities in the water (originating, e.g., from material adhering to the glass walls) of sufficient amount and catalytic effectiveness to determine mainly the observed relaxation time. However, it does not seem very probable to us that this is the case, since in one of our experiments mineral oil was used instead of water. It exhibited a relaxation time of the same order of magnitude, while the entirely different chemical nature should be expected to result in a different composition of impurities. Nevertheless there may be an accidental coincidence and more experiments will be necessary to clarify the role of impurities.

Another experiment of interest was carried out with ice. The water was frozen in a small container and placed into the transmitter-receiver assembly. No noticeable signal was observed while the water was still frozen but the signal started to show up with the beginning of the melting process. We interpret this result as indicating a very long relaxation time in ice, since it was shown in I, Section 4, that the magnitude of the signal decreases indefinitely for sufficiently increasing T_1.

It seems reasonable, from theoretical considerations, that the relaxation time in a solid should be considerably longer than in a liquid and in this respect there is nothing remarkable in the behavior of ice. It was the more surprising to find another solid, namely paraffin, to behave in an entirely different manner. With the same method of observation as indicated in Fig. 5 and 6 for

* We wish to thank Dr. R. A. Ogg for kindly preparing the sample for us and for valuable discussions relating to the chemical aspect of our experiments.

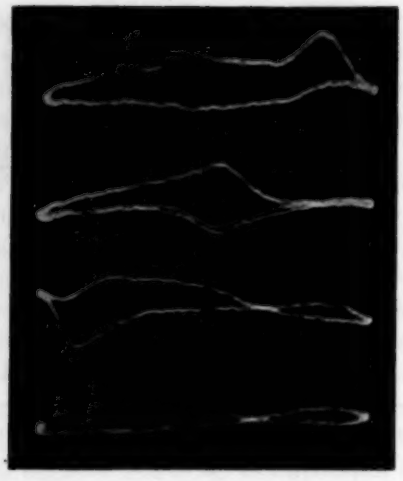

FIG. 11. Photographic record of the proton signal in paraffin. The four traces from top to bottom are in the text referred to as *a*, *b*, *c*, and *d*.

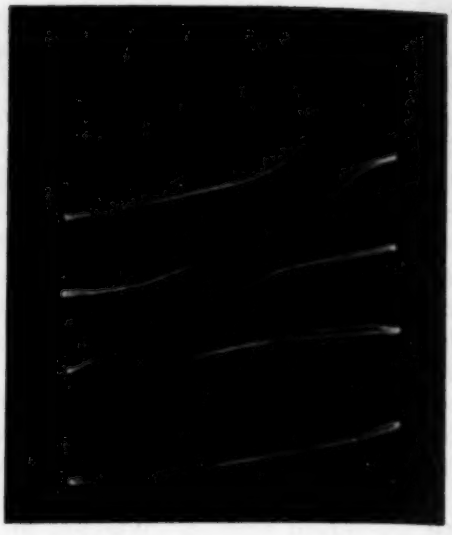

FIG. 12. Photographic record of the proton signal in a concentrated solution of $Fe(NO_3)_3$ in water. The four traces from top to bottom are in the text referred to as *a*, *b*, *c*, *d*.

water it was found that even during the ½ second which it took the signal to travel across the screen, it showed instantaneous reversal after passing the midpoint and that there was no observable dependence of the aspect of the signal upon the previous values of H_{dc}. While this indicates already a relaxation time considerably shorter than that of water, its actual value could be directly ascertained by observation under conditions equal to those of Fig. 7. The photographic record is shown in Fig. 11 with the traces *a*, *b*, *c* referring to the same values of H_0 as the corresponding ones on Fig. 8. A fourth "zero" trace *d* is shown on the plate where the resonance field H^* was well outside the sweep range so that there appears no signal. As on Fig. 10, there appears a spurious signal which slightly separates the forth and back sweep on the oscillograph to make the trace *d* look like the "infinity," sign of mathematics. This accidental separation of the two sweeps is actually quite desirable in this case since, contrary to the case of water on Fig. 8 where they coincide and show the complete identity of the signals on the two traces, there is here a marked difference. On trace *a*, where the resonance occurs near the minimum of H_0, both signals are still positive, the signal on the back sweep (below) being, however, considerably smaller than that on the forth sweep (above). The explanation is obviously that on the forth sweep the previous value of δ during almost a complete cycle was positive but that for the back sweep it is no more the average value of δ as in the case of water, which determines its magnitude, since this would be the same for the two sweeps. Instead the short time interval of about 1/240 second during which δ is negative until returning to zero, suffices, not to make the back signal negative, but at least to diminish it considerably. The identical behavior in reverse is shown on trace *c* where resonance occurs near the maximum of H_0 with both signals negative and the one on the back sweep (above) being smaller in magnitude than that on the forth sweep (below). With $H_{dc}=H^*$ and the signal therefore appearing at the center of the oscillogram, the time interval of 1/120 second is sufficient for complete reversal of the signal, as shown on trace *b*.

This leads to the conclusion that, contrary to our expectations, the relaxation time in paraffin is only of the order of 1/100 second. For a solid this is indeed extraordinarily short and only an unsuspectedly large amount of impurities can explain it, provided that the true explanation will not be found in a yet unknown and entirely different mechanism.

The results of a last set of experiments are shown on Fig. 12. Here we were dealing with a concentrated solution of $Fe(NO_3)_3$ in water in

order to obtain a case in which, because of the atomic moments of the Fe ions, the relaxation time is short compared to the time required to pass through resonance conditions. We obtain thus the case of "slow passage," discussed in I, Section 5. The shape of the signal is here in complete agreement with the theoretical formula, I (53), having a zero at resonance and an up- and down-swing for positive and negative values of δ, respectively. Except for their position, there is no difference in the signals received on the three traces *a*, *b*, *c* which pertain to the corresponding values of H_{dc}, represented in Fig. 6. A "zero" trace *d* is again added, showing the slight separation of forth- and back-sweep.

With the time, required to sweep through the signal of about 1/600 second we estimate the relaxation time to be here of the order of 10^{-4} to 10^{-5} sec. Other data, showing the dependence of the relaxation time upon the concentration of the paramagnetic salt will be published shortly.

The shape of the signal obtained with $Fe(NO_3)_3$ solutions makes it particularly easy to locate the resonance value of H_{dc} by setting the magnet current to such a value that the zero point of the signal is located at the exact center of the oscillogram. With the whole resonance width amounting to only about 1 percent of the total field, this setting can be easily adjusted to within the order of one per permille.

We have verified that the value of the resonance field determined in this manner agrees with the gyromagnetic ratio for protons determined by Kellogg, Rabi, Ramsey, and Zacharias.* After determining the resonance frequency and without altering the magnet current, the modulating a.c. field was turned off, the transmitter-receiver assembly removed and a carefully measured flip coil brought to the original position of the sample between the pole pieces in order to determine the value of the resonant field H^*. With a frequency $\nu = 7.765 \times 10^6$ sec.$^{-1}$ it was found that the resonance field had the value $H^* = 1826$ gauss which leads to a value of the gyromagnetic ratio

$$\gamma = 2\pi \frac{7.765 \times 10^6}{1826} = 2.672 \times 10^4.$$

The agreement within one-quarter of a percent with the value $\gamma = 2.665 \times 10^4$, obtained with molecular beams, must be considered accidental since our field measurement can only claim an accuracy of about 1 percent. We have also verified, although with somewhat less accuracy, that the ratio ν/H^* for the resonance signal, obtained from water, remains the same for $\nu = 7.8 \times 10^6$, $\nu = 8.8 \times 10^6$, and $\nu = 10.7 \times 10^6$.

*J. M. B. Kellogg, I. I. Rabi, N. F. Ramsey, Jr., and J. R. Zacharias, Phys. Rev. **56**, 728 (1939).

PHYSICAL REVIEW VOLUME 70, NUMBERS 7 AND 8 OCTOBER 1 AND 15, 1946

Propagation of Radiation in a Medium with Random Inhomogeneities*

PETER G. BERGMANN
Sonar Analysis Group, 64th Floor, 350 Fifth Avenue, New York 1, New York

(Received May 13, 1946)

By means of the methods of geometrical optics, approximate formulae are being derived which correlate the statistical properties of the inhomogeneities of the transmitting medium with the fluctuations to be expected in the signal level of radiative energy. Through a further simplification of the formulae obtained, it is possible to predict the dependence of signal fluctuation on range without detailed knowledge of the statistical parameters of the "microstructure" of the transmitting medium.

INTRODUCTION

WHEN radiative energy is propagated over considerable distances, the transmitting medium is rarely the homogeneous expanse it is assumed to be in elementary theory. The medium is bounded, and it may have an internal structure, such as a density gradient. In addition, the most important non-solid media of propagation, the atmosphere and the ocean, are known to possess a rapidly changeable random structure of comparatively small dimensions, which is caused by local heating, convective currents, and similar factors. In this paper, the modification of the radiative field which is caused by random structure will be derived for the case of small changes and on the assumption of a wave-length so short that the formulae of ray optics are valid. The results obtained may find application in the propagation of either electromagnetic or sound waves of high frequencies in the atmosphere or in a similarly extended medium.

THE PROBLEM

We shall restrict ourselves at once to the application of ray optical methods. Treatment of the same problem by means of wave optics is planned for the future. The basic equations of ray optics in the stationary case may be written in the form

$$\left.\begin{aligned}(\nabla S)^2&=n^2,\\ \nabla\cdot\left(\frac{I}{n}\nabla S\right)&=0.\end{aligned}\right\} \tag{1}$$

In these equations, the function $S(\mathbf{r})$ is the optical path length counted from the radiative source to the point $\mathbf{r}$ along the connecting ray path. Each constant value of $S>0$ corresponds to a wave front in the ray optical approximation. $n(\mathbf{r})$ is the local index of refraction, and $I(\mathbf{r})$ is the intensity of the radiative field, measured in units of energy passing per unit time through a unit area cross section perpendicular to the rays. In electromagnetic theory, I is the averaged magnitude of Poynting's vector, while in acoustics, I is the mean square pressure divided by ρc. The first of the Eqs. (1) expresses Huygens' principle that the distance between consecutive wave fronts is inversely proportional to the local index of refraction; while the second equation is the law of conservation of energy. Absorption and scattering are disregarded. For the following discussion, it is convenient to introduce the level L, defined as the logarithm (on some base) of I/n.[1] We shall measure the level in nepers, that is on the base e. In terms of level, Eqs. (1) may be rewritten in the form

$$\left.\begin{aligned}(\nabla S)^2&=n^2,\\ \nabla S\cdot\nabla L+\nabla^2 S&=0.\end{aligned}\right\} \tag{2}$$

It will now be assumed that n is very nearly equal to unity. We shall set

$$n=1+\lambda n', \tag{3}$$

with λ a constant parameter,

$$\lambda\ll 1. \tag{4}$$

* This work represents in part results of research carried out by the Sonar Analysis Group under contracts between Columbia University and the Office of Scientific Research and Development and between Woods Hole Oceanographic Institution and the Bureau of Ships, Navy Department.

[1] The quantity I/n has no direct physical significance and is chosen merely for convenience. However, because n very nearly equals unity, according to the assumptions made, I/n does not differ significantly from I. In most practical cases, n differs from unity by an amount less than 10^{-4}.

An approximate solution of Eqs. (1) will be obtained in terms of definite integrals.

APPROXIMATE SOLUTION OF THE BASIC EQUATIONS

If n' vanishes, the solution of Eq. (1) for a point source is

$$\left.\begin{aligned} S_0 &= r, \\ L_0 &= b(\Omega) - 2\ln r, \end{aligned}\right\} \tag{5}$$

where r is the distance from the source and b is a constant or, in the case of a directional source, a function of the angle Ω. That the pair S_0, L_0, is a solution can be verified directly by substituting the expressions (5) into Eqs. (2) with n equal to unity. We shall call S_0, L_0 the zero approximation.

The first approximation is obtained if Eq. (2) is expanded into a power series with respect to the parameter λ. Denoting all first-order variables by primes, we obtain the following conditions for the first approximation:

$$\left.\begin{aligned} \mathbf{r}_0 \cdot \nabla S' &= n', \\ \mathbf{r}_0 \cdot \nabla L' &= -\nabla^2 S' - \nabla L_0 \cdot \nabla S', \end{aligned}\right\} \tag{6}$$

where $\mathbf{r}_0$ is the unit vector pointing directly away from the source.

Fortunately, the two Eqs. (6) need not be solved simultaneously. They can be solved with the further condition that the variables S' and L' are to vanish at the location of the source.

The solution of the first Eq. (6) is provided by the integral

$$S'(\mathbf{r}) = {}^{*}\int_{\rho=0}^{r} n'(\rho)\, d\rho. \tag{7}$$

The symbol ${}^{*}\int_0^r$ refers to integration along a straight line from the location of the source to the point characterized by the radius vector $\mathbf{r}$. ρ is the variable of integration. For what follows, we shall require the gradient and the Laplacian of S'. Figure 1 shows how the path of integration must be transformed if a differentiation of an integral of the type (7) is to be carried out. Considering the unspecified integral

$$J(\mathbf{r}) = {}^{*}\int_0^r A(\rho)\, d\rho, \tag{8}$$

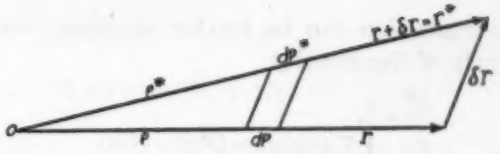

FIG. 1. Variation of the line integral.

we find that the variation of this integral may be written as

$$\delta J(\mathbf{r}) = {}^{*}\int_0^r \delta[A(\rho)\, d\rho] = {}^{*}\int_0^r \delta A(\rho)\, d\rho + {}^{*}\int_0^r A(\rho)\, \delta d\rho. \tag{9}$$

The local variation $\delta A(\rho)$ is, according to the figure,

$$\delta A(\rho) = \frac{\rho}{r} \nabla_\rho A(\rho) \cdot \delta\mathbf{r} \tag{10}$$

while the variation of $d\rho$ equals

$$\delta d\rho = \frac{\mathbf{r}_0 \cdot \delta\mathbf{r}}{r} d\rho. \tag{11}$$

We find, therefore,

$$\begin{aligned} \delta J(\mathbf{r}) &= \frac{1}{r}\delta\mathbf{r} \cdot {}^{*}\int_0^r [\rho \nabla_\rho A(\rho) + \mathbf{r}_0 A(\rho)]\, d\rho \\ &= \frac{1}{r}\delta\mathbf{r} \cdot {}^{*}\int_0^r \nabla_\rho [\rho A(\rho)]\, d\rho. \end{aligned} \tag{12}$$

The gradient of S', Eq. (7), is thus

$$\nabla S'(\mathbf{r}) = \frac{1}{r} {}^{*}\int_0^r \nabla_\rho (\rho n')\, d\rho. \tag{13}$$

Iteration of this process of differentiation leads to the result

$$\nabla^2 S'(\mathbf{r}) = \nabla\left(\frac{1}{r}\right) \cdot {}^{*}\int_0^r \nabla_\rho (\rho n')\, d\rho + \frac{1}{r^2} {}^{*}\int_0^r \nabla_\rho \cdot [\rho \nabla_\rho\, \rho n')]\, d\rho. \tag{14}$$

This expression can be further simplified with the help of the identity

$$\mathbf{r}_0 \cdot \int_0^r \nabla_\rho Q(\rho) d\rho \equiv Q(\mathbf{r}) - Q(0). \tag{15}$$

We obtain, after a straightforward computation,

$$\nabla^2 S'(\mathbf{r}) = -\frac{2}{r} n'(\mathbf{r}) + \frac{1}{r^2} \int_0^r \rho^2 \nabla_\rho^2 n'(\rho) d\rho. \tag{16}$$

We shall now write out the explicit expressions occurring on the right-hand side of the second Eq. (6). We have for ∇L_0 the expression

$$\nabla L_0 = \nabla b - \frac{2}{r} \mathbf{r}_0, \tag{17}$$

with the further condition

$$\mathbf{r}_0 \cdot \nabla b = 0. \tag{18}$$

The second Eq. (6) therefore assumes the form

$$\mathbf{r}_0 \cdot \nabla L' = -\frac{1}{r^2} \int_0^r \rho^2 \nabla_\rho^2 n' d\rho - \frac{1}{r} \nabla b \cdot \int_0^r \rho \nabla_\rho n' d\rho \equiv B(\mathbf{r}). \tag{19}$$

The two terms on the right-hand side of Eq. (19) can be interpreted quite simply. The first term corresponds to the "lens action" of local inhomogeneities, while the second term, which depends on the directivity of the source, represents the change in local intensity caused by the lateral displacement of the "beam." In what follows we shall consider a non-directional source and drop the second term.

The solution of Eq. (19) is the integral

$$\left.\begin{aligned} L' &= \int_0^r B(\rho) d\rho \\ &= -\int_0^r \left(\frac{1}{\rho} - \frac{1}{r}\right) \rho^2 \nabla_\rho^2 n' d\rho, \end{aligned}\right\} \tag{20}$$

by a simple transformation of the double integrals.

Equations (7) and (20) are solutions of the differential Eq. (6). If conditions at the source are disregarded, these solutions are not unique; it is possible to write down the general solution of Eq. (6). The difference between two solutions of the first Eq. (6) is a function of the angle only. The most general solution is, therefore,

$$\left.\begin{aligned} S_g' &= S_0' + \phi(\Omega), \\ \mathbf{r}_0 \cdot \nabla \phi &= 0. \end{aligned}\right\} \tag{21}$$

S_0' is the particular solution (7), and $\phi(\Omega)$ is an arbitrary function of the solid angle Ω. The addition $\phi(\Omega)$ produces a discontinuous addition to the variable S at the source, and is, thus, inconsistent with the assumption that for vanishing r, S' is to vanish. We find that the expressions (7) and (20) represent the only solution which satisfies the conditions at the source.

As for the higher approximations, the expansion described here leads, at each stage, to equations for $S^{(n)}$ and $L^{(n)}$, which have the same type left-hand sides as Eq. (6). The right-hand sides, however, get progressively more involved. At any rate, each successive approximation has a unique solution, which can be expressed in the form of explicit line integrals. These higher approximations will not be considered in the remaining sections of this paper.

THE SELF-CORRELATION FUNCTION OF THE INDEX OF REFRACTION

In the following sections, we shall derive the mean and the standard deviation of S, the optical path length from the source, and of L, the level at a fixed point $\mathbf{r}$. First, however, the microstructure must be characterized by certain statistical properties. If we consider a configuration of microstructure patterns, or a time series of distributions of n' in the same medium, then we shall assume that there is a possibility of averaging all quantities which depend on the spatial distribution of n' and its derivatives. The averaged quantities shall be enclosed in angular brackets, $\langle\ \rangle$. Obviously, it is reasonable to define the standard wave velocity so that

$$\langle n'(x, y, z) \rangle = 0. \tag{22}$$

The significance of this normalization is that the deviation of n' from unity is equally likely to be

positive or negative. The second assumption is that the spatial correlation function,

$$\langle n'(x_1, y_1, z_1)n'(x_2, y_2, z_2)\rangle,$$

exists and is a function of the coordinate differences only,

$$\left.\begin{aligned}\langle n'(x_1, y_1, z_1)n'(x_2, y_2, z_2)\rangle \\ \equiv N(x_1-x_2, y_1-y_2, z_1-z_2) \\ \equiv N(x_2-x_1, y_2-y_1, z_2-z_1).\end{aligned}\right\} \quad (23)$$

In other words, it is assumed that the statistical characteristics of the microstructure, while not necessarily isotropic, are homogeneous.

The function N satisfies a number of inequalities. A few shall be listed here. From the inequality

$$[n'(0)\pm n'(\mathbf{r})]^2 \geqslant 0 \quad (24)$$

we have

$$0 \leqslant \langle [n'(0)\pm n'(\mathbf{r})]^2\rangle = 2[N(0)\pm N(\mathbf{r})] \quad (25)$$

or, for all coordinate differences $\mathbf{r}$,

$$\left.\begin{aligned}N(0) &\geqslant 0, \\ |N(\mathbf{r})| &\leqslant N(0).\end{aligned}\right\} \quad (26)$$

An inequality between the N-values belonging to two arguments $\mathbf{r}_1$ and $\mathbf{r}_2$ is obtained by means of another positive definite expression. Introduce a parameter α (or β or γ) which serves to number the cases which constitute the "population" for purposes of averaging and then consider the square of the determinant

$$D = \begin{vmatrix} n_\alpha'(0), & n_\alpha'(\mathbf{r}_1), & n_\alpha'(\mathbf{r}_2) \\ n_\beta'(0), & n_\beta'(\mathbf{r}_1), & n_\beta'(\mathbf{r}_2) \\ n_\gamma'(0), & n_\gamma'(\mathbf{r}_1), & n_\gamma'(\mathbf{r}_2) \end{vmatrix}, \quad (27)$$

averaged three times, over α, β, and γ. This triple mean square is

$$\left.\begin{aligned}\langle D^2\rangle = 6\{N^3(0)+2N(\mathbf{r}_1)N(\mathbf{r}_2)N(\mathbf{r}_1\pm\mathbf{r}_2) \\ -N(0)[N^2(\mathbf{r}_1)+N^2(\mathbf{r}_2)+N^2(\mathbf{r}_1\pm\mathbf{r}_2)]\}.\end{aligned}\right\} \quad (28)$$

The resulting inequality takes the form

$$\left.\begin{aligned}N^3(0)+2N(\mathbf{r}_1)N(\mathbf{r}_2)N(\mathbf{r}_1\pm\mathbf{r}_2) \\ -N(0)[N^2(\mathbf{r}_1)+N^2(\mathbf{r}_2) \\ +N^2(\mathbf{r}_1\pm\mathbf{r}_2)] \geqslant 0.\end{aligned}\right\} \quad (29)$$

This inequality can be transformed if we solve it with respect to $N(\mathbf{r}_1\pm\mathbf{r}_2)$. We find the inequality

$$\frac{1}{N(0)}[N(\mathbf{r}_1)N(\mathbf{r}_2)-R] \leqslant N(\mathbf{r}_1\pm\mathbf{r}_2) \leqslant \frac{1}{N(0)}[N(\mathbf{r}_1)N(\mathbf{r}_2)+R], \quad (30)$$

$$R \equiv \{[N^2(0)-N^2(\mathbf{r}_1)][N^2(0)-N^2(\mathbf{r}_2)]\}^{\frac{1}{2}}.$$

It follows that N will be continuous everywhere if it is continuous at the point 0. For if $\mathbf{r}_2$ is a very small coordinate difference $\boldsymbol{\delta}$, and if

$$N(\boldsymbol{\delta}) = N(0)(1-\epsilon), \quad (31)$$

where ϵ is again a small quantity, then (30) goes over into

$$\left.\begin{aligned}-\epsilon N(\mathbf{r})-[\epsilon(2-\epsilon)]^{\frac{1}{2}}[N^2(0)-N^2(\mathbf{r})]^{\frac{1}{2}} \\ \leqslant N(\mathbf{r}\pm\boldsymbol{\delta})-N(\mathbf{r}) \leqslant -\epsilon N(\mathbf{r}) \\ +[\epsilon(2+\epsilon)]^{\frac{1}{2}}[N^2(0)-N^2(\mathbf{r})]^{\frac{1}{2}}.\end{aligned}\right\} \quad (32)$$

Both the lower and the upper bound converge toward zero with ϵ. It follows further from the inequality (32) that the rate of change of N, defined as

$$\lim_{|\delta|=0}\left\{\frac{1}{|\boldsymbol{\delta}|}[N(\mathbf{r}+\boldsymbol{\delta})-N(\mathbf{r})]\right\}, \quad (33)$$

is everywhere bounded if the following limit exists

$$\lim_{|\delta|=0}\left\{\frac{1}{|\boldsymbol{\delta}|}\left[1-\frac{N(\boldsymbol{\delta})}{N(0)}\right]^{\frac{1}{2}}\right\}, \quad (34)$$

for fixed direction of $\boldsymbol{\delta}$. If that limit vanishes, $N(\mathbf{r})$ is constant everywhere and equal to $N(0)$.

Another set of inequalities can be obtained by considering positive definite expressions of the type

$$Q = {}^*\int_0^r \phi(\rho)n'(\rho)d\rho \cdot {}^*\int_0^r \phi^*(\sigma)n'(\sigma)d\sigma \geqslant 0, \quad (35)$$

where the asterisk indicates transition to the conjugate complex. If we choose in particular for the arbitrary function $\phi(\rho)$ the function $e^{ik\rho}$, then we obtain the following

$$\left.\begin{aligned}Q &= {}^*\int_0^r\int_0^r e^{ik(\rho-\sigma)}N(\rho-\sigma)d\rho d\sigma \\ &= 2\,{}^*\int_0^r (r-\rho)\cos k\rho \cdot N(\rho)d\rho \geqslant 0\end{aligned}\right\} \quad (36)$$

or

$$\int_0^r \left(1-\frac{\rho}{r}\right) \cos k\rho \cdot N(\rho)d\rho \gtrless 0. \tag{37}$$

THE MEAN SQUARE DEVIATION OF S'

From Eq. (7), we shall now compute an expression for the mean square deviation of the optical path length from the geometrical path length. We have

$$\left.\begin{aligned}\sigma_S^2 &= \langle (S_0+\lambda S'+\lambda^2 S'')^2\rangle - \langle S_0+\lambda S'+\lambda^2 S''\rangle^2 \\ &= \lambda^2[\langle S'^2\rangle - \langle S'\rangle^2] + \text{higher terms.}\end{aligned}\right\} \tag{38}$$

In this expression, $\langle S'\rangle$, the mean deviation of the optical from the geometrical path length, vanishes,

$$\langle S'\rangle = {}^*\int_0^r \langle n'(\rho)\rangle d\rho = 0. \tag{39}$$

For $\langle S'^2\rangle$ we find

$$\langle S'^2\rangle = {}^*\int_{\rho,\sigma=0}^{r}\int N(\rho-\sigma)d\sigma d\rho. \tag{40}$$

This double integral can be transformed as follows:

$$\left.\begin{aligned}\langle S'^2\rangle &= \int_{\sigma=0}^{r}\int_{\tau=-\sigma}^{r-\sigma} N(\tau)d\tau d\sigma \\ &= \int_{\tau=0}^{r}\int_{\sigma=0}^{r-\tau} N(\tau)d\sigma d\tau + \int_{\tau=-r}^{0}\int_{\sigma=-\tau}^{r} N(\tau)d\sigma d\tau,\end{aligned}\right\} \tag{41}$$

and finally

$$\langle S'^2\rangle = 2\,{}^*\int_0^r (r-\rho)N(\rho)d\rho. \tag{42}$$

We find, thus, that the mean optical path length equals the actual distance r, while the r.m.s. deviation is given in this approximation by the expression

$$\sigma_S = \left[2\,{}^*\int_0^r (r-\rho)N(\rho)d\rho\right]^{\frac{1}{2}}. \tag{43}$$

The integral is to be extended over the straight line connecting the source with the point at which the observer is located.

It may be assumed that in most practical cases the function $N(\mathbf{r})$ decreases rapidly for large values of the argument. As a result, expression (42) may be replaced, in fair approximation, by

$$\sigma_S^2 \sim 2r\,{}^*\int_0^\infty N(\rho)d\rho. \tag{44}$$

Without any knowledge of the details of the function N, it can be predicted that, for sufficiently large distances, the r.m.s. fluctuation of the optical path length will increase with the square root of the distance.

THE SIGNAL LEVEL FLUCTUATION

From Eqs. (19) and (20), it is possible to obtain an expression for signal level fluctuation. By an argument analogous to that leading to the mean square deviation of the optical path length, we find first that

$$\sigma_L^2 = \langle L'^2\rangle. \tag{45}$$

This expression is, in turn, equal to

$$\langle L'^2\rangle = {}^*\int_{\rho,\sigma=0}^{r}\int \left(\frac{1}{\rho}-\frac{1}{r}\right)\left(\frac{1}{\sigma}-\frac{1}{r}\right) \times \rho^2\sigma^2\langle \nabla_\rho{}^2 n'(\rho)\nabla_\sigma{}^2 n'(\sigma)\rangle d\sigma d\rho. \tag{46}$$

The integrand can be simplified, first of all, by the introduction of the iterated Laplacean of $N(\mathbf{r})$, in accordance with the identity

$$\langle \nabla^2 n'(\rho)\nabla^2 n'(\sigma)\rangle \equiv \nabla^2\nabla^2 N(\rho-\sigma). \tag{47}$$

Equation (46) then assumes the form

$$\langle L'^2\rangle = {}^*\int_{\rho,\sigma=0}^{r}\int \left(\frac{1}{\rho}-\frac{1}{r}\right)\left(\frac{1}{\sigma}-\frac{1}{r}\right) \times \rho^2\sigma^2\nabla^2\nabla^2 N(\rho-\sigma)d\sigma d\rho. \tag{48}$$

It is now possible to convert the double integral into a single integral by means of transformations similar to those leading to Eq. (42) above. We obtain the expression

$$\langle L'^2\rangle = \frac{1}{15}\frac{1}{r^2}\,{}^*\int_{\rho=0}^{r} (r^2+3\rho r+\rho^2) \times (r-\rho)^3\nabla^2\nabla^2 N(\rho)d\rho. \tag{49}$$

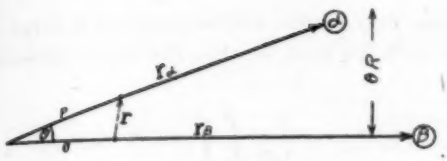

FIG. 2. Two receiving stations.

If $N(\rho)$ is small for large values of the argument, then the expression (49) can be approximated by the much cruder approximation

$$\langle L'^2\rangle \sim \frac{1}{15} r^3 \int_{\rho=0}^{\infty} \nabla^2\nabla^2 N(\rho)\, d\rho. \tag{50}$$

New observations, made recently at the Laboratory of the University of California, Division of War Research, at San Diego, appear to show that the fluctuation of supersonic sound signals over paths in the deep ocean, well removed from both surface and bottom, shows an increase with increasing distance, but the rate of increase did not agree quantitatively with Eq. (50).

CORRELATION AT TWO RECEIVING STATIONS

In the case of two stations receiving the same signals (Fig. 2), the levels received at either station are given by the expression (20), so that we have

$$\left.\begin{aligned} L_\alpha' &= -\int_0^{r_\alpha} \left(\frac{1}{\rho}-\frac{1}{r_\alpha}\right)\rho^2\nabla_\rho{}^2 n'(\rho)\, d\rho, \\ L_\beta' &= -\int_0^{r_\beta} \left(\frac{1}{\sigma}-\frac{1}{r_\beta}\right)\sigma^2\nabla_\sigma{}^2 n'(\sigma)\, d\sigma. \end{aligned}\right\} \tag{51}$$

The average product of L_α' and L_β' is given by the expression

$$\langle L_\alpha' L_\beta'\rangle = \int_{\rho=0}^{r_\alpha}\int_{\sigma=0}^{r_\beta} \left(\frac{1}{\rho}-\frac{1}{r_\alpha}\right)\left(\frac{1}{\sigma}-\frac{1}{r_\beta}\right) \times \rho^2\sigma^2\nabla^2\nabla^2 N(\mathbf{r})\, d\sigma\, d\rho, \tag{52}$$

where the two integrals are to be extended over two different paths. $\mathbf{r}$ is a vector which connects the two points (σ) and (ρ), as indicated in Fig. 2. This double integral cannot be converted into a single integral, because the vector $\mathbf{r}$ assumes values depending on two parameters. However, it is possible to replace the expression (52) by an approximate expression which, like (50), gives

FIG. 3. Area of integration in the r-plane.

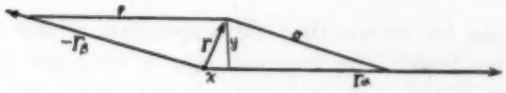

FIG. 4. Coordinate transformation in the r-plane.

information on the dependence on distance for large distances. First of all, we shall assume that the argument $N(\mathbf{r})$ is significantly different from zero only for small values of the argument $\mathbf{r}$, let us say for

$$|\mathbf{r}| < l, \tag{53}$$

and further, that l itself is small compared with the lateral separation of the stations α and β, that is,

$$l \ll \tfrac{1}{2}\theta(r_\alpha + r_\beta). \tag{54}$$

It will further be assumed that θ is a small angle and that

$$\frac{|r_\alpha - r_\beta|}{r_\alpha + r_\beta} \ll 1. \tag{55}$$

The average vector from source to receivers will be called $\mathbf{R}$,

$$\mathbf{R} \equiv \tfrac{1}{2}(\mathbf{r}_\alpha + \mathbf{r}_\beta). \tag{56}$$

In that case, the only portion of the integral which contributes significantly is the obtuse circular section in the r-plane indicated in Fig. 3. In this region, the expression (52) may be replaced, in fair approximation, by

$$\langle L_\alpha' L_\beta'\rangle \sim \int\int \rho\sigma\nabla^2\nabla^2 N(\mathbf{r})\, d\rho\, d\sigma. \tag{57}$$

This integral, in turn, can be further transformed. If we describe the area of integration by rectangular coordinates, x and y, Fig. 4,

$$\left.\begin{aligned} x &= \rho - \sigma\cos\theta, \\ y &= \sigma\sin\theta, \end{aligned}\right\} \tag{58}$$

or

$$\left.\begin{aligned} \rho &= x + y\cot\theta, \\ \sigma &= y\,\mathrm{cosec}\,\theta, \end{aligned}\right\} \tag{59}$$

with the Jacobian

$$\frac{\partial\rho}{\partial x}\frac{\partial\sigma}{\partial y} - \frac{\partial\rho}{\partial y}\frac{\partial\sigma}{\partial x} = \mathrm{cosec}\,\theta, \tag{60}$$

Eq. (53) assumes the form

$$\langle L_\alpha' L_\beta' \rangle \sim \operatorname{cosec}^2\theta \iint_{x,y} y(x+y\cot\theta) \times \nabla^2\nabla^2 N(x,y,z)\,dxdy. \quad (61)$$

It can be shown that the expression which remains under the integral sign is changed but little if the circular sector is expanded into a semicircle. Thus, the expression (57) can be further simplified into

$$\langle L_\alpha' L_\beta' \rangle \sim \frac{1}{2\theta^2}\int\int_{x,y=-\infty}^{\infty} xy\nabla^2\nabla^2 N\,dxdy + \frac{1}{2\theta^3}\int\int_{x,y=-\infty}^{\infty} y^2\nabla^2\nabla^2 N\,dxdy. \quad (62)$$

Of these two terms, the second one is large compared with the first, so that the final expression is

$$\langle L_\alpha' L_\beta' \rangle \sim \frac{1}{2\theta^3}\int\int_{x,y=-\infty}^{\infty} y^2\nabla^2\nabla^2 N\,dxdy, \quad (63)$$

where y is the direction perpendicular to $\mathbf{R}$ in the plane of source and receivers.

To obtain the usual correlation coefficient, the expression (63) has to be divided through by (50). It is found that the correlation coefficient is independent of the distance between source and receivers and inversely proportional to the cube of the distance between the two receiving stations perpendicular to the line connecting the source with the location of the receivers, δ, as indicated in Fig. 2.

PHYSICAL REVIEW VOLUME 70, NUMBERS 7 AND 8 OCTOBER 1 AND 15, 1946

A Calculation of the Binding Energies of H^3 and He^4 with a New Potential

MU-HSIEN WANG
Department of Physics, National University of Chekiang, Meitan, Kweichow, China

(Received May 15, 1946)

The binding energies of the nuclei H^3 and He^4 are calculated by the method of equivalent two-body, using the potential suggested by Wang. The range at which the potential between two nucleons is cut off is the same as that for the case of the deuteron, and the same range for the equivalent two-body is deduced accordingly. The binding energies thus calculated are 7.3 Mev and 15.1 Mev, respectively.

I. METHOD OF CALCULATION

THE nuclear potential proposed by Wang[1] was previously applied by the author to the calculation of the binding energy of the deuteron and of the neutron-proton scattering.[2] In the present work the binding energies of the nuclei H^3 and He^4 are computed by using the same potential in the method of the equivalent two-body.

Let $C\phi(r)$ be the potential between any two nucleons. If the Gaussian wave function $N\exp[-\frac{1}{2}\nu(r_{12}^2+r_{13}^2+r_{23}^2)]$ is used, the variation energy for H^3 is[3]

$$E(H^3) = \frac{9\nu\hbar^2}{2M} - 3C\frac{4}{\pi^{\frac{1}{2}}}\int_0^\infty \exp(-x^2) \times \phi[x/(3\nu/2)^{\frac{1}{2}}]x^2dx, \quad (1)$$

where

$$x = (3\nu/2)^{\frac{1}{2}}r_{12} \quad (\text{or } r_{13}, r_{23}),$$

and r_{12} is the distance between particles 1 and 2. For the nucleus He^4, taking $N\exp[-\frac{1}{2}\nu(r_{12}^2+r_{13}^2+r_{14}^2+r_{23}^2+r_{24}^2+r_{34}^2)]$ as the wave function, we have

$$E(He^4) = \frac{9\nu\hbar^2}{M} - 6C\frac{4}{\pi^{\frac{1}{2}}}\int_0^\infty \exp(-x^2) \times \phi[x/(2\nu)^{\frac{1}{2}}]x^2dx, \quad (2)$$

[1] K. C. Wang and H. L. Tsao, Phys. Rev. 66, 155 (1944); Nature 155, April 28 (1945).
[2] Mu-Hsien Wang, Phys. Rev. 66, 103 (1944).
[3] William Rarita and R. D. Present, Phys. Rev. 51, 788 (1937).

TABLE I

ϵ, erg	$\frac{5.00\times10^{-5}}{2\epsilon}-1$	coth $(370\epsilon^{\frac{1}{2}})$
10.8×10^{-6}	1.32	1.20
11.5×10^{-6}	1.17	1.18
11.7×10^{-6}	1.14	1.17

TABLE II.

ϵ, erg	$\frac{5.00\times10^{-5}}{2\epsilon}-1$	coth $(388\epsilon^{\frac{1}{2}})$
11.5×10^{-6}	1.18	1.16
11.6×10^{-6}	1.16	1.15+
12.0×10^{-6}	1.08	1.15

where

$$x=(2\nu)^{\frac{1}{2}}r_{12} \quad (\text{or } r_{13}, r_{14}, \cdots).$$

Now, let $D\Phi(r)$ be the potential for the equivalent two-body problem. Using the wave function $N\exp[-\mu r^2/2]$, we get for the variation energy for the equivalent two-body:

$$E_{eq}=\frac{3\mu\hbar^2}{2M}-D\frac{4}{\pi^{\frac{1}{2}}}\int_0^\infty \exp(-x^2) \times\Phi(x/\mu^{\frac{1}{2}})x^2dx, \quad (3)$$

where

$$x=\mu^{\frac{1}{2}}r.$$

In order that $E(H^3)$, as given by (1), may equal E_{eq}, we should have

$$\mu=3\nu, \qquad D=3C, \qquad \Phi(r)=\phi(2^{\frac{1}{2}}r). \quad (4)$$

Similarly, to have $E(He^4)=E_{eq}$, we must set

$$3\mu/2=9\nu, \qquad D=6C, \qquad \Phi(r)=\phi(3^{\frac{1}{2}}r). \quad (5)$$

In our case, the potential is

$$C\phi(r)=V_0=\text{const.} \quad \text{for } r\leq a,$$

$$C\phi(r)=-Ae^{K/r} \quad \text{or} \quad -\frac{B}{r}e^{K/r} \quad \text{for } r>a,$$

where

$$r=r_{12} \quad (\text{or } r_{13}, r_{14}, \cdots),$$

and where a has the same meaning as in the deuteron; its value was found in reference 2. To determine the cut-off distance, r_0, to be used in the equivalent two-body method, we compare Eq. (3) in turn with Eqs. (1) and (2), and find that

$$r_0=a/2^{\frac{1}{2}} \text{ for } H^3, \quad (6)$$

and

$$r_0=a/3^{\frac{1}{2}} \text{ for } He^4. \quad (7)$$

If the zero cut-off method is employed, the potential for H^3 has therefore the form (9a, b) or the form (10a, b), and the potential for He^4 has the form (11a, b) or the form (12a, b).

The binding energy, ϵ, of H^3 and of He^4 is then the proper value of the wave equation

$$M\Delta\psi-\hbar^2(\epsilon+V)\psi=0,$$

where V is the potential. The condition for the smooth joint of the wave function at r_0 is[2]

$$|V(r_0)|/2\epsilon-1=\coth(\beta r_0), \quad (8)$$

where $\beta=(M\epsilon/\hbar^2)^{\frac{1}{2}}$.

II. THE BINDING ENERGY OF H^3

(a) For the potential

$$D\Phi(r)=0 \text{ for } r\leq r_0=a/2^{\frac{1}{2}}, \quad (9a)$$

and

$$D\Phi(r)=-3A\exp(K/2^{\frac{1}{2}}r) \text{ for } r>r_0, \quad (9b)$$

where[2] $A=4.78\times10^{-45}$, $K=3.84\times10^{-11}$ cm, $a=4.21\times10^{-13}$ cm, Eq. (8) becomes:

$$5.00\times10^{-5}/2\epsilon-1=\coth(370\epsilon^{\frac{1}{2}}).$$

The numerical results are given in Table I. The estimated binding energy of H^3 is therefore 11.5×10^{-6} erg, or 7.23 Mev.

(b) For the potential

$$D\Phi(r)=0 \quad \text{for } r\leq r_0=a/2^{\frac{1}{2}}, \quad (10a)$$

and

$$D\Phi(r)=-\frac{3B}{2^{\frac{1}{2}}r}\exp(K/2^{\frac{1}{2}}r) \quad \text{for } r>r_0, \quad (10b)$$

where[2] $a=4.42\times10^{-13}$ cm, $B=1.84\times10^{-55}$, we have

$$5.00\times10^{-5}/2\epsilon-1=\coth(388\epsilon^{\frac{1}{2}}).$$

The results are given in Table II. The estimated binding energy of H^3 is therefore 11.6×10^{-6} erg, or 7.30 Mev. These results are in good agreement with the experimental value 8.3 Mev.

III. THE BINDING ENERGY OF He^4

(a) For the potential

$$D\Phi(r)=0 \text{ for } r\leq r_0=a/3^{\frac{1}{2}}, \quad (11a)$$

TABLE III

ϵ, erg	$\frac{1.00\times10^{-4}}{2\epsilon}-1$	coth $(302\epsilon^{\frac{1}{2}})$
23.6×10^{-6}	1.12	1.12
23.8×10^{-6}	1.11	1.11
24.0×10^{-6}	1.08	1.10

TABLE IV

ϵ, erg	$\frac{1.00\times10^{-4}}{2\epsilon}-1$	coth $(317\epsilon^{\frac{1}{2}})$
23.8×10^{-6}	1.11	1.10
24.0×10^{-6}	1.08	1.09
24.2×10^{-6}	1.07	1.09

and

$$D\Phi(r)=-6A\exp(K/3^{\frac{1}{2}}r) \text{ for } r>r_0, \quad (11b)$$

where the constants have the same values as in Section II (a), Eq. (8) turns out to be

$$1.00\times10^{-4}/2\epsilon-1=\coth(302\epsilon^{\frac{1}{2}}),$$

and yields Table III. According to this table, the binding energy of He^4 is 23.8×10^{-6} erg, or 15.0 Mev.

(b) For the potential

$$D\Phi(r)=0 \quad \text{for } r\leq r_0=a/3^{\frac{1}{2}}, \quad (12a)$$

and

$$D\Phi(r)=-\frac{6B}{3^{\frac{1}{2}}r}\exp(K/3^{\frac{1}{2}}r) \quad \text{for } r>r_0, \quad (12b)$$

where the constants have the same values as in Section II (b), Eq. (8) becomes

$$1.00\times10^{-4}/2\epsilon-1=\coth(317\epsilon^{\frac{1}{2}}),$$

and yields Table IV. According to this table, the binding energy of He^4 is 24.0×10^{-6} erg, or 15.1 Mev.

The values of the binding energy of He^4 computed above are about 45 percent less than the experimental value 27.8 Mev. The results for He^4 are therefore not as good as those for H^3. This may mean that the method of the equivalent two-body tends to be a poor approximation as the number of particles increases.

In conclusion, the author wishes to express his thanks to Dr. K. C. Wang for helpful discussions.

PHYSICAL REVIEW VOLUME 70, NUMBERS 7 AND 8 OCTOBER 1 AND 15, 1946

Recurrence Phenomena in Small Cosmic-Ray Bursts*

JAMES W. BROXON
University of Colorado, Boulder, Colorado

(Received July 11, 1946)

Chree's method of superposed epochs was employed in the statistical investigation of variations in the frequency of occurrence of small cosmic-ray bursts which produced 2.9 to 3.6 millions of pairs of ions in a shielded spherical ionization chamber of 13.3 liters effective volume containing air at 160 atmospheres. The data employed were obtained by Long and Whaley in the same investigation (during a little more than 18 months in 1938 and 1939) which supplied the data for the author's work on recurrences in variations of cosmic-ray intensity and their relation to geomagnetic and heliophysical activities. The analysis was carried out only for the range of day numbers from −45 to +45. Irregular secondary pulses were found both preceding and subsequent to both positive and negative primary pulses. Both subsequent and preceding difference curves and the combination difference curve displayed secondary pulses with peaks at about 27 days preceding and subsequent to the primary pulses. The secondary pulses amounted to about 3 or 4 percent of the average frequency of approximately 37 small bursts per day, and about 10 percent of the larger variations constituting the primary pulses.

THE data regarding bursts which are discussed in this paper were observed by Long[1] and Whaley[2,3] in the same investigation during eighteen months in 1938 and 1939, which yielded data used heretofore by the writer.[4,5]

* Presented at the meeting of the American Physical Society at St. Louis, November 30–December 1, 1945; Phys. Rev. 69, 46 (1946).

[1] V. A. Long, Ph.D. Thesis, University of Colorado, August 14, 1940.

[2] R. M. Whaley, M.A. Thesis, University of Colorado, June 3, 1940.

[3] V. A. Long and R. M. Whaley, Phys. Rev. 59, 470 (1941).

[4] J. W. Broxon, Phys. Rev. 59, 773 (1941).

[5] J. W. Broxon, Phys. Rev. 62, 508 (1942).

These data were obtained at an altitude of 5400 ft., latitude 40° N, longitude 105° 15′ W. After correction for bursts and barometric variations, the ionization currents produced by the cosmic radiation displayed an annual variation of about 1.3 percent amplitude with maximum in late January or February, almost diametrically out of phase with the annual variation of local outdoor temperature. Also, a preliminary analysis of one month's data by Long[1] indicated a diurnal variation of about 0.2 percent amplitude. The author's[4] analysis by Chree's method of superposed epochs showed recurrences in fluctuations of the (corrected) cosmic-ray intensity at intervals of about 28 days, with secondary pulses deviating some 0.2 percent from the mean. Further analysis[5] showed that the primary pulses in the intensity of the cosmic radiation were in general phase opposition to corresponding pulses in the terrestrial magnetic character and in sunspot areas. The peaks of the opposed pulses in magnetic character occurred one day prior to those of the primary pulses of the cosmic radiation, while the corresponding lead in the case of the pulses in sunspot area was three or four days.

Because of the sensitivity of the apparatus, Long and Whaley were able to distinguish cosmic-ray bursts which were appreciably smaller than those commonly observed with recording apparatus. After careful consideration of criteria for distinguishing between bursts and statistical fluctuations, they concluded that bursts corresponding to a deflection of 0.5 mm on the photographic record could be distinguished quite reliably. They concluded that there was only about 0.1 percent probability that a 1-mm burst (the smallest they read and considered in their study of magnitude-frequency relations) as selected by them might actually be a statistical fluctuation. A 1-mm burst corresponds to the formation of 2.9×10^6 pairs of ions in the chamber. The 13.8-liter chamber containing air at 160 atmospheres was spherical, with a concentric spherical collecting electrode (with 620 volts collecting P.D., compensated) of 9.5 cm diameter, leaving an effective volume of about 13.3 liters. This was shielded by 5 inches of lead and the stone building in which it was housed. Considering the dimensions of the chamber, and arbitrarily assuming a mean linear ion density of 100 pairs per cm of path of a cosmic-ray particle in air at N.T.P., Long[1] concluded that a 1-mm burst might correspond to as few as 65 cosmic-ray particles passing through the chamber.

For their investigation of magnitude-frequency relations, Long and Whaley arranged the bursts in groups or classes corresponding to 0.5 mm differences in the deflections produced on the photographic record, the first class comprising a narrower range than the others. Thus all bursts from 1.0 to 1.2 mm, inclusive, were classified as 1-mm bursts. The next group, corresponding to deflections from 1.3 to 1.7 mm, inclusive, were classified as 1.5-mm bursts, and so on for larger bursts. While the frequency of occurrence of large bursts (which extended to 56 mm) appeared to be entirely random in time, there were indications of both diurnal and annual variation in the frequency of the 1-mm bursts. Long[1] found the frequency of this class to be some 25 or 30 percent greater in the neighborhood of (local) noon than around midnight, on the average, for the first 12 months. Also, their average frequency during February and March was about 2.5 times as great as it was during July, August, and September of either year. In this connection, it may be mentioned that the monthly average frequency of occurrence of the 3-mm bursts (which were less frequent than the 1-mm bursts in the ratio of 1 to 58; the difference would be greater if the 3-mm class were restricted to the narrower range) varied somewhat more irregularly with the season, and was greatest in September of 1938 and August of 1939.

In view of the fact that the smallest bursts did not appear to occur entirely at random, but did show indications of diurnal and annual variations corresponding somewhat to those of the cosmic-ray intensity as indicated by the ionization current, it was decided to investigate the possibility that the method of Chree might indicate recurrences in the frequency of these small bursts. The high frequency of occurrence of the 1-mm bursts was also an item considered by the writer in deciding to apply the method to data extending over only 18 months. Burst data were used for precisely the same (Greenwich) days as in the investigations[4, 5] of the pulses

in cosmic-ray intensity, with the exception of the last day, December 1, 1939. The frequencies designated represent the number of bursts per 24-hour day, corrections being applied for the days when data were not available for all 24 hours. When such correction was necessary, the nearest integral number was employed; no fractions were retained in designating the number of 1-mm bursts per 24-hour day. Also no correction factor was applied on account of the fact that the central system was grounded during two minutes of each hour. The extreme frequencies of occurrence of the 1-mm bursts were 5 and 115 per day. Both of these represented remarkably large departures from the mean, particularly the latter. The grand average of the corrected values for all days was 36.15 per 24-hour day for the 1-mm bursts. If further corrected for the two-minute grounding period during each hour, this would represent a mean frequency per day of 37.4 bursts in the range representing the formation of about 2.9 to 3.6 millions of pairs of ions in the chamber.

In classifying bursts and restricting attention to those within specified limits it is important that these limits be definite and constant. Changes of sensitivity of the apparatus could affect the boundaries between classes if corrections were not applied. Although the temperature of the apparatus varied only about 1°C during the year and a half of observation, some changes of sensitivity as great as 5 percent did occur. In classifying the bursts, corrections for variations of sensitivity were not made. In the case of the 1-mm bursts, it is estimated that observational errors of this order of magnitude were quite likely to occur. This is apparent if one considers the difficulty of distinguishing accurately among bursts at the lower limit of this narrow range, the finite width and distinctness of the photographic record as well as the time of collection of the ions being involved.

Although considerations of accuracy of observation made the undertaking far from promising in that random variations might be expected to outweigh possible regularities in the variation of frequency, it was decided to proceed with an investigation over a limited range of day numbers by Chree's method of superposed epochs. Accordingly, the five days with the greatest number of 1-mm bursts in each of the 18 complete months of the investigation were selected as the zero days for the positive pulses, while the

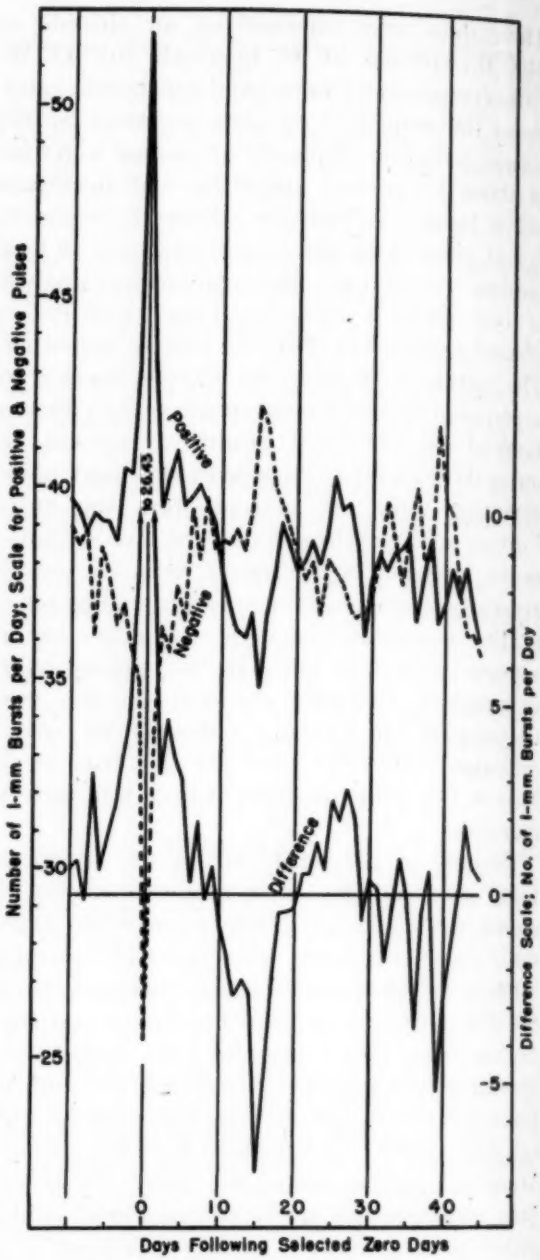

FIG. 1. Primary and subsequent pulses in the frequency of occurrence of 1-mm bursts. For the positive-pulse curve, the zero days are the five of greatest frequency of 1-mm bursts in each of the first fifteen months, June, 1938, through August, 1939. For the negative-pulse curve, the zero days are the five of least frequency of 1-mm bursts in each of the same months. The difference curve was obtained by subtracting ordinates of the negative-pulse curve from those of the positive-pulse curve for the same day numbers.

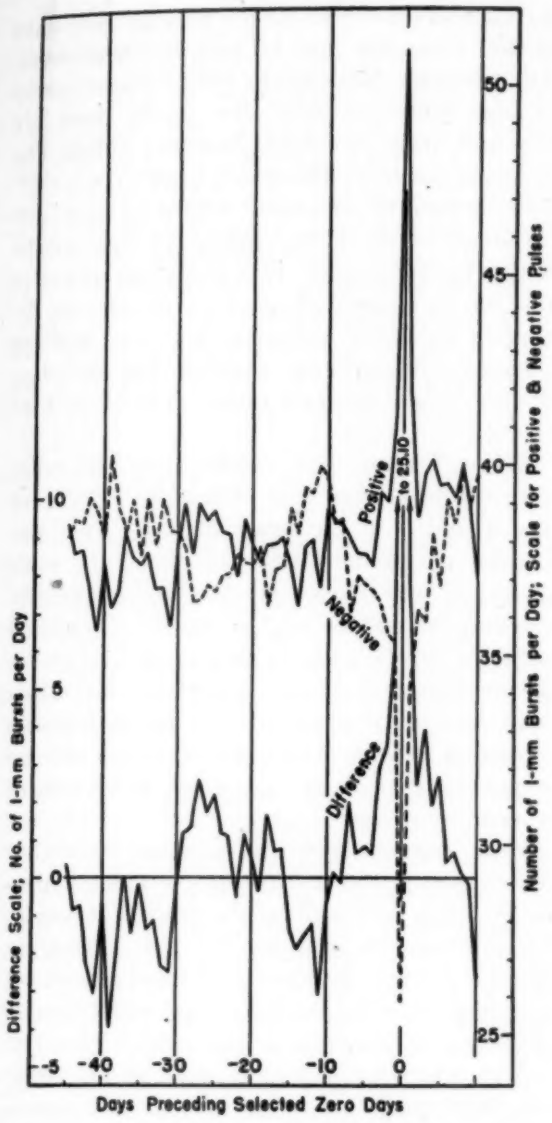

FIG. 2. Primary and previous pulses in the frequency of occurrence of 1-mm bursts. For these curves, zero days were selected from the last fifteen months, September, 1938, through November, 1939.

five with the smallest number of 1-mm bursts in each month were selected as the zero days for the negative pulses. When dealing with the large numbers of very small bursts, it might be supposed that, if they did not occur at random, then the frequency of occurrence would be greatest when the cosmic-ray intensity (as measured by the average ionization current) was greatest, and least when the intensity was least. If so, then one might suppose that upon investigating the four groups of 90 zero days each, there would be found a considerable degree of coincidence among the two groups selected for the positive pulses, and likewise among those selected for the negative pulses. On the other hand, one might suppose that a converse relation could exist, for the ionization currents had been corrected for bursts as well as for variations of barometric pressure, and the number of ions formed by thirty-seven 1-mm bursts exceeds 0.2 percent of the number of ions formed in the chamber in one day as represented by the average ionization current of 38.2 ions per cc per sec.; the secondary pulses in the ionization current as yielded by the Chree method amounted to about 0.2 percent of the average. Actually, 17 zero days selected for their large number of 1-mm bursts were identical with days selected on the basis of large average cosmic-ray ionization current and 22 zero days selected for their small number of 1-mm bursts were identical with those selected for their small average current. On the other hand, 9 zero days selected for their large number of 1-mm bursts were identical with those selected on the basis of small average current, and 13 zero days selected for their small number of 1-mm bursts were identical with those selected for their large average current. While the evidence appears slightly to favor the first of the two suppositions suggested above, there appears to be no considerable correlation between zero days selected upon the basis of large or small average currents, and those selected upon the basis of large or small number of 1-mm bursts.

Proceeding with the analysis by Chree's method as in the investigation of average ionization currents,[4] primary and subsequent pulse curves were constructed for the limited range of day numbers, $n=-10$ to $n=45$, for the first 15 months. These are shown in Fig. 1. For the solid line marked "positive," the zero days were the five with the greatest number of 1-mm bursts in each month from June, 1938, through September, 1939. For the broken line marked "negative," the zero days were the five with the least number of 1-mm bursts in each of the same months. As usual, the "difference" curve was obtained by subtracting ordinates of the "negative" curve from the corresponding ordinates of the "positive" curve.

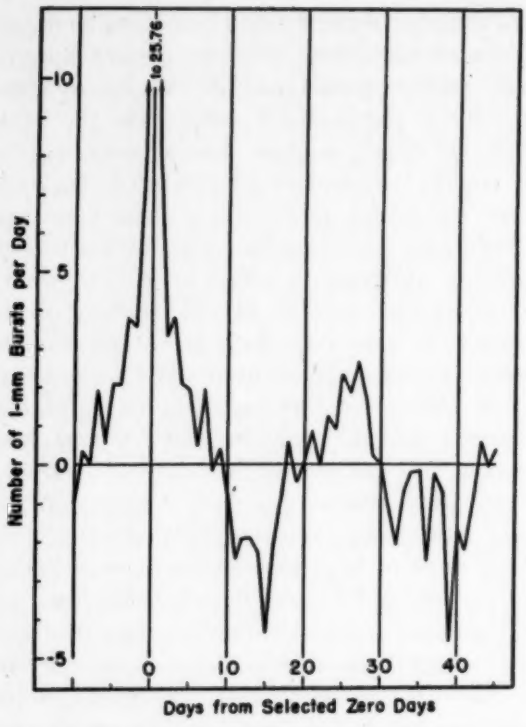

FIG. 3. Combination of difference pulses of Fig. 1 and Fig. 2. The ordinate for any day n is the average of the "difference" value for day number n in Fig. 1 and that for day number $-n$ in Fig. 2.

Though the curves are quite irregular, the "positive" and "negative" curves of Fig. 1 do display rather definite loops, indicating subsequent secondary pulses in both the positive and negative curves. The highest peak in the subsequent positive pulse is at day number $n=25$, though the shape of the pulse makes it somewhat difficult to decide where it is centered. The greatest dip in the subsequent negative pulse is at $n=28$. The subsequent difference pulse has its highest tip at $n=27$, though its shape might be taken as indicating that it is centered at a slightly smaller day number.

Figure 2 shows the corresponding curves for day numbers $n=-45$ to $n=10$ with zero days selected from the last 15 months, September, 1938, through November, 1939. These curves are also quite irregular, but again there are loops indicating preceding secondary pulses. The preceding positive pulse has a peak at $n=-27$, with another of the same height at $n=-29$. The shape of the pulse appears to lend weight to the former value. The preceding negative pulse has its greatest dip at $n=-28$, though the shape of the pulse indicates that it is centered at a smaller negative day number. The preceding difference pulse shows a rather definite peak at $n=-27$.

Figure 3 shows the combination difference curve formed from the difference curves of Figs. 1 and 2 in the usual manner. This also displays a secondary pulse of about the same magnitude and shape as the subsequent and preceding secondary pulses in the individual difference curves, with its highest peak at $n=27$. The magnitude indicates preceding and subsequent secondary positive and negative pulses amounting to some 3 to 4 percent of the average frequency for all days, and about 10 percent of the primary pulses.

While irregularities are perhaps somewhat greater than in the case of daily average ionization currents produced by the cosmic radiation, this investigation appears to the author to provide definite indication of recurrences of variations in the frequency of these small cosmic-ray bursts at intervals in the neighborhood of 27 days preceding and subsequent to the larger variations which determine the primary pulses. This is perhaps somewhat surprising in view of the experimental difficulties associated with the precise measurement of burst magnitudes, as indicated above. Perhaps observational errors are fairly well compensated in this statistical treatment of such a large number of bursts.

Perturbations in the Ultraviolet Band Spectrum of P_2

E. J. MARAIS*
Merensky Institute for Physics, University of Stellenbosch, South Africa

(Received June 6, 1946)

The emission spectrum of the ultraviolet band system of P_2 has been photographed in the third and fourth orders of a 21-ft concave grating. Strong rotational perturbations were found in the $v'=5$, 7, 8, and 9 vibrational levels of the upper electronic state. These perturbations were fully determined. It is shown that the vibrational perturbations of the bands which result from the $v'=5$ level are caused by the rotational perturbations in this level. The following values were obtained for the equilibrium constants:

$B'_e=0.2416_4$ cm^{-1} $\quad B''_e=0.3032_7$ cm^{-1}
$\alpha'_e=0.00165$ cm^{-1} $\quad \alpha''_e=0.00142$ cm^{-1}
$I'_e=115.84\times10^{-40}$ g cm^2 $\quad I''_e=92.31\times10^{-40}$ g cm^2
$r'_e=2.12\times10^{-8}$ cm $\quad r''_e=1.893\times10^{-8}$ cm

SECTION A. INTRODUCTION

THE spectrum of the diatomic phosphorus molecule consists of two band systems. A prominent ultraviolet band system stretches from λ3400A to λ1800A, while a weak system has been reported in the visible region. Only P and R branches are present. This is a characteristic of a $^1\Sigma,^1\Sigma$, electronic transition. Herzberg[1] showed that it represents a $^1\Sigma^+_u$, $^1\Sigma^+_g$ transition. The lower $^1\Sigma^+_g$ level is the ground state of the molecule, because the same system is also observed in absorption. The emission spectrum of phosphorus was first observed by Geuter.[2] Jakowlewa[3] was the first to suggest a vibrational analysis. Herzberg[1] confirmed and extended this analysis and fully interpreted the predissociation phenomenon, which he discovered in this band system. This effect is very effectively shown in Fig. 1. He also showed that vibrational perturbations occurred in the $v'=2$ and 5 levels and suggested that research should be done on the rotational structure of the bands which result from these vibrational levels. In this connection Herzberg, Herzberg, and Milne[4] analyzed the (2,15) band. They found that the lines, with J'-values larger than 46, followed the usual run. The lines nearer the head of the band, with J'-values smaller than 46, however, showed an increasing deviation and the series could not be followed very far. The reason for this deviation is obviously a strong shift of the lines near the heads of the $v'=2$ bands on account of rotational perturbations. This is confirmed by the above-mentioned shift of these band heads, as reported by Herzberg.[1] With the same object in view Rao[5] analyzed the (5,18) and (5,21) bands and could not detect any perturbations in the rotational structure of these bands. Analyses were made by him for lines which had J'-values larger than 29 and 43, respectively. These lines are very far removed from the heads of these bands. It was therefore impossible to detect perturbations near the heads of these bands. Herzberg[1] also discovered rotational perturbations in the $v'=9$ level.

A strong alternation in intensity is observed in successive rotational lines of each branch of the bands of the homonuclear P_2 molecule. This is clearly shown in the case of the (9,29) band where the weak and strong lines of the two series fall together, respectively (cf. Fig. 2). Ashley,[6] Jenkins,[7] and Rao[8] fully worked out the phenomenon for P_2 and found the alternation ratio to be 3. This represents a high alternation, the weak lines being very much weaker than the strong lines. The strong lines correspond to odd

* Now research officer in the National Physical Laboratory, South Africa.
[1] G. Herzberg, Ann. d. Physik 15, 677 (1932).
[2] P. Geuter, Zeits. f. wiss. Phot. 5, 1 (1907).
[3] A. Jakowlewa, Zeits. f. Physik 15, 677 (1931).
[4] G. Herzberg, L. Herzberg, and G. G. Milne, Can. J. Research 18A, 139 (1940).
[5] K. N. Rao, Ind. J. Phys. 17, 135 (1943).
[6] Muriel F. Ashley, Phys. Rev. 44, 919 (1933).
[7] F. A. Jenkins, Phys. Rev. 47, 783 (1935).
[8] K. N. Rao, Ind. J. Phys. 17, 149 (1943).

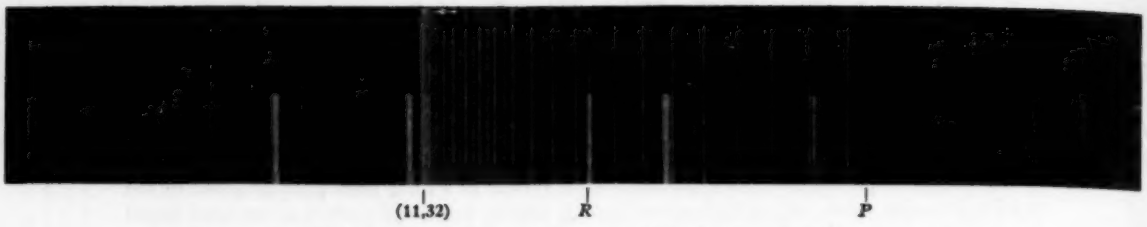

FIG. 1. (11,32) band of P_2. The positions at which the P and R branches stop, as a result of predissociation, are indicated.

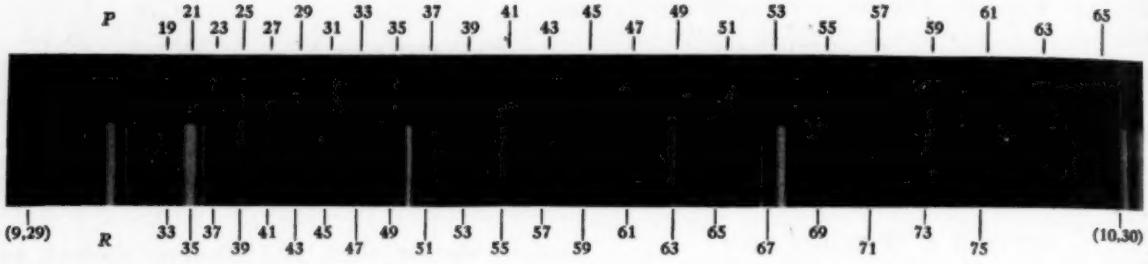

FIG. 2. (9,29) band of P_2, showing alternating intensities and perturbed lines. The numbers refer to J''-values.

values of J'' while the weak lines correspond to even values of J''. As was shown by Ashley,[6] the P-nuclei obey the Fermi-Dirac statistics.

Rotational analyses of a number of bands were made by Herzberg,[1] Ashley,[6] G. Herzberg, L. Herzberg, and Milne,[4] and Rao.[5] The dispersion obtained by previous research workers was very low, and varied between 2.38A to 3.5A/mm. The chief purpose of the present investigation was to obtain higher dispersion spectrograms in order to study the perturbations in the spectrum.

B. EXPERIMENTAL

A II-shaped Geissler tube of Pyrex was used to obtain the P_2 spectrum. The tube was evacuated by a two-stage Apiezon oil diffusion pump, designed by Sloan and Jenkins,[9] backed by a Cenco-Hyvac oil rotation pump. Both limbs of the discharge tube were connected through two liquid-air traps to the rest of the vacuum system to prevent impurities reaching the discharge tube. The material was purified by slowly redistilling "extra fine" red phosphorus four times in vacuum from one Pyrex vessel to the next by means of an electrical oven. The red phosphorus sublimed and condensed as the yellow modification in the second receptacle. The final receptacle was connected to the capillary of the discharge tube. When the yellow modification comes into the discharge it again changes to the red modification. An uncondensed discharge was obtained between the circular aluminum electrodes by using a 5-K.V.A. 220- to 20,000-volt step-up transformer. The light from the capillary of the discharge tube passed through a quartz window. The quartz window was kept clear by constantly heating it with a small gas flame.

A very high phosphorus vapor pressure is necessary to conduct the electric discharge. The method used by Herzberg[1] was found most satisfactory. Hydrogen was circulated in the vacuum system to conduct the discharge. Oxygen-free hydrogen was obtained by the electrolysis of NaOH solution in a specially constructed voltameter. Under the most favorable excitation conditions the discharge became dark green and the hydrogen spectrum (and therefore the hydrogen continuum running into the ultraviolet band spectrum of P_2) was altogether suppressed. It was impossible to prevent the emission of the strong PH band at λ3390A. A current of 12 amp. was used through the primary of the transformer. An exceptionally strong source was developed so that, using the corning glass "Red Ultra No. 5840" filter, which has a very weak transmission in this region, fourth-order spectrograms were obtained on the 21-ft. concave grating, mounted according to Paschen, for the bands between

[9] D. H. Sloan and F. A. Jenkins, Rev. Sci. Inst. 6, 80 (1935).

TABLE I. Rotational structure and combination differences of the P_2 bands.

J.	P(cm⁻¹)		R(cm⁻¹)		$\Delta_2F''(J)$ (cm⁻¹)	$\Delta_2F'(J)$ (cm⁻¹)
(11,31) ν_{head} = 30458.0 cm⁻¹.						
9	(2*mm*)	304,49.65	(5*dd*)	304,58.16		8.51
10	(0)	48.54			10.80	
11	(2*m*)	47.36		—		
12	(0)	46.13	(2*m*)	57.49		11.36
13		—	(4)	57.08	13.70	
14	(2)	43.79	(1*mm*)	56.63	14.71	12.84
15	(3*m*)	42.37	(4)	56.07	15.73	13.70
16	(1*m*)	40.90	(1)	55.58	16.74	14.68
17	(3)	39.33	(3*m*)	54.96	17.76	15.63
18	(1)	37.82	(1*d*)	54.29	18.78	16.47
19	(4)	36.18	(4)	53.62	19.82	17.44
20	(2)	34.47	(1)	52.75	20.79	18.28
21	(4)	32.83	(4)	51.91	21.82	19.08
22	(2)	30.93	(1)	50.95	22.81	20.02
23	(4)	29.10	(4)	49.95	23.83	20.85
24	(2*d*)	27.12	(1)	48.97	24.83	21.85
25	(4)	25.12	(4)	47.86	25.82	22.74
26	(2*dd*)	23.15	(2)	46.65	26.87	23.50
27	(4)	20.99	(5*d*)	45.41	27.86	24.42
28	(2)	18.79		—	28.92	
29	(4)	16.49	(4)	42.78		26.29
30		—	(2)	41.45	30.91	
31	(4)	11.87	(4)	39.86	31.94	27.99
32	(1)	09.51	(1*d*)	38.33	32.91	28.82
33	(4)	06.95	(4)	36.72	33.97	29.77
34	(1)	04.36	(2)	35.06	34.94	30.70
35	(4)	304,01.78			35.96	
36	(1)	303,99.10				
(10,31) ν_{head} = 30033.2 cm⁻¹						
9	(1*mm*)	300,24.83	(3*d*)	300,33.33		8.50
10					10.64	
11	(1*m*)	22.69	(2*mm*)	33.09		10.40
12					12.79	
13	(1)	20.30	(2)	32.40		12.10
14			(00)	32.05	14.71	
15	(2)	17.69	(3)	31.59		13.90
16			(1)	31.11	16.72	
17	(3)	14.87	(3)	30.55	17.69	15.68
18	(0)	13.42	(0*d*)	29.93	18.75	16.51
19	(3)	11.80	(2*m*)	29.29		17.49
20			(1*dd*)	28.44	20.80	
21	(3)	08.49	(4)	27.76	21.67	19.27
22	(1)	06.77	(1*mm*)	26.90	22.81	20.13
23	(3)	04.95	(4)	26.01	23.77	21.06
24	(0)	03.13	(1*mm*)	25.03	24.82	21.90
25	(3)	300,01.19	(4*d*)	24.03	25.80	22.84
26	(0)	299,99.23	(1*m*)	22.98	26.86	23.75
27	(3)	97.17	(4)	21.79	27.87	24.62
28	(1*m*)	95.11	(0)	20.64	28.88	25.53
29	(3)	92.91	(4)	19.38	29.72	26.47
30	(1*mm*)	90.92	(0)	18.02	30.93	27.10
31	(3)	88.45	(4)	16.66	31.88	28.21
32	(0)	86.14	(1)	15.24	32.92	29.10
33	(3)	83.74	(3)	13.71	33.92	29.97
34	(1)	81.32	(1*m*)	12.11	34.91	30.79
35	(3)	78.80	(3*mm*)	10.56	35.88	31.76
36	(1)	76.23	(1*m*)	08.86	36.96	32.63
37	(3)	73.60	(3)	07.13	37.92	33.53
38	(1*m*)	70.94	(0)	05.32	38.94	34.38
39	(3)	68.19	(3)	03.50	39.91	35.31
40	(1*mm*)	65.41	(1*m*)	300,01.57	40.98	36.16
41	(3)	62.52	(3)	299,99.61	41.95	37.09
42	(1*mm*)	59.62	(0)	97.58	42.98	37.96
43	(4)	56.63	(3)	95.48	44.00	38.85
44	(1)	53.58	(1)	93.34	45.00	39.76
45	(4)	50.48	(3*m*)	91.10	46.01	40.62
46	(1)	47.33	(0)	88.85	46.98	41.52
47	(4)	44.12	(3)	86.52	48.01	42.40
48	(1)	40.84	(1)	84.14	49.01	43.30
49	(4)	37.51	(3)	81.66	50.03	44.15
50	(1)	34.11	(0)	79.09	51.01	44.98
51	(4)	30.65	(2)	76.71	51.98	46.06
52	(1)	27.11		—	53.02	
53	(4)	23.69	(2)	71.31		47.62
54		—	(0)	68.56	55.02	
55	(4)	16.29	(2)	65.73	56.03	49.44
56	(2)	12.53	(00)	62.73	57.03	50.20
57	(4)	08.70	(2)	59.90	57.90	51.20
58	(1)	04.83			59.01	
59	(4)	00.89				
(10,29) ν_{head} = 31221.9 cm⁻¹						
9	(2*mm*)	312,13.12	(4*dd*)	312,21.76		8.64
10	(0)	12.05			10.86	
11	(2)	10.90		21.19		10.29
12	(00)	312,09.58			12.84	
13	(3)	08.35	(3)	312,20.46		12.11
14	(0)	06.97	(00)	19.96	14.91	12.99
15	(3)	05.55	(6)	19.41	15.98	13.86
16	(1*m*)	03.98	(0)	18.83	16.91	14.85
17	(3)	02.50	(6)	18.18	17.97	15.68
18	(1)	312,00.86	(0)	17.40	19.01	16.54
19	(4)	311,99.17	(6)	16.63	19.98	17.46
20	(1*d*)	97.42	(0)	15.76	21.05	18.34
21	(5)	95.58	(6)	14.83	22.07	19.25
22	(2*m*)	93.69	(1)	13.84	23.12	20.15
23	(4)	91.71	(4)	12.76	24.17	21.05
24	(2)	89.67	(1)	11.65	25.17	21.98
25	(5)	87.59	(4)	10.43	26.22	22.84
26	(1)	85.43	(2)	09.17	27.23	23.74
27	(4)	83.20	(4)	07.82	28.24	24.62
28	(2)	80.93	(1*m*)	06.44	29.25	25.51
29	(6)	78.57	(5*dd*)	04.86	30.26	26.29
30	(2)	76.18	(1)	03.48	31.20	27.30
31	(6)	73.66	(4)	01.87	32.36	28.21
32	(2)	71.12	(2)	312,00.20	33.37	29.08
33	(6)	68.50	(5)	311,98.45	34.40	29.95
34	(2)	65.80	(1*m*)	96.67	35.41	30.87
35	(6)	63.04	(5*dd*)	94.78	36.43	31.74
36	(3)	60.24	(2*m*)	92.87	37.41	32.63
37		57.37	(5)	90.90	38.42	33.53
38	(2)	54.45	(2)	88.83	39.52	34.38
39	(6)	51.38	(5)	86.72	40.50	35.34
40	(3)	48.33	(2)	84.52	41.54	36.19
41	(6)	45.18	(5)	82.26	42.55	37.08
42	(3)	41.97	(2)	79.94	43.58	37.97
43	(6)	38.68	(6)	77.55	44.57	38.87
44	(1*dd*)	35.37	(2)	75.07	45.61	39.70
45	(8*d*)	31.94	(6)	72.55	46.61	40.61
46	(3*m*)	28.46	(2)	69.95	47.63	41.49
47	(5)	24.92	(6)	67.29	48.74	42.37
48	(3)	21.21	(2)	64.56	49.70	43.35
49	(6*m*)	17.59	(6*dd*)	61.79	50.68	44.20
50	(1)	13.88	(2)	58.88	51.75	45.00
51	(5)	10.04	(5)	56.10	52.74	46.06
52	(1)	06.14		—	53.78	
53	(5)	311,02.32	(5)	49.96		47.64
54	(1*m*)	310,98.33	(2)	46.82	55.85	48.49
55	(8*d*)	94.11	(5)	43.63	56.80	49.52
56	(1)	90.02	(2)	40.35	57.82	50.33
57	(6)	85.81	(3*dd*)	37.00	58.74	51.19
58	(2*d*)	81.61			59.82	
59	(4)	77.18				
(9,29) ν_{head} = 30792.6 cm⁻¹						
9	(1*m*)	307,83.97	(5*d*)	307,92.61		8.64
10					10.88	
11	(2)	81.73	(2*dd*)	92.12		10.49
12					12.86	
13	(4)	79.26	(3)	91.37		12.11
14					14.89	
15	(3)	76.48	(6)[3]	90.33		13.85
16					17.00	
17	(2)	73.33	(6)[3]	90.33		17.00
18					19.05	
19	(7)[2]	71.28	(4)	88.38		17.10
20			(2*d*)	87.55	21.09	
21	(2*m*)	67.29	(4)	86.61	22.14	19.32
22	(1)	65.41	(1*m*)	85.63	23.15	20.22
23	(2)	63.46	(4)	84.65	24.15	21.19
24	(1)	61.48	(0)	83.62	25.18	22.14
25	(5*d*)	59.47	(4)	82.46	26.23	22.99
26	(1)	57.39	(1*m*)	81.27	27.25	23.88
27	(4)	55.21	(4*d*)	79.98	28.26	24.77
28	(1)	53.01			29.25	
29	(4)	50.73	(4)	77.35		26.62
30	(1*d*)	48.48	(1)	75.94	31.31	27.46
31	(4)	46.04	(3)	74.43	32.35	28.39
32	(1)	43.59	(1)	72.90	33.38	29.31
33	(5)	41.05	(7)[3]	71.28	34.39	30.23
34	(3)	38.51	(1*dd*)	69.72	35.45	31.21
35	(4)	35.83	(3)	67.85	36.58	32.02
36	(2)	33.14	(2)	66.05	37.48	32.91
37	(5)	30.37	(3)	64.17	38.46	33.80
38	(3)	27.59	(1)	62.24	39.51	34.65
39	(5)	24.66	(4)	60.23	40.52	35.57
40	(1)	21.72	(1)	58.18	41.55	36.46
41	(5)	18.68	(4)	56.05	42.57	37.37
42	(2)	15.61	(1)	53.85	43.60	38.24
43	(5)	12.45	(4)	51.61	44.59	39.16
44	(2)	09.26	(1*mm*)	49.32	45.62	40.06
45	(4)	05.99	(4)	46.93	46.67	40.94
46	(2)	307,02.65	(1)	44.49	47.68	41.74

TABLE I.—*Continued.*

J.	P(cm⁻¹)		R(cm⁻¹)		$\Delta_2F''(J)$ (cm⁻¹)	$\Delta_2F'(J)$ (cm⁻¹)
			(9,29) ν_{head} =30792.6 cm⁻¹.—*Continued*			
47	(4)	306,99.25	(5)	307,41.98	48.68	42.73
48	(1)	95.81	(1)	39.40	49.67	43.59
49	(4)	92.31	(4)	36.77	50.69	44.46
50	(2)	88.71	(1)	34.06	51.71	45.35
51	(4)	85.06	(4)	31.32	52.72	46.26
52	(3)	81.34	(2)	28.49	53.75	47.15
53	(4)	77.57	(4)	25.61	54.75	48.04
54	(2)	73.74	(1)	22.66	55.77	48.92
55	(4)	69.84	(4)	19.64	56.77	49.80
56	(1)	65.89	(3)	16.51	57.79	50.62
57	(4)	61.85	(4)	13.39	58.77	51.54
58	(1)	57.74	(1*d*)	10.19	59.81	52.45
59	(4)	53.58	(3)	06.89	60.80	53.31
60	(1)	49.39	(1)	03.54	61.84	54.15
61	(3)	45.05	(3)	307,00.09	62.85	55.04
62	(1)	40.69	(1)	306,96.56	63.85	55.87
63	(4)	36.24	(3)	92.81	64.88	56.57
64	(1)	31.68			65.90	
65	(4)	26.91	(3)	86.62		59.71
66					67.86	
67	(4*m*)	18.76	(3)	78.62		59.86
68					69.85	
69	(5)	306,08.77	(3)	70.95		62.18
70					71.78	
71	(1*mm*)	305,99.17	(3)	62.84		63.67
72					73.91	
73	(3)	88.93	(3)	54.51		65.58
74					76.01	
75	(5*d*)	78.50	(2)	45.90		67.40
76					77.74	
77	(1*mm*)	68.16				
78						
			(9,28) ν_{head} =31396.9 cm⁻¹			
9	(6)[2]	313,88.11	(4*dd*)	313,96.85		8.74
10					11.07	
11	(6*d*)[2]	85.78	(1*m*)	96.24		10.46
12					13.06	
13	(6*d*)[2]	83.18	(3)	95.45		12.27
14					15.14	
15	(6*d*)[2]	80.31	(6*d*)[2]	94.23		13.92
16					17.10	
17	(5)[2]	77.13	(6*d*)[2]	94.23		17.10
18					19.09	
19	(1*mm*)	75.14	(6*d*)	92.04		16.90
20			(2*d*)	91.14	21.15	18.32
21	(5)	70.89	(6)	90.20	22.21	19.31
22	(2)	68.93	(3)	89.17	23.31	20.24
23	(6)	66.89	(6)[2]	88.11	24.32	21.22
24	(2)	64.85	(1*d*)	87.04	25.38	22.19
25	(6)	62.73	(6*d*)[2]	85.78	26.51	23.05
26	(1)	60.53	(1*d*)	84.55	27.48	24.02
27	(6)	58.30	(6*d*)[2]	83.18	28.61	24.88
28	(2*d*)	55.94	(3*d*)	81.92	29.57	25.98
29	(6)	53.61	(6*d*)[2]	80.31	30.68	26.70
30	(2)	51.24	(3)	78.80	31.61	27.56
31	(6)	48.70	(5)[2]	77.13	32.66	28.43
32	(2)	46.14	(1*mm*)	75.35	33.62	29.21
33	(6)	43.51	(4)	73.71	34.54	30.20
34	(2)	40.81	(1*m*)	71.89	35.66	31.08
35	(6)	38.05	(6)	70.04	36.67	31.99
36	(2)	35.22	(3*d*)	68.14	37.71	32.92
37	(6)	32.33	(6)	66.10	38.77	33.77
38	(2)	29.37	(3)	64.04	39.76	34.67
39	(6)	26.34	(6)	61.91	40.77	35.57
40	(2)	23.27	(1)	59.72	41.82	36.45
41	(9)	20.09	(6*d*)	57.48	42.85	37.39
42	(2)	16.87	(2)	55.14	43.90	38.27
43	(6)	13.58	(6)	52.72	44.93	39.14
44	(2)	10.21	(2)	50.26	45.93	40.05
45	(6)	06.79	(6)	47.74	46.93	40.95
46	(2)	313,03.33	(2*dd*)	45.03	47.99	41.70
47	(7)	312,99.75	(6)	42.48	48.90	42.73
48	(2*d*)	96.13	(2)	39.74	50.04	43.61
49	(6)	92.44	(6)	36.94	51.04	44.50
50	(2)	88.70	(2)	34.07	52.07	45.37
51	(6)	84.87	(5)	31.14	53.12	46.27
52	(2)	80.95	(1*m*)	28.13	54.14	47.18
53	(7)	77.00	(6)	25.07	55.17	48.07
54	(2)	72.96	(2)	21.93	56.18	48.97
55	(7)	68.89	(6)	18.68	57.17	49.79
56	(1)	64.76	(2)	15.41	58.19	50.65
57	(6)	60.49	(6)	12.07	59.19	51.58
58	(1)	56.22	(1*m*)	08.67	60.22	52.45
59	(6)	51.85	(4)	05.17	61.24	53.32
60	(2)	47.43	(2)	313,01.58	62.29	54.15
61	(6)	42.88	(6)	312,97.94	63.28	55.06
62	(1)	38.30	(2*dd*)	94.24	64.30	55.94
63	(6)	312,33.64	(6)	312,90.19	65.37	56.55
64	(1)	28.87			66.31	
65	(6)	23.88	(4)	83.60		59.72
66					68.38	
67	(5*m*)[2]	15.22	(5)	75.11		59.89
68					70.25	
69	(5*dd*)[2]	312,04.86	(5)	66.95		62.09
70					72.37	
71	(1*dd*)	311,94.58	(3)	58.39		63.81
72					74.42	
73	(3)	83.97	(5)	49.56		65.59
74					76.44	
75	(3)	73.12	(2)	40.45		67.33
76					78.55	
77	(1*dd*)	61.90				
			(8,28) ν_{head} =30963.6 cm⁻¹			
9	(1*d*)	309,54.99	(4*d*)	309,63.69		8.70
10					10.95	
11	(2*m*)	52.74	(1*mm*)	63.29		10.55
12					12.99	
13	(2)	50.30	(2)	62.59		12.29
14	(0)	48.96			15.03	
15	(2*d*)	47.56	(4)	61.70		14.14
16	(0)	46.09			17.12	
17	(3)	44.58	(3)	60.51		15.93
18	(1*d*)	43.01	(00)	59.78	19.14	16.77
19	(3)	41.37	(3)	59.10	20.11	17.73
20	(0)	39.67	(0)	58.27	21.24	18.60
21	(3)	37.86	(3)	57.47	22.23	19.61
22	(0)	36.04	(0)	56.52	23.31	20.48
23	(3)	34.16	(3)	55.51	24.33	21.35
24	(2)	32.19	(0)	54.51	25.32	22.32
25	(3*d*)	30.19	(3)	53.37	26.38	23.18
26	(0)	28.13	(2)	52.20	27.42	24.07
27	(3)	25.95	(3)	50.98	28.45	25.03
28	(1)	23.75	(0)	49.67	29.49	25.92
29	(3*m*)	21.49	(3)	48.30	30.51	26.81
30	(1)	19.16	(1*d*)	46.85	31.54	27.69
31	(3)	16.76	(4)	45.35	32.54	28.59
32	(1*d*)	14.31	(1*d*)	43.80	33.58	29.49
33	(3)	11.77	(4)	42.22	34.61	30.45
34	(1*d*)	09.19	(1*d*)	40.53	35.68	31.34
35	(4)	06.54	(4)	38.77	36.71	32.23
36	(1)	03.82	(1*d*)	36.98	37.71	33.16
37	(4)	309,01.06	(3)	35.09	38.77	34.03
38	(1)	308,98.21	(1*d*)	33.17	39.78	34.96
39	(4)	95.31	(3)	31.14	40.81	35.83
40	(1*d*)	92.36	(1)	29.10	41.81	36.74
41	(4)	89.33	(3)	26.97	42.87	37.64
42	(1)	86.23	(1*d*)	24.78	43.88	38.55
43	(4)	83.09	(3)	22.53	44.92	39.44
44	(2)	79.86	(1*d*)	20.20	45.95	40.34
45	(4)	76.58	(3)	17.81	46.96	41.23
46	(1)	73.24	(0)	15.36	48.00	42.12
47	(3)	69.81	(3)	12.85	48.94	43.04
48	(1*d*)	66.42	(1*dd*)	10.26	50.03	43.84
49	(4)	62.82	(3)	07.63	51.05	44.81
50	(1)	59.21	(2)	04.92	52.08	45.71
51	(4)	55.55	(3)	309,02.15	53.09	46.60
52	(1)	51.83	(1*d*)	308,99.30	54.13	47.47
53	(4)	48.02	(3)	96.41	55.12	48.39
54	(1)	44.18	(1*d*)	93.45	56.16	49.27
55	(4)	40.25	(4)	90.38	57.20	50.13
56	(1)	36.25	(0*m*)	87.31	58.20	51.06
57	(4)	32.18	(3)	84.08	59.26	51.90
58	(1)	28.05	(1)	80.83	60.23	52.78
59	(3)	23.85	(4)	77.48	61.27	53.63
60	(1)	19.56	(0)	74.00	62.28	54.44
61	(4)	15.20	(2)	70.40	63.28	55.20
62	(0)	10.72			64.31	
63	(3)	308,06.09	(2)	61.88		55.79
64					66.35	
65	(3)	307,95.53	(3)	58.03		62.50
66					68.41	
67	(2*dd*)	89.62	(2)	49.69		60.07
68					70.43	
69	(4)	79.26	(2)	42.72		63.46
70					72.37	
71	(1*d*)	70.35	(2)	34.02		63.67
72					74.55	
73	(5*d*)	59.47	(1)	25.97		66.50
74					76.40	
75	(0)	49.57	(2)	16.99		67.42
76					78.48	
77	(3)	38.51	(2)	308,08.09		69.58
78					80.50	
79	(3)	27.59	(2)	307,98.94		71.35

TABLE I.—*Continued.*

J.	P(cm⁻¹)		R(cm⁻¹)		$\Delta_2F''(J)$ (cm⁻¹)	$\Delta_2F'(J)$ (cm⁻¹)
	(8,27) ν_{head} = 31574.4 cm⁻¹					
9	(1*d*)	315,65.63	(4*d*)	315,74.50		8.87
10	(0*dd*)[1]	64.54			11.05	
11	(1*dd*)	63.45	(1*m*)	73.94		10.49
12	(0)	62.26			13.02	
13	(1*mm*)	60.92	(3)	73.25		12.33
14	(0)	59.62			15.15	
15	(1)	58.10	(4)	72.24		14.14
16	(0)	56.63			17.24	
17	(2)	55.00	(4)	70.98		15.98
18	(0)	53.42	(0*d*)	70.13	19.31	16.71
19	(2)	51.67	(4)	69.47	20.21	17.80
20	(0)	49.92	(1*d*)	68.64	21.40	18.72
21	(3)	48.07	(4*d*)	67.66	22.46	19.59
22	(0)	46.18	(1*d*)	66.63	23.45	20.45
23	(3)	44.21	(4*d*)	65.59	24.47	21.38
24	(1)	42.16	(0*dd*)[1]	64.54	25.52	22.38
25	(4)	40.07	(4*d*)	63.23	26.65	23.16
26	(1*d*)	37.89	(0)	61.93	27.57	24.04
27	(4)	35.66	(3)	60.64	28.57	24.98
28	(1)	33.36	(0)	59.27	29.65	25.91
29	(4)	30.99	(3)	57.79	30.72	26.80
30	(1)	28.55	(1)	56.28	31.75	27.73
31	(4)	26.04	(3)	54.67	32.80	28.63
32	(1*m*)	23.48	(1)	53.02	33.82	29.54
33	(4)	20.85	(3)	51.22	34.90	30.37
34	(1*mm*)	18.12	(1)	49.47	35.87	31.35
35	(4)	15.35	(4)	47.59	36.93	32.24
36	(1)	12.54	(0)	45.68	37.96	33.14
37	(4)	09.63	(4)	43.65	39.02	34.02
38	(1*mm*)	06.66	(1)	41.58	40.00	34.92
39	(5)	03.65	(4)	39.46	41.06	35.81
40	(1)	315,00.52	(1)	37.26	42.09	36.74
41	(5)	314,97.37	(4)	35.00	43.15	37.63
42	(2)	94.11	(1)	32.66	44.17	38.55
43	(5)	90.83	(4)	30.27	45.21	39.44
44	(1*d*)	87.45	(1)	27.78	46.24	40.33
45	(5)	84.03	(4)	25.26	47.23	41.23
46	(2)	80.55	(1)	22.63	48.29	42.08
47	(5)	76.97	(4)	19.99	49.30	43.02
48	(1*d*)	73.33	(1)	17.23	50.37	43.90
49	(5)	69.62	(4)	14.43	51.32	44.81
50	(4)[1]	65.91	(1)	11.56	52.42	45.65
51	(3*m*)	62.01	(4)	08.62	53.52	46.61
52	(3)	58.04	(1)	05.59	54.50	47.55
53	(4)	54.12	(4)	315,02.52	55.52	48.40
54	(2)	50.07	(1*d*)	314,99.37	56.56	49.30
55	(3)	45.96	(4)	96.11	57.60	50.15
56	(2)	41.77	(1)	92.81	58.58	51.04
57	(5)	37.53	(4)	89.40	59.61	51.87
58	(1*m*)	33.20	(1)	85.95	60.61	52.75
59	(5)	28.79	(4)	82.40	61.67	53.61
60	(1)	24.28	(1)	78.73	62.71	54.45
61	(5)	19.69	(4)	74.90	63.74	55.21
62	(1)	14.99			64.74	
63	(5)	314,10.16	(4)[1]	65.91		55.75
64					66.81	
65	(7*d*)[1]	313,99.10	(2*mm*)	61.70		62.60
66			(1*m*)	57.21	68.83	
67	(3*dd*)[1]	92.87	(2)	52.86	69.96	59.99
68	(0)	87.25			70.94	
69	(3*d*)[1]	81.92	(2)	45.46		63.54
70					72.85	
71	(1*mm*)	72.61	(3)	36.24		63.63
72			(0)	31.75	74.93	
73	(1)	61.31	(2)	27.73		66.42
74			(0)	22.79	76.96	
75	(2)	50.77	(3)	18.19		67.42
76			(0)	13.53	78.97	
77	(2)	39.22	(2)	314,08.76	79.99	69.54
78	(1*m*)	33.54			81.00	
79	(1*m*)	27.76	(7*d*)[1]	313,99.10		71.34
	(7,24) ν_{head} = 33008.0 cm⁻¹					
9	(0)	329,99.45	(2*dd*)	330,08.32		8.87
10					11.35	
11	(1)	96.97	(1*mm*)	07.60		10.63
12					13.35	
13	(1*m*)	94.25	(2)	06.59		12.34
14					15.42	
15	(2*m*)	91.17	(3)	05.39		14.22
16					17.53	
17	(3)	87.86	(3*m*)	03.92		16.06
18					19.70	
19	(3)	84.22	(2)	02.12		17.90
20					21.78	
21	(3)	80.34	(3)	330,00.05		19.71
22					23.92	

J.	P(cm⁻¹)		R(cm⁻¹)		$\Delta_2F''(J)$ (cm⁻¹)	$\Delta_2F'(J)$ (cm⁻¹)
	(7,24) ν_{head} = 33008.0 cm⁻¹.—*Continued*					
23	(3)	329,76.13	(3)	329,97.66		21.53
24					26.02	
25	(3)	71.64	(3)	94.97		23.33
26					28.12	
27	(2*m*)	66.85	(3)	91.98		25.13
28					30.29	
29	(5)[1]	61.69	(3)	88.71		27.02
30					32.33	
31	(3*d*)	56.38	(3)	85.11		28.73
32					34.46	
33	(3)	50.65	(3)	81.21		30.56
34					36.56	
35	(3*d*)	44.65	(3)	76.94		32.29
36					38.68	
37	(3)	38.26	(3)	72.35		34.09
38					40.83	
39	(3)	31.52	(2*m*)	67.28		35.76
40					42.93	
41	(3*m*)	24.35	(5)[1]	61.69		37.34
42					45.14	
43	(3)	16.55	(2*d*)	54.57		38.02
44					47.14	
45	(3)	07.43	(2)	55.54		48.11
46					49.24	
47	(2*m*)	329,06.30	(2)	48.27		41.97
48					51.33	
49	(3)	328,96.94	(3)	41.36		44.42
50					53.49	
51	(3)	87.87	(1)	33.66		45.79
52					55.55	
53	(3)	78.11	(2)	28.80		50.69
54					57.66	
55	(2)	71.14	(3)	21.20		50.06
56					59.74	
57	(2)	61.46	(3)	13.62		52.16
58					61.84	
59	(3)	51.78	(2*m*)	329,05.68		53.90
60					63.91	
61	(2)	41.77	(3)	328,97.85		56.08
62					66.02	
63	(3)	31.83	(3)	89.48		57.65
64					68.09	
65	(3)	21.39	(3)	80.86		59.47
66						
67			(2*m*)	71.91		
68						
69			(2)	62.68		
70						
71			(2)	53.14		
72						
73			(2)	43.33		
74						
75			(2)	33.15		
76						
77			(2*d*)	22.75		
	(7,23) ν_{head} = 33644.8 cm⁻¹					
9	(3*m*)[1]	336,35.94	(2*dd*)	336,44.85		8.91
10					11.43	
11	(4)[1]	33.42	(1*mm*)	44.00		10.58
12					13.46	
13	(4)[1]	30.54	(2)	42.99		12.45
14					15.59	
15	(4)[1]	27.40	(3)	41.66		14.26
16					17.70	
17	(5)[1]	23.96	(4)	40.07		16.11
18					19.87	
19	(6)[1]	20.20	(3)	38.16		17.96
20					21.99	
21	(7)[1]	16.17	(3*m*)[1]	35.94		19.77
22					24.07	
23	(2*mm*)	11.87	(4)[1]	33.42		21.55
24					26.15	
25	(2)	07.27	(4)[1]	30.54		23.27
26					28.25	
27	(2)	336,02.29	(4)[1]	27.40		25.11
28					30.38	
29	(3)	335,97.02	(5)[1]	23.96		26.94
30					32.57	
31	(3)	91.39	(6)[1]	20.20		28.81
32					34.73	
33	(3)	85.47	(7)[1]	16.17		30.70
34					36.96	
35	(3)	79.21	(2*mm*)	11.54		32.33
36					39.02	
37	(5)	72.52	(2*m*)	06.75		34.23
38					40.95	

TABLE I.—*Continued.*

J.	*P*(cm⁻¹)		*R*(cm⁻¹)		$\Delta_2F''(J)$ (cm⁻¹)	$\Delta_2F'(J)$ (cm⁻¹)
	(7,23) ν_{head} =33644.8 cm⁻¹.—*Continued*					
39	(5*dd*)[1]	335,65.80	(2)	336,01.39		35.59
40					43.21	
41	(3)	58.18	(2)	335,95.38		37.20
42					45.27	
43	(3)	50.11	(2*dd*)[2]	88.51		38.40
44					47.75	
45	(3*d*)	40.76	(2)[2]	88.51		47.75
46					49.21	
47	(3)	39.30	(2)	81.23		41.93
48					51.71	
49	(3)	29.52	(3*d*)	73.98		44.46
50					53.79	
51	(3)	20.19	(5)[2]	65.80		45.61
52					55.76	
53	(2*mm*)	10.04	(3)	60.72		50.68
54					57.98	
55	(3)	335,02.74	(3)	52.79		50.05
56					60.05	
57	(4)	334,92.74	(3)	44.78		52.04
58					62.15	
59	(3)	82.63	(2)	36.54		53.91
60					64.31	
61	(3)	72.23	(1*m*)	28.29		56.06
62					66.49	
63	(3)	61.80	(2)	19.50		57.70
64					68.54	
65	(3)	50.96	(2*dd*)	10.30		59.34
66						
67			(2*d*)	335,00.92		
68						
69			(2)	334,91.39		
70						
71			(2)	81.40		
72						
73			(2)	71.08		
74						
75			(2*d*)	60.31		
76						
77			(2*dd*)	49.32		
	(6,23) ν_{head} =33204.3 cm⁻¹					
9			(4*dd*)	332,03.52		
10					11.75	
11	(1*mm*)	331,91.77	(3*m*)	02.80		11.03
12					13.34	
13	(3)	89.46	(2*dd*)	01.66		12.20
14					15.26	
15	(3*m*)	86.40	(2)	332,00.70		14.30
16					17.58	
17	(2*d*)	83.12	(3)	331,99.21		16.09
18					19.77	
19	(3)	79.44	(4)	97.40		17.96
20					21.89	
21	(3)	75.51	(4)	95.38		19.87
22					24.06	
23	(3*m*)	71.32	(4)	93.02		21.70
24					26.18	
25	(3)	66.84	(5)	90.28		23.44
26					28.21	
27	(3)	62.07	(4*d*)	87.34		25.27
28					30.39	
29	(4)	56.95	(5)	84.13		27.18
30					32.54	
31	(4*m*)	51.59	(7*d*)	80.60		29.01
32					34.65	
33	(3)	45.95	(5*m*)	76.82		30.87
34					36.79	
35	(3)	40.03	(4)	72.70		32.67
36					38.98	
37	(4)	33.72	(3)	68.29		34.57
38					41.08	
39	(3)	27.21	(4)	63.57		36.36
40					43.20	
41	(5)	20.37	(3*m*)	58.58		38.21
42					45.33	
43	(3)	13.25	(3*m*)	53.27		40.02
44					47.51	
45	(5*d*)	331,05.76	(5)	47.63		41.87
46					49.52	
47	(3)	330,98.11	(3)	41.78		43.67
48					51.67	
49	(3)	90.11	(3)	35.56		45.45
50					53.76	
51	(4)	81.80	(3)	29.06		47.26
52					55.87	
53	(3)	73.19	(3*d*)	22.26		49.07
54					57.97	

J.	*P*(cm⁻¹)		*R*(cm⁻¹)		$\Delta_2F''(J)$ (cm⁻¹)	$\Delta_2F'(J)$ (cm⁻¹)
	(6,23) ν_{head} =33204.3 cm⁻¹.—*Continued*					
55	(3)	330,64.29	(3*m*)	331,15.18		50.89
56					60.09	
57	(3)	55.09	(3)	07.77		52.68
58					62.24	
59	(3*m*)	45.53	(3)	331,00.05		54.52
60					64.58	
61	(1*mm*)	35.47	(3)	330,92.00		56.53
62					66.42	
63	(3)[2]	25.58	(3)	83.67		58.09
64					68.53	
65	(3)[2]	15.14	(2)	74.95		59.81
66						
67			(2)	65.90		
68						
69			(2)	56.41		
70						
71			(2*m*)	46.42		
72						
73			(1*mm*)	35.70		
74						
75			(3)[2]	25.58		
76						
77			(3)[2]	15.14		
	(6.21) ν_{head} =34496.1 cm⁻¹					
15	(1)	344,78.19	(3)	344,92.55		14.36
16					17.86	
17	(2)	74.69	(2)	90.87		16.18
18					20.05	
19	(2)	70.82	(2)	88.81		17.99
20					22.15	
21	(2)	66.66	(4)	86.50		19.84
22					24.35	
23	(2*m*)	62.15	(4)	83.83		21.68
24					26.49	
25	(2)	57.34	(2*mm*)	80.86		23.52
26					28.68	
27	(3*d*)	52.18	(2)	77.57		25.39
28					30.74	
29	(3*d*)	46.83	(4*m*)	73.91		27.08
30					32.91	
31	(3)	41.00	(3)	70.02		29.02
32					35.06	
33	(3)	34.96	(3)	65.76		30.80
34					37.24	
35	(3)	28.52	(3*m*)	61.20		32.68
36					39.39	
37	(3)	21.81	(4*m*)	56.33		34.52
38					41.51	
39	(4)	14.82	(2)	51.09		36.27
40					43.69	
41	(3)	344,07.40	(3)	45.59		38.19
42					45.87	
43	(3)	343,99.72	(2*m*)	39.72		40.00
44					48.01	
45	(4*d*)	91.71	(2)	33.53		41.82
46					50.14	
47		83.39	(2)	27.06		43.67
48					52.31	
49	(2)	74.75	(4)	20.25		45.50
50					54.48	
51	(4)	65.77	(2)	13.09		47.32
52					56.62	
53	(4)	56.47	(2)	344,05.54		49.07
54					58.69	
55	(4)	46.85	(3*d*)	343,97.63		50.78
56					60.74	
57	(4)	36.89	(2)	89.59		52.70
58					62.99	
59	(2)	26.60	(2)	81.12		54.52
60					65.13	
61	(2)	15.99	(2)	72.33		56.34
62						
63			(2*m*)	63.11		
64						
65			(1*m*)	53.52		
66						
67			(2)	43.69		
68						
69			(1)	33.19		
70						
71			(1)	22.32		

TABLE I.—*Continued.*

J.	P(cm⁻¹)		R(cm⁻¹)		$\Delta_2F''(J)$ (cm⁻¹)	$\Delta_2F'(J)$ (cm⁻¹)
	(5,21) ν_{head} = 34047.6 cm⁻¹					
13	(1*d*)	340,32.21	(1)	340,44.74	15.66	12.53
14						
15	(1*mm*)	29.08	(1*d*)	43.09	18.00	14.01
16						
17	(1*mm*)	25.09	(1)	41.38	20.01	16.29
18						
19	(1*m*)	21.37	(2*d*)	39.09	22.26	17.72
20						
21	(4)	16.83	(4)²	36.46	24.39	19.63
22						
23	(2)	12.07	(2)	33.18	26.65	21.11
24						
25	(8)²	06.53	(1*mm*)	29.45	28.66	22.92
26						
27	(1*m*)	340,00.79	(1*mm*)	25.09	30.82	24.30
28						
29	(2*d*)	339,94.27	(4)²	36.46	32.70	42.19
30						
31	(1*dd*)	340,03.76	(1*d*)	30.94	35.04	27.18
32						
33	(1)	339,95.90	(2)	25.45	37.27	29.55
34						
35	(1)	88.18	(3)	19.75	39.40	31.57
36						
37	(1*mm*)	80.35	(4)²	13.62	41.46	33.27
38						
39	(2)	72.16	(4)²	13.62	43.71	41.46
40						
41	(1)	69.91	(8)²	340,06.53	45.92	36.62
42						
43	(1)	60.61	(2)	339,99.85	47.98	39.24
44						
45	(3)	51.87	(2*m*)	93.41	50.11	41.54
46						
47	(3)	43.30	(4)	86.73	52.27	43.43
48						
49	(2*m*)	34.46	(2)	79.84	54.56	45.38
50						
51	(5)²	25.28	(2)	73.63	56.62	48.35
52						
53	(2)	17.01	(2)	66.07	58.78	49.06
54						
55	(1*m*)	339,07.29	(2)	58.42	60.84	51.13
56						
57	(1*mm*)	338,97.58	(3)	50.55	62.94	52.97
58						
59	(1*mm*)	87.61	(2)	42.38	65.09	54.77
60						
61	(1*mm*)	77.29	(2*m*)	34.03	67.31	56.74
62						
63	(1*mm*)	66.72	(5)²	25.28	69.38	58.56
64						
65	(1)	55.90	(2)	16.22		60.32

J.	P(cm⁻¹)		R(cm⁻¹)		$\Delta_2F''(J)$ (cm⁻¹)	$\Delta_2F'(J)$ (cm⁻¹)
	(5,20) ν_{head} = 34703.0 cm⁻¹					
9			(3*m*)	347,02.90	11.49	
10						
11	(1*mm*)	346,91.41	(1*m*)	01.41	13.48	10.00
12						
13	(5*dd*)²	87.93	(2)	347,00.21	15.99	12.28
14						
15	(3*d*)²	84.22	(2)	346,98.59	17.92	14.37
16						
17	(1*dd*)	80.67	(3)	96.66	20.12	15.99
18						
19	(3)	76.54	(2)	94.24	22.27	17.70
20						
21	(2)	71.97	(1*mm*)²	91.41	24.35	19.44
22						
23	(7)	67.06	(5*dd*)²	87.93	26.44	20.87
24						
25	(2)	61.49	(3*d*)²	84.22	28.82	22.73
26						
27	(2)	55.40	(4)²	79.49	30.89	24.09
28						
29	(2)	48.60	(3*d*)	90.89	33.08	42.29
30						
31	(1)	57.81	(2*m*)	85.16	35.26	27.35
32						
33	(2)	49.90	(4)²	79.49	37.50	29.59
34						
35	(3)	41.99	(3)	73.55	39.64	31.56
36						
37	(3)	33.91	(7)²	67.06	41.81	33.15
38						
39	(5)²	25.25	(7)²	67.06	44.13	41.81
40						
41	(3)	22.93	(1*m*)	59.53	46.21	36.60
42						
43	(4)	13.32	(2*m*)	52.64	48.32	39.32
44						
45	(3)	346,04.32	(4)	45.87	50.47	41.55
46						
47	(4)	345,95.40	(4)	38.94	52.61	43.54
48						
49	(3)	86.33	(3)	31.67	54.81	45.34
50						
51	(3)	76.86	(5)²	25.25	57.02	48.39
52						
53	(3)	68.23	(4*mm*)	17.20	59.16	48.97
54						
55	(4*d*)	58.04	(3*m*)	09.27	61.25	51.23
56						
57	(4)	48.02	(4)	346,01.03	63.39	53.01
58						
59	(4)	37.64	(2)	345,92.46	65.46	54.82
60						
61	(3)	27.00	(3)	83.66	67.63	56.66
62						
63	(4)	16.03	(2)	74.52	69.76	58.49
64						
65	(4)	04.76	(3)	64.99		60.23

λ3350A and λ3028A. Using a corning glass "Purple Corex A No. 9863" filter, third-order spectrograms were obtained for bands between λ3093A and λ2800A. The exposure time was 2–3 hours. In the third- and fourth-order spectrograms the much higher dispersion of 0.85A/mm and 0.65A/mm, respectively, were obtained. The grating was very successfully mounted according to a method described by Naudé.[10]

C. ROTATIONAL ANALYSIS

The analyses of several bands, which were made by previous investigators, were extended and a large number of bands were analyzed for the first time. The rotational analysis and the combination differences of some of these bands are given in Table I. The number in brackets before each wave number gives the visual estimation of the intensity of the line on the photographic plate. When the line is broad or diffuse, probably caused by the superposition of two or more lines, a "*d*" is added to the intensity (e.g., 1*d*). Lines which were difficult to measure are indicated with an "*m*" (e.g., 2*m*). The superscript outside the bracketed number gives the number of lines to which the same wave number was ascribed, if more than one. For some bands

[10] S. M. Naudé, South African J. Sci. 41, 128 (1945).

TABLE II. Rotational constants of the electronic states.

v'	B'_v(cm^{-1})	v''	B''_v(cm^{-1})	v''	B''_v(cm^{-1})
3	0.2359_8	16	0.2783_5	25	0.2639_1*
4	0.2341_7	17	0.2769_8*	26	0.2619_8*
5	0.2321_9	18	0.2753_6	27	0.2604_3
6	0.2308_2	20	0.2720_5*	28	0.2587_7
7	0.2289_2*	21	0.2704_8	29	0.2566_8
8	0.2275_3	22	0.2686_8	30	0.2552_3
9	0.2258_6	23	0.2670_7	31	0.2535_5
10	0.2242_3	24	0.2655_4*	32	0.2516_6
11	0.2227_2				

the weak lines were so weak that they could not be accurately measured. For this reason the weak lines are excluded from the analysis of several bands.

Rotational Constants

When the new quantum theory is applied to a molecule with zero-average electronic angular momentum, the following expression for the rotational term value $F(J)$, of the level corresponding to the rotational quantum number J, is obtained:

$$F(J)=B_vJ(J+1)-D_vJ^2(J+1)^2+\cdots, \quad (1)$$

where B_v and D_v are rotational constants. The combination differences are defined as follows:

$$\Delta_2F'(J)=F'(J+1)-F'(J-1)$$
$$=R(J)-P(J),$$

and

$$\Delta_2F''(J)=F''(J+1)-F''(J-1),$$
$$=R(J-1)-P(J+1).$$

Hence, the general expression for the combination differences is:

$$\Delta_2F(J)=4B_v(J+\tfrac{1}{2})+8D_v(J+\tfrac{1}{2})^3+\cdots$$
$$\text{i.e. } 4B_v=\Delta_2F(J)/(J+\tfrac{1}{2})-8D_v(J+\tfrac{1}{2})^2+\cdots. \quad (2)$$

A value of $4B_v$ is obtained by dividing each $\Delta_2F(J)$ obtained from the rotational analysis by $(J+\frac{1}{2})$. Finally the term $8D_v(J+\frac{1}{2})^2$ is subtracted algebraically from the corresponding $\Delta_2F''(J)/(J+\frac{1}{2})$, using approximate D_v-values obtained as indicated by Herzberg.[11] The resulting B_v-values, which were calculated from the most trustworthy combination differences, were then averaged for every vibrational level. In the case of perturbed vibrational levels of the upper electronic state the combination differences which appeared unperturbed were used for the determination of these constants. The rotational constants obtained from unpublished analyses are included in Table II. Those indicated by an asterisk are newly obtained. Applying the method of least squares for the determination of these constants, very good agreement was obtained.

Equilibrium Constants

Corresponding to the equilibrium distance, r_e, of the atoms apart we have the equilibrium constants B_e, I_e, and r_e. Least square solutions were made of the equation:

$$B_v=B_e-\alpha_e(v+\tfrac{1}{2})-\text{constant}\,(v+\tfrac{1}{2})^2+\cdots.$$

For the upper and lower electronic states, respectively, this equation was found to be:

$$B'_v=0.241{,}66-0.001{,}65(v'+\tfrac{1}{2})$$
$$-0.000{,}001{,}1(v'+\tfrac{1}{2})^2+\cdots$$
$$B''_v=0.303{,}27-0.001{,}42(v''+\tfrac{1}{2})$$
$$-0.000{,}005{,}2(v''+\tfrac{1}{2})^2+\cdots.$$

I_e and r_e were calculated from the equations:

$$I_e=(27.994\times10^{-40})/B_e$$

and

$$I_e=\mu r_e^2.$$

The values of the equilibrium constants are tabulated in Table III together with the most reliable values obtained by previous investigators. The results obtained for the lower electronic

TABLE III. Equilibrium constants of the upper and lower electronic states.

Upper $^1\Sigma_u^+$ electronic state				Lower $^1\Sigma_g^+$ electronic state		
Constant	Author	Herzberg and col. (reference 4)	Ashley (reference 6)	Constant	Author	Herzberg and col. (reference 4)
B'_e(cm^{-1})	0.2416_8	0.2415	0.2415_1	B''_e(cm^{-1})	0.3032_7	0.3031
α'_e(cm^{-1})	0.00165	0.00153	0.00164	α''_e(cm^{-1})	0.00142	0.00138
I'_e(g cm^2)	115.84×10^{-40}	115.92×10^{-40}		I''_e(g cm^2)	92.31×10^{-40}	92.36×10^{-40}
r'_e(cm)	2.12×10^{-8}	2.123×10^{-8}	2.12×10^{-8}	r''_e(cm)	1.893×10^{-8}	1.895×10^{-8}

[11] G. Herzberg, *Molecular Spectra and Molecular Structure of Diatomic Molecules* (Prentice Hall Inc., New York, 1939).

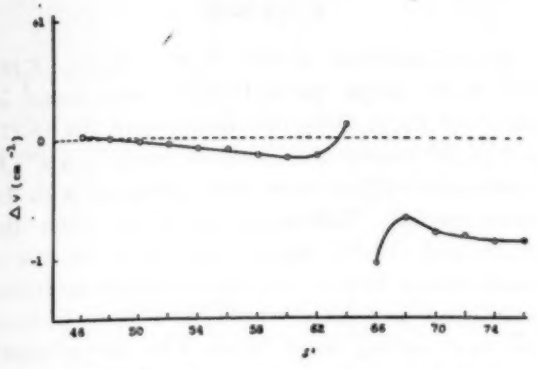

FIG. 3. Rotational perturbations in the $v'=9$ level.

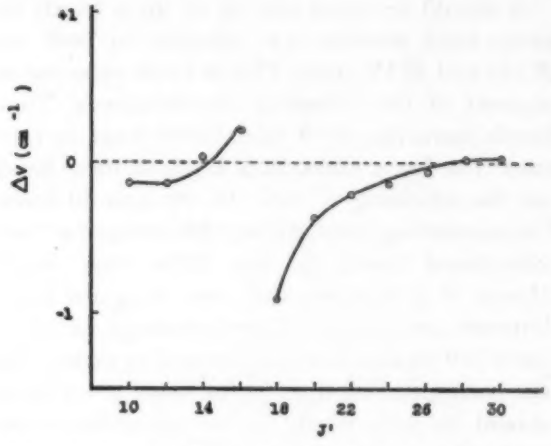

FIG. 4. Rotational perturbations in the $v'=9$ level.

state are not only based on bands of high v''-values but also on bands of low v''-values, which were analyzed by G. Herzberg, L. Herzberg, and Milne.[4]

D. PERTURBATIONS

The author discovered rotational perturbations in all the bands which result from the $v'=9$, 8, 7, and 5 vibrational levels. Hence, perturbations occur in the rotational term series of these vibrational levels of the upper electronic state. Using the high dispersion spectrograms it was possible to determine these perturbations. The perturbed lines were found by using the "unperturbed" $\Delta_2F''(J)$ combination differences obtained from the analysis of other bands which have the same lower vibrational level v''. The validity of an analysis was tested by comparing the "perturbed" $\Delta_2F'(J)$-values, obtained from the analysis with corresponding $\Delta_2F'(J)$-values obtained in the analysis of the bands which have the same perturbed v' vibrational level. In discussions below the J'-values of the perturbed levels will be given. For the purpose of inspecting Table I with reference to perturbations it should be remembered that if, for example, the $J'=6$ rotational level is perturbed then the band lines $P(7)$ and $R(5)$, which result from this upper rotational level, will suffer perturbations of the same sign and magnitude.

TABLE IV. Rotational perturbations of the $v'=9$, 8, 7 and 5 vibrational levels.

	$\Delta\nu$ in cm^{-1}					$\Delta\nu$ in cm^{-1}				
J'	$v'=9$	$v'=8$	$v'=7$	$v'=5$	J'	$v'=9$	$v'=8$	$v'=7$	$v'=5$
10	−0.13	—	—	+5.69	46	+0.02	—	−3.77	−0.37
12	−0.13	—	—	+6.04	48	+0.00	—	−2.48	+0.07
14	+0.03	—	—	+6.10	50	−0.03	—	−1.80	+0.45
16	+0.21	—	—	+6.55	52	−0.05	—	−0.69	−0.27
18	−0.91	—	—	+6.59	54	−0.08	—	−2.70	+0.12
20	−0.37	—	—	+7.01	56	−0.09	+0.02	−2.29	+0.19
22	−0.21	—	—	+7.40	58	−0.14	+0.07	−2.18	+0.20
24	−0.14	—	—	+8.21	60	−0.16	+0.17	−2.03	+0.22
26	−0.07	—	—	+9.03	62	−0.14	+0.47	−2.30	+0.13
28	+0.01	—	—	+10.25	64	+0.11	+2.00	−2.34	+0.06
30	+0.02	—	—	−4.70	66	−1.04	−1.58	−2.39	—
32	—	—	+0.02	−2.86	68	−0.66	−0.73	—	—
34	—	—	+0.05	−1.40	70	−0.78	−1.71	—	—
36	—	—	+0.15	−0.10	72	−0.81	−1.06	—	—
38	—	—	+0.29	+1.30	74	−0.86	−1.43	—	—
40	—	—	+0.59	−3.71	76	−0.86	−1.06	—	—
42	—	—	+1.16	−1.85	78	—	−1.08	—	—
44	—	—	+2.87	−0.85	—	—	—	—	—

$v'=9$ level

The (9,27), (9,28), (9,29), and (9,30) bands were analyzed. Only the (9,29) and (9,28) bands are given in Table I. The $\Delta_2F''(J)$ combination differences were compared with corresponding combination differences obtained from the (8,27), (8,28), (8,29), (10,29), and (10,30) bands. Perturbations, which have a maximum shift at and around the level with $J'=66$ were found. Unfortunately in all these bands the P-branch enters the next strong band head at the position where the strongest perturbations are found (cf. Fig. 2). The high dispersion spectrograms made it possible to adopt the following procedure. The bands, which the perturbed P lines enter, were analyzed. In this way the extra lines, which belong to the perturbed P-series of the previous band, were found. Very often the perturbed P-lines were superimposed on lines of these bands, but it was very convincing to see how "extra" lines were taken up in the analyses. Perturbations were also discovered near the heads of these bands with a maximum shift at $J'=18$.

It should be noted that in all these bands the same wave number was allotted to both the $R(15)$ and $R(17)$ lines. This is to be expected on account of the following circumstances. These bands have the $v'=9$ vibrational level in common. The lower vibrational levels of these bands are the adjoining $v''=27$, 28, 29, and 30 levels. Corresponding combination differences for these vibrational levels do not differ very much. Hence, if it happens that two lines are superimposed, as a result of perturbations, in one of the $v'=9$ bands then it is natural to expect that the corresponding lines in the other $v'=9$ bands should be very nearly if not altogether superimposed.

A feature which was of great importance in the analysis of the system and determining the perturbations was the fact that lines of the two branches of a band often fell together in pairs (cf. Fig. 2).

The unperturbed values of the wave numbers were calculated according to Eq. (1). $\Delta\nu(=\nu_{\text{calculated}}-\nu_{\text{determined}})$ were determined and this is tabulated in Table IV for all the vibrational levels in which perturbations occur. The perturbations in the $v'=9$ level are graphically represented in Figs. 3 and 4.

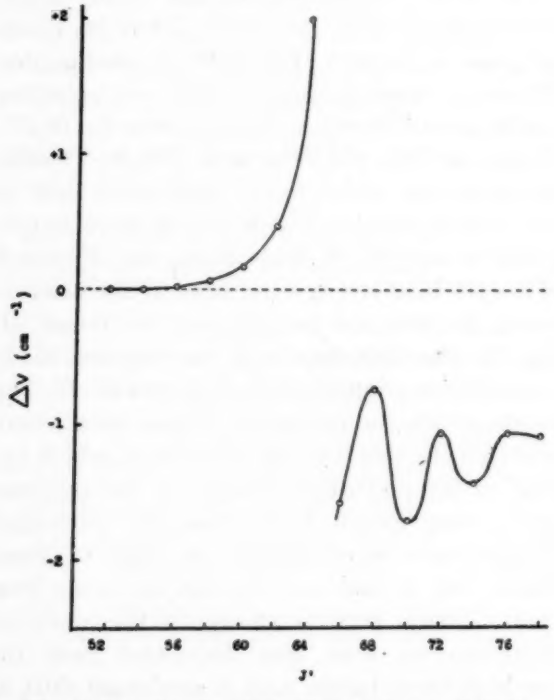

FIG. 5. Rotational perturbations in the $v'=8$ level.

$v'=8$ level

In the analysis of the (8,26), (8,27), (8,28) and (8,29) bands perturbations were found in the $v'=8$ level. Only the analyses of the (8,27) and (8,28) bands are given in Table I. $\Delta_2F''(J)$ combination differences were compared with the corresponding differences obtained from the (9,28) and (10,29) bands. Just as in the case of bands which have $v'=9$, the strongest perturbations occur in a band where the P-branch enters the next strong band head. The perturbations in this level are given in Table IV, and are graphically represented in Fig. 5.

$v'=7$ level

The (7,23) and (7,24) bands are the first bands to be analyzed, which have $v'=7$. Combination differences were also compared with the corresponding differences obtained from the (6,23) band. Strong perturbations were found around the $J'=46$ level. The perturbations are given in Table IV and are graphically represented in Fig. 6.

$v'=5$ level

It was mentioned in Section A that, according to Herzberg, all the bands which have $v'=5$ are vibrationally perturbed. With the object of inspecting the rotational analysis of such bands the (5,20) and (5,21) bands were analyzed. $\Delta_2F''(J)$ combination differences were compared with the corresponding differences obtained from the (6,21) band. The following rotational perturbations were found: perturbations occur around the level $J'=50$, very strong perturbations around the level $J'=40$, and exceptionally strong perturbations around the level $J'=28$. In terms of J'-values the intervals between the levels which suffer maximum perturbation are approximately the same. Here also, as in the case of $v'=9$ bands, the same wave number was ascribed to the lines $R(37)$ and $R(39)$ in both bands. It was assumed that the high quantum number lines ($J'=\pm56$ and higher) were unperturbed because the series could easily be found in this region. Furthermore the B'_v value, calculated from combination differences obtained from these lines, obeyed the linear B'_v-v' relation satisfactorily. On this assumption the perturbation

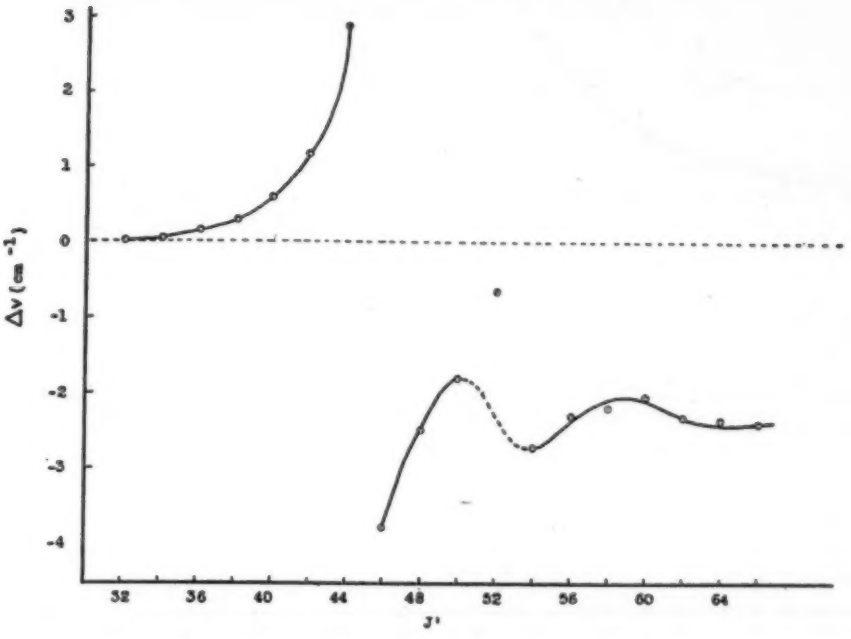

FIG. 6. Rotational perturbations in the $v'=7$ level.

values, given in Table IV were calculated. These are graphically represented in Fig. 7. It is clear from Fig. 7 that the lines near the head of these bands still suffer perturbations of $+6$ cm^{-1}. Herzberg[1] found that the heads of bands which have $v'=5$ are displaced by an amount $+3.2$ cm^{-1}. The present rotational analysis clearly shows, in contradistinction to the conclusions drawn by Rao,[5] that the vibrational perturbation of the bands which result from the $v'=5$ level is caused by rotational perturbations of the lines forming the heads of these bands. The discrepancy, *viz.* that the perturbation value calculated from the rotational analysis is approximately $+6$ cm^{-1}, while Herzberg found it to be 3.2 cm^{-1}, is no doubt explained as follows: The perturbation values given for the $v'=5$ level in Table IV should be considered to be relatively but not absolutely correct, because calculations were made on the assumption that the high quantum number lines are not perturbed. Although the series are normal for these high quantum number lines it is highly probable that all these lines are shifted by a constant amount from their normal positions. According to Figs. 3, 5, and 6 the perturbation does not go back to zero for higher J'-values after the position of maximum perturbation. Hence, according to the classification by Dieke[12] these perturbations should be classified as A-perturbations. If this was true for the other levels it should also be true for the $v'=5$ level. To get Fig. 7 quantitatively correct the zero-axis must therefore be shifted so that the calculated perturbation of approximately $+6$ cm^{-1}, near the heads of the $v'=5$ bands, is decreased to approximately $+3$ cm^{-1}. The unsymmetrical position of the curve, representing the perturbations between $J'=28$ and 38, with respect to the zero axis is possibly explained as being caused by this effect (cf. Fig. 7). Coster and Brons[13] got a perturbation curve for the $v''=1$ level of a CO electronic state, similar to the curve for the $v'=5$ level of P_2.

E. GENERAL DISCUSSION

According to expectation the perturbations increased in a "resonance-like" manner with increasing J', until a maximum value of the perturbation is obtained; then suddenly changes sign and decreases (cf. Figs. 3–7). It is however remarkable that the decrease is not altogether in a resonance-like manner but an oscillatory effect is evident (cf. Figs. 5 and 6, and to a lesser

[12] G. H. Dieke, Phys. Rev. **47**, 870 (1935).
[13] D. Coster and F. Brons, Physica **1**, 155 (1934).

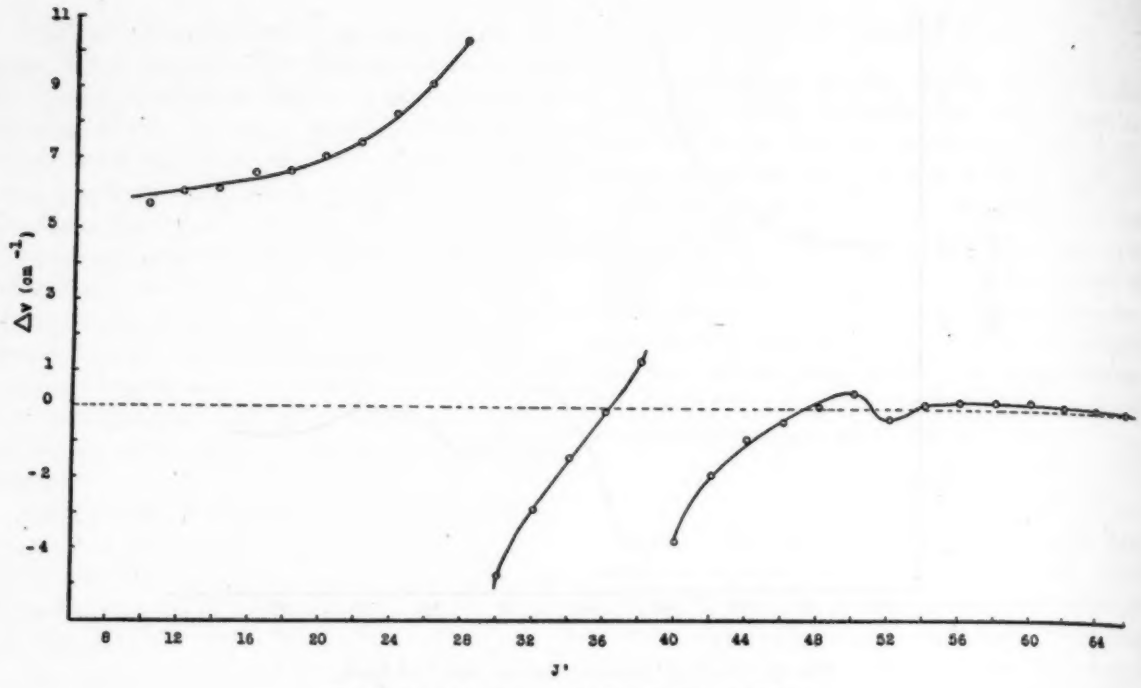

FIG. 7. Rotational perturbations in the $v'=5$ level.

extent Figs. 3 and 7). Perturbations similar to the perturbations in the $v'=8$ and 9 levels also appear in the $v'=4$ level.

F. THE PERTURBING STATE

As was shown above the perturbation of the P_2 molecule does not go back to zero for higher J'-values after the position of maximum perturbation. Hence, according to Kronig, $\Delta\Lambda=\pm1$ for the perturbing state. Because the perturbed state is a $^1\Sigma$ state it is clear that $\Delta\Lambda=-1$. Hence applying the Kronig[14] selection rules in conjunction with this fact the perturbing state must be a $^1\Pi_u$ state. By using the excitation method described in Section B, however, no indication of another band system could be found in the region λ3400A to λ6000A.

G. MISSING LINES

In the analysis of the (10,29), (10,30), and (10,31) bands it was found that the $R(52)$ and $P(54)$ lines were missing. These lines result from the $J'=53$ level in the $v'=10$ vibrational level. In the (11,31) and (11,32) bands not only the $R(28)$ and $P(30)$ lines, which result from the $J'=29$ level, but also the $R(11)$ and $P(13)$ lines, which result from the $J'=12$ level in the $v'=11$ vibrational level, were missing. That these lines were missing was usually quite obvious on the spectrograms. Herzberg was aware of this effect in the $P(13)$ line of the (11,32) band and he indicated this line by the word "*fehlt.*" These might be instances of very strong intensity perturbations.

The author is particularly indebted to Dr. S. M. Naudé,* for the kind interest taken by him in the research, which was conducted under his supervision. The author should like to express his appreciation to the H. B. Webb-Curators and National Research Board for financial assistance.

[14] R. de L. Kronig, Zeits. f. Physik **50**, 347 (1928).

* Now director of the National Physical Laboratory of South Africa.

PHYSICAL REVIEW VOLUME 70, NUMBERS 7 AND 8 OCTOBER 1 AND 15, 1946

On the Deep Configurations of Ti I, Ti II, V II, V III

ABRAHAM MANY
Department of Physics, The Hebrew University, Jerusalem, Palestine

(Received May 13, 1946)

The theoretical formulas for $d^n s^2$, $d^{n+1}s$, d^{n+2} are compared with the experimental data of Ti II, V III, Ti I, V II. In Ti II and V II the agreement is considerably improved by taking into account the interactions between configurations.

INTRODUCTION

IT is a known fact[1] that in the iron group the configurations $3d^n 4s^2$, $3d^{n+1}4s$, $3d^{n+2}$ overlap considerably. As they are all even, their proximity gives rise to strong interactions and we must, therefore, expect a mixing up of the terms and large deviations from the first-order formulas. Consequently the iron group is most suitable for investigating configuration interactions when we confine ourselves to (LS) coupling. On the one hand, in the elements of the preceding periods the distance between configurations of the same parity is comparatively great, so that the interactions are small, and on the other hand, in the succeeding periods the (LS) coupling is increasingly broken down.

As the only detailed studies of these configurations in the iron group are those which have been made by Ufford[2] and Marvin,[3] and as these studies were since made more theoretical although experimental data have been obtained, it has been thought worth while to consider systematically the spectra arising from these configurations. We confined ourselves however to four spectra as they alone afford sufficient data for detailed study.

In each of the spectra which was studied we fitted the experimental values to the theoretical formulas first by neglecting configuration interactions (first-order comparison), and then, when the overlapping of the configurations was considerable, we took those interactions into account. In both cases we evaluated the Slater-Condon F's and G's by the method of least squares, calculated the terms and compared the agreements in the two cases.

Following Ufford[2] we worked on the assumption that the radial integrals containing electrons of identical n and l values are equal, regardless of the fact that these electrons belong to different configurations. The question whether it is justifiable to do so will be discussed in detail in the case of V II, as in that case there could have been some doubts as to the soundness of the assumption.

The experimental data were mainly taken from the tables of Bacher and Goudsmit.[4] In V II we used the classification of Meggers and Moore[5] as it is given by Bowman,[6] because the original paper was unfortunately not at our disposal.

The theoretical formulas are taken from Racah.[7]

Ti II

In the three configurations ds^2, d^2s, d^3, 15 of the 16 terms predicted by theory are known. This spectrum was considered by Ufford,[2] but it will be shown that a better agreement with the experimental data may be obtained by a fuller use of the least squares, and also by a change in the assignments of a couple of terms.

In the first-order comparison we fitted the experimental values to the theoretical formulas by means of least squares and calculated the mean error μ and mean deviation Δ which are defined by

$$\mu^2=\Sigma\Delta_i^2/n-m, \quad \Delta^2=\Sigma\Delta_i^2/n,$$

where Δ_i is the deviation of each term, n the number of terms, and m the number of adjust-

[1] E. U. Condon and G. H. Shortley, *Theory of Atomic Spectra* (Cambridge University Press, New York, 1935), p. 330.
[2] C. W. Ufford, Phys. Rev. **44**, 732 (1933).
[3] H. H. Marvin, Phys. Rev. **47**, 521 (1935).
[4] R. F. Bacher and S. Goudsmit, *Atomic Energy States* (McGraw-Hill Book Company, Inc., New York, 1932).
[5] W. F. Meggers and C. E. Moore, J. Research Nat. Bur. Stand. **25**, 83 (1940).
[6] D. S. Bowman, Phys. Rev. **59**, 386 (1941).
[7] G. Racah, Phys. Rev. **62**, 438 (1942); **63**, 367 (1943).

TABLE I. Calculated terms of the deep configurations of Ti II.

Column (1). Neglecting configuration interactions, using old assignments. Column (2). Neglecting configuration interactions, using proposed assignments. Column (3). With configuration interactions, using old assignments. Column (4). With configuration interactions, using proposed assignments.

Term	Obs.	(1) Calc.	(1) Diff.	(2) Calc.	(2) Diff.	(3) Calc.	(3) Diff.	(4) Calc.	(4) Diff.
$a\,^4F$	225	454	+229	−146	−371	898	+673	214	−11
$b\,^4F$	1085	123	−962	701	−384	515	−570	1160	+75
$d^2s\ ^3F$	4783	5928	+1145	5832	+1049	5153	+370	5079	+296
$d^2s\ ^1D$	8730	9373	+643	9630	+900	8711	−19	8947	+217
$d^3\ ^1G$	9065	8489	−576	8402	−663	8837	−228	8749	−316
$d^3\ ^4P$	9452	9872	+420	9621	+169	9572	+120	9310	−142
$d^3\ ^2P$	9934	11739	+1805	11658	+1724	10020	+86	9932	−2
$d^2s\ ^4P$	9968	10203	+235	10468	+500	9955	−13	10256	+288
$d^3\ ^2D^-$	12706	12441	−265	12413	−293	13651	+945	13637	+931
$d^3\ ^1H$	12730	11739	−991	11658	−1072	12163	−567	12055	−675
$d^2s\ ^1G$	15261	13922	−1339	14187	−1074	14066	−1195	14328	−933
$d^2s\ ^1P$	16589	15676	−913	15598	−991	16519	−70	16464	−125
$d^3\ ^1F$	20918	21487	+569	21424	+506	21386	+468	21317	+399
$d^2s\ ^1S$	21338	30031	(+8693)*	30605	(+9267)*	30154	(+8816)*	30757	(+9419)*
$ds^2\ ^1D$	25100	25100	0	25100	0	25100	0	25100	0
$d^3\ ^1D^+$	—	33022	—	33152	—	33625	—	33674	—
Mean error			±1147		±1090		±742		±622
Mean deviation			± 867		± 824		±525		±440
Parameters:									
$A(d^2s)$		9303		9330		8676		8735	
$A(d^3)$		9872		9621		9572		9310	
$A(ds^2)$		25100		25100		25656		25587	
$B=F_2-5F_4$		650		651		604		606	
$C=35F_4$		1922		1981		2071		2128	
G_2		1824		1710		1474		1362	
$H_2=R^3(dd, ds)/35$		—		—		172		172	

* This term has not been taken into account in the least squares calculations.

able parameters. In all the calculations we excluded $d^2s\ ^2S$ as it fits badly[8] in most spectra arising from d^2s. The results of the calculation are shown in Table I, column (1).

It must be remembered that, according to theory, the two quartets F should be in the same order and at the same distance as the quartets P, while in the given classification the order is inverted. The question arises whether the assignments of one pair of quartets should be interchanged, and, if so, of which of the two pairs. We examined all possibilities and found that the best agreement is obtained by interchanging the assignments of the quartets F, i.e., by assigning $_a{}^4F$ to d^3 and $_b{}^4F$ to d^2s.

With this exchange we repeated the last calculation and obtained the results shown in Table I, column (2). We must admit that the agreement in column (2) has not been appreciably improved, but it will be shown that the interaction calculations will justify the exchange in assignments.

We proceeded to the second step in the comparison by taking the configuration interactions into account. As most of the formulas obtained by introducing interactions are not linear, we used the usual approximate method of least squares.[9] As the approximate values of the parameters we took the results of the first-order comparison, and the approximate value of the interaction parameter H_2 was roughly evaluated by its effect on the position of the doublets PFG. The derivatives needed in Eq. (13-93) of Margenau[9] were obtained by the explicit formulas in the case of the second-order equations. In the case of the fourth-order equation they were obtained by the following method. We inserted in the matrix the approximate parameters and evaluated the roots of the secular equation. From these roots we found the orthogonal transformation which diagonalizes the numerical matrix and applied that transformation to the original matrix (in terms of the parameters). It is easy to show that the coeffi-

[8] Reference 1, p. 204.

[9] H. Margenau and G. M. Murphy, *The Mathematics of Physics and Chemistry* (Van Nostrand Company, New York, 1943), p. 500.

cients of the different parameters in the diagonal elements of the transformed matrix are the values of the required derivatives.

By the use of these methods the theoretical formulas became linear formulas containing as adjustable constants the correction terms of the parameters. We made two calculations. In the first calculation we used the old assignments and in the second we used the exchanged assignments of the quartets F. The results are shown in Table I, columns (3) and (4). The agreement of the quartets F in the proposed assignments is now much better than in the old assignments. It will be observed that the agreement of the remaining terms is practically the same in the two calculations, the mean deviation, excluding the quartets F, being ± 506 and ± 475. This shows the advantage of using least squares in comparing the theoretical formulas with experimental data; an incorrect assignment in the classification when many terms are known does not appreciably change the values of the parameters, as its effect is mainly balanced by the other terms.

To sum up, the agreement with experimental data has been greatly improved by taking configuration interactions into account; the mean error has been reduced from ± 1090 to ± 622. It is interesting to note that even the agreement of the unperturbed terms (the quartets F and P, and ^2H) is improved.

Finally we shall compare our results with those of Ufford. Using the parameters evaluated by him, one obtains a mean deviation of ± 859 cm^{-1}. By the full use of the method of least squares, the mean deviation is reduced to ± 525 when the same assignments of the quartets F are retained and to ± 440 when the assignments are exchanged as proposed above.

TABLE II. The deep configurations of V III.

Term	Obs.	Calc.	Diff.
$d^3\ ^4F$	336	387	+51
$d^3\ ^4P$	11668	11873	+205
$d^3\ ^2G$	12089	12015	−74
$d^3\ ^2D^-$	16317	17197	+880
$d^3\ ^2H$	16907	15844	−1063
$d^3\ ^2P$	—	15844	—
$d^3\ ^2F$	—	27329	—
$d^3\ ^2D^+$	—	42756	—
$d^2s\ ^4F$	44343	44343	0
$d^2s\ ^2F$	49602	49602	0
$d^2s\ ^4P$	—	55829	—
$d^2s\ ^2D$	—	55634	—
$d^2s\ ^2G$	—	60994	—
$d^2s\ ^2P$	—	61087	—
$d^2s\ ^2S$	—	82926	—
Mean error			±989

Parameters: $A(d^3)=11873$, $A(d^2s)=53975$, $B=F_2-5F_4=766$, $C=35F_4=2855$, $G_2=1753$.

V III

In the deep configurations, 8 terms have been classified by White.[10] It must be pointed out that, according to theory, $d^3\ ^2H$ and $d^3\ ^2P$ should be, in the first approximation, at the same height, while in White's classification ^2P lies at about 5600 cm^{-1} lower than ^2H and is even lower than $d^3\ ^4P$. This cannot be ascribed to a repulsion from $d^2s\ ^2P$, as the configuration d^2s is so high that the interactions between it and d^3 must be much smaller than the corresponding interactions in Ti II, and in the latter ^2P is shifted by only 1700 cm^{-1}. Moreover, White's classification of $d^3\ ^2P$ is based on the only multiplet $3d^3\ ^2P-3d^2(^3F)4p\ ^2D^0$, or more exactly on the only line $\lambda=1289$A which is assigned to the transition $^2P_{3/2}-^2D_{5/2}^0$, the existence of the other two lines of this multiplet being only inferred by assuming that they coincide by

TABLE III. The deep configurations of Ti I.

Term	Obs.	Calc.	Diff.
$d^2s^2\ ^3F$	223	712	+489
$d^3s\ ^5F$	6721	6020	−701
$d^2s^2\ ^1D$	7255	7194	−61
$d^2s^2\ ^3P$	8547	9119	+572
$d^3(^4F)s\ ^3F$	11673	11182	−491
$d^2s^2\ ^1G$	12118	11118	−1000
$d^3s\ ^5P$	14055	14427	+372
$d^2s^2\ ^1S$	15167	25916	(+10749)*
$d^3s\ ^3G$	15170	15072	−98
$d^3s\ ^3D^-$	17467	18660	+1193
$d^3(^2P)s\ ^3P$	18101	17874	−227
$d^3s\ ^3H$	18133	17874	−259
$d^3s\ ^1G$	18288	17653	−635
$d^3(^4P)s\ ^3P$	18873	19589	+716
$d^3s\ ^1P$	20063	20456	+393
$d^3s\ ^1D^-$	20210	21241	+1031
$d^3s\ ^1H$	20796	20456	−340
$d^3(^2F)s\ ^3F$	—	26282	—
$d^3s\ ^1F$	29818	28863	−955
$d^3s\ ^3D^+$	—	36779	—
$d^3s\ ^1D^+$	—	39361	—
Mean error			±772

Parameters: $A(d^2s^2)=5196$, $A(d^3s)=18299$, $B=F_2-5F_4=560$, $C=35F_4=1840$, $G_2=1291$.

* This term has not been taken into account in the least squares calculation.

[10] H. E. White, Phys. Rev. **33**, 674 (1929).

TABLE IV. Calculated terms of the deep configurations of V II.

Column (1). Neglecting configuration interactions. Column (2). With configuration interactions. Column (3). Assuming that the parameters B and C differ in the two configurations.

Term		Obs.	(1) Calc.	(1) Diff.	(2) Calc.	(2) Diff.	(3) Calc.	(3) Diff.
d^4	^5D	206	−1502	−1708	−1136	−1342	427	+221
d^3s	^5F	2926	4810	+1884	4697	+1771	3790	+864
$d^3(^4F)s$	^3F	8904	10913	+2009	10122	+1218	9893	+989
d^4	^3P	11709	12286	+577	11940	+231	12656	+947
d^4	^3H	12634	10857	−1777	11122	−1512	11509	−1125
d^4	^3F	13558	12715	−843	13423	−135	13160	−398
d^3s	^5P	13647	14694	+1047	14578	+931	13924	+277
d^4	^3G	14572	14152	−420	14055	−517	14651	+79
d^3s	^3G	16446	16264	−182	16472	+26	16194	−252
d^4	^1G	17911	18043	+132	17917	+6	17819	−92
d^4	^3D	18317	18764	+447	18494	+177	19050	+733
d^3s	^1G	19113	19316	+203	19295	+182	19245	+132
$d^3(^3P)s$	^3P	19147	19559	+412	19447	+300	19572	+425
d^4	^1I	19191	17037	−2154	17319	−1872	17050	−2141
d^4	^1S	19902	21321	+1419	21561	+1659	20806	+904
$d^3(^4P)s$	^3P	20238	20797	+559	20859	+621	20027	−211
d^3s	^3H	20303	19559	−744	19406	−897	19572	−731
d^3s	^3D	20601	20711	+110	21056	+455	20972	+371
d^4	^1D	20981	22980	+1999	20931	−50	22597	+1616
d^3s	^1P	22274	22610	+336	22328	+54	22623	+349
d^3s	^1H	23391	22610	−781	22328	−1063	22623	−768
d^3s	^1D	25191	23763	−1428	25577	+386	24024	−1167
d^4	^1F	26840	26920	+80	26400	−440	26476	−364
d^4	^3F	30302	32106	+1804	32407	+2105	31366	+1064
$d^3(^3F)s$	^3F	30637	29442	−1195	29313	−1324	29706	−931
d^4	^3P	32169	32534	+365	33021	+852	31870	−299
d^3s	^1F	34229	32494	−1735	33008	−1221	32757	−1472
d^4	^1G	36425	36501	+76	36883	+458	35276	−1149
d^3s	^3D	44139	42625	−1514	42401	−1738	43935	−204
d^3s	^1D	44658	45677	+1019	45332	+674	46987	+2329
d^4	^1D	—	50013	—	50488	—	48093	—
d^4	^1S	—	65143	—	65347	—	61853	—
Mean error				±1295		±1142		±1083
Mean deviation				±1182		±1021		± 948
Parameters:								
$A(d^4)$			12335		12697		13624	
$A(d^3s)$			19271		19029		18501	
$B=F_2-5F_4$			659		659		d^3s:676, d^4:628	
$C=35F_4$			2431		2417		d^3s:2725, d^4:2142	
G_2			1526		1484		1526	
$H_2=R^2(dd, ds)/35$			—		153		—	

chance with two other lines. Consequently we concluded that the levels 11207 cm^{-1} and 11387 cm^{-1} given by White most probably do not exist, and we excluded $d^3\ ^2P$ from the calculation. The results are shown in Table II.

It is not worth while to consider configuration interactions as the configurations are very widely separated.

Ti I

As only one term of the configuration d^4 is known, we considered only d^3s and d^2s^2 in which 18 of the 21 terms predicted by theory are known. Here also $d^2s^2\ ^1S$ fits badly, and we excluded it from the calculations. The results of the first-order comparison are shown in Table III. The agreement is satisfactory—a mean error of ±772 amounts only to 2.5 percent of the configurations' width. This is only to be expected as the configurations d^3s and d^2s^2 overlap very slightly, and d^4 is probably very high. As a result the interactions are small and it is not worth while to consider them.

V II

According to the classification of Meggers and Moore[5] all except two of the terms are known in the configurations d^3s and d^4, but d^2s^2 is altogether unknown. In making a preliminary calculation we got rid of the non-linear formulas

by taking means of each two terms of the same kind. The parameters obtained were $A(d^4)=10741$, $A(d^3s)=18403$, $B=581$, $C=2589$, $G_2=1361$, and from them the terms were calculated. It was found that the observed value of the term ^1D (44658) agrees better with the calculated value of $d^3s\ ^1D^+$ (44451) than with that of $d^4\ ^1D^+$ (47699). This suggests that the observed value should be assigned to $d^3s\ ^1D^+$ and not to $d^4\ ^1D^+$, the term to which Meggers and Moore assigned it, and in fact subsequent calculations confirmed this new assignment. Those subsequent calculations also gave rise to doubts as to the correctness of the assignments of the two $d^3s\ ^3P$. In addition the examination of the separations of the two triplets could not give any information, as theoretically those separations are almost equal (they are in the ratio 4:5). Therefore, in some of the calculations made by least squares we used only the mean of the two triplets, and it was found that the agreement was considerably improved by exchanging the assignments of the $d^3s\ ^3P$ terms, i.e., by assigning the observed value 19147 to $d^3(^2P)s\ ^3P$ and the observed value 20238 to $d^3(^4P)s\ ^3P$. Consequently these proposed assignments for $^1D^+$ and ^3P were used in all calculations which are reported in this paper.

The first-order calculation gave the results shown in Table IV, column (1). Introducing interactions between d^3s and d^4 we obtained the results in Table IV, column (2). It will be seen that the introduction of the interactions brings about some improvement of the agreement, although not a very considerable one.

A first-order comparison was made also by Bowman,[6] who assumed that the parameters F_2 and F_4 differ in the two configurations d^3s and d^4. From his results it is found that the parameters B differ by 40 percent and the parameters C differ by 20 percent in the two configurations. According to Ufford[2] and Racah[11] it is difficult to admit such differences. Since Bowman's calculations are based on Ostrofsky's[12] formulas for d^4 in which there are some mistakes, we repeated those calculations. We assumed as Bowman did that the parameters B and C differ in the two configurations, but we used the correct formulas for d^4 and the proposed assignments, and made full use of the least squares. The results are shown in Table IV, column (3). The parameters B then differed by only 7 percent but C differed by 25 percent. We must admit that a better agreement is obtained by assuming different values for B and C than by assuming unified parameters, but the gain in mean error is not great enough to justify such a procedure which has no sufficient theoretical basis.

I am deeply grateful to Professor G. Racah for suggesting this problem and for his constant assistance to me throughout my work.

[11] G. Racah, Phys. Rev. **61**, 537 (1942).
[12] M. Ostrofsky, Phys. Rev. **46**, 604 (1934).

A Five-Dimensional Field Theory

K. C. WANG AND K. C. CHENG
Department of Physics, National University of Chekiang, Meitan, Kweichow, China

(Received June 1, 1946)

With the assumption of a five-dimensional space-time the field equations and the interactions of the field and particles are obtained. In this theory, the electrodynamics is in agreement with the classical theory. In the case of the meson theory, the vector, pseudoscalar, and pseudovector theories are obtained.

I. INTRODUCTION

CURRENT field theories are of Maxwellian and scalar types. These theories are genetically unrelated. Here we propose a unified treatment under the assumption of a five-dimensional space-time continuum. Instead of the ordinary four-dimensional space-time we have five, including four space-like (x, y, z, x_0) and one time-like (t) dimensions. If a proper assumption is made on the nature of the charge distributions in the fifth dimension (x_0), the field equations and the interactions with particles can be obtained.

As the momentum and velocity of a particle in the fifth dimension have never been observed, they are assumed to be zero. We also assume the density distribution along the fifth dimension to vary as $\cos(kx_0+\epsilon)$ or $\sin(kx_0+\epsilon)$, equivalent to the saying that the particle in the five-dimensional space is a long line extending in the fifth dimension, and the density varying as $\cos(kx_0+\epsilon)$ along that dimension.

II. THE FIELD EQUATIONS AND THE LAGRANGIAN

We define the five field vector

$$A_\mu=(A_x, A_y, A_z, i\phi, A_0), \tag{1}$$

the field tensor

$$F_{\mu\nu}=\partial A_\mu/\partial x_\nu-\partial A_\nu/\partial x_\mu, \quad \mu,\nu=0,1,2,3,4 \tag{2}$$

the charge density

$$j_\mu=(\rho\dot{x}, \rho\dot{y}, \rho\dot{z}, i\rho, \rho\dot{x}_0), \tag{3}$$

the magnetic moment tensor

$$M_{\mu\nu}=\begin{pmatrix} 0 & \pi_z & \pi_y & \pi_x & ix \\ -\pi_z & 0 & M_x & -M_y & -iN_z \\ -\pi_y & -M_x & 0 & M_z & -iN_y \\ -\pi_x & M_y & -M_z & 0 & -iN_x \\ -ix & iN_z & iN_y & iN_x & 0 \end{pmatrix}, \tag{4}$$

and the field equations

$$\frac{\partial F_{\mu\nu}}{\partial x_\nu}=4\pi j_\mu+\frac{\partial M_{\mu\nu}}{\partial x_\nu},$$

or writing explicitly

$$\begin{aligned} &\Delta\mathbf{A}-\frac{1}{c^2}\frac{\partial^2\mathbf{A}}{\partial t^2}-k^2\mathbf{A}=-\frac{4\pi}{c}\mathbf{j} \\ &\qquad -\text{rot }\mathbf{M}+\frac{1}{c}\frac{\partial\mathbf{N}}{\partial t}+\frac{\partial\boldsymbol{\pi}}{\partial x_0}, \\ &\Delta\phi-\frac{1}{c^2}\ddot{\phi}-k^2\phi=-4\pi\rho-\text{div }\mathbf{N}-\frac{\partial x}{\partial x_0}, \\ &\Delta A_0-\frac{1}{c^2}\ddot{A}_0-k^2A_0=-4\pi\rho\dot{x}_0-\text{div }\boldsymbol{\pi}-\frac{1}{c}\frac{\partial x}{\partial t}, \end{aligned} \tag{5}$$

and the interaction energy between field and charge density

$$\mathcal{E}=\int(M_{\mu\nu}+j_\mu A_\mu)dxdydzdx_0. \tag{6}$$

Since all the charge quantities vary as $\cos(kx_0+\epsilon)$, each of the variables $(\mathbf{A}, \phi, A_0)$ can be separated into two parts: $(\mathbf{A}_1+\mathbf{A}_2, \phi_1+\phi_2, \mathbf{A}_0+0)$ with

$$\begin{aligned} &\Delta\mathbf{A}_1-\frac{1}{c^2}\frac{\partial^2\mathbf{A}_1}{\partial t^2}-k^2\mathbf{A}_1=-\frac{4\pi}{c}\mathbf{j}-\text{rot }\mathbf{M}+\frac{1}{c}\frac{\partial\mathbf{N}}{\partial t}, \\ &\Delta\mathbf{A}_2-\frac{1}{c^2}\frac{\partial^2\mathbf{A}_2}{\partial t^2}-k^2\mathbf{A}_2=-k\boldsymbol{\pi}, \\ &\Delta\phi_1-\frac{1}{c^2}\ddot{\phi}_1-k^2\phi_1=-4\pi\rho-\text{div }\mathbf{N}, \\ &\Delta\phi_2-\frac{1}{c^2}\ddot{\phi}_2-k^2\phi_2=kx, \\ &\Delta A_0-\frac{1}{c^2}\ddot{A}_0-k^2A_0=-4\pi\rho\dot{x}_0-\text{div }\boldsymbol{\pi}-\frac{1}{c}\frac{\partial x}{\partial t}. \end{aligned} \tag{7}$$

Thus all quantities with subscript 1 vary as $\cos(kx_0+\epsilon)$, while the quantities with subscript 2 vary as $\sin(kx_0+\epsilon)$. Since

$$\langle\cos^2(kx_0+\epsilon)\rangle_{Av}=\langle\sin^2(kx_0+\epsilon)\rangle_{Av}=\tfrac{1}{2};$$
$$\langle\cos(kx_0+\epsilon)\sin(kx_0+\epsilon)\rangle_{Av}=0,$$

Eq. (6) can be written in the form

$$\mathcal{S}=\int\left\{(\mathbf{M}\cdot\mathbf{H}_1)-(\mathbf{N}\cdot\mathbf{E}_1)-\pi\,\mathrm{grad}\,\mathbf{A}_0-\frac{1}{c}xA_0+\left(x\frac{\partial\phi_2}{\partial x_0}-\pi\frac{\partial\mathbf{A}_2}{\partial x_0}\right)-\frac{1}{c}\mathbf{j}\cdot\mathbf{A}_1+\rho\phi_1\right\}dxdydz, \quad (8)$$

except with different choice of the charge units.

On the other hand the field equations in space free of charges are derivable from the following Lagrangian:

$$\mathfrak{L}=-\frac{1}{8\pi}\int\left(\frac{\partial A_\mu}{\partial x_\nu}-\frac{\partial A_\nu}{\partial x_\mu}\right)dxdydzdx_0. \quad (9)$$

If we put $Q_\mu=A_\mu$, $P_\mu=\partial\mathfrak{L}/\partial Q_\mu$, we get the Hamiltonian function,

$$\mathfrak{H}=\sum P_\mu\dot{Q}_\mu-\mathfrak{L}=\frac{1}{8\pi}\int\left\{\left[(\mathrm{grad}\,\mathbf{A})^2+\frac{1}{c^2}\frac{\partial\mathbf{A}^2}{\partial t}+k^2A^2\right]+\left[(\mathrm{grad}\,A_0)^2+\frac{1}{c^2}A_0^2+k^2A_0^2\right]-\left[(\mathrm{grad}\,\phi)^2+\frac{1}{c^2}\dot{\phi}^2+k^2\phi^2\right]\right\}dxdydzdx_0. \quad (10)$$

Here it is to be reminded that $(\phi_1+\phi_2,\ \mathbf{A}_1+\mathbf{A}_2)$ can be separated into independent terms in the Hamiltonian function, since $\langle\cos^2(kx_0+\epsilon)\rangle_{Av}=\frac{1}{2}$, etc.

III. THE HAMILTONIAN EQUATION CONTAINING FIELD AND PARTICLE

The five-dimensional Hamiltonian function for a particle in the Dirac's form of a particle with spin $\frac{1}{2}$ is

$$c\beta_\mu\left(p_\mu+\frac{e}{c}A_\mu\right)+m_0c^2=0, \quad (11)$$

where β_μ satisfies the relations $\beta_\mu\beta_\nu+\beta_\nu\beta_\mu=2\delta_{\mu\nu}$ and $\beta_0=\beta_1\beta_2\beta_3\beta_4$. Now by assumption that $v_0=0$, $p_0=0$, we see that $\psi^+\beta_4\beta_0\psi=0$ at least for a free particle. Thus to the first approximation

$$j_\mu=\psi^+\beta_4\beta_\mu\psi=\psi^+\beta_4(\beta_1,\beta_2,\beta_3,\beta_4,0)\psi.$$

(*i*) In the case of electrodynamics, we have $k=0$, $j_0=0$, $M_{\mu\nu}=0$, then all the equations of the field and particles in our theory will conform with the ordinary equations.

(*ii*) In the case of the meson theory, we adopt the "single force hypothesis," i.e., $j_\mu\equiv0$. Put

$$M_{\mu\nu}=f\psi^+\beta_4\cdot\tfrac{1}{2}(\beta_\mu\beta_\nu-\beta_\nu\beta_\mu)\psi=f\psi^+\beta_4\begin{pmatrix}0&\beta_4\beta_3\beta_2&\beta_4\beta_1\beta_3&\beta_4\beta_2\beta_1&-i\beta_1\beta_2\beta_3\\-\beta_4\beta_3\beta_2&0&\beta_1\beta_2&\beta_1\beta_3&i\beta_1\beta_4\\-\beta_4\beta_1\beta_3&-\beta_1\beta_2&0&\beta_2\beta_3&i\beta_2\beta_4\\-\beta_4\beta_2\beta_1&-\beta_1\beta_3&-\beta_2\beta_3&0&i\beta_3\beta_4\\i\beta_1\beta_2\beta_3&-i\beta_1\beta_4&-i\beta_2\beta_4&-i\beta_3\beta_4&0\end{pmatrix}\psi. \quad (12)$$

In accordance with Eqs. (8), (10), and (11), we obtain the complete Hamiltonian function of the particle and the field:

$$\mathfrak{H}_c=c\beta_\mu p_\mu+m_0c^2+f\left[\boldsymbol{\sigma}\cdot\mathbf{H}_1+i\beta_4\boldsymbol{\alpha}\cdot\mathbf{E}_1+\beta_4\boldsymbol{\sigma}\cdot\mathrm{grad}\,A_0-\frac{i}{c}\beta_1\beta_2\beta_3A_0+\beta_4k(\boldsymbol{\sigma}\cdot\mathbf{A}_2)-ik\beta_1\beta_2\beta_3\phi_2\right]$$
$$+\frac{1}{8\pi}\int\left\{\left[(\mathrm{grad}\,\mathbf{A})^2+\frac{1}{c^2}\frac{\partial\mathbf{A}^2}{\partial t}+k^2\mathbf{A}^2\right]+\left[(\mathrm{grad}\,A_0)^2+\frac{1}{c^2}A_0^2+k^2A_0^2\right]-\left[(\mathrm{grad}\,\phi)^2+\frac{1}{c^2}\phi^2+k^2\phi^2\right]\right\}dxdydz.$$

Here we see that $\boldsymbol{\sigma}\cdot\mathbf{H}_1+i\beta_4\boldsymbol{\alpha}\cdot\mathbf{E}_1$ corresponds to the current vector meson coupling and the term $\beta_4\boldsymbol{\sigma}\cdot\mathrm{grad}\,A_0$ is the pseudoscalar coupling, while the last two terms give the pseudovector coup-

ling. Thus all types of coupling necessary come in our scheme with equal importance.

Finally it should be noted that in our theory all quantities must be expressible in the tensor form in consistence with the assumption of the five-dimensional space, or, in other words, all quantities must be invariant under the five-dimensional rotation. As a consequence the coupling constants must be alike for all kinds of coupling.

IV. CONCLUSION

We have obtained the field equations and the interactions of the field and the particles with the assumption of the five-dimensional space-time. The electrodynamics in our theory is in agreement with the classical theory. In the case of the meson theory we obtained the vector, pseudoscalar and pseudovector couplings. But an important and also rather stringent consequence of our theory is that all coupling must appear in equal importance, i.e., the coupling constants must be alike for all kinds of coupling. Moreover, our theory corresponds to the weak coupling of the current theories.*

* Cf. W. Pauli and S. Kusaka, Phys. Rev. 63, 400 (1943). In this paper they have shown that weak coupling is in better agreement with the experiment.

PHYSICAL REVIEW VOLUME 70, NUMBERS 7 AND 8 OCTOBER 1 AND 15, 1946

Accuracy of the Earth-Flattening Approximation in the Theory of Microwave Propagation*

C. L. PEKERIS†
Columbia University, New York, New York

(Received July 1, 1946)

A study was made of the maximum ranges and elevations for which the earth-flattening approximation in the theory of microwave propagation is valid. It is found that at a range equal to half the radius of the earth the error introduced by the earth-flattening approximation is only 2 percent, and this independently of the wave-length. The fractional error Δ in the height-gain functions is found to be proportional to the 5/2th power of the elevation, and to the inverse power of the wave-length. Values of Δ for various wave-lengths and elevations are shown in Table I. For wave-lengths of the order of several centimeters the earth-flattening approximation breaks down at elevations greater than a few thousand feet.

1. INTRODUCTION

THE central problem in the theory of microwave propagation is the determination of the electromagnetic field produced by a dipole antenna situated at some elevation above the ground. The electromagnetic field is affected primarily by the polarization of the antenna (vertical or horizontal dipole), the properties of the ground, the variation with elevation of the refractive index of the air, and by the spherical shape of the earth's surface. The last mentioned factor is, of course, very serious for propagation into regions below the horizon. It also introduces great complexity into the mathematical solution of the problem,[1] especially in the presence of a variable refractive index in the atmosphere.

Considerable simplification of the analysis has been achieved in recent years through a device due originally to Schelleng, Burrows, and Ferrell,[2] and later developed by M. H. L. Pryce,[3] whereby

* This paper is based on work done for the Naval Research Laboratory under contract with the Navy's Office of Research and Inventions. Publication assisted by the Ernest Kempton Adams Fund for Physical Research of Columbia University.

† Columbia University Mathematical Physics Group, on leave of absence from Massachusetts Institute of Technology.

[1] See Arnold Sommerfeld's article in Frank-Mises, *Differentialgleichungen der Physik* Vol. II, p. 918.

[2] Schelling, Burrows, and Ferrell, Proc. I. R. E. 21, 427 (1933).

[3] M. H. L. Pryce, unpublished report. See also J. E. Freehafer, Radiation Laboratory Report 447, 1943.

space is transformed so as to make the surface of the earth plane and the rays curved.[4] The transformation is accomplished simply by the use in the wave equation of a modified index of refraction N, in place of the actual index of refraction μ, defined by

$$N(r)=r\mu(r)/a\mu(a), \tag{1}$$

where r denotes the distance from the center of the earth, and a the radius of the earth. It is known qualitatively that the flattening-of-the-earth-approximation is valid for determining the field up to moderate ranges and elevations.[5] The purpose of this investigation is to determine precisely the maximum ranges and elevations for which the flattening of the earth can be considered a good approximation.

2. THE EARTH-FLATTENING APPROXIMATION

When the fractional change of the index of refraction over a distance of a wavelength is small, the electromagnetic field is determined by a Hertzian potential Ψ which satisfies the wave equation

$$\nabla^2\Psi+k^2\mu^2\Psi=0, \tag{2}$$

$$k=2\pi/\lambda \text{ in air}, \tag{3}$$

$$k^2\mu^2=(\epsilon\omega^2-i\sigma\omega)/c^2 \text{ in the ground}, \tag{4}$$

where a time factor $e^{i\omega t}$ has been assumed. For vertical polarization Ψ represents the vertical component of the electric Hertzian potential, and the field intensity is proportional to $|\Psi|^2$. Similarly, in the case of horizontal polarization the field is still essentially determined by a single Hertzian potential Ψ.[6]

In the problem of radiation from a dipole antenna, the solution of Eq. (2) must satisfy the following boundary conditions:

(*a*) Ψ should reduce to the form e^{-ikR}/R for small distances R from the source,
(*b*) Ψ should represent an outgoing wave at great distances from the source, and
(*c*) The tangential components of the electric and magnetic fields should be continuous at the earth's surface.

We shall limit the discussion to the special, but important, case when the index of refraction μ is a function of elevation only, i.e., $\mu=\mu(r)$. Without loss of generality we can also confine the discussion to solutions of Ψ which are symmetrical with respect to the radius vector through the source. Using polar coordinates (r, θ), we seek to build up a solution of (2) satisfying the boundary conditions in terms of elementary solutions of the form

$$\psi=P(\theta)\cdot U(r). \tag{5}$$

Substituting in (2) we find that P and U must satisfy the equations

$$\frac{d^2P}{d\theta^2}+\frac{\cos\theta}{\sin\theta}\frac{dP}{d\theta}+a^2k_m^2P=0, \tag{6}$$

$$\frac{d^2U}{dr^2}+\frac{2}{r}\frac{dU}{dr}+\left[k^2\mu^2(r)-\frac{a^2k_m^2}{r^2}\right]U=0. \tag{7}$$

Here we have written $a^2k_m^2$ (a denoting the radius of the earth, and k_m having the dimension of a reciprocal length) for the customary separation constant $n(n+1)$. The appropriate solutions of (6) are of course $P_n(\cos\theta)$, where n must be an integer in order to secure finiteness of P at $\theta=\pi$. We shall, however, relinquish the requirement of finiteness of P at $\theta=\pi$, as well as $\theta=0$, by using what amounts to a linear combination of $P_n(\cos\theta)$ and $Q_n(\cos\theta)$. The resulting solution for Ψ, which can be made to satisfy the boundary conditions, will be useful everywhere except in the immediate

[4] In a memorandum submitted by the writer to Professor Carl Eckart on October 23, 1943, it was pointed out that the portion of the coverage diagram situated below the horizon shown in Fig. 5 of the paper by B. v. d. Pol and H. Bremmer, in Phil. Mag. **27**, 270 (1939), agrees with the solution for a flat earth when the index of refraction of the air μ varies with elevation h like $(1+h/a)$, where a denotes the radius of the earth. The solution of the latter problem had been obtained by the writer in May, 1943 (see a paper by the writer in J. Acous. Soc. Am. **18**, 295 (1946) In the field in which the writer was then active the flat earth with a variable index of refraction presented itself *ab initio*. It was suggested on many occasions that the treatment of that problem could perhaps be simplified by curving the earth and straightening the rays, a procedure the opposite of which was then being practiced by microwave propagation researchers.

[5] See Freehafer's discussion in Radiation Laboratory Report 447.

[6] See reference 1, page 948; M. C. Gray, Phil. Mag. **27**, 421 (1939); R. Burrows and M. C. Gray, Proc. I. R. E. **29**, 16 (1941).

neighborhood of the radius vector through the source and through the antipodes. The k_m are then found to be a set of complex characteristic values determined by the boundary conditions.

In the earth-flattening approximation one adopts, instead of the polar coordinates r and θ, the set of coordinates (ρ, h) defined by

$$\rho = a\theta, \tag{8}$$

$$h = r - a. \tag{9}$$

In terms of these coordinates, Eqs. (6) and (7) can be written as

$$\frac{d^2P}{d\rho^2} + \frac{1}{\rho}\frac{dP}{d\rho} + k_m^2 P = -\frac{1}{\rho}\frac{dP}{d\rho}\left(\frac{1}{3}\frac{\rho^2}{a^2} + \frac{1}{45}\frac{\rho^4}{a^4} + \cdots\right), \tag{10}$$

$$\frac{d^2U}{dh^2} + \left[k^2\mu^2(h) - k_m^2 + 2k_m^2\frac{h}{a}\right]U = -\frac{2}{a}\frac{dU}{dh} + 3k_m^2\frac{h^2}{a^2}U + \cdots, \tag{11}$$

upon expanding $\cos\theta/\sin\theta$ in powers of d/a, and $1/r$ in powers of h/a. Mathematically the earth-flattening approximation consists essentially in neglecting the right-hand sides of Eqs. (10) and (11), which are roughly of the order of ρ/a and h/a relative to the terms on the left-hand sides. One is then left with a system of equations which are appropriate for a flat earth, the only change being that the term $k^2\mu^2(h)$ is replaced by $[k^2\mu^2(h) + (2k_m^2h)/a]$. Since under actual conditions $\mu(h) \simeq 1$ and $k_m \simeq k$, the latter expression is equal to $k^2N^2(r)$ to within terms of the order of h^2/a^2, where $N(r)$ is defined in Eq. (1).

Barring certain pathological cases which we need not consider here[4] it is possible to obtain solutions of (2) satisfying the boundary conditions in terms of *normal modes* as follows

$$\Psi = -i\pi \sum_1^\infty H_0^{(2)}(k_m\rho)\, U_m(h_1)\, U_m(h_2), \tag{12}$$

where h_1 and h_2 denote the heights of transmitter and receiver respectively, and $U_m(h)$ satisfies the equation

$$\frac{d^2U_m}{dh^2} + (k^2N^2 - k_m^2)\, U_m = 0. \tag{13}$$

The solution (12) was arrived at in recent years by W. H. Furry, T. Pearcey, G. L. Roe, and the writer, the method of derivation having been used for the first time by H. Lamb in a classical paper written in 1904.[7]

3. THE ERROR INVOLVED IN THE EARTH-FLATTENING APPROXIMATION

We now turn to our principal task, which is an estimation of the error involved in the neglect of the terms appearing on the right-hand sides of Eqs. (10) and (11). Taking first Eq. (10), we seek a solution of the form

$$P(\rho) = P_0(\rho) + (1/a^2k_m^2)P_2(\rho) + (1/a^4k_m^4)P_4(\rho) + \cdots. \tag{14}$$

Substituting in (10) we find that

$$\frac{d^2P_0}{d\rho^2} + \frac{1}{\rho}\frac{dP_0}{d\rho} + k_m^2P_0 = 0, \quad P_0(\rho) = H_0^{(2)}(k_m\rho), \tag{15}$$

$$\frac{d^2P_2}{d\rho^2} + \frac{1}{\rho}\frac{dP_2}{d\rho} + k_m^2P_2 = -\frac{\rho}{3}\frac{dP_0}{d\rho}, \qquad P_2(\rho) = -\frac{1}{12}(k_m\rho)^2H_2^{(2)}(k_m\rho). \tag{16}$$

Hence

$$P(\rho) = H_0^{(2)}(k_m\rho) - \frac{\rho^2}{12a^2}H_2^{(2)}(k_m\rho) + 0(1/a^4k_m^4). \tag{17}$$

$P_2(\rho)$ is certainly small relative to $P_0(\rho)$ for small values of ρ, while for large values of $k_m\rho$, $H_2^{(0)}(k_m\rho) \to -H_0^{(0)}(k_m\rho)$, so that the correction term to $P_0(\rho)$ is of the order of $\rho^2/12a^2$, independently of frequency. For $\rho = a/3$ this correction term is less than one percent, and for $\rho = a/2$ it is around two percent. *We therefore conclude*

[7] H. Lamb, Phil. Trans. Roy. Soc. **A203**, 1 (1904).

*that the earth-flattening approximation is valid to within two percent up to ranges of about half the radius of the earth, and this independently of the frequency.**

Coming now to the height-gain functions $U(h)$, which in the earth-flattening approximation satisfy the homogeneous equation (13) rather than the exact inhomogeneous equation (11), we must consider separately the part of the solution in the interior of the earth and the part in the atmosphere. With regard to the solution in the ground it is clear qualitatively that the earth-flattening approximation will be valid only if the electromagnetic energy is confined to a thin skin layer of the ground. This condition will be realized the more closely the more conductive the ground is. Over the sea we may expect relatively little energy to be carried in the water, especially for the low order modes.

Our principal interest is to estimate the maximum heights for which the earth-flattening is a valid approximation. For this purpose we need to investigate the asymptotic behavior of the solutions of (11) for large heights. Now at great heights $\mu^2(h)$ decreases linearly with h under standard atmospheric conditions, and the expression in brackets in (11) becomes a linear function of h, which is characteristic for the so-called *standard atmosphere*. It follows that in our particular application we can limit ourselves to the case of a standard atmosphere where

$$\mu^2(h)=1-\frac{1}{2}\frac{h}{a}. \tag{18}$$

As far as the boundary condition at the surface is concerned we can assume for the sake of simplicity that $U_m(0)=0$, because the mode of variation of $U_m(h)$ at great heights is not affected thereby.†

It is convenient to introduce non-dimensional coordinates as follows

$$N^2=1+qh, \quad q=\frac{3}{2a}, \quad k_m^2=k^2(1-\Lambda_m), \tag{19}$$

$$H=(k^2q)^{-1/3}, \quad z=h/H, \quad \Lambda_m=(k/q)^{-1/3}D_m. \tag{20}$$

Using these in (11) we obtain

$$\frac{d^2U}{dz^2}+(z+D_m)U=\frac{2H}{a}\left(-\frac{dU}{dz}+z^2U\right). \tag{21}$$

As before, we seek a solution of (21) of the form

$$U(z)=U_0(z)+\frac{H}{a}U_1(z)+\cdots, \tag{22}$$

and find that

$$\frac{d^2U_0}{dz^2}+(z+D_m)U_0=0, \tag{23}$$

$$U_0=Cu^{1/2}H_{1/3}^{(2)}(u), \quad u=\tfrac{2}{3}(z+D_m)^{3/2}, \tag{24}$$

$$\frac{d^2U_1}{dz^2}+(z+D_m)U_1=-2\frac{dU_0}{dz}+2z^2U_0, \tag{25}$$

$$U_1=\left(-\frac{2}{5}z^2+\frac{8}{15}D_mz-\frac{16}{15}D_m^2\right)\dot{U}_0-\frac{3}{5}zU_0. \tag{26}$$

Now

$$\dot{U}_0=C(z+D_m)^{1/2}u^{1/2}H_{-2/3}^{(2)}(u),$$

so that

$$\frac{1}{U_0}\frac{dU_0}{dz}=\frac{(z+D_m)^{1/2}H^{(2)}_{-2/3}(u)}{H_{1/3}^{(2)}(u)}\to -i(z+D_m)^{1/2}, \tag{27}$$

for large z. It follows that for large z

$$U_1\to i\tfrac{2}{5}z^{5/2}U_0.$$

The correction factor to be applied to the solution $U_0(z)$ obtained under the earth-flattening approximation is therefore

$$1+i\frac{2H}{5a}z^{5/2}=1+i\frac{2h^{5/2}}{5a^{3/2}}\equiv 1+i\Delta, \tag{28}$$

$$\Delta=\frac{2}{5}\frac{h^{5/2}}{aH^{3/2}}=\frac{\sqrt{6}}{5}\frac{kh^{5/2}}{a^{3/2}}. \tag{29}$$

* This investigation was prompted by alarming results which the writer obtained with the earth-flattening approximation when instead of the distance along the surface of the earth $\rho=a\theta$, the distance from the earth's axis $\rho=a\sin\theta$ was adopted for the horizontal coordinate. In this case the correction term to $P_0(\rho)$ is of the order of $\rho^3k/6a^2$ instead of $\rho^3/12a^3$. The former varies with wave-length, and for a wave-length of 10 cm is greater than 1 already at a range of 10 miles!

† Essentially what is needed for the following argument is merely relation (27).

TABLE I. Fractional error $\Delta(h)$ of the height-gain function under the earth-flattening approximation for various elevations h and wave-lengths λ.

λ_{cm}	H	$\Delta(1000')$	$\Delta(2000')$	$\Delta(3000')$	$\Delta(4000')$	$\Delta(5000')$	$\Delta(6000')$
10	33.62′	0.0031	0.0176	0.0484	0.0993	0.1735	0.2737
3	15.07′	0.0103	0.0585	0.1613	0.3310	0.5783	0.9122
1	7.24′	0.0310	0.1756	0.4839	0.9930	1.735	2.737

It is seen that the correction term Δ increases with elevation like $h^{5/2}$, and is proportional to the frequency. In Table I are listed values of Δ for various elevations and wave-lengths.

It is clear from the table that for the wave-lengths listed the earth-flattening approximation breaks down at elevations of several thousand feet. In the case of a 10-cm wave, for example, the height-gain function is in error by 17 percent at an elevation of 5000 feet.

PHYSICAL REVIEW VOLUME 70, NUMBERS 7 AND 8 OCTOBER 1 AND 15, 1946

Surface Layers on Quartz and Topaz*

D. D'EUSTACHIO
Bliley Manufacturing Corporation, Erie, Pennsylvania†

(Received July 15, 1946)

X-ray studies of single crystals of quartz and topaz show that there exist on the surfaces of these crystals disturbed layers which are not removed by etching, and that they exert an effect on etched surfaces to a depth of 5 or more microns. The disturbance is not caused by plastic flow. Good, single crystal quartz wafers, 35 microns thick, change when they are etched to 15 microns. The thin plates no longer appear to be single crystal. This "polycrystalline" state is stable at room temperature. Thin crystals undergo further changes when flexed, resulting in a two to threefold broadening of the Cu $K\alpha$ rocking curves. Similar results were observed with topaz. It is shown that this effect is different from, and may not be related to, the well-known broadening of the Bragg reflections that result from grinding crystal surfaces. As an explanation for the observed phenomena, it is suggested that at least part of the surface energy is in the form of structure irregularity and there results a very thin, glass-like layer that is unstable because it is effectively at a higher temperature than the rest of the crystal. Consequently, recrystallization to a more stable form occurs.

INTRODUCTION

MANY workers have reported that the surfaces of crystals, particularly if they have been ground or polished, are covered with misaligned material.[1–5] In 1943 C. J. Davisson[6] and E. H. Armstrong[7] investigated the surface of ground quartz crystals and found crystallites which were turned through more than 3°. Davisson measured the actual misalignment. A quartz crystal was adjusted in a Bragg spectrometer to give maximum reflection for the Cu $K\alpha$ line from the $(20\bar{2}3)$ planes. Photographs were taken, the first with the crystal as adjusted, the second with the crystal turned 15′ from the maximum reflecting position, the next with the crystal turned 30′, etc., until the quartz had been rotated through several degrees. The series showed two lines, one from the background radiation with position dependent on crystal orientation, and the second at the Bragg position for Cu $K\alpha$. The intensity of the undisplaced line fell off to zero with increasing angle. Since the crystallites showed a decided preference for the orientation of the main crystal, Davisson concluded that the line could not be caused by small particles of quartz broken off in grind-

* A report on part of this work was presented at the January, 1946, Meeting of the American Physical Society. Cf. D. D'Eustachio and S. B. Brody, Phys. Rev. **69**, 256 (1946).

† Now Collman Manufacturing Corporation, Erie, Pennsylvania.

[1] S. K. Allison, Phys. Rev. **41**, 13, 688 (1932).

[2] M. Y. Colby and Sidon Harris, Phys. Rev. **43**, 562 (1933).

[3] R. M. Bozorth and F. E. Haworth, Phys. Rev. **45**, 821 (1934).

[4] C. C. Murdock, Phys. Rev. **45**, 117 (1934).

[5] Jesse W. M. DuMond and V. L. Bollman, Phys. Rev. **50**, 97 (1936).

[6] C. J. Davisson, private communication.

[7] E. H. Armstrong, paper presented at the Cleveland Meeting of the A.A.A.S., September, 1944.

ing and wedged into cracks on the surface. D'Eustachio and Brody[8] have pointed out the difficulties with supposing that this misalignment is produced by mechanical forces acting on the crystal surfaces during lapping or grinding. They have shown that fresh surfaces of valence crystal fragments undergo changes during the first few hours of their existence as surfaces, and that these changes may well be a recrystallization of the surface.

This paper reports on a series of experiments with single crystals of quartz and topaz, which show that disoriented layers are an integral part of the crystal, that they exist on the surfaces of etched crystals, that they exert an effect on etched surfaces to a depth of 5 or more microns. Plastic flow is not a factor in the formation of the layers.

EXPERIMENTAL TECHNIQUE

Two series of experiments were carried out. The first made use of the same technique that Davisson[6] employed. Photographs were taken of ground, etched, and freshly cracked quartz surfaces, using reflections from $(10\bar{1}1)$, $(01\bar{1}1)$, $(20\bar{2}3)$, $(30\bar{3}1)$, $(10\bar{1}0)$ and (0003) planes. Two etchants were used, a solution of 30 percent hydrofluoric acid in water, and fused sodium hydroxide. The intensities of the reflections were estimated both from photographic films and from current readings with an ionization chamber. Similar experiments were carried out with (002) and (110) reflections from topaz, except that in this case only molten sodium hydroxide was used as an etchant.

In the second series of experiments, the distribution of intensity in the Cu $K\alpha$ reflection at and near the Bragg angle was measured as a function of crystal thickness. Measurements were made photographically and with an ionization chamber. Single crystals of quartz and topaz approximately 2×4 mm and from 10 to 100 microns thick were used.

The thin quartz crystals were prepared in the following manner. Wafers about 1 mm thick were sawed at 13° with the $(10\bar{1}1)$ plane. Most of the plates were lapped mechanically to 75 microns, etched with 30 percent hydrofluoric acid to 50 microns, and then finished to 10–15 microns by one of these methods:

(1) Grinding on both sides.
(2) Alternate grinding and HF etching on both sides.
(3) Grinding one side only, followed by HF etching on both sides.
(4) HF etching only on both sides.
(5) HF etching one side only, protecting the other side with ceresin wax.

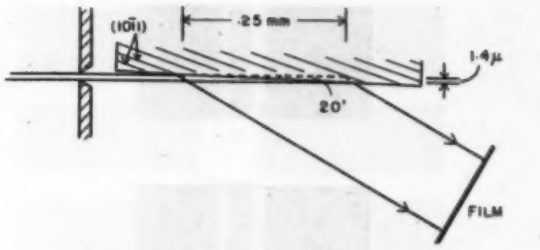

FIG. 1. A schematic diagram showing the relationship between x-ray beam and crystal for the experiment on thin crystals.

When sodium hydroxide was used as an etchant the mechanical lapping was discontinued when the crystals were 100 microns thick. The plates were etched to the desired thickness by immersion in molten sodium hydroxide. After being washed in water the crystals were rinsed for about one minute in 30 percent hydrofluoric acid to remove all traces of sodium salts, and then washed again. Thickness of plates was measured to ±1 micron. The particular angle of cut used was chosen because it permits examination of the crystals with a beam of x-rays that is nearly parallel to the surface. The Bragg angle for the $(10\bar{1}1)$ plane is 13° 20′. Hence, a well collimated beam of x-rays can be used to investigate a large area. See Fig. 1.

The linear absorption coefficient for quartz is 92 cm^{-1}. Consequently, the intensity of the incident beam will be reduced to 1 percent of the original value after traversing 0.25 mm of material. Referring to Fig. 1, one sees that this corresponds to a penetration of 1.4 microns. It was found that under the experimental conditions available, an exposure of $\frac{1}{4}$ second did not produce any blackening of the film, while $\frac{1}{2}$ second gave a barely observable darkening. Therefore, the reflection for a layer about $1\frac{1}{2}$

[8] D. D'Eustachio and S. B. Brody, J. Opt. Soc. Am. 35, 544 (1945).

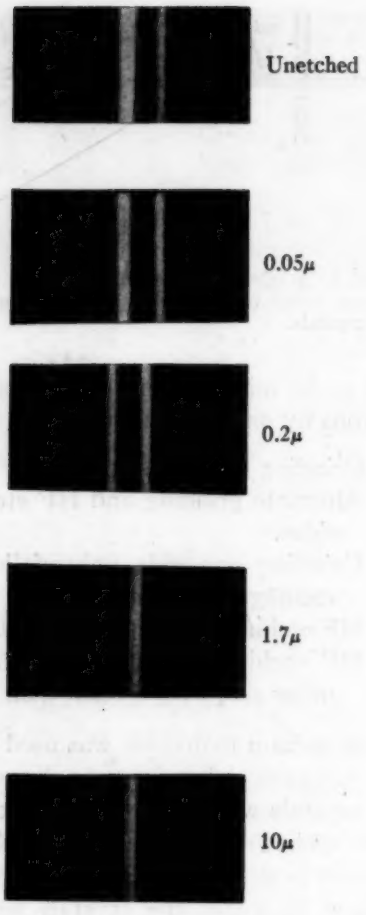

FIG. 2. The effect of etching on the disoriented layer. The line to the left remained undisplaced as the crystal was rotated. The numbers give the thickness, in microns, of the layer that has been etched off. (Cu $K\alpha$ $(10\bar{1}1)$ reflection.)

microns thick was recorded by using 25-second exposures.

Experiments were also carried out with thin plates cut so that the incident radiation made a larger angle with the surface. These were used to investigate the interior of the crystals. They were prepared in the same manner as above.

Topaz was not studied in great detail. It was used primarily to determine whether the behavior described below occurred in other crystals than quartz. Topaz plates were cut parallel to (002) plane, ground to 100 microns, and etched in molten sodium hydroxide in successive steps to 10 microns.

A Philips, air-cooled, copper tube, operating at 34 kv and with currents between 5 ma and 8 ma, was used in all the experiments. The beam was collimated with a pair of slits 0.10 mm by 4 mm, spaced 8 cm apart. A nickel filter that reduced the intensity of Cu $K\beta$ to 1 percent of the original intensity was used throughout. Two film-to-crystal distances were used, 5 cm and 10 cm. To eliminate mounting stresses in the thinnest crystals it was necessary to support them from one corner by a glass fiber ~0.3 micron in diameter.

RESULTS

Disoriented material was observed on all thick specimens of quartz and topaz studied. The photographs still showed two lines after more than 5 mm had been etched from the surface with fused sodium hydroxide. After 1–2 microns were removed by etching, the amount of "disoriented material," as indicated by the intensity of the undisplaced line, became independent of the manner in which the surface was prepared. On unetched surfaces the misalignment increased markedly as the "abrasive vigor" with which the surface was prepared increased. Cleaved topaz and carefully fractured quartz exhibited approximately as much "disoriented material" as etched specimens. Many of the films obtained from unetched crystals showed the undisplaced line after the crystal had been turned through 10°. No reliable evidence for disorientation beyond 1.5 degrees has been found on well-etched material.

A series of pictures showing the effect of etching on quartz with hydrofluoric acid is reproduced in Fig. 2. The crystal was rotated 40′ from the Bragg position. It will be observed

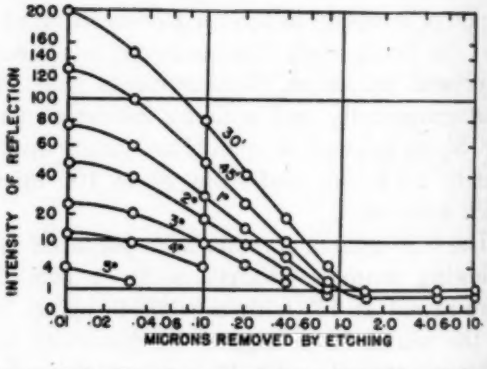

FIG. 3. A family of curves for the intensity of the undisplaced line as a function of depth of etching. The number above each curve gives the angular displacement from the Bragg position.

that after 1.7 microns were removed from the surface the intensity of the undisplaced line remained constant. This result is also shown in Fig. 3 in which the intensity of the undisplaced reflection is plotted against thickness of the layer that has been etched away.

Since "misaligned material" has been found on deeply etched crystals the misalignment cannot be due simply to mechanical disturbance or plastic flow caused by grinding or polishing the surface. Kirkpatrick[9] has pointed out that it is necessary to measure the angle of deviation very accurately to distinguish between Bragg reflection due to crystal imperfection and non-Bragg reflection of the type predicted by Zachariasen[10] and reported by Siegel and Zachariasen[11] and others. Some of the films obtained by the present writer from lightly etched crystals showed two "undisplaced" lines when the deviation from the Bragg position was 2–3 degrees. One of the lines was actually undisplaced, and the other showed a shift in general agreement with Zachariasen's theory. No attempt was made to obtain similar pictures with strongly etched plates because the indicated exposures were too long. Thus, it is necessary to examine more critically the conclusion that one is dealing with a surface phenomenon. The experiments on thin crystals were performed to check this point. These experiments were also intended to give some information about the thickness of the layers.

Figure 4a shows the Cu $K\alpha$ reflection from the $(10\bar{1}1)$ plane in quartz for a crystal 30 microns thick, photographed with the x-rays at grazing incidence, and in Fig. 4b is shown the same crystal after the thickness was reduced to 10 microns. Care was always taken to have the entire surface of the crystal bathed in x-rays. This could be done easily since the small angle of incidence resulted in a beam area approximately 4 mm by 2 mm. The manner in which the crystal was made thinner is significant. The crystal was first reduced from 75 microns to 30 microns by alternately grinding and etching; then to 10 microns by etching material away from the side

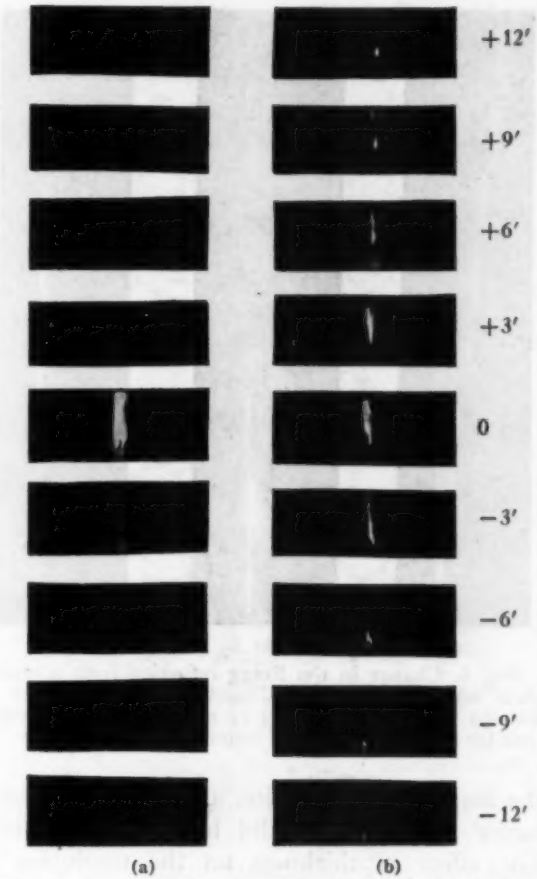

FIG. 4. Change in the character of Bragg reflection from a quartz plate when reduced in thickness by etching. (a) 30 microns. (b) 10 microns thick. The angles given are the deviation from the position for maximum reflection. Exposure times = 25 seconds in all cases.

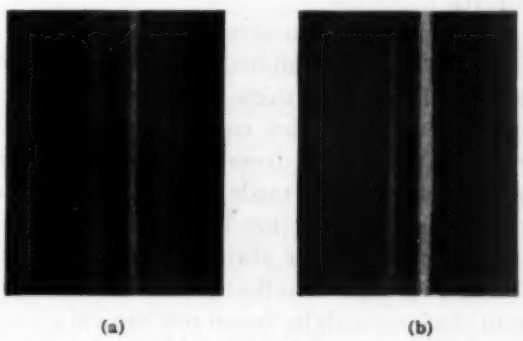

FIG. 5. Resolving power of quartz as a function of thickness. (a) Cu $K\alpha_1$ and Cu $K\alpha_2$ as resolved by a crystal 30 microns thick. (b) 10 microns thick.

that was *not* being photographed. The surface of the plate no longer appears to be good, single crystal. In addition to the variation in the intensity of reflection from different parts of

[9] Paul Kirkpatrick, Phys. Rev. **61**, 452 (1941).
[10] W. H. Zachariasen, Phys. Rev. **57**, 597 (1940).
[11] S. S. Siegel and W. H. Zachariasen, Phys. Rev. **57**, 795 (1940).

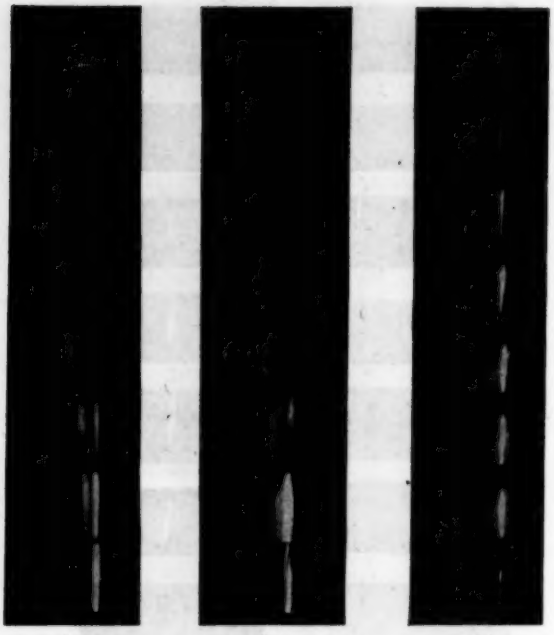

FIG. 6. Change in the Bragg reflection from a quartz plate when reduced in thickness by grinding. (a) 60 microns. (b) 20 microns. (c) 12 microns thick. Exposure time for first picture in each series 25", all others 3 hr.

the surface, the reflection also persisted over a larger angle than it did for thicker crystals. The effect of thickness on the resolution of copper $K\alpha_1$ and $K\alpha_2$ as reflected from the $(10\bar{1}1)$ plane in quartz, is shown in Fig. 5. Changes occur long before they would be expected to occur if the crystal were not becoming more imperfect.

The marked non-uniform reflection shown in Fig. 4b was only exhibited by quartz plates less than 10–15 microns thick. The reflection from a plate 50 microns thick cannot be distinguished from that obtained from a slab 1 mm thick. As the plates were made thinner the non-uniformity in the reflection increased gradually at first and then rather abruptly. All attempts to obtain the type of reflection shown in Fig. 4b from thick crystals by rough mechanical abrasion failed. Two plates lapped to 125 microns with 240 mesh silicon carbide at the rate of 0.005" per minute gave reflections that appeared as homogeneous under the technique described as plates ground slowly with the finest available abrasive. The critical thickness of topaz for the effect described above has not been fully determined, but it appears to be less than 15 microns.

It is possible to combine the Davisson method with the thin crystal experiment. As already noted, with sufficiently long exposures one always obtains in these experiments a pair of lines: one from the characteristic radiation and the "disordered" crystal (which line remains undisplaced), and the second from the continuous background radiation and the main body of the crystal. This latter line is separated from the first by an amount proportional to the angular displacement of the crystal from its Bragg position. When an experiment of this type is carried out with a quartz crystal so cut that the incident x-ray beam makes a very small angle with the crystal, both lines broaden. Since the x-ray beam has a slight divergence, the line due to the continuous background radiation will be somewhat broader than the one arising from the characteristic radiation. The width of the lines is not affected by small changes of the angle between the crystal and the incident beam as long as the disordered material is essentially an ideal mosaic (the mosaic blocks in this case however, must be considered as being distributed over a very much larger angle than is usually ascribed to mosaic crystals). Unlike the previous experiment, here it was desirable to record reflections from the interior of the crystal. This was done by changing the angle of cut slightly (to increase the incident angle) and increasing the exposure appropriately. The expected effect from a ground quartz surface is shown in Fig. 6a. However, the crystal must be thicker than 40–50 microns for this result to be ob-

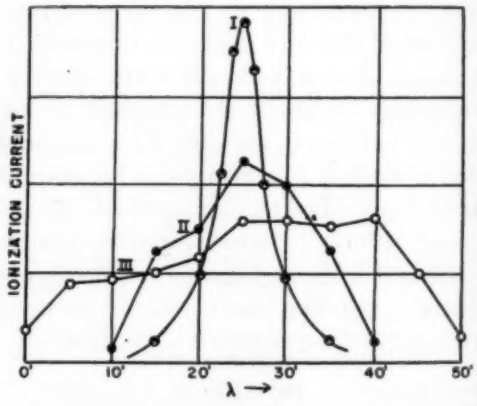

FIG. 7. Rocking curves from quartz. (I) crystal 150 microns thick, (II) crystal 10 microns thick, (III) crystal 10 microns thick after flexing.

served. When thinner quartz crystals were used the line produced by the background radiation broadened, became less uniform, and the integrated intensity increased. Finally, when the crystal was 12 microns thick the continuous radiation produced a band nearly 3° wide. This change is shown in Fig. 6b and 6c. Etching removed the strong undisplaced line, but did not make the broad band narrower. This same result has been obtained with topaz.

Quartz plates 100 microns or less in thickness are quite flexible and can readily be bent around very small cylinders without breaking. Crystals have never been observed however, to acquire a permanent set, even after they have been held in the bent position for three weeks. Nevertheless, when quartz plates are sufficiently thin, bending them produces marked changes in the x-ray diffraction pattern. The nature of the change is shown by the rocking curves, Fig. 7. Curve I was obtained from a quartz crystal 150 microns thick. Curve II was obtained from the same crystal when it was 10 microns and curve III after the crystal was bent 50 times around a cylinder of 1.0-cm radius. The magnitude of the change produced decreased rapidly as the radius of the cylinder was increased. It was necessary to bend a plate many hundred times around a cylinder of 3-cm radius to get a noticeable change in the diffraction pattern. The effect could not be observed with crystals 30–40 microns thick.

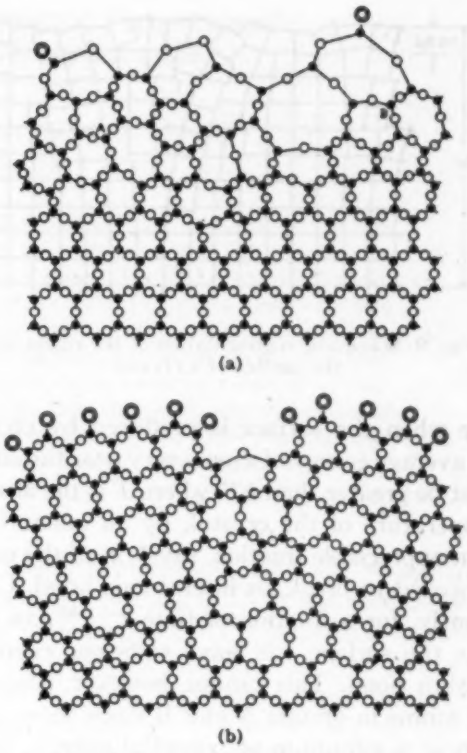

FIG. 8. Schematic representation of changes occurring on a crystal surface shortly after its formation. (a) New surface. (b) Older surface.

DISCUSSION

In interpreting the results from thick crystals it might be supposed that the disorder found on unetched crystals arises from plastic flow, a result of grinding, and that the undisplaced line on etched specimens is due to internal effects. As part of the work reported in this paper, a search was made for evidence of plastic flow in quartz. None was found, and since the effects observed with thin crystals become a function of crystal thickness when the crystals are very thin, one must be dealing with a surface effect.

D'Eustachio and Brody,[7] in their experiments on freshly fractured crystalline materials, observed time-dependent changes which were tantamount to recrystallization of the surface. As an explanation for the phenomenon they suggested that immediately upon the formation of a surface on valence crystals at least part of the surface energy is in the form of structure irregularity and a thin, highly stressed (possibly glassy), layer is formed. This layer is unstable and initiates recrystallization. The nature of the changes as visualized by this theory is illustrated schematically in Fig. 8: (a) representing the region in the vicinity of the surface immediately after formation, and (b) the same region at a slightly later time. Very few atomic layers are initially disturbed by the rupture. There will be no long range order near the surface, but there will be small groups of atoms (A and B in Fig. 8a) which, though displaced with respect to the original crystal, will (accidentally?) have a high degree of short range order. Such groups will act as centers of growth leading to "disoriented" crystallites. Using a thermodynamic argument, it is not difficult to see how this "recrystallization" occurs. Since it has been assumed that only a few surface layers are disturbed by the formation of the surface (and it is difficult to see how this can be other-

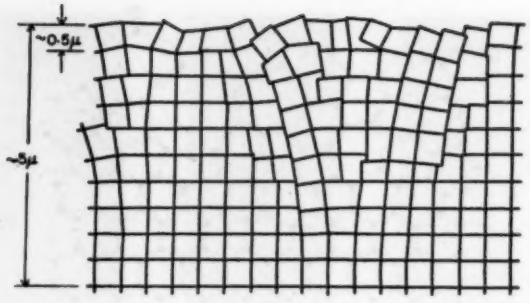

FIG. 9. Schematic representation of the region near the surface of a crystal.

wise when the surface is produced by etching) the average energy of atoms very near the surface must be greater than kT, where T is the absolute temperature of the crystal, by an amount that is an appreciable fraction, say $1/n$, of the energy U needed to break an interatomic bond. Consequently, for a fraction of time $e^{-U/nkT}$, an atom near the surface will have sufficient energy to break a bond. This cannot, however, happen to the atoms in groups A and B since these are at or near a minimum of potential energy. So the nuclei will grow. This growth will not eliminate all structure irregularities because the growing crystallites in general will be disoriented with respect to the original crystal. There results instead a diffusion of imperfections into the interior of the crystal. This is the condition shown in Fig. 8b. The experimental results show that some disturbance must penetrate a number of microns, but that the badly disoriented layer is less than half a micron thick. Just how or why the process can continue to the depth indicated by experiment is not clear. There is evidence from frequency measurements of quartz oscillator plates that a stable state is not attained unless the surface is covered with a monolayer. Such a layer is shown in Fig. 8. The final state may perhaps be represented as shown in Fig. 9. Presumably, the interpenetration of two of these surface layers causes further changes, resulting in the "polycrystalline" material that composes the thinnest plates.

It should not be difficult to cause the displaced atoms connecting the crystallites nearest the surface to undergo further changes. Bending the plates around small cylinders (particularly if the radius of the cylinder is chosen so as to stress the plates almost to the rupture point) can obviously supply the needed energy.

Finally, it is necessary to account for the marked decrease in disoriented material on etched surfaces. It is known from comparison of electron microscope pictures of ground and etched quartz crystals that a very large decrease in the surface area occurs on etching. Thus, the observed decrease in disoriented material is partly due to the change in surface area. It has also been observed that freshly ground quartz surfaces which were left undisturbed for a few weeks were covered with a fine, white powder. Spectroscopic examination showed this powder to contain silicon, and there is little doubt that the material is quartz.[12] Some of this flaking off will occur in the cracks that cover a ground surface and the particles may remain wedged in place. These will tend to retain the orientation of the original crystal though displacement of a few degrees can occur. Being small, their large total surface will contribute strongly to the undisplaced reflection.

The author is indebted to Mr. Samuel Gordon of the Philadelphia Academy of Natural Sciences for an excellent specimen of topaz.

[12] See C. Frondel, Am. Mineralogist **30**, 422 (1945).

Elastic, Piezoelectric, and Dielectric Properties of Sodium Chlorate and Sodium Bromate

W. P. MASON
Bell Telephone Laboratories, Murray Hill, New Jersey
(Received July 15, 1946)

The elastic, piezoelectric, and dielectric constants of sodium chlorate ($NaClO_3$) and sodium bromate ($NaBrO_3$) have been measured over a wide temperature range. The value of the piezoelectric constant at room temperature is somewhat larger than that found by Pockels. The value of the Poisson's ratio was found to be positive and equal to 0.23 in contrast to Voigt's measured value of -0.51. At high temperatures the dielectric and piezoelectric constants increase and indicate the presence of a transformation point which occurs at a temperature slightly larger than the melting point. A large dipole piezoelectric constant (ratio of lattice distortion to dipole polarization) results for these crystals but the electromechanical coupling factor is small because the dipole polarization is small compared to the electronic and ionic polarization and little of the applied electrical energy goes into orienting the dipoles.

I. INTRODUCTION

SODIUM chlorate ($NaClO_3$) is a water soluble crystal which crystallizes in the cubic tetrahedral class. As a consequence of its symmetry, it has three elastic constants, one piezoelectric constant, and one dielectric constant. Its isomorphous salt, sodium bromate ($NaBrO_3$), crystallizes in the same crystal class. Measurements were made of the piezoelectric constant of sodium chlorate as early as 1893 by Pockels[1] who obtained a value of 4.84×10^{-8} for the piezoelectric constant d_{14}. Voigt[2] measured the elastic constants and came to the conclusion that the crystal had a negative Poisson's ratio; i.e., the crystal expands sidewise as it elongates lengthwise. The measurements made here do not confirm this conclusion. Since this crystal has such a simple structure, has no water of crystallization, and will stand a high temperature (up to 250°C), it was thought worth while to investigate its properties even though the indicated piezoelectric effect was quite small.

X-ray crystal structure studies[3] show that sodium chlorate has four molecules per unit cell. Each molecule consists of three oxygens arranged in the form of an equilateral triangle with a separation of 2.38A between oxygen centers as shown by Fig. 1. The chlorine is located at a distance of 0.48A above the plane of the oxygen atoms in a line through the center of gravity of the oxygens. The sodium lies above the chlorine at a distance of 6.12A. On account of the large separation of the sodium from the chlorate ion, it is probably the latter which acts as the dipole in

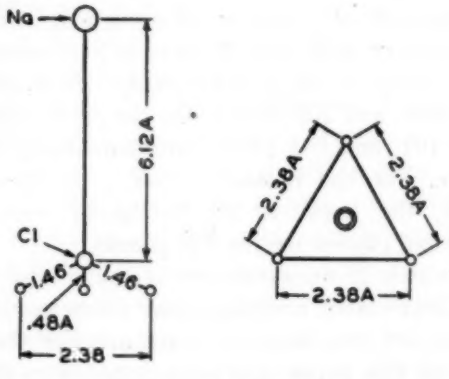

FIG. 1. Arrangement of atoms in sodium chlorate molecule.

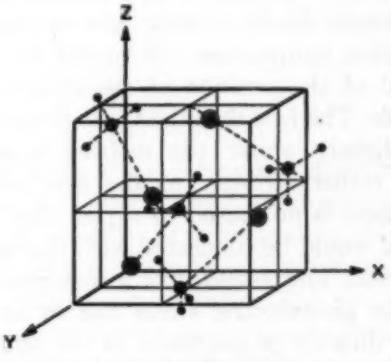

FIG. 2. Arrangement of sodium chlorate molecules in unit crystal cell.

[1] W. Voigt, *Lehrbuch Der Kristall Physik*, p. 873.
[2] W. Voigt, *Lehrbuch Der Kristall Physik*, p. 741.
[3] R. W. G. Wyckoff, *The Structure of Crystals* (Chemical Catalog Company, New York), p. 276.

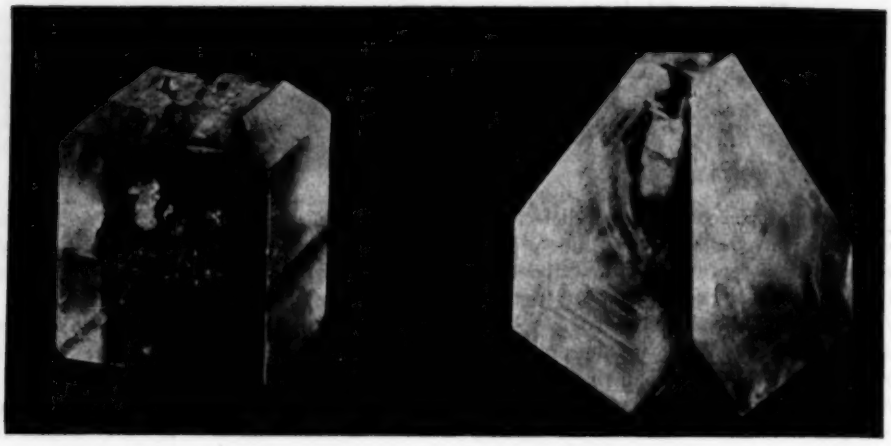

FIG. 3. Photograph of sodium chlorate crystal (left) and sodium bromate crystal (right).

the temperature variable part of the dielectric constant. The arrangement of the four molecules in the unit cell is shown by Fig. 2.

The experimental results for the dielectric constant show that there is a component of the polarization which is practically independent of the temperature and another component which increases with temperature and becomes large as the melting point is approached. This is presumably caused either by an actual orientation of the chlorate dipoles as they become unfrozen at the higher temperature, or caused by an apex reversal of the position of the chlorine in the molecule. The fact that the Curie temperature is only slightly above the melting temperature points rather strongly to the first alternative since there is no reason to expect that an apex reversal would be connected with the melting of the crystal. The piezoelectric measurements show that the piezoelectric stress due to an applied field is directly proportional to the temperature variable component of the polarization and hence it is the change in orientation of the dipoles which causes the distortion of the crystal lattice and hence the piezoelectric effect.

Similar measurements have been made for the isomorphous salt sodium bromate. The temperature independent dielectric constant is larger than for sodium chlorate, indicating that the polarizability of the bromine is larger than that for the chlorine. For equal temperature separations from the Curie point (which is close to the melting point) the temperature variable portion of the polarization is nearly the same size as that for sodium chlorate, indicating that the effective dipole moment is nearly the same. The piezoelectric measurements show that a given dipole polarization produces over twice the lattice distortion and hence piezoelectric effect for sodium bromate as for sodium chlorate.

II. SYMMETRY CONSIDERATIONS AND THE RESULTING PIEZOELECTRIC EQUATIONS

Crystals of sodium chlorate and sodium bromate have been grown by A. N. Holden from a saturated water solution by slowly reducing the temperature and depositing the salt on a prepared seed. The process will be described in a forthcoming paper. Both crystals belong to the cubic tetrahedral class but there is an interesting difference in their crystal habits. Figure 3 shows a photograph of a sodium chlorate and a sodium bromate crystal. The chlorate crystal assumes a cubic form of which the principal faces are the 001, 010, and 100 planes. On the cube edges the 110, 101, and 011 planes are sometimes in evidence. For the bromate crystal, on the other hand, the habit is the tetragonal one. The principal planes are the 111 planes.

Because of the symmetry of the crystal, there are three elastic constants, one piezoelectric constant, and one dielectric constant. For the purpose of this paper it is advantageous to express the piezoelectric relations in the form of a ratio of the strain to the electric displacement. This follows from the fact that it is found that the

strain is nearly proportional to the temperature variable part of the polarization. Since a system of equations, which involves quantities that can be directly measured, cannot be based on the polarization or a part of the polarization, the electrical displacement is employed. As will be shown, the polarization constants are easily obtained from these and the measured dielectric constants.

On this basis the piezoelectric equations for sodium chlorate or sodium bromate can be written

$$\begin{aligned}
&S_1=s_{11}T_1+s_{12}T_2+s_{12}T_3, \quad && S_6=s_{44}{}^{D}T_6+g_{14}\frac{D_z}{4\pi},\\
&S_2=s_{12}T_1+s_{11}T_2+s_{12}T_3, \quad && E_x=\frac{D_x}{\epsilon_1{}^{T}}-g_{14}T_4,\\
&S_3=s_{12}T_1+s_{12}T_2+s_{11}T_3, \quad && E_y=\frac{D_y}{\epsilon_1{}^{T}}-g_{14}T_5, \qquad (1)\\
&S_4=s_{44}{}^{D}T_4+g_{14}\frac{D_x}{4\pi}, && E_z=\frac{D_z}{\epsilon_1{}^{T}}-g_{14}T_6,\\
&S_5=s_{44}{}^{D}T_5+g_{14}\frac{D_y}{4\pi},
\end{aligned}$$

where $S_1, \cdots, S_6$ are the six strain components, $T_1, \cdots, T_6$ the six stress components, $E_x, \cdots, E_z$ the three field strengths in the three directions, $D_x, \cdots, D_z$ the three electric displacements which at the surface are equal to the surface charges times 4π, s_{11}, s_{12}, $s_{44}{}^{D}$ the three elastic constants, g_{14} the piezoelectric constant which measures the ratio of the strain to the surface charge in the absence of a stress, and $\epsilon_1{}^{T}$ the dielectric constant, that is the same in every direction. The elastic constant $s_{44}{}^{D}$ has a superscript D to show that it is the ratio of the strain to the applied stress when the electric displacement is constant or zero. Similarly the dielectric constant $\epsilon_1{}^{T}$ has a superscript T to indicate that it is the "free" dielectric constant measured in the absence of an applied stress.

Another form of the piezoelectric equations in which the stresses are expressed as a function of the strain is also of interest. These can be obtained from Eqs. (1) by solving for the stresses in terms of the strains. These become

$$\begin{aligned}
&T_1=c_{11}S_1+c_{12}S_2+c_{12}S_3, \quad && T_6=c_{44}{}^{D}S_6-h_{14}\frac{D_z}{4\pi},\\
&T_2=c_{12}S_1+c_{11}S_2+c_{12}S_3, \quad && E_x=\frac{D_x}{\epsilon_1{}^{S}}-h_{14}S_4,\\
&T_3=c_{12}S_1+c_{12}S_2+c_{11}S_3, \quad && E_y=\frac{D_y}{\epsilon_1{}^{S}}-h_{14}S_5, \qquad (2)\\
&T_4=c_{44}{}^{D}S_4-h_{14}\frac{D_x}{4\pi}, && E_z=\frac{D_z}{\epsilon_1{}^{S}}-h_{14}S_6,\\
&T_5=c_{44}{}^{D}S_5-h_{14}\frac{D_y}{4\pi},
\end{aligned}$$

where

$$\begin{aligned}
c_{11}&=\frac{s_{11}+s_{12}}{s_{11}(s_{11}+s_{12})-2s_{12}{}^{2}},\\
c_{12}&=\frac{-s_{12}}{s_{11}(s_{11}+s_{12})-2s_{12}{}^{2}},\\
c_{44}{}^{D}&=\frac{1}{s_{44}{}^{D}}, \quad h_{14}=g_{14}c_{44}{}^{D},\\
\frac{4\pi}{\epsilon_1{}^{S}}&=\frac{4\pi}{\epsilon_1{}^{T}}+g_{14}h_{14}=\frac{4\pi}{\epsilon_1{}^{T}}+\frac{g_{14}{}^{2}}{s_{44}{}^{D}}.
\end{aligned} \qquad (3)$$

Here $\epsilon_1{}^{S}$ denotes the "clamped" dielectric constant, i.e., the dielectric constant measured in the absence of a strain. It is related to the "free" dielectric constant as indicated in Eq. (3).

If we wish to test whether the piezoelectric strain is caused by the temperature variable part of the polarization, we can write

$$\begin{aligned}
\frac{D_x}{4\pi}=\sigma_x&=\frac{E_x}{4\pi}+P_{x0}+P_x'\\
&=\frac{E_x}{4\pi}[1+4\pi\eta_0]+P_x'=\frac{E_x\epsilon_0}{4\pi}+P_x', \qquad (4)
\end{aligned}$$

where ϵ_0 is the temperature and strain independent part of the dielectric constant. Introducing this value into Eq. (2) and eliminating common terms, the equations involving the

piezoelectric effect become

$$T_4=c_{44}{}^{*}S_4-f_{14}P_x', \quad E_x=\frac{4\pi P_x'}{\epsilon_1{}^{S}-\epsilon_0}-f_{14}S_4, \tag{5}$$

where

$$f_{14}=\frac{h_{14}\epsilon_1{}^{S}}{\epsilon_1{}^{S}-\epsilon_0}, \quad c_{44}{}^{*}=c_{44}{}^{D}+\frac{h_{14}{}^{2}\epsilon_0\epsilon_1{}^{S}}{4\pi(\epsilon_1{}^{S}-\epsilon_0)}$$

$c_{44}{}^{*}$ is the elastic compliance with P_x' held constant or zero. f_{14} is the ratio of the stress to the temperature variable part of the polarization in the absence of an internal strain. Hence if the piezoelectric constant g_{14} or h_{14} and the constant and temperature variable parts of the dielectric constant are determined, the ratio of stress to temperature variable polarization can be evaluated.

The method of evaluating the piezoelectric constant employed has been to utilize a longitudinally vibrating crystal cut with its length at 45° from two of the axes and with its thickness along the third axis. The measurements made are an evaluation of the capacity at low frequencies (free dielectric constant) and the resonant and anti-resonant frequencies. Since the relation between these quantities has been discussed at length in another publication,[4] only the pertinent equations will be given here.

The frequency of resonance of the longitudinally vibrating plated crystal and the measured density determine the elastic compliance at constant field according to the equation

$$s^{E}=\frac{1}{(2lf_R)^{2}\rho}, \tag{6}$$

where l is the length of the crystal, f_R the resonant frequency, and ρ the density. The separation Δf between resonant and antiresonant frequencies, determines the electromechanical coupling constant k, according to the formula

$$k=\frac{1}{\left(1+\frac{4}{\pi^{2}}\frac{f_R}{\Delta f}\right)^{\frac{1}{2}}}, \tag{7}$$

where k the coupling factor is defined in terms of the fundamental constants by the equation

$$k=g\left(\frac{\epsilon^{T}}{4\pi s^{E}}\right)^{\frac{1}{2}}. \tag{8}$$

In this equation g is the longitudinal piezoelectric constant relating the strain to the applied charge, ϵ^{T} the free dielectric constant normal to the

TABLE I. Measured properties of sodium chlorate.

Temperature in degrees C	Z-cut; L=22.5° from X L=20.13 mm W=2.69 mm T=1.00 mm	Z-cut; L=45° from X L=20.38 mm W=2.71 mm T=1.01 mm	0° Z-cut L=29.90 mm W=6.02 mm T=1.04 mm	$\Delta f/f_R$ for 45° Z-cut	Free dielectric constant $\epsilon_1{}^{T}$
28	193.2 kc cm	181.8 kc cm	108.6	0.000281	5.76
40	192.2	180.9	108.3	0.000317	5.8
75	190.2	179.3	108.2	0.000393	5.94
100	187.2	177.2	106.2	0.000465	6.05
130	183.4	173.5	104.2	0.000584	6.21
140	182.3	172.5	103.8	0.00065	6.27
150	181.3	171.3	103.1	0.000725	6.34
160	—	170.3	102.5	0.000807	6.41
170	178.6	169.2	102.0	0.000894	6.49
180	177.5	168.3	101.2	0.00098	6.57
190	176.1	167.1	100.4	0.00115	6.70
200	175.1	166.2	99.9	0.00134	6.81
210	173.1	164.5	99.1		
220	172.2	163.3	98.3		
230	170.3	161.3	97.2		
240	168.5	160.2	96.2		

[4] See W. P. Mason, Phys. Rev. 69, 173–195 (1946).

SUBSTANCE	COEF. OF THERMAL EXPANSION ($10^6 \times \Delta l/l$ PER DEGREE C)			$\Delta l/l = a(t-25) + b(t-25)^2$	
	-40° TO 0°	0° TO 50°	50° TO 90°	$10^5 \times a$	$10^8 \times b$
S.B.	37.5	39.2	41.7	3.94	1.0
S.C.	40.8	43.4	45.2	4.38	3.8

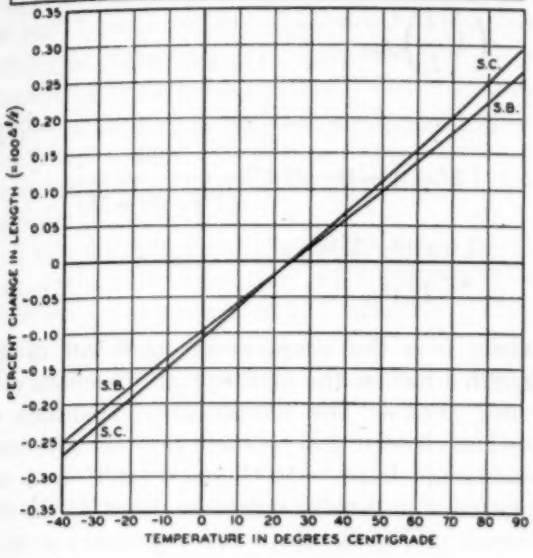

FIG. 4. Percent linear thermal expansion of sodium bromate and sodium chlorate.

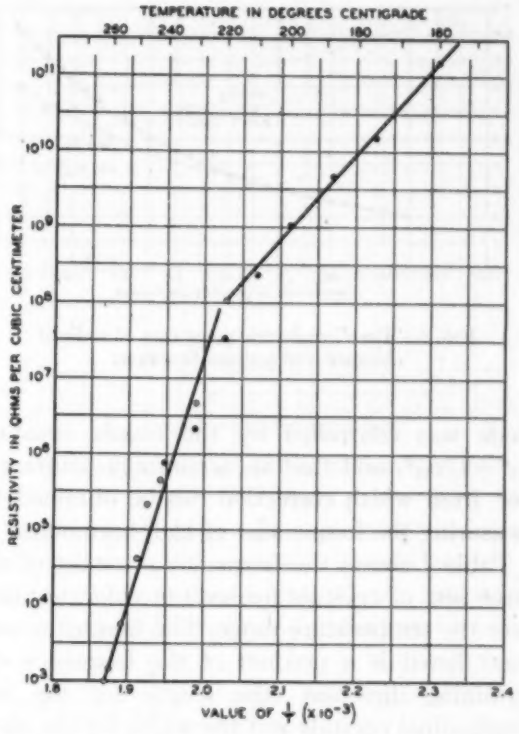

FIG. 5. Resistivity as a function of temperature.

applied voltage, and s^E the inverse of Young's modulus along the length of the crystal measured at constant field.

Measurements with longitudinally vibrating crystals will determine one elastic constant and a relation between the other two. To determine the shear elastic constant requires a measurement of a shear vibrating crystal. It has been shown previously[4] that a face shear mode of a long thin crystal will determine the shear elastic constant according to the equation

$$s^E = \frac{1}{(2l_w f_R)^2 \rho}, \tag{9}$$

where l_w is the width of the shear vibrating crystal. The coupling for a shear mode is determined by Eq. (7) if the coupling is defined as in Eq. (8) using the shear piezoelectric constant and the shear elastic constant.

III. MEASUREMENT OF PRIMARY ELASTIC, PIEZOELECTRIC, AND DIELECTRIC CONSTANTS OF SODIUM CHLORATE AND SODIUM BROMATE

All of the constants of these crystals can be measured by measuring the properties of three oriented cuts. All cuts are taken normal to one of the crystallographic axes, which for convenience will be designated the Z axis. One cut has its length 45° from the other two axes, one cut has its length 22.5° from one of the axes, and the third cut has its length along one of the crystallographic axes. The first two cuts are driven in their lowest longitudinal mode and are made long compared to their width or thickness so that the uncorrected compliance constant $s_{11}^{E'}$ is determined. As a function of orientation this compliance is given by the equation.

$$s_{11}^{E'} = s_{11}(\cos^4\varphi + \sin^4\varphi) + (2s_{12} + s_{44}^E)\sin^2\varphi\cos^2\varphi. \tag{10}$$

Hence measurements of the resonant frequencies, the expansion coefficient of the material, and the density at 25°C will determine two values of $s_{11}^{E'}$ for two different angles and hence s_{11} and $(2s_{12}+s_{44}^E)$ can be evaluated over a range of temperatures. The third crystal is cut thin, and with its width dimension much smaller than its length. It was demonstrated in a previous paper[4] that the resonant frequency of the face shear

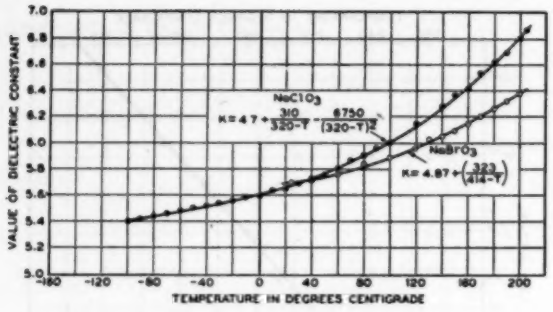

FIG. 6. "Free" dielectric constants of sodium chlorate and sodium bromate.

mode was controlled by the elastic constant $c_{44}^E = 1/s_{44}^E$, and that an accurate measurement free from width correction can be obtained by measuring the frequencies of high harmonics.

Table I shows the frequency constant of the three sets of crystals for sodium chlorate taken over the temperature range. The frequency constant listed is a product of the frequency determining direction (the length for the two longitudinal crystals and the width for the shear crystal), measured at 25°C, by the frequency of vibration. Since the frequency of vibration is given by the formula

$$f=\frac{1}{2l}\left(\frac{1}{\rho s^E}\right)^{\frac{1}{2}} \tag{11}$$

and $f_c = fl_0$ where l_0 is the length measured at 25°C, the elastic constant s^E is given by the formula

$$s^E=\frac{1}{\left(2f_c\frac{l}{l_0}\right)^2\rho}$$

$$=\frac{1}{[2f_c(1+\alpha(\Theta-25))]^2\frac{\rho_0}{[1+\alpha(\Theta-25)]^3}}, \tag{12}$$

$$=\frac{1+\alpha(\Theta-25)}{(2f_c)^2\rho_0},$$

where α is the temperature coefficient of the length which is the same for all directions of a cubic crystal. The temperature expansions of sodium chlorate and bromate crystals have been measured[5] from −50°C to +110°C and are plotted as a percent expansion from 25° by the curves of Fig. 4. Since this represents a small correction to the elastic constant, the curves have been extrapolated up to the highest temperature used.

As the temperature increased, it was found that the dielectric and piezoelectric constants also increased. At 200°C the leakage resistance of the crystal became noticeable and became low enough at 210°C and higher to make the measurement of the dielectric constant and the anti-resonant frequency unreliable. The resistivity

TABLE II. Elastic compliances and piezoelectric constants of sodium chlorate.

Temperature in °C	Expansion of length compared to length at 25°C	Value of $s_{11}^{E'}$ for 22.5° crystal	Value of $s_{11}^{E'}$ for 45° crystal	Value of s_{44}^E	Value of piezoelectric constant g_{14}	Value of piezoelectric constant h_{14}	Value of f_{14}	Value of d_{14}
28	1.000	2.69×10^{-12} cm²/dyne	3.045×10^{-12}	8.54×10^{-12}	13.7×10^{-3}	1.61×10^{4}	8.75×10^{4}	$6.2\times10^{-$
40	1.00055	2.705	3.075	8.60	14.6	1.69	8.85	6.6
75	1.00215	2.825	3.175	8.86	16.2	1.83	8.75	7.6
100	1.0033	2.895	3.265	9.05	17.8	1.96	8.75	8.5
130	1.0047	3.005	3.360	9.30	19.9	2.14	8.8	9.9
140	1.00512	3.038	3.402	9.41	20.8	2.22	8.78	10.4
150	1.00557	3.080	3.445	9.49	22.1	2.34	9.05	11.2
160	1.00604	3.130	3.49	9.56	23.2	2.42	9.05	11.9
170	1.00647	3.185	3.525	9.72	24.4	2.52	9.10	12.7
180	1.00695	3.205	3.565	9.85	25.6	2.60	9.10	13.5
190	1.0074	3.255	3.62	10.00	27.6	2.77	9.20	14.8
200	1.00787	3.305	3.675	10.13	29.8	2.94	9.40	16.2
210	1.00832	3.360	3.735	10.3				
220	1.00877	3.402	3.795	10.48				
230	1.00925	3.482	3.882	10.71				
240	1.00967	3.565	3.96	10.93				

[5] This measurement was made by Miss E. J. Armstrong.

curve as a function of temperature is shown plotted by Fig. 5. At 245°C the resistivity was low enough so that no appreciable piezoelectric response was obtained and, at the melting point of 263°C, the resistivity was less than 1000 ohms per cubic centimeter. This indicates that as the crystal approaches its melting point, it becomes highly ionized with the chlorate ion separating from the sodium ion for a large number of molecules. This behavior is usual for an ionic crystal.

Table I shows also the ratio $\Delta f/f_R$ for the 45° cut, and the free dielectric constant measured at 1000 cycles, as a function of temperature. These quantities were measured with the crystals in holders for which all stray capacities were tied to ground and since the impedances in the measuring circuits were low, these can be neglected. Hence no corrections had to be made and the measured results are given directly. From the data given in Table I, all the constants can be evaluated. The data for the dielectric constants of sodium chlorate and sodium bromate are shown plotted in Fig. 6. The dielectric constant can be expressed as a function of temperature by the empirical equation

$$\epsilon = 4.7 + \frac{310}{320-\Theta} - \frac{6750}{(320-\Theta)^2}. \tag{13}$$

This indicates that there is a part equal to 4.7 that is independent of temperature and another part that varies with temperature and becomes large for temperatures approaching 320°C. The first part is caused by the electronic and ionic polarizabilities while the temperature variable part is caused by changes in orientation of dipoles or to displacement of loosely bound ions such as exist in glass. This happens more freely as the temperature increases. Since no adequate treatment of the dielectric constant has been made for temperatures below a transition point, an empirical formula has to be resorted to in order to locate the temperature transition point. For sodium bromate, since the measured values are taken considerably below the transition point, a single term is sufficient to fit the curve and we have

$$\epsilon = 4.87 + \frac{(323)}{(414-\Theta)}. \tag{14}$$

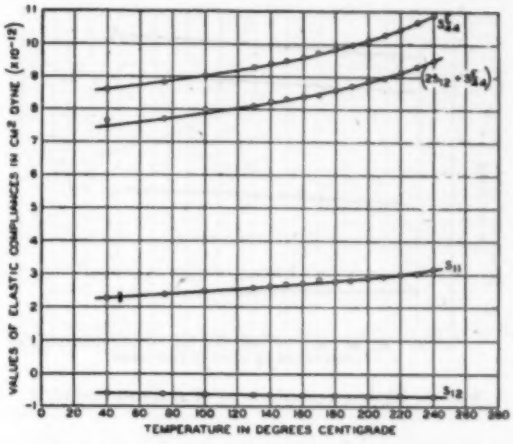

FIG. 7. Elastic compliances of sodium chlorate.

Table II shows a calculation of the elastic compliances of the three crystals shown in Table I. Since the value of $s_{11}^{E'}$ as a function of the orientation for a crystal cut normal to Z can be written

$$s_{11}^{E'} = s_{11}(\sin^4\varphi + \cos^4\varphi) + (2s_{12}+s_{44}^{E})\sin^2\varphi\cos^2\varphi,$$

the values of s_{11} and $(2s_{12}+s_{11}^{E})$ are given by

$$\begin{aligned} s_{11} &= 2s_{11}^{E'}{}_{22.5°} - s_{11}^{E'}{}_{45°}, \\ (2s_{12}+s_{44}^{E}) &= 6s_{11}^{E'}{}_{45°} - 4s_{11}^{E'}{}_{22.5°}. \end{aligned} \tag{15}$$

Since s_{44}^{E} is evaluated in column 5 of Table II, all three elastic constants can be determined and they are shown plotted by Fig. 7. Since the elastic constant s_{44}^{D} is related to s_{44}^{E} by the equations

$$s_{44}^{D} = s_{44}^{E} - g_{14}^2\epsilon_1^T/4\pi, \tag{16}$$

it can be evaluated from the data of Table II and Fig. 7. It differs from s_{44}^{E} by too small an amount to plot on the curve and hence is not shown.

The only previous data is that published by Voigt[2] who found

$$\begin{aligned} s_{11} &= 2.46\times10^{-12}\ \text{cm}^2/\text{dyne}, \\ s_{12} &= +1.252\times10^{-12}, \\ s_{44} &= 8.36\times10^{-12} \end{aligned} \tag{17}$$

at room temperature. These data resulted in a negative Poisson's ratio (one which causes the cross-sectional dimensions to increase as the

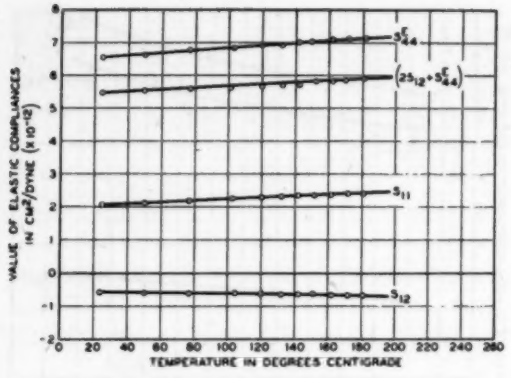

FIG. 8. Elastic compliances of sodium bromate.

length increases) of -0.51, a point that was stressed by Voigt. The present data, however, do not support this conclusion for the value of s_{12} found is negative giving a Poisson's ratio of 0.23, which is an ordinary value to be expected.

The values of the piezoelectric constants g_{14} and h_{14} are given by the sixth and seventh columns. Since the Voigt piezoelectric constant d_{14} (relating the piezoelectric strain to the applied field) is related to g_{14} by

$$d_{14}=g_{14}\frac{\epsilon_1{}^T}{4\pi}, \tag{18}$$

the value of d_{14} at room temperature is 6.1×10^{-8}, which is somewhat larger than Pockels' value of 4.84×10^{-8}.

We note from Table II that both g_{14} and h_{14} increase considerably as the temperature rises. To test whether the piezoelectric strain is proportional to that part of the polarization which varies with temperature, use is made of Eq. (5) and the data on the dielectric constant given in Eq. (11). The resulting value of f_{14} is shown in the next to the last column and within the experimental accuracy is a constant 9×10^4. This indicates that there is a one to one correspondence between the rotation of the dipoles in the unit cell and the shear stress on the unit cell.

Similar measurements have been made on three sodium bromate crystals cut with the same orientations with respect to the crystallographic axes. The dielectric constant as a function of temperature is shown by Fig. 6. This variation satisfies the formula

$$\epsilon^T=4.87+323/(414-\Theta). \tag{14}$$

Since the melting point is known to be about 400°C, this indicates again that if there is a Curie temperature it is near the melting point. The three elastic compliances are shown plotted in Fig. 8. They show a linear variation and do not have the curvature of sodium chlorate since the temperature is farther from the melting point. The piezoelectric constants are shown by Fig. 9. From these data it can be shown that the piezoelectric constant f_{14} is independent of the temperature and equal to 18×10^4. It is over twice as large as the constant for sodium chlorate.

IV. DISCUSSION OF RESULTS

From the experimental data obtained it appears possible to conclude that the dielectric constant is made up of a part which is relatively temperature independent and another part that varies nearly inversely as the difference between a temperature θ, possibly a Curie temperature, and the actual temperature. However the dielectric constant data place this Curie temperature above the melting point. The fact that one component of the dielectric constant varies with temperature indicates that this component may be caused by dipoles that become unfrozen as the temperature increases. This polarization might be caused by an actual rotation of the dipoles as is usually assumed, or it might be caused by an inversion of the position of the chlorine in the chlorate ion as has been found to occur in the similar nitrate ion NO_3. Either assumption would give a component of the polarization that varied with temperature. There is no reason to suppose, however, that the temperature of an apex inversion would be in any way connected with the melting point, whereas if the component is caused by an actual rotation of the dipoles, the dipoles might well become free rotationally at about the same temperature that they become free translationally. At that tem-

TABLE III. Comparison of the dipole piezoelectric effect in four crystals.

Material	f_{14}	Electromechanical coupling factor at 25°C
KH_2PO_4	3×10^4	0.11
$NH_4H_2PO_4$	16×10^4	0.29
$NaClO_3$	9×10^4	0.03
$NaBrO_3$	18×10^4	0.04

perature all the free dipoles could show a cooperative effect and hence a dielectric Curie point, so that the evidence seems to point to an actual rotation of the dipoles as the cause of the temperature variable part of the polarization. The temperature independent part of the dielectric constant is presumably caused in part by electronic polarization of the component sodium, oxygen, and chlorine of the molecules. Since the square of the refractive index of both salts is about 2.5 there is also an appreciable temperature independent polarization caused presumably by displacements of the lattice ions. At present there is no adequate theory for connecting the number of molecules per cc and the average dipole moment per molecule with the susceptibility of a solid below a Curie point.

The measurements of the piezoelectric constant given in Section III show conclusively that the gross distortion of the lattice under an applied charge (the piezoelectric effect) is directly proportional to that portion of the polarization which varies with temperature, i.e., the part due to change in orientation of the dipoles. A comparison of this dipole piezoelectric effect, which has been measured for four crystals, is shown by Table III. This table shows that this constant varies for different crystals by a factor of about 6 to 1 being highest for sodium bromate and lowest for potassium dihydrogen phosphate. The next column shows the value of the electromechanical coupling factor which is a measure of the amount of the total applied electrical energy that appears in mechanical form under static conditions. An examination of the data shows that this is low for sodium chlorate and sodium bromate because the electronic and ionic polarization is large compared to the dipole polarization and hence only a small fraction of the total input electrical energy goes into orienting the dipoles. KDP which has a smaller dipole piezoelectric constant has a larger electromechanical coupling because of the fact that the dipole polarization represents about three fourths of the total polarization, whereas for sodium chlorate it is only 0.2 of the total. Ammonium dihydrogen phosphate obtains its large coupling because of the fact that over fifty percent of the total polarization is dipole polarization and in addition the dipole piezoelectric constant is large.

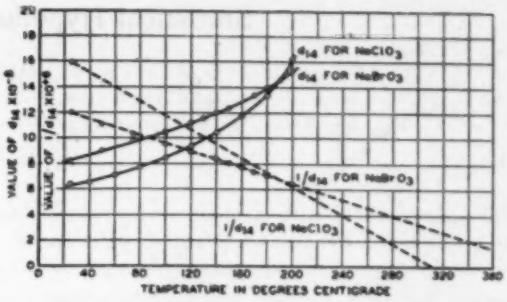

FIG. 9. Piezoelectric constants d_{14} for $NaClO_3$ and $NaBrO_3$ as a function of temperature.

PHYSICAL REVIEW VOLUME 70, NUMBERS 7 AND 8 OCTOBER 1 AND 15, 1946

Statistical Hypotheses in Stellar Dynamics

HERBERT JEHLE
Institut d'Astronomie, Université libre de Bruxelles, Belgium, and
Jefferson Physical Laboratory, Harvard University, Cambridge, Massachusetts

(Received April 11, 1945)

This paper starts with a short review of the usual methods of stellar dynamics and analyzes the underlying hypotheses. The most successful approach to stellar dynamics has been the one which neglects interactions between nearby stars (because they are weak) and takes into consideration the motion of stars in a smooth field of force only, produced by the smeared-out mass distribution of the stellar system. This method is based on nothing but mechanics. It is, however, a semi-empirical one because it is confined to systems in such a state and for so short a duration that stellar encounters may be neglected. It does not explain how stellar systems reached their present state. This as well as the explanation of statistical distributions cannot be hoped to be achieved by merely using mechanics. It is necessary to introduce statistical hypotheses to provide the means for attacking problems of a statistical character, such as a theory of stellar systems including interactions of individual stars. A similar situation is exemplified by Clausius-Boltzmann's hypothesis concerning molecular chaos (*Stosszahlansatz*) which in its statistical interpretation provides the essential basis for deriving the second law of thermodynamics from the kinetic theory of gases. Compare with the discussion of the principles of kinetic theory by P. and T. Ehrenfest, Enzyclopaedie d. math. Wiss. 4, Art. 32, and R. C. Tolman, *Principles of Statistical Mechanics*. One attack on the general statistical problem is the method of force fluctuations. But this method is limited: In order to be able to calculate the relevant data about force fluctuations, it is necessary to assume the distances between, and the velocity- and mass-distributions of the stars, all numerical data about which have to be borrowed from observation. Besides, the actual interaction of nearby masses is a play between single stars, multiple stars, and star clusters, and it is impossible to calculate force fluctuations between those complex subsystems of a stellar system without a great number of artificial assumptions. Therefore we should like to examine the consequence of a more basic hypothesis: Provided the large scale development of a stellar system is so slow that it can approximately be regarded as sliding from one statistical equilibrium state (as concerns the mutual adjustments of the elements) to another, we assume that statistically independent elements of a stellar system (e.g. galactic clusters or multiple stars or independent single stars as elements of their stellar system—our galaxy) cannot be crowded into Boltzmann phase space $x_1, x_2, x_3, v_1, v_2, v_3$ more closely than with an expectation value of one element per volume σ^3 where σ is a constant, characteristic for the system. This is plausible because too great densities in position space, in the absence of large mean square deviations of velocities, give cause to an aggregation of formerly independent clusters or stars into larger statistically independent units. This assumption indicates the limits of determinacy of the mass distribution function $f(x_1, x_2, x_3, v_1, v_2, v_3)$ if we try to evaluate f on the basis of star counts in too small volumes in Boltzmann phase space. It also indicates the expected minimum distance between statistically independent elements in position space for a given mean square deviation of velocities. As we cannot expect a stellar system to be flattened into a disk more narrow than this minimum distance, a "minimum relation" between intervals in position space and intervals in velocity space follows, in mathematical analogy to the quantum-mechanical uncertainty principle. Our assumption is analogous to the Pauli principle (Thomas-Fermi atom). It is interesting to note that this exclusion principle forms the basic assumption in the astronomical case, and that the minimum relation is a consequence of it. Our hypothesis pays attention to micro-aspects of the streaming field and therefore implies an assumption about interaction of neighboring elements. (The word micro refers to the fine grained details of a streaming field and shall not imply that the independent elements are labeled and distinguished.) In the second part we investigate the transformation of the two classical hydrodynamical equations (continuity equation in position space, and Bernouilli equation) into a wave equation of the Schroedinger type and justify this procedure in the light of the foregoing remarks. The main idea is that we exploit the indeterminacy of the hydrodynamical streaming field (originating from our basic assumption). As the hydrodynamical quantities are defined but as local averages taken over rather big volumes in position space, we can transform the complicated hydrodynamical equations into a much simpler wave equation whose wave function provides the same local averages. There is no modification of the classical equations of motion involved in this procedure. It merely implies a statement about residual velocities ("pressure function") and force fluctuations. The wave-mechanical picture implicitly satisfies the minimum relation. In the wave picture we replace our basic hypothesis by the assumption that the distribution (numbers and intensities) of excited ψ_{nlm} states (n goes up to about 10^6) corresponds statistically to the distribution (in numbers and masses) of statistically independent elements of a stellar system. From this and further analysis it is clear that when confronting an observed stellar system with its ψ picture, we have to take averages over volumes containing enough elements to make the hydrodynamical quantities determinate and therefore make inferences about superpositions of *many* stationary ψ states. None of the discrete effects of ordinary quantum mechanics shows up in the present theory because of this.

PART I

1. Introduction and Some Definitions

THE present paper studies statistical problems which arise in stellar dynamics. As, however, we are not only interested in stellar systems but in any system of particles which are under the influence only of gravitational forces, we choose the name "gravitational system" or shortly "system" instead of "stellar system." We denote by this term a swarm of masses like our own or an external galaxy, or a globular or irregular star cluster, or our solar system or a system of satellites, in their evolution when they were more chaotic swarms of masses, and other systems of such kinds. A gravitational system might also be defined negatively as one in which electrodynamics, radiation, thermodynamics of solids, liquids, and gases, and collision phenomena are irrelevant.

A notion of fundamental importance is that of a "statistically independent element" or shortly "element" of such a gravitational system. Let us illustrate this in the case of our galaxy: A star or a smaller mass either moves independently in our galaxy, or it is a part of a number of stars and other masses, which at least for some time-interval form a smaller unit, which as a whole moves as one statistically independent element in our galaxy. Such an element is, e.g., a globular cluster, or a galactic cluster (or a single or multiple star or a planetary system), all as elements of our galaxy.—Constituent stars are the elements of a star cluster if this is considered as a gravitational system.—In general we may consider some set of particles as constituting one statistically independent element when this set stays together (usually because of its own gravitational attraction, cf. Section 5), thus acting as one unit of the total system. Evidently an element may acquire new masses or may be broken up. If we form any statistical average in our galactic system, it is clear that we have to attribute to a galactic cluster a statistical weight different from that of a small star or even smaller mass.

We plot the elements of the system in a 7-dimensional space-time spanned out by the rectangular cartesian coordinates and the velocity components, $x_1, x_2, x_3, v_1, v_2, v_3, t$. This is a Maxwell-Boltzmann phase space (μ space) as v, stands for momentum per unit mass. And we assume for a little while that the elements are so numerous and small, and form such a smooth swarm that we may define a distribution function $f(x_1, x_2, x_3, v_1, v_2, v_3, t)$.[1] $f\,dx_1dx_2dx_3dv_1dv_2dv_3$ denotes the probable amount of mass in $dx_1dx_2dx_3dv_1dv_2dv_3$, cf. the remark given before Section 4.1.

It is an essential point of this paper to analyze how far a definition of a distribution function is possible and to draw the necessary conclusions from the actual lack of determinacy of f.

The application of this theory to galaxies, or to our solar system, are both in reach of Newtonian mechanics. Consequently, relativistic corrections do not amount to much. We should not, however, forget that the proper theoretical description of the dynamics of a gravitational system is given by general relativity.

2. Hypotheses about "Initial Conditions" and about Interaction of Matter in Gravitational Systems

If we knew the detailed initial conditions (or let us better call it the prehistoric states) of gravitational systems, and if we were able to calculate the intricate detailed interaction of matter in such systems all through their development, we would have no need to introduce statistical hypotheses into stellar dynamics, nor into the theory of our solar system. This is not, however, a possible procedure. Thus let us consider the statistical approaches, involving two kinds of hypotheses.

One kind of hypotheses consists in assumptions about the prehistoric macroscopic (coarse grained) statistical distribution of matter in the system in question, and its total mass and age. When we need to introduce assumptions about prehistoric macrodistribution of matter, it is best to assume some kind of chaotic disorder depending on the kind of system we consider.

Another kind of hypotheses concerns the most probable kind of interaction of matter inside gravitational systems during their evolution (and near equilibrium). By this second kind of hy-

[1] The mathematical inadequacies of this Maxwellian model are discussed by N. Wiener and A. Wintner, "The discrete chaos," Am. J. Math. 65, 279 (1943).

potheses we relieve ourselves of the following steps: (a) the need of introducing first-kind hypotheses about the prehistoric microscopic (fine grained) statistical distribution, (b) calculating the development from prehistoric to present-day states of immense numbers of individual systems of many (million) bodies each, accurately, (c) translating the numerical results about present-day states into a statistical language.

3. Classical Stellar Dynamics, Neglecting Interactions of Individual Stars

The first possibility, widely used in stellar dynamics is to assume the "star passage" interactions as negligible; the flow of the statistical distribution of matter (because of Liouville's theorem) obeys the Boltzmann-Gibbs equation

$$0=\sum_1^3\left(\frac{\partial f}{\partial t}+v_\nu\frac{\partial f}{\partial x_\nu}-\nabla_\nu\bar{U}\frac{\partial f}{\partial v_\nu}\right), \qquad (3.1)$$

where $\bar{U}(x_1, x_2, x_3, t)$ is the gravitational potential derived from the smoothed-out mass distribution of the system concerned. The bar on the top of U indicates that $\bar{U}$ is free from granulations of U originating from the fact that the actual mass distribution gives a potential field with deep holes at each element of the system. Equation (3.1) expresses that f stays constant if we move along with the stars in phase space. If there exist 6 integrals $I_1, \ldots, I_6$ of the Lagrangian subsidiary equations, the general integral of Gibbs-Boltzmann's equation (3.1) is

$$f(x_1, \ldots, v_3, t) = \text{arbitrary function of } (I_1, \ldots, I_6). \qquad (3.2)$$

If, however, the gravitational potential allows only, say, 2 integrals I_1 and I_2 and if we start with any distribution in the $(x_1 \ldots v_3)$ space, then the famous ink-stirring argument of Gibbs[2] applied to our μ space $(x_1, \ldots v_3)$ shows that the *coarse grained* distribution $f(x_1, \ldots v_3)$ tends to average out; it finally adopts a constant value on a sub-manifold

$$I_1=\text{const.}, \qquad I_2=\text{const.}$$

Thus,

$$f(x_1, \ldots v_3, t)\rightarrow \text{arbitrary function of } (I_1, I_2). \qquad (3.3)$$

Such a final state, called dynamical equilibrium, is reached in a comparatively short time.[1] The ink-stirring argument can be regarded as a consequence of the assumption that there are no regularities in the microscopic initial conditions of the masses of the system. The latter assumption provides also for the distribution to be independent of angle variables (I_4, I_5 corresponding to action variables I_1, I_2). The deviation of the actual field of force from the smoothed $-\nabla_\nu\bar{U}$ has a similar effect: Such deviations though they might change action variables but slightly may bring about a great change in angle variables if we consider a long time interval.

Though the classical assumptions about the interaction of elements are changed in the following parts, the ink-stirring argument in the μ space will retain its fundamental role all the way through because it relates the fine grained density with the course grained density $f(x_1, \ldots v_3, t)$, (cf. Section 5).

It is evident that methods based on (3.1) admit many more solutions f than can actually exist in nature. Though the influence $\delta f/\delta t$ (cf. Eq. (4.01)) of passages or interactions does not alter very much *actual* present-day distributions f during not too long intervals of time (e.g. a time interval necessary to establish dynamical equilibrium), it is generally necessary to take account of these interactions.

This is illustrated by a simple example: Two well-developed galaxies which have two nearly parallel galactic planes and which rotate around about the same axis, but in opposite directions, may very slowly approach and finally penetrate each other. The combined system very quickly adopts a dynamical equilibrium which, however, is far from anything like a steady solution of (4.01) as the stars revolve in opposite directions.

For the problem falling under this section we refer to S. Chandrasekhar, *Principles of Stellar Dynamics*,* and P. M. Stehle, *Star Streaming*.**

[2] Cf. H. Poincaré, *Lecons sur les hypothèses cosmogoniques* (1913), pp. 95–101, or Ehrenfest, *Encyclopaedie der Math. Wissenschaften*. The ink and the water do not diffuse into each other, but form filaments.

[1] A. S. Eddington, AN (1921), p. 9, MN (1915); Smithsonian Report 1931, 239; B. Lindblad, Stockholm Obs. Ann. 12, No. 4 (1936).

* (University of Chicago Press, Chicago, Illinois, 1942.)

** (Dissertation, Princeton, 1944.)

This investigation formulates stellar dynamics in the covariant notation of the absolute differential calculus. It was started by H. P. Robertson.

4. Assumptions about Stellar Encounter Terms

The second possibility is to take into account the effects originating from the discreteness of the statistically independent elements. Because of individual attractions between elements, the actual forces $-\nabla_\nu \bar{U}+\delta F_\nu$ are slightly different from the smoothed forces, $-\nabla_\nu \bar{U}$. The irregular forces δF_ν cause a slow change $\delta f/\delta t$ of f,

$$\frac{\delta f}{\delta t}=\sum_1^3\left(\frac{\partial f}{\partial t}+v_\nu\frac{\partial f}{\partial x_\nu}-\nabla_\nu\bar{U}\frac{\partial f}{\partial v_\nu}\right). \qquad (4.01)$$

Integrating this Boltzmann-Gibbs' equation over the velocity space, we get the hydrodynamical equations—first, the equation of continuity

$$\sum_1^3 \nabla_\nu(\rho\langle v_\nu\rangle)+\partial\rho/\partial t=0. \qquad (4.02)$$

(The left-hand side of (4.01) corresponds to displacements mainly in the v directions, and vanishes therefore when integrated over the v space); secondly, integrating after multiplication with v_μ, Euler's equation of motion:

$$-\int\int\int v_\mu(\delta f/\delta t)dv+\frac{\partial}{\partial t}(\rho\langle v_\mu\rangle)+\sum_1^3\frac{\partial}{\partial x_\nu}(\rho\langle v_\mu v_\nu\rangle)+\rho\frac{\partial\bar{U}}{\partial x_\mu}=0, \qquad (4.03)$$

or sometimes written in the form

$$-\int\int\int v_\mu(\delta f/\delta t)dv+\sum_1^3\nabla_\nu(\rho\langle(v_\mu-\langle v_\mu\rangle)(v_\nu-\langle v_\nu\rangle)\rangle)+\rho\left(\sum_1^3\langle v_\nu\rangle\nabla_\nu\langle v_\mu\rangle+\partial\langle v_\mu\rangle/\partial t\right)+\rho\nabla_\mu\bar{U}=0, \qquad (4.04)$$

where $\int\int\int dv$ stands for $\int\int\int dv_1dv_2dv_3$,

$$\rho=\int\int\int f dv, \quad \rho\langle v_\nu\rangle=\int\int\int v_\nu f dv,$$

$$\rho\langle v_\mu v_\nu\rangle=\int\int\int v_\mu v_\nu f dv, \qquad (4.05)$$

(4.02) and (4.03) together with the hydrodynamical equations of higher degree in v_μ (7.9) (which as we shall see are of no great interest to us), are equivalent to (4.01). Because of the law of conservation of mass (in this paper we deal with the non-relativistic form of the problems), ρ and f have evidently to be interpreted as statistical densities of mass (not of number of particles) because we put elements of different mass in the same μ space.

4.1 On the basis of Eq. (4.01), a statistical theory for "stellar gas" has been developed in analogy to the kinetic theory of gases. By making use of an encounter model and of Boltzmann's hypothesis about molecular chaos (*Stosszahlansatz*), the interaction term $\delta f/\delta t$ has been calculated by a passage integral

$$\frac{\delta f}{\delta t}=\int\int\int\int\int(f'f_0'-ff_0)bV\times dbd\psi du_0dv_0dw_0. \qquad (4.11)$$

In order to obtain solutions of this problem (4.01), (4.11) at all, it was necessary to be satisfied with steady solutions, and in some very simple cases only it was possible to obtain such a distribution function f. Setting aside the mathematical difficulties, there are serious objections against the application to astronomy of this method, invented for gases:

In general, single stars are not statistically independent elements. We have to take the clustering tendency into account. The statistically independent elements of a stellar system are partly single stars, partly star clusters of different diameter, mass, and compactness. Passages cause a loosening of these clusters and a decrease or increase in stars constituting them (cf. Section 5).

Contrary to the dynamics of gases, in stellar systems we have not to do with strong, short range forces which, whenever two elements meet, completely alter their velocities (jumps (4.11) into and out of the smooth streaming field in μ space), but with very weak long-range forces. And the stellar system is not included in a box.

There is no equipartition of energy to be expected in such a situation. Such lack of equipartition of energy is made most strikingly evident in the simultaneous presence in a gravita-

tional system of elements of very different mass and similar velocity.

4.2 These passage forces are only the small fluctuations δF_ν of the total field of

$$\text{force} = -\nabla_\nu \bar{U} + \delta F_\nu. \qquad (4.21)$$

The force fluctuations δF_ν comprise both dynamical friction and random fluctuations of force. (The mean value and mean square deviation of δF_ν are functions of $(x_1, x_2, x_3, v_1, v_2, v_3, t)$ which, like $\bar{U}$ depend on f.) They cause an additional displacement of the elements in their streaming in μ space, a slow convection and diffusion (chiefly in the velocity directions) superposed on the streaming (3.1) governed by $-\nabla_\nu \bar{U}$ only.[4] In this way it is possible to calculate $\delta f/\delta t$ properly, not by the passage integral (4.11). It is useful to translate the diffusion process in question into the space of the integrals $I_1, I_2, \ldots$, because it is the diffusion between different sub-manifolds which is of interest only, as *on* a sub-manifold we have already the ink-stirring effect described in 3. (*N.B.* Both the ink-stirring on a sub-manifold and the diffusion are essentially irreversible processes.) Reasonable statistical hypotheses about δF_ν (which replace the encounter hypothesis, i.e., (4.11)) enable us to carry through this force fluctuation method.

4.3 As already mentioned in the introduction, we have to introduce a hypothesis indicating how far apart from each other are the statistically independent elements of a gravitational system. In other words we have to make a hypothesis stating up to which degree of fineness the distribution function $f(x_1, \ldots v_3, t)$ is determined by the detailed observational data of a system. Such a hypothesis is fundamental to the theory of gravitational systems, because it states the limits up to which $f(x_1, \ldots v_3, t)$ can have an unambiguous meaning. It is obvious that it too contains implicitly an assumption about the force fluctuations δF_ν (4.21),[5] and these force fluctuations determine the diffusion process $\delta f/\delta t$ in μ space. Instead of the usual procedure of introducing specialized assumptions about force fluctuations[6] we start with a more basic hypothesis, which we have to make anyhow and which yields the effect (7.7) of force fluctuations as a by-product.

5. Hypotheses about this Indeterminacy of f

We have first to define the density of elements, or its inverse, the volume per element in the neighborhood of a point $(x_1, x_2, x_3, v_1, v_2, v_3, t)$. To do this we plot a graph analogous to that of Prandtl and Chandrasekhar. We take round the point $x_1, \ldots v_3$ at the time t a sphere in position space and a sphere in velocity space. The product of the position-space volume and velocity-space volume we call "volume." (In order not to run into too large position-space volumes, let us take the radius of the velocity-space sphere approximately equal to the size of the square root of the mean square deviation of the velocity distribution at the point (x_1, x_2, x_3, t), and its center at $x_1, x_2, x_3, \langle v_1\rangle, \langle v_2\rangle, \langle v_3\rangle$.) We then plot the total mass inside the volume divided by the volume as ordinate against the volume taken as abscissa. The ordinate, if it converges before the zigzag line shows an upward or downward trend, tends towards what we call f (Fig. 1). In the abnormal case when a system has but one or a few extraordinarily large statistically independent elements besides smaller elements (i.e. if the density does not converge), these are too few in number to define a statistical distribution. Whenever the number of elements is too small, this statistical theory like every other one loses its significance (not its consistency) because of the wide gap between sample and collective.—The expectation value of the number of jumps per unit phase space volume is what we call density of numbers of elements or shortly density of

[4] H. A. Kramers, Physica **7**, 284 (1940). S. Chandrasekhar and J. v. Neumann, Astrophys. J. **94**, 511 (1941); **95**, 489 (1942); **97**, 1 (1943); **97**, 255 (1943); Rev. Mod. Phys. **15**, 31 (1943). H. Jehle, Zeits. f. Astrophys. **19**, 133 (1939) (in this paper the force fluctuation method has not been carried through).

[5] The largest elements' predominant role for force fluctuations has been pointed out by Professor Onsager.

[6] S. Chandrasekhar, reference 4. In order to find out the effect $\delta f/\delta t$ of δF_ν in this usual procedure, one has to make detailed assumptions about the dependence of the force fluctuations' statistical averages $\langle \delta F_\nu\rangle_{Av}$ and $\langle (\delta F_\nu)^2\rangle_{Av}$ upon $(x_1, \cdots v_3, t)$ and on $f(x_1, \cdots v_3, t)$. In the actual Brownian case these are provided for by requiring equipartition of energy to be compatible with assumptions about δF_ν; in the stellar case, by making statistical hypotheses about stellar encounters based on a model of a stellar system composed of equal single stars, but all quantitative details of the model have to be borrowed from observation. The force fluctuation method in astronomy has its limitation in the arbitrariness which comes from the multitude of assumptions needed for the calculation of force fluctuations.

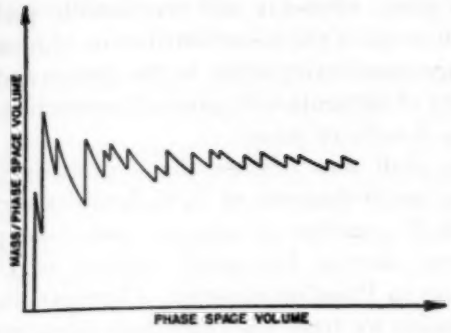

FIG. 1. Definition of mass density f in six-dimensional phase space.

elements. The word "jumps" ought not to be taken literally as elements have finite size; thus there are no discontinuities in the graph.

We are going to make the following hypothesis. For each gravitational system there exists a characteristic constant, σ, limiting the unambiguous determinacy of $f(x_1, x_2, \ldots, v_3, t)$. f can be defined if we choose blocks in μ space which are large compared with blocks

$$\int \cdots \int dx_1 \cdots dv_3 = \delta x_1 \delta x_2 \cdots \delta v_3,$$

representing the volume per statistically independent element in the phase space region under consideration. We introduce the more convenient notation $\delta x_1 \delta x_2 \ldots \delta v_3$ instead of the integral as long as without loss of generality it is possible to think of roughly blockshaped volumes of approximate extension δx_1, etc. We assume that

$$\delta x_1 \delta x_2 \ldots \delta v_3 \geqq \sigma^3. \tag{5.1}$$

This hypothesis means that statistically independent elements cannot be crowded together with densities exceeding σ^{-3}. Thus in a large block, say of volume $N\delta x_1 \cdots \delta v_3$, the probable number of elements is N, and the chance fluctuation from this probable value is of the order $N^{\frac{1}{2}}$, i.e., the relative fluctuation is $N^{-\frac{1}{2}}$. For a sufficiently large N we can call f well determined.

The volume $\delta x_1 \ldots \delta v_3$ per element is of course to be distinguished from the size of the element, described e.g., by the radius of the cluster constituting one element. Besides its size, its total mass and quantities measuring its compactness characterize an element.—We do not at present discuss eventual modifications of the above assumption brought about by the presence of the spinning of the elements.

We have a continual adjustment of the elements of a stellar system towards each other and *versus* the total stellar system, an adjustment concerning size, mass, and number of "particles" in the elements. Such adjustment tends toward what may best be called "statistical equilibrium." (This definition of statistical equilibrium is more useful than defining it as a steady solution of (4.01) plus (4.11), i.e., something like a state of equipartition of energy which never occurs.) Our hypothesis obviously refers to a statistical equilibrium distribution.

We shall describe more in detail this adjustment of the elements. An element, composed of a swarm of particles, as time goes on, will reduce or build up its size. To study this, let us consider the kinds of forces acting on the particles (stars or other bodies) of a statistically independent element. There is (1) its own gravitation field, i.e., (1a) its own smoothed field of force and (1b) its own force fluctuations; (2) in addition to (1), the outside field of force coming from the other elements of the total stellar system, i.e., (2a) the smooth external gravitation field $-\nabla_r \bar{U}$ and (2b) the force fluctuations δF_r of the gravitation field of the whole system.

The force (1a) is the basic cause for holding the element together. The force fluctuations (1b) occasionally impart such energy to one of the particles constituting the element that it gets a velocity greater than the velocity of escape and therefore evaporates from the element. This process has carefully been calculated by Chandrasekhar. On the other hand the force fluctuations (1b) have an effect on a particle coming from outside and accidentally penetrating into the swarm: They distribute the particle's kinetic energy over the many degrees of freedom of the other particles of the swarm and thereby capture the outside particle if it had not too great a velocity with respect to the swarm.—The field (2a) can have disruptive effects on an element because of tidal action, but it can also help to build up an element by causing outside particles or elements to adopt velocities close to the velocity of the element; (2b) has disruptive influence on an element. It is impossible to study

all these effects quantitatively without introducing many statistical hypotheses. So we are fully justified in replacing such calculations of sizes and densities of elements, and force fluctuations by a more fundamental statistical hypothesis like (5.1). The statistical equilibrium we are referring to specifies the outcome of the evaporation and building up processes of the elements, caused by their interaction. It is plausible to assume (5.1) because a too tight crowding of elements in position space in the absence of sufficient velocity deviations causes an association of formerly independent elements into fewer, larger ones.

Our theory is limited to the extent that actual systems cannot but approximately be considered to shift along a sequence of equilibrium states. We may assume the elements to be in approximate statistical equilibrium if the time constants characterizing the macroscopic (coarse grained) change of hydrodynamical quantities are larger than the relaxation times characterizing mutual adjustment of elements. This limitation is, however, but very weak and the theory developed in Part II based on the present assumption, provides a good enough approximation also if there is no statistical equilibrium—as long as we are interested in the dynamical results rather than in the distribution of numbers of independent elements. Non-equilibrium cases arise particularly if the gravitation field $\bar{U}$ changes quickly in time. An extreme situation occurs when two formerly distinct global systems join into a single one. The elements of the combined system being a mixture of the former elements, some regrouping of elements will take place. Occasionally a smaller system joining a larger one might form one statistically independent element of the latter.

The equations of motion based on the smooth field of force $\bar{U}$ may admit one or several first integrals $I_1, I_2, \ldots$, often only approximately. So the motion of an element is more or less confined to a sub-manifold defined by these integrals. The imperfection of the validity of such integrals (because $\bar{U}$ has not perfect symmetry) and the effect of the force fluctuations δF_ν, however, both will help the element to get round different sub-manifolds, more or less conserving its identity during such wanderings. Insofar as this process takes place, elements will occasionally perhaps tend to acquire the same distribution of mass (or average mass) everywhere in the system and the density of elements will approach proportionality to the density of mass.

We shall now discuss the hypothesis (5.1). Many redistributions of local densities such as we shall consider at present, can take place without causing but small changes of $\bar{U}$ according to Poissons equation. Therefore, in this discussion we treat (as a first approximation) $\bar{U}$ as given and independent of t. Let the system start off with some particular distribution of elements. The following effect will take place. Consider several blocks on[7] a sub-manifold $I_1 = \text{const.}$, $I_2 = \text{const.}$ say, each of them having the same unit volume and containing at the outset quite different numbers of elements. Because of Liouville's theorem each originally blockshaped unit volume is conserved as time goes on, but the shapes of the volumes get deformed into long filaments. A block of unit volume picked at a shortly later time is made up from many different pieces of filament-like, deformed earlier blocks. It therefore contains an average of the original numbers of elements per unit volume. In other words, the density of elements on a sub-manifold quickly becomes uniform, because of the ink-stirring effect, and then stays constant as time goes on. (The density of elements is usually different on different sub-manifolds.) Therefore as long as we do not consider $\bar{U}$ time dependent and disregard the slow diffusion caused by δF_ν, and as long as we do not make a quantitative assumption about the size of σ, (5.1) is trivial. This consideration, however, makes us realize that (5.1) is the only possible form of an assumption which can be introduced with respect to finite size of elements (not e.g., a maximum density in position space).

We like to leave the quantitative assumption about σ open, because the observed facts should have the last word about it. If, however, from dimensionality arguments we consider what possible values we might give to σ, we realize that for a gravitational system, apart from universal constants, only its mass is an available constant.

[7] When we speak about "on a sub-manifold," we mean a 6-dimensional neighborhood of the sub-manifold in question.

So we may assume

$$\sigma = \sigma_0 M, \tag{5.2}$$

where M is the total mass of the gravitational system concerned, and σ_0 a universal constant of the order of magnitude G/c.[8] It is plausible that the total mass of a system has some influence on the density limit σ^{-3} of its elements because both the smooth field of force and the force fluctuations of the whole system have their effect on the elements. But we take (5.2) again as an assumption and do not want to make any calculations about densities of elements to justify it, because in order to be able to do so, we would have to make many other assumptions. Thus σ is evidently different if we consider the whole galaxy with each of its clusters counting as one element, or if we consider such a cluster by itself. If two systems merge into a single system, there is a change of σ; evidently it will take considerable time till the combined system actually comes close to statistical equilibrium.

For our solar system σ/c has about the value 10^5 cm, for our galaxy 10^{16} cm. These quantitative assumptions can be checked against observed data in particular about the strongest possible flattening of a system, and (in our galaxy) against observations about the minimum relation (5.8) and about distributions of statistically independent elements (5.1). For the present, let us, however, take the quantitative formulation (5.2) of our hypothesis as an assumption which, as we shall see in a later paper, fits the observed data.

Let

$$(\Delta x_\nu)^2 = \langle (x_\nu - \langle x_\nu \rangle_M)^2 \rangle_M,$$

the averages in this case being understood as averages over all the elements of the system, if plotted in position space. The total extension of the stellar system in the x_ν direction is something of the order of Δx_ν, actually it is larger than Δx_ν. The total extension of the system if plotted in the velocity space is of the order of Δv_ν, where Δv_ν is defined like Δx_ν. The v_ν extension of the system, plotted in phase space, at a certain location x_1, x_2, x_3 is of the order of $\Delta_x v_\nu$, where

$$(\Delta_x v_\nu)^2 = \langle (v_\nu - \langle v_\nu \rangle)^2 \rangle$$

in the present case the averages being, as usually in this paper, "local" averages. If we denote by $\langle \Delta_x v_\nu \rangle_M$ an average value of $\Delta_x v_\nu$, averaged over position space, we have

$$\Delta v_\nu \gtrapprox \langle \Delta_x v_\nu \rangle_M, \tag{5.3}$$

the $>$ sign referring to the contribution of a not constant $\langle v_\nu \rangle$ towards Δv_ν.—If we then choose a one-element block $\delta x_1 \ldots \delta v_3$ of volume $\gtrapprox \sigma^3$ (the meaning of $\gtrsim$ is as in (5.1)), such that $\delta v_\nu \approx \Delta_x v_\nu$, and

$$\delta v_1 \delta v_2 \delta v_3 \approx \Delta_x v_1 \Delta_x v_2 \Delta_x v_3,$$

this block covers a substantial fraction of the occupied region of the v_1, v_2, v_3 subspace at x_1, x_2, x_3. Therefore

$$\delta x_1 \delta x_2 \delta x_3 \gtrapprox \sigma^3 / \Delta_x v_1 \Delta_x v_2 \Delta v_3, \tag{5.4}$$

because of (5.1), contains about one element altogether, irrespective of velocity, and a block some N times as large would make the density ρ in position space well determined. In other words

$$\delta x \gtrapprox (\sigma^3 / \Delta_x v_1 \Delta_x v_2 \Delta_x v_3)^{\frac{1}{3}} = \sigma / \Delta_x v \tag{5.5}$$

indicates roughly a unit block width or (1/0.554) times the average distance between two neighboring elements in position space. (Average distance between neighbors in a homogeneous statistical distribution is independent of the direction considered, i.e., isotropic.) From this aspect our hypothesis means that if $\Delta_x v$ is a large quantity, i.e., if we have large residual velocities, statistically independent elements may be close together in position space, whereas if $\Delta_x v$ is small, then the elements have to be far apart in order not to tend to associate.

Let us now consider the extensions Δx_ν and Δv_ν of a strongly flattened system. The smallest of the Δx_ν may be called the width Δx_3 of the system. We may reasonably assume that this cannot be smaller than of the order of magnitude of the above unit block width δx, or about the distance between two neighboring elements. Because otherwise the elements being confined to

[8] If we use relativistic units (cf. A. Einstein, *The Meaning of Relativity*), we have the following relationships between numerical values: (ct) in c.g.s. $= (t)$ in relativistic units, $(8\pi GM/c^3)$ in c.g.s. $= (M)$ in relativistic units. Therefore we get the formulae in relativistic units if we replace the quantities on the left-hand sides by those on the right-hand sides, i.e. by simply putting $c = 1$ and $G = 1/8\pi$, that takes care of everything. In relativistic units (5.2) becomes $= M/8\pi$, and this is a plausible assumption as there is no other constant available for a gravitational system than its mass M.

the immediate neighborhood of the x_1, x_2 plane would present a physically impossible distribution: It would be a statistical distribution if its x_1, x_2 values are considered and at the same time well-ordered (flat) in the x_3 direction without a physical reason for. The fact that statistically independently moving elements have some distance from each other in the x_1, x_2 directions makes them spread over a domain of width Δx_3 which becomes at least as wide as the block width $\langle \delta x \rangle_M$ (5.5), the $\langle\ \rangle_M$ indicating a suitable average taken over position space. Thus

$$\Delta x_3 \gtrapprox \langle \delta x \rangle_M. \tag{5.6}$$

Forgetting anisotropy of local residual velocity distribution $\Delta_x v_x$ we may make the approximation $\Delta_x v_1 \approx \Delta_x v_2 \approx \Delta_x v_3$ for the present rough calculation.—In case of systems which are far from such isotropic velocity distribution, the inequality sign in (5.5) is so strong that the conclusion (5.8) holds *a fortiori*. Therefore we get

$$\Delta v_3 \gtrapprox \langle \Delta_x v_3 \rangle_M \approx \langle \Delta_x v \rangle_M. \tag{5.7}$$

The Eqs. (5.5)–(5.7) lead to the minimum relation

$$\Delta x_3 \Delta v_3 \gtrapprox \sigma. \tag{5.8}$$

So the relation (5.4) which expresses the phase-space volume required per element, limits the area (5.8). We would have arrived at the same result by a similar consideration with roles of x_x and v_x interchanged. With a more accurate definition of total extension in terms of Δx_x, $\Delta_x v_x$, and a numerical factor different from one in (5.6) we could have arrived at

$$\Delta x_3 \Delta v_3 \gtrapprox \sigma/4\pi, \tag{5.8'}$$

a formula matching (8.5).

A description of a system by a function f is certainly meaningful if the blocks

$$N \delta x_1 \delta x_2 \delta x_3 \gtrapprox N\sigma^3/\Delta_x v_1 \Delta_x v_2 \Delta_x v_3 \tag{5.4'}$$

are small compared with the large-scale structure of the system in question. We have said that f apart from a certain percent error is unambiguously defined only on basis of volumes $\geqq N\sigma^3$. We may subdivide the μ space occupied by our system into cubic blocks (cube shaped in x space, and also in v space), one block next to the other, and attribute one value of f to each block. We then form, by smoothing inside the error limits, and by *interpolation* a continuous function $f(x_1, \ldots v_3, t)$ which shows no irregular variations inside a block. We assume that to such a function f the Boltzmann-Gibbs equation and the integrated hydrodynamical equations will apply, and such an f is directly comparable with observation. We should not, however, forget that the smoothness of f is a convention of the way how we interpolated. We will always understand f as such a smooth function.—Still a word about the gravitation potential, $\bar{U}$ obeys Poisson's equation with a density

$$\rho = \int\int\int f dv_1 dv_2 dv_3. \tag{5.9}$$

PART II. TRANSFORMATION THEORY OF THE HYDRODYNAMICAL EQUATIONS

6. Introduction

It is known that a wave equation of the time-dependent Schroedinger type,

$$((\bar{\sigma}^2/2)\nabla^2 + (\bar{\sigma}/i)\partial/\partial t - c^2 - U)\psi = 0, \tag{6.1}$$

(in atomic physics $\bar{\sigma}$ was $\hbar/m$) admits a hydrodynamical interpretation[9] i.e., (6.1) can be looked at as being equivalent to hydrodynamical equations. We are going to follow up this interpretation in Sections 7 and 8. A theory of gravitational systems consists of two logically independent parts: (a) The laws of motion, expressed in Boltzmann-Gibbs' Eq. (4.01), or in the hydrodynamical Eqs. (4.02), (4.03) and hydrodynamical equations of higher degree in v_x[7.9]. The theory developed below which may be called cosmological wave mechanics because it transforms the hydrodynamical Eqs. (4.02), (4.03) into a wave equation, certainly has to and does comply with these classical laws for a system of particles, unlike ordinary wave mechanics which refers to the motion of one or several individual particles, replacing the classical laws of motion by new ones. (b) Statistical hypotheses which we are going to formulate in a wave-mechanical language.

[9] Cf. E. Madelung, Zeits. f. Physik **40**, 322 (1927). The approaches of R. Fuerth in Frank-Mises **2**, 615 (1935) ff., Zeits. f. physik. Chemie **B26**, 187 (1934), and some other of the papers on wave mechanics occasionally deal with some points related to the present theory. We include the rest energy term c^2 because of later relativistic formulation.

This new wave mechanics is in certain respects mathematically analogous to that of De Broglie and Schroedinger, but the physical interpretation of the present ψ waves differs essentially from the interpretation given in quantum mechanics. In our astronomical case we describe the evolution of a system by a ψ wave in ordinary 3-plus 1-dimensional space-time and we assume ψ to satisfy (6.1). ψ is, however, not normalized. An independent assumption concerns $\bar{\sigma}/c$; apart from a numerical factor of the order of magnitude one it is assumed to be the gravitational radius of the total system described by such a ψ wave. This implies values of the order of magnitude 10^5 for the numbers n, l, m, characterizing stationary ψ_{nlm}, in the case of a central gravitation field both in our galaxy and for the primordial solar system.

The analogy of the basic hypothesis of Part I of this paper to Pauli's exclusion principle in the old quantum theory (Thomas Fermi atom) and the formal analogy of the minimum relation to the indeterminacy relation lead us to suspect that there is some meaning behind the expression of hydrodynamical equations of stellar dynamics in the formalism of wave mechanics.

In order to get a clearer picture of the logical structure of this theory, we are starting over in this Part II, stating afresh all the assumptions we are going to make, independent of Part I. So we replace the basic hypothesis of Part I by a hypothesis in wave-mechanical formulation: If the potential field $\bar{U}(x_1, x_2, x_3, t)$ changes in time slowly enough and if it has approximate spatial symmetry properties, so that there are approximately stationary solutions of the wave equation (6.1) characterized by 3 numbers (e.g., n, l, m, corresponding to 3 integrals I_1, I_2, I_3), then we assume the following statement about numbers of elements: Let us expand the ψ function describing a system into stationary ψ_{nlm}

$$\psi = \sum_{n,l,m} c_{nlm}\psi_{nlm}, \tag{6.2}$$

and ask for the distribution of statistically independent elements of this system as a function of the integrals (action variables) I_1, I_2, I_3 corresponding to n, l, m. The answer is that we have an expectation value of one element per stationary state and that the expectation value of its mass is $|c_{nlm}|^2$ (ψ_{nlm} being understood as normalized). Considering the fact that usually several stationary states are not excited, i.e., several $c_{nlm}=0$, it comes to the same if we state that each stationary state is in the average occupied by one or less than one statistically independent element. As an illustration consider, in the ψ picture of a stellar system, the $|c_{nlm}|^2$ values belonging to a certain $n\,l\,m$ range which is small compared with the total $n\,l\,m$ range of the system, and count how many of these $|c_{nlm}|^2$ have values falling between 0 and 5, 5 and 10, 10 and 15, etc. Our statement means that provided we have statistical equilibrium, the expectation value of numbers of statistically independent elements inside the range of $I_1\,I_2\,I_3$ values corresponding to our $n\,l\,m$ range, and of mass between 0 and 5, 5 and 10, etc., is given by the corresponding numbers of $|c_{nlm}|^2$. This is the simplest unambiguous assumption we can make about distribution of numbers and masses of elements in a system close to statistical equilibrium. We note that $|c_{nlm}|^2$ has to be interpreted as mass because $|\psi|^2$ according to (7.2), (7.5) has to be interpreted as density of mass.

We like to give the connection of this hypothesis with the one of Part I, and thereby give the justification for the present hypothesis. It is well known from quantum mechanics that if we fill all stationary ψ states up to a certain frequency limit with one particle (element) per state, we get in the average just one particle (element) per volume

$$\delta x_1\delta x_2\delta x_3\delta v_1\delta v_2\delta v_3 = (2\pi\bar{\sigma})^3 \tag{6.3}$$

for the inner regions. This is shown by using the Brillouin-Kramers-Wentzel approximation, leading to the Bohr-Sommerfeld quantum conditions.[10] Note that in our case this does not mean that the same amount of mass belongs to each occupied stationary ψ state. The amplitudes with which the different stationary ψ are represented are accordingly subject to no restriction. The quantity $\bar{\sigma}$ in (6.3) comes from (6.1). In order to make (6.3) identical with (5.1) we have to put

$$\bar{\sigma} = \sigma/2\pi. \tag{6.4}$$

[10] Cf. L. Brillouin, "L'atome de Thomas Fermi," Actualités scientifiques 160, 19–25 (1934).

If still the question were raised whether our hypothesis is not too specific in stating the relative distribution of heavy and light elements, we have to note that it refers to a statistical equilibrium which is usually realized but approximately. For the applications of the theory where it is merely used as a mathematical shortcut to solve complicated dynamical problems (and where we are not interested in relative distributions of mass among the elements), it is pretty irrelevant how far we are from statistical equilibrium.

We consider now the problem: Which ψ is to be coordinated to a given stellar system? From the foregoing it is clear that the presence of many statistically independent elements means that many stationary states are simultaneously represented, i.e., ψ is a superposition of many stationary ψ's. We have to keep in mind that the wave picture and its coordinated hydrodynamical quantities represent a statistical collective, whereas nature offers but a sample with a limited number of elements. Therefore the problem of determining the collective, i.e., ψ, given an observed stellar system, has no unique solution; it is a Bayes problem. The correct procedure, just as in ordinary quantum mechanics, would be to set up a Gibbs ensemble of ψ functions.[11] From the observed data we have to make inferences about the Dirac v. Neumann density matrix. In most of the applications, however, we may altogether disregard the density matrix and only investigate the behavior of one appropriate ψ function (a superposition of several stationary ψ) for one system. This procedure provides a sufficient insight into the results characteristic for the wave-mechanical method.

It is possible to infer the ψ function with not too crude inaccuracy only if we have many elements, and they correspond to a superposition of many stationary ψ's. (There is, however, no coordination of one of the individual elements to one of the stationary states.) A single element would indeed allow to infer but very little about the ψ function representing it. It is therefore evident that the existence of discrete stationary states cannot show up directly in the space distributions $\rho(x_1, x_2, x_3, t)$ permitted by the theory (cf. Eq. (7.5)).

If the gravitation potential $\bar{U}$ changes so quickly in time that there exist not even approximately stationary ψ solutions, it is difficult to specify assumptions about numbers of elements in wave-mechanical language. This difficulty has its counterpart in the absence of statistically steady distributions (statistical equilibrium) of numbers of elements in phase space, if $\bar{U}$ changes too quickly in time. In some respects a similar situation prevails if $\bar{U}$ has not the symmetry necessary to provide for 3 integrals (action variables).

To illustrate the wave picture we mention 2 theorems concerning the motion of a wave packet representing a swarm of particles. A wave packet's center of gravity moves as the swarm's center does according to Newton (Ehrenfest's theorem). And a small swarm's volume in phase space, according to Liouville's theorem, is preserved as the swarm moves in the field (if we consider the effect of the smooth field $-\nabla_\nu \bar{U}$ only, disregarding the force fluctuations δF_ν, and its own gravitation field). The wave packet too preserves the phase space volume it occupies, under the same conditions.[12]

Still a word about Poisson's equation. We assume that U is given by

$$U = -G\int\int\int (|\psi|^2/r)dx_1dx_2dx_3, \quad (6.5)$$

and split

$$U = \bar{U} + \delta U \quad (6.6)$$

into its smooth part $\bar{U}$ which is a smooth function of x_1, x_2, x_3, t and which because of (7.5) is identified with the $\bar{U}$ used in Section 3 (cf. (5.9)), and into its irregular part δU whose gradient $-\nabla_\nu(\delta U)$ stands in analogy to δF_ν (4.21), representing force fluctuations.

The principal idea behind this investigation is that the wave-mechanical method offers an essential advantage over the straightforward application of the hydrodynamical equations:

[11] P. A. M. Dirac, *Quantum Mechanics* (Oxford University Press, New York, 1935), second edition, p. 139; J. v. Neumann, *Grundlagen* Verlagsbuch handlung Julius Springer, Berlin, 1932, p. 157; R. C. Tolman, *Principles of Statistical Mechanics* (Oxford University Press, New York, 1938), p. 326 ff.

[12] J. H. Van Vleck, Phil. Sci. 8, 275 (1941); J. E. and M. G. Mayer, *Statistical Mechanics*, p. 61.

Instead of finding solutions $f(x_1, \ldots, v_3, t)$ of a Boltzmann-Gibbs equation in 6 plus 1 independent variables, or solutions $\rho(x_1, x_2, x_3, t)$, $\langle v_\nu \rangle(x_1, x_2, x_3, t)$, $\langle v_\nu v_\mu \rangle(x_1, x_2, x_3, t)$ of the hydrodynamical equations we have only to look for solutions $\psi(x_1, x_2, x_3, t)$ of one wave equation in 3 plus 1 independent variables. It is the author's opinion that besides this obvious point the wave-mechanical theory, wherever its statements go beyond the corresponding statements of ordinary hydrodynamical theory, is to be considered correct because it provides for a more adequate formulation of statistical hypotheses. The ψ picture, because of its features of discreteness, has a closer connection to an actual stellar system made up from discrete elements, than has a microscopically smooth hydrodynamical picture (cf. the following section).

7. Interpretation of the Wave Equation

To justify our procedure we examine the conditions under which the wave equation (6.1) is equivalent with the hydrodynamical equations (4.02), (4.03). Let

$$\psi = |\psi| \exp(iS/\bar{\sigma}).^{13} \tag{7.1}$$

The complex wave equation splits into two real equations

$$-\sum_1^3 \nabla_\nu(|\psi|^2 \nabla_\nu S) + (\partial/\partial t)|\psi|^2 = 0, \tag{7.2}$$

$$\partial S/\partial t - \sum_1^3 \tfrac{1}{2}(\nabla_\nu S)^2 + (\bar{\sigma}^2/2|\psi|)\nabla^2|\psi| - U - c^2 = 0. \tag{7.3}$$

(7.2) invites an interpretation as continuity equation in position space, (7.3) as a generalized Bernouilli equation whose third term represents a "pressure potential."[14]

The remarks in the footnote should serve but for a short survey. Actually an Euler equation (4.04) or (4.03) is made up of quantities ρ, $\rho\langle v_\nu \rangle$, etc., which represent averages over blocks containing many statistically independent elements. So it is but averages $\langle|\psi|^2\rangle$, $\langle|\psi|^2\nabla_\nu S\rangle$ etc., of wave-mechanical quantities which we can confront with observable quantities like ρ, $\rho\langle v_\nu \rangle$, etc. We are therefore going to confront the non-integrated Euler Eq. (4.03) for the hydrodynamical averages $\langle v_\nu \rangle$, etc., directly with the corresponding wave-mechanical equation. This wave-mechanical equation is obtained by differentiating (7.3) with respect to x_μ, then multiplying it by $-|\psi|^2$ and finally taking averages (over position space volumes containing many elements)—these averages[15] are indicated by angular brackets without the subscript Av.

$$0 = (\partial/\partial t)\langle -|\psi|^2 \nabla_\mu S\rangle + \sum \nabla_\nu \langle |\psi|^2 (\nabla_\mu S)(\nabla_\nu S) - \tfrac{1}{4}\bar{\sigma}^2 |\psi|^2 \nabla_\mu \nabla_\nu \log|\psi|^2\rangle + \langle|\psi|^2\rangle \nabla_\mu \bar{U} + \langle|\psi|^2 \nabla_\mu(\delta U)\rangle. \tag{7.4}$$

---

[13] The bar on top of σ has nothing to do with averaging.

[14] Let us assume but for the purpose of this footnote that the streaming field may be definable in all details, and we denote the microscopic streaming velocity then by $\mathbf{v}$. And let us for the moment combine the first and the last term of the Euler equation (4.04) into a term $\rho\nabla_\mu U$. As is well known we can integrate this Euler equation

$$\rho\{\partial \mathbf{v}/\partial t + (\mathbf{v}\cdot\nabla)\mathbf{v}\}_\mu + \Sigma \nabla_\nu p_{\nu\mu} + \rho\nabla_\mu U = 0,$$

or

$$\{\partial \mathbf{v}/\partial t + \tfrac{1}{2}\nabla(\mathbf{v}^2) - \mathbf{v}\times[\nabla\times\mathbf{v}]\}_\mu + (1/\rho)\Sigma \nabla_\nu p_{\nu\mu} + \nabla_\mu U = 0,$$

if

$$\nabla\times\mathbf{v} = 0 \quad \text{or} \quad \mathbf{v} = -\nabla S$$

and if

$$(1/\rho)\Sigma \nabla_\nu p_{\nu\mu} = \nabla_\mu P.$$

P is usually called pressure potential, where "pressure" refers to nothing but transfer of momentum by virtue of the mean square deviations of velocity. The last equation means that, e.g., because of some equation of state we may have a relation between pressure and density and then can integrate

$$P = \int_0^p (1/\rho)dp.$$

The integration of the Euler equation gives the generalized Bernouilli equation

$$\partial S/\partial t - \Sigma\, \tfrac{1}{2}(\nabla_\nu S)^2 - P - U = \text{const.}$$

Confronting this equation term by term with (7.3) we readily see the meaning of the term

$$-(\bar{\sigma}^2/2|\psi|)\nabla^2|\psi|.$$

It is not a correction term to the classical (Hamilton Jacobi) equation of motion, but it represents the pressure potential in the Bernouilli equation, a term always present when we have to do with hydrodynamical equations of motion of many particles. We shall come back to this point when discussing (7.8). The Euler equation in this footnote refers to a microscopically defined unrealistic streaming-field $\mathbf{v}$, and the integration is possible if the curls of $\mathbf{v}$ are concentrated upon discrete singularities (usually lines), and if there exists a pressure potential. In the text, however, we want to follow up a rigorous interpretation of the wave-mechanical equations, confronting them directly with the (not integrated) Euler Eq. (4.03) which holds without restrictions in the general case.

[15] When averaging we remark that we can decompose any of the wave-mechanical functions like $(-|\psi|^2\nabla_\nu S)$ into a smooth and an irregular part, i.e., $F = F_{sm} + F_{irr}$ where $\langle F_{irr}\rangle = 0$, and also $\langle \nabla_\nu F_{irr}\rangle = 0$, therefore

$$\langle \nabla_\nu F\rangle = \langle \nabla_\nu F_{sm}\rangle = \nabla_\nu F_{sm} = \nabla_\nu \langle F\rangle.$$

Similarly for the continuity equation

$$0=\sum\nabla_\nu\langle-|\psi|^2\nabla_\nu S\rangle+(\partial/\partial t)\langle|\psi|^2\rangle, \quad (7.2)$$

(7.4) and (7.2) are equivalent to (4.03) and (4.02) if we identify

$$\rho=\langle|\psi|^2\rangle, \quad (7.5)$$

$$\rho\langle v_\nu\rangle=-\langle|\psi|^2\nabla_\nu S\rangle, \quad (7.6)$$

$$\int\int\int v_\mu(\delta f/\delta t)dv=-\langle|\psi|^2\nabla_\mu(\delta U)\rangle, \quad (7.7)$$

$$\rho\langle v_\mu v_\nu\rangle=\langle|\psi|^2(\nabla_\nu S)(\nabla_\mu S) -\tfrac{1}{4}\bar\sigma^2|\psi|^2\nabla_\nu\nabla_\mu\log|\psi|^2\rangle. \quad (7.8)$$

These equations together with the hypotheses in Section 6 form the assumptions of the present theory. They go beyond the assumption formulated in Part I. The averaging process derives from ψ a streaming field which (unlike $|\psi|$, $\nabla_\nu S$, etc., itself) is smooth over regions ($N\gg1$)

$$N\delta x_1\delta x_2\delta x_3\gtrapprox N\sigma^3/\Delta_x v_1\Delta_x v_2\Delta_x v_3. \quad (5.4')$$

Indeed only after such a smoothing process a comparison is possible with hydrodynamical quantities, because these are averages, definable only on basis of blocks $N\delta x_1\delta x_2\delta x_3$ or larger ones. (ρ, $\rho\langle v_\nu\rangle$, $\rho\langle v_\mu v_\nu\rangle$ are averages taken over the statistically independent elements contained in a block (5.4')), and because the hydrodynamical equations do only hold for such smoothed quantities ρ, $\langle v_\nu\rangle$, etc. Strictly speaking, the word "averages" always means expectation values of mass, etc. per unit volume, it refers to a collective about which we can infer the more the larger N, i.e., the less details we request about the streaming field.

The main point of this transformation theory is to exploit the indeterminacy of the micro details of the hydrodynamical streaming field. After realizing that hydrodynamical quantities are only defined as averages we can simplify the set of hydrodynamical equations by transforming them into a single wave equation without any restrictions of generality (cf. Section 8), except that this transformation implicitly contains an assumption (7.7), (7.8), cf. also (8.2), (8.5), about the effect of stellar encounters, an assumption physically more adequate than the great number of assumptions needed in a straightforward calculation of force fluctuations.

Another way of looking at our procedure: We start with hydrodynamical Eqs. (4.02), (4.03). Realizing the coarse grained definition of the hydrodynamical quantities we can represent them by wave-mechanical expressions (7.5)–(7.8) which obey the wave Eq. (6.1) and thereby satisfy the hydrodynamical equations automatically. The rather artificially looking representation (7.8), and also (7.7) impose restrictions on the classes of hydrodynamical fields which can be represented by ψ waves. Equation (7.8) concerns an assumption about mean square deviation of velocity. An assumption of this kind has to be introduced in any case. It has been chosen of that particular form (7.8) not only to make it possible to transform hydrodynamical equations into a simple wave equation but because of its compatibility with the basic assumption of Part I (cf. Eq. (8.5)).

Before discussing these equations let us note that cosmological wave mechanics does not make any statements about third and higher moments of v_ν like $\langle(v_\mu-\langle v_\mu\rangle)(v_\nu-\langle v_\nu\rangle)(v_\lambda-\langle v_\lambda\rangle)\rangle$. Thus there cannot arise any inconsistency from hydrodynamical equations of third and higher degree in v_ν. The hydrodynamical equation of third degree e.g., reads

$$\sum\{\rho[\langle(v_\mu)\nabla_\mu+\partial/\partial t\rangle\langle(v_\lambda-\langle v_\lambda\rangle)(v_\nu-\langle v_\nu\rangle)\rangle +\langle(v_\nu-\langle v_\nu\rangle)(v_\mu-\langle v_\mu\rangle)\rangle\nabla_\mu\langle v_\lambda\rangle +\langle(v_\lambda-\langle v_\lambda\rangle)(v_\mu-\langle v_\mu\rangle)\rangle\nabla_\mu\langle v_\nu\rangle] +\nabla_\mu[\rho\langle(v_\mu-\langle v_\mu\rangle)(v_\nu-\langle v_\nu\rangle)(v_\lambda-\langle v_\lambda\rangle)\rangle]\} +\text{terms containing } \delta f/\delta t=0. \quad (7.9)$$

This fact only shows that cosmological wave mechanics makes less detailed statements about $f(x_1, x_2, x_3, v_1, v_2, v_3, t)$ than Boltzmann-Gibbs' Eq. (4.01).

8. Discussion

Let us first consider Eq. (7.6) which states that the velocity $\langle v_\nu\rangle$ of the streaming field is an average over a potential streaming field $-\nabla_\nu S$. S, however, as its definition (7.1) shows, may be a many-valued function of x_1, x_2, x_3, the various values differing by multiples of $2\pi\bar\sigma$, though ψ is assumed to be single valued. (The simplest example is provided by the superposition of two

overlapping stationary ψ functions in the Kepler problem, belonging to two different angular momenta, m_1, and m_2.) Thus a contour integral $\oint\sum -\nabla_\nu S dx_\nu$, or the corresponding smooth $\oint\sum\langle v_\nu\rangle dx_\nu$, does not vanish in general.[16]

The singularities of S round which S is many valued are at the zeros of ψ; $\psi=0$ in general defines lines in x_1, x_2, x_3, space, which may move as time goes on. $\oint\sum -\nabla_\nu S dx_\nu$ round such a singularity is thus an integer multiple of $2\pi\bar{\sigma}$. In the ψ picture of an actual gravitational system there are enormous numbers of these singularities. The question arises whether the discrete curls of the $-\nabla_\nu S$ field do not stand in contradiction with the continuous character of the observed $\langle v_\nu\rangle$ field, or whether they fall under the category of fine grained structure of the wave mechanical picture, which smoothes out when we average over volumes (5.4′). The latter alternative which states that the fine grained structure of the ψ picture is nothing but an interpolation escaping in its details any observational test turns out to be the case: What we can compare with observation is the behavior of the contour integral $\oint\sum\langle v_\nu\rangle dx_\nu$ if we choose various closed paths. The wave-mechanical $\oint -\sum\nabla_\nu S dx_\nu$ makes jumps $2\pi\bar{\sigma}$ if we deform the closed path. In order now to carry out the averaging, we construct a ring-shaped tube with the given closed path as axis, the thickness of the tube given by $N^{\frac{1}{3}}\delta x$ (cf. (5.5)). dx_ν being a length element along the path, our average is

$$\oint\sum\langle v_\nu\rangle dx_\nu=\oint -\sum(\langle|\psi|^2\nabla_\nu S\rangle/\langle|\psi|^2\rangle)dx_\nu, \tag{8.1}$$

the averages being taken over the cross sections of the tube. It is evident that (8.1) makes no jumps if the path is steadily deformed, cutting singularities of S. (7.6) therefore defines a general streaming field $\langle v_\nu\rangle$ with a continuous distribution of curl.

There are several features of the ψ function similar to that just discussed: $|\psi|^2$ is not a very smooth function in general, there are many maxima and minima. But we have to average over blocks (5.4′) and in this averaging process the ripples of $|\psi|^2$, characteristic for its microstructure, smooth out. (That can be most easily seen for the superposition of two plane waves going in opposite directions, forming a standing wave.) These ripples of $|\psi|^2$ are of importance for δU calculated by the Poisson equation. The lack of smoothness of the $|\psi|^2$ field and of the S field (wave picture) stands in correspondence to the discreteness of the actual elements of the system (particle picture).

Let us now discuss (7.7). $\iiint v_\nu(\delta f/\delta t)dv$ is the increase of momentum of unit volume $\iiint dx_1dx_2dx_3$ per unit time originating from the fact that force fluctuations speed up (or slow down) some elements; $-\langle|\psi|^2\nabla_\nu(\delta U)\rangle$ is the contribution of force fluctuations toward the force acting on unit volume $\iiint dx_1dx_2dx_3$. (7.7), (6.5), (6.6) thus represent our assumptions about $\delta f/\delta t$ (cf. Section 4.3).

Equation (7.8) needs some more detailed discussion. Consider first a ψ wave of a system flattened in the x_3 direction whose $\nabla_3 S$ is a constant or zero all over. Then $\langle v_3\rangle=-\nabla_3 S$ and (7.8) becomes

$$\begin{aligned}\rho\langle(v_3-\langle v_3\rangle)^2\rangle&=-\tfrac{1}{4}\bar{\sigma}^2\langle|\psi|^2\nabla_3\nabla_3\log|\psi|^2\rangle\\&=\bar{\sigma}^2(-\tfrac{1}{4}\langle\nabla_3\nabla_3|\psi|^2\rangle+\langle(\nabla_3|\psi|)^2\rangle).\end{aligned}\tag{8.2}$$

For example, if at some instant

$$\psi\propto\exp\{-\tfrac{1}{4}(x_3/\Delta x_3)^2+i(\nabla_3 S/\bar{\sigma})x_3\}, \tag{8.3}$$

i.e.,

$$|\psi|^2\propto\exp\{-\tfrac{1}{2}(x_3/\Delta x_3)^2\}, \tag{8.4}$$

we get from (8.2)

$$\rho\langle(v_3-\langle v_3\rangle)^2\rangle=\tfrac{1}{4}\bar{\sigma}^2\langle|\psi|^2\rangle/(\Delta x_3)^2,$$

or

$$\Delta x_3\Delta v_3=\tfrac{1}{2}\bar{\sigma}. \tag{8.5}$$

This shows that the wave picture because of (7.8) involves an assumption about the residual velocities in a gravitational system. This assumption which for the wave packet has the form of (8.5), is just identical with the minimum relation (5.8) required by the analysis of observational data. The pressure $\rho\langle(v_\nu-\langle v_\nu\rangle)^2\rangle$, because it is defined as an average of (8.2) over blocks (5.4′), is positive not only in the special case (8.3).—We note that a three-dimensional version of a wave packet (8.3) has not much physical significance as it would contain about

[16] Overlooking this fact, S. Rosseland raised the objection (Astrophysica Norvegica 3, 88 (1939)) that in the wave picture "the angular momentum round the axis will be the same per unit mass at all places of the system."

one statistically independent element only. The relation (7.8) *replaces* the polytropic or similar relation between pressure and density sometimes introduced into stellar dynamics without any physical justification.[17] This short calculation shows the close relationship between the assumption (7.8) or (8.2) about pressure and the fundamental assumption (5.1) of Part I about density of elements in phase space. It indicates that we are well justified in making this assumption about pressure after we have adopted the assumption about density of elements as a basis. The reasoning for the density assumption given in Part I makes, however, sense but in the case of mass points and clusters of mass points, moving in their gravitation field, not in hydrodynamics of ordinary fluids.

(8.3) can be written as a Fourier integral, $(\Delta k_\nu)^2=\langle(k_\nu-\langle k_\nu\rangle_{kl})^2\rangle_{kl}$

$$\psi \propto \int_{-\infty}^{+\infty} \exp\{-\tfrac{1}{4}[(k_3-\langle k_3\rangle_{kl})/\Delta k_3]^2-ik_3x_3\}dk_3, \tag{8.6}$$

where (this follows from Fourier analysis and (7.1))

$$\langle k_3\rangle_{kl}=-\nabla_3 S/\bar{\sigma}, \quad \Delta k_3=1/2\Delta x_3, \tag{8.7}$$

which, combined with (7.6), (8.5) gives

$$\langle k_3\rangle_{kl}=\langle v_3\rangle/\bar{\sigma}, \quad \Delta k_3=\Delta v_3/\bar{\sigma}. \tag{8.8}$$

(8.8) shows that the distribution of v_ν in the wave packet follows from the k_ν distribution by multiplication with $\bar{\sigma}$. We derived this result after we defined the v_ν distribution by (7.6), (7.8). We could also have defined the v_ν distribution as that of $\bar{\sigma}k_\nu$, i.e., (8.8) and therefrom derived (7.6), (8.5) via (8.7).

It would be interesting to study in all generality the relationship between the hydrodynamical interpretation (7.5)–(7.8) on the one hand, and a statement to the effect that the total velocity distribution in a stellar system be given by its k distribution as exemplified by (8.7), (8.8) on the other hand. Space forbids us to reproduce some calculations in this direction. Similarly a detailed proof would be desirable of the compatibility of the hydrodynamical interpretation (7.5) to (7.8) with the hypothesis that $|c_{nlm}|^2$ represents the statistical distribution of the elements over the integrals I_1, I_2, I_3 corresponding to n, l, m.

These problems concern the transformation theory from one representation of the ψ function to another. We are confronted here with a somewhat more detailed situation than in the quantum-mechanical transformation theory because of our interest in all the hydrodynamical quantities (7.5)–(7.8), not only in $|\psi|^2$. Apart from the hydrodynamical equations obtained from the Boltzmann Gibbs Eq. (4.01) by integration over the velocity space, we have also to study the Boltzmann Gibbs equation integrated over position space and integrated over the space of angle variables, respectively, and confront them with the corresponding equations in ψ.

The following are the De Broglie relations for a wave parcel moving in an external gravitation field. Forgetting about the finite extension of the wave parcel and considering the one-dimensional case, we write the time dependent form of (8.6)

$$\psi=\exp i(\omega t-kx).$$

The wave equation (6.1) implies

$$\bar{\sigma}\omega=\tfrac{1}{2}\bar{\sigma}^2k^2+c^2+U, \tag{8.9}$$

i.e., total energy = kin. energy + rest. energy + pot. energy. Therefore, we have the phase velocity

$$V=\frac{\omega}{k}=\frac{1}{\bar{\sigma}k}(\tfrac{1}{2}\bar{\sigma}^2k^2+c^2+U)\approx\frac{c^2}{\bar{\sigma}k} \tag{8.91}$$

and the group velocity

$$v=d\omega/dk=\bar{\sigma}k\approx c^2/V, \tag{8.92}$$

which is identical with (8.7).

9. Some General Remarks

Superposition Principle

At first sight the linear superposition principle in ψ seems to be in contradiction to the apparent non-linearity in f of the Boltzmann-Gibbs Eq. (4.01). Let us talk about the fact that f is quadratic in ψ according to (7.5)–(7.8) later, and first look after the linearity and non-

[17] To "specify the physical relation between pressure and density . . . , say a polytropic relation" (Rosseland, reference 16, p. 92) is equivalent with the introduction of a statistical assumption, not a consequence of plain mechanics.

linearity of the wave-mechanical equation for ψ on the one hand, and, respectively, the linearity or non-linearity of the Boltzmann-Gibbs equation for f on the other hand. Examining this point more closely, we immediately realize that if we consider the forces $-\nabla_\nu(\bar{U}+\delta U)$ (in the wave-mechanical case), and $-\nabla_\nu\bar{U}+\delta F_\nu$ (for the Boltzmann-Gibbs equation) as given, respectively, then we have a linear superposition principle for ψ, and for f (including ρ, $\rho\langle v_\nu\rangle$, $\rho\langle v_\mu v_\nu\rangle$ cf. (4.02), (4.03)), respectively. If, however, we determine the smooth field $-\nabla_\nu\bar{U}$ as well as its fluctuations $-\nabla_\nu(\delta U)$ and δF_ν, respectively, by Poisson's equation and Chandrasekhar's equations, respectively, out of $|\psi|^2$ and f, respectively, and thus combine the gravitation field equation with the wave equation and Boltzmann-Gibbs equation, respectively, then we no longer have linear superposition, neither in ψ nor in f. It is interesting to study this latter case in the example of two galaxies rotating in opposite directions around about the same axis (by chance) and approaching and finally penetrating each other: According to the ψ picture the superposition corresponding to the penetrated case has a ripply $|\psi|^2$ distribution which, through the δU produced by it, causes transitions to many new ψ states, thus not permitting an unperturbed superposition of the two original galaxies. According to the classical description, strong fluctuations δF_ν of the field of force arise and thus disturb the superposition $f_{\mathrm{I}}+f_{\mathrm{II}}$.

From now on we consider the gravitation field and its fluctuations as given. Evidently linear superposition in ψ in general means something different from linear superposition in f which is quadratic in ψ. The wave equation admits a linear superposition

$$\psi=\psi_{\mathrm{I}}+\psi_{\mathrm{II}}, \tag{9.1}$$

and because of the hydrodynamical interpretation of the wave equation, the quantities $\rho=\langle|\psi|^2\rangle=\langle|\psi_{\mathrm{I}}+\psi_{\mathrm{II}}|^2\rangle$ etc., satisfy the hydrodynamical equations too. But we have in general $\rho\neq\rho_{\mathrm{I}}+\rho_{\mathrm{II}}=\langle|\psi_{\mathrm{I}}|^2\rangle+\langle|\psi_{\mathrm{II}}|^2\rangle$ etc. On the other hand the hydrodynamical equations admit a linear superposition, i.e., with ρ_{I} and ρ_{II} also $\rho_{\mathrm{I}}+\rho_{\mathrm{II}}$ etc., are a solution. (Under this category falls a Gibbs ensemble, i.e., a mixture $|\psi_{\mathrm{I}}|^2+|\psi_{\mathrm{II}}|^2$ of ψ functions with random phase distributions.) Thus both ρ and $\rho_{\mathrm{I}}+\rho_{\mathrm{II}}$ satisfy the hydrodynamical equations.

Let us now study the case where the two superposition principles become identical. We readily see that the hydrodynamical quantities defined by (7.5)–(7.8), admit a linear superposition principle too, provided the distributions of the wave numbers $\mathbf{k}_{\mathrm{I}}$ and $\mathbf{k}_{\mathrm{II}}$ of the superimposed ψ_{I} and ψ_{II} do not cover the same nor approximately the same ranges.—In that case quantities like $\langle\psi_{\mathrm{I}}\psi_{\mathrm{II}}^*+\psi_{\mathrm{II}}\psi_{\mathrm{I}}^*\rangle$, averaged over a block large enough to contain many statistically independent elements, will average out to zero. The superposition principle for the hydrodynamical quantities appears thus as a special case of the more general linear superposition principle in ψ. Indeed we have

$$\begin{aligned}\langle|\psi|^2\rangle&=\langle\psi\psi^*\rangle\\&=\langle\psi_{\mathrm{I}}\psi_{\mathrm{I}}^*+\psi_{\mathrm{II}}\psi_{\mathrm{II}}^*+\psi_{\mathrm{I}}\psi_{\mathrm{II}}^*+\psi_{\mathrm{II}}\psi_{\mathrm{I}}^*\rangle\\&=\langle\psi_{\mathrm{I}}\psi_{\mathrm{I}}^*\rangle+\langle\psi_{\mathrm{II}}\psi_{\mathrm{II}}^*\rangle.\end{aligned}\tag{9.2}$$

Similarly

$$|\psi|^2\nabla_\nu S=\frac{\bar{\sigma}}{2i}(\psi^*\nabla_\nu\psi-\psi\nabla_\nu\psi^*);$$

this is also bilinear, therefore we get as average

$$\langle|\psi|^2\nabla_\nu S\rangle=\langle|\psi_{\mathrm{I}}|^2\nabla_\nu S_{\mathrm{I}}\rangle+\langle|\psi_{\mathrm{II}}|^2\nabla_\nu S_{\mathrm{II}}\rangle. \tag{9.3}$$

For (7.7) where $\delta U(x_1, x_2, x_3)$ is considered a given quantity (the same for ψ_{I}, ψ_{II} as well as for ψ), the statement is evident. Finally we can transform (7.8)

$$\begin{aligned}&-\tfrac{1}{4}\bar{\sigma}^2|\psi|^2\nabla_\mu\nabla_\nu\log|\psi|^2+|\psi|^2(\nabla_\nu S)(\nabla_\mu S)\\&=\tfrac{1}{4}\bar{\sigma}^2[\nabla_\nu\psi^*\nabla_\mu\psi+\nabla_\nu\psi\nabla_\mu\psi^*-\psi\nabla_\mu\nabla_\nu\psi^*-\psi^*\nabla_\mu\nabla_\nu\psi];\end{aligned}$$

this is again bilinear and therefore we have for the averages

$$\langle[\ ]\rangle=\langle[\ ]_{\mathrm{I}}\rangle+\langle[\ ]_{\mathrm{II}}\rangle,\ \text{Q.E.D.} \tag{9.4}$$

We are, however, primarily interested in investigating the cases for which linear superposition in ψ leads to results different from linear superposition in f. That happens if there are definite phase relationships in space (and time) between the superposed ψ's. In that case, interference effects will have to show up. Indeed, the formation of structures like spiral arms in galaxies comes from the superposition of an original

ψ with another ψ excited from the original ψ by a perturber. There is a definite phase-relationship between original ψ and new ψ. The superposition, as the analysis shows, leads to structures with well established symmetry properties (180° symmetry) such as pairs of spiral arms, even the details of which have to have this symmetry. The observed facts confirm this feature of our theory very well. It has its counterpart in the classical treatment of tidal effects which, however, cannot easily be carried through in quantitative details with the usual hydrodynamical methods.

Gibbs Ensemble

The question might be raised whether both, linear superpositions of ψ, say $\psi=\sum c_{nlm}\psi_{nlm}$ with density

$$|\psi|^2=|\sum c_{nlm}\psi_{nlm}|^2,$$

and mixtures (Gibbs ensembles) with diagonal elements of the density matrix $\sum P_{nlm}|\psi_{nlm}|^2$ necessarily have to enter into this theory. The answer is yes.

There is no theoretical possibility to dispose of superpositions and to work but with mixtures. Such disposal would mean to express all distributions in terms of $\sum P_{nlm}|\psi_{nlm}|^2$. But it would be absurd to distinguish one particular set of eigenfunctions (say ψ_{nlm} in the case of an attracting mass center) excluding a distribution over another set (say the eigenfunctions of the same problem referring to a different direction of polar axis, or referring to parabolical coordinates).—Besides we are essentially interested in interference phenomena which would be lost in an attempt to describe a stellar system only by mixtures of stationary states. We are interested both in large scale interference structures described above, and in small scale unobservable interference ripples which play an important role in producing δU following Poissons equation, i.e., (6.6), (6.5) which works with the non-averaged $|\psi|^2$.

On the other hand, in a rigorous theoretical treatment we cannot dispose of the Gibbs ensemble, in general made up from a mixture of some kind of ψ functions, say

$$\psi_\alpha=\sum c_{\alpha,\,nlm}\psi_{nlm}.$$

When given an observed system (i.e., a sample), we have to choose the collective from a Gibbs ensemble of collectives and find that the system belongs with the probability P_α to the ψ_α, the diagonal elements of the density matrix being

$$\sum_\alpha P_\alpha|\psi_\alpha|^2.$$

In quantum mechanics one can, by a single observation, pin down a specific ψ_α state; we cannot. Our case is more like the usual one in probability theory where the available number of elements never can single out just one ψ_α collective.

We discussed the averaging process of wave-mechanical expressions over blocks $N\delta x_1\delta x_2\delta x_3$. It provided us with smooth hydrodynamical quantities. We might conjecture that the averages of ψ quantities over those blocks can be replaced by strictly local averages over the Gibbs ensemble. The averaging over blocks levels out micro-structures of the ψ picture due to variations of amplitude and phase of ψ inside blocks, variations which do not show up macroscopically. Similarly the Gibbs ensemble provides a mixture of ψ functions whose phase distribution is at random to the extent that this does not upset the given macrostructure of the system.

Other remarks

If we consider a galaxy consisting amongst other elements, of several kinds of clusters, we have two entirely different problems: (a) The motion of these clusters and other elements in the galaxy. (b) The internal motions inside each of the clusters: (a) and (b) refer to different "systems," different ψ's and different $\bar{\sigma}$'s, the elements in (a) being the clusters, etc., the elements in (b) the individual stars constituting the respective cluster. A "sub" ψ wave describing a cluster (b) moves in the gravitation field of its own and in the external field of the galaxy; it gives among other things information about disintegration of the cluster due to tidal forces and chance-encounters just as in the classical treatment.[18]

[18] B. J. Bok, Harvard Circular 384. S. Chandrasekhar, reference 4. If we take together all the sub ψ waves describing (b) and plot them in the same position space, arranged just as the clusters are located these days, we do not get a "ψ picture of the galaxy as a whole." Such a collection of sub ψ waves would correspond to the par-

Self-Consistency

On the one hand we have to study the connection which the hydrodynamical equations of motion establish between gravitation field and statistical distribution function f. On the other hand we have to satisfy Poisson's equation for the gravitation potential and thereby secure a self-consistent field. This problem is, however, so complicated that the usual hydrodynamical methods have to stop half-way, ignoring the Poisson equation and therefore self-consistency. The main idea of the transformation theory developed in Part II is to provide a mathematical shortcut which makes it possible to attack dynamically more complicated problems, and also self-consistent fields; an integration of the wave equation is attainable even for rather complicated gravitation fields. With this powerful mathematical tool we may hope not only to calculate self-consistent steady fields but self-consistent transient fields. In particular we are interested in the explanation of the asymptotic behavior of stellar systems like the flattening process of a galaxy.—Our solar system seems to have developed from a more chaotic distribution of masses, which first became flattened into a disk shaped body and which through their interactions had a tendency to group into preferential orbits. To such a system it is possible to apply a wave-mechanical hydrodynamical description. There is a vast field of dynamically more complicated problems about our solar system (restricted problems of 4 bodies, resonance problems, and others) which in this way become accessible to solution merely because of the simplicity of our mathematical tool.

ticular sample of clusters as we encounter them today, but not to a statistical distribution of clusters in the big system. The latter is represented by a "super" ψ wave which tells nothing about internal structure of the clusters.

PHYSICAL REVIEW VOLUME 70, NUMBERS 7 AND 8 OCTOBER 1 AND 15, 1946

Properties of 94(239)

J. W. KENNEDY, G. T. SEABORG, E. SEGRÈ, AND A. C. WAHL
Radiation Laboratory and Department of Chemistry, University of California, Berkeley, California

(Received May 29, 1941)*

WE would like to report that we have observed the fission of 94^{239} with slow neutrons. The cross secton for the fission of 94^{239} with slow neutrons is even larger than that of U^{235}. The cross section was determined by comparing the number of fissions obtained with a sample containing 94^{239} with the number obtained with a sample of ordinary uranium under conditions which were as identical as possible in every detail. Two separate methods were used to prove that the fissions in the 94^{239} sample could not be attributed to the presence of uranium impurity: (1) complete and identical chemical tests on the isolation of rare earth carrier material for element 94 from non-irradiated uranium, i.e., "blank tests," in which the absence of uranium impurity in the final product was established by showing the absence of uranium alpha-particles and (2) demonstration that the ratio of the cross section for slow neutrons to that for fast neutrons for the fission of 94^{239} is different from the same ratio for natural uranium. This latter experiment has not yet been carried out in its optimum form, and we hope to submit a later report giving details of an improved experiment.

The details follow:

A sample of uranyl nitrate ($UO_2(NO_3)_2 \cdot 6H_2O$) weighing 1.2 kilograms was distributed in a large paraffin block, placed directly behind the beryllium target of the 60-inch Berkeley cyclotron, and given over a period of about two days a 3500 microampere-hour bombardment with neutrons from beryllium plus 16-Mev deuterons. This uranyl nitrate was placed in a continuously operating glass extraction apparatus, two liters of diethyl ether were added, and practically all of the uranyl nitrate was extracted into the ether phase. The 93^{239} was isolated from the aqueous

* This letter was received for publication on the date indicated but was voluntarily withheld from publication until the end of the war. The original text has been somewhat changed, by omissions, in order to conform to present declassification standards.

phase with rare earth fluoride carrier by the method of McMillan and Abelson[1] and the mixture of 3 mg of La and 3 mg of Ce which was "carrying" the 93^{239} was reprecipitated as fluoride six times in order to remove any uranium impurity. This sample of 93^{239} at the time of its purification (which included purification from element 94) had an activity of 125 millicuries as determined with the aid of an ionization chamber, connected to an FP-54 vacuum tube electrometer, which had been calibrated in an absolute manner for 93^{239} radiation by the use of a Geiger counter and the method of aliquots. After the 93^{239} had decayed into 94^{239}, preliminary fission tests were made on this sample which then contained 0.5 microgram of 94^{239}. This sample was placed near the screen window of an ionization chamber which was imbedded in paraffin near the beryllium target of the 37-inch Berkeley cyclotron. This gave a small, but detectable, fission rate when a 6-microampere beam of deuterons was used. However, this count was too small to be sure that the fissions were not caused by uranium impurity and the fission rate with fast neutrons (i.e., when the chamber was surrounded with cadmium) was too small to determine with any accuracy at all.

This sample, which had a thickness of total material amounting to 4.8 mg per cm^2, was then subjected to a chemical procedure[2] designed to isolate the 94^{239} in much less material. The procedure was carefully tested in blank experiments with the aid of element 94 from deuteron-activated uranium as tracer to show that the yield was practically 100 percent. In this manner the 0.5 microgram of 94^{239} was isolated with lanthanum fluoride in which the thickness of total material amounted to 0.16 mg per cm^2. (In a blank experiment in which the same amount of lanthanum fluoride was isolated from non-irradiated uranium by an identical chemical procedure the alpha-count was less than $\frac{1}{4}$ per minute. Correcting for the geometrical factor, as determined with the aid of a known amount of uranium of the same thickness, this means that the sample contained less than 3 micrograms of U^{238} impurity and hence less than 0.03 microgram of U^{235} impurity. This is the upper limit of uranium impurity which may be present, as determined by the limitations on the method of detection, and the actual amount might very well be much less than this.) A standard uranium sample, probably in the form of anhydrous oxide, of a thickness and area very nearly the same as that of the 94^{239} sample, was prepared by the electolysis of ordinary uranium out of absolute ethyl alcohol solution. This uranium standard contained 200 micrograms of U^{238} and hence 1.46 micrograms of U^{235}. The easily measurable fission rates of the 0.5 microgram 94^{239} sample and the 1.46 microgram U^{235} sample were compared when placed near the screen window of an ionization chamber imbedded in paraffin near the beryllium target of the 37-inch Berkeley cyclotron. When the ionization chamber and samples were completely surrounded with a shield of cadmium and boron carbide (B_4C) the fission rates dropped to negligibly small values.

Worth appending here is the information which we have obtained about the alpha-activity of 94^{239}. During the decay of the 125-millicurie sample of 93^{239} the sample was placed near an ionization chamber connected to a linear, pulse amplifier in order to watch for the growth of alpha-particles. A strong magnetic field was used to bend out the beta-particles. An alpha-particle activity was observed to grow with a half-life of about 2.3 days, which is the half-life to be expected for growth from 93^{239}. The alpha-count grew to the value 240 per minute. After the sample was thinned to 0.16 mg per cm^2 the alpha-count became 800 per minute. Correcting for the geometrical factor, as determined with the aid of a known amount of uranium of the same thickness as this sample, the total alpha-emission of the sample amounted to about 60,000 per minute. This corresponds to a half-life of about 3×10^4 years.

[1] E. M. McMillan and P. H. Abelson, Phys. Rev. **57**, 1185 (1940).
[2] G. T. Seaborg, A. C. Wahl, and J. W. Kennedy, Phys. Rev. **69**, 367 (1946).

Letters to the Editor

PROMPT publication of brief reports of important discoveries in physics may be secured by addressing them to this department. The closing date for this department is the third of the month. Because of the late closing date for the section no proof can be shown to authors. The Board of Editors does not hold itself responsible for the opinions expressed by the correspondents. Communications should not in general exceed 600 words in length.

Neutron Diffraction and Nuclear Resonance Structure

L. B. BORST, A. J. ULRICH, C. L. OSBORNE, AND B. HASBROUCK
Monsanto Chemical Company, Clinton Laboratories, Oak Ridge, Tennessee
September 4, 1946

THE phenomena of neutron diffraction have been described and the present status of studies with monochromatic neutrons produced by this means have been given recently.[1] The first work in this laboratory in 1944 led to the characterization of the prominent resonance level in samarium. This level was found to obey the Breit-Wigner resonance formula within experimental error. Figure 1 shows the original data and the best fitting resonance curve. The deviation of some of the points at low energies are caused by higher order reflections.

Table I summarizes the characteristics of some of the resonances studied. The cross section σ_0 given is the total cross section at resonance and includes contributions from resonance and potential scattering. Gamma is the half-width of the resonance at half-maximum. The integral under the resonance may be considered as an index of the importance of the resonance.

In the cases of indium and rhodium, the resolution of the instrument was not sufficient to evaluate the true constants of the resonance. The cross sections tabulated, therefore, represent lower limits, and the resonance widths represent upper limits.

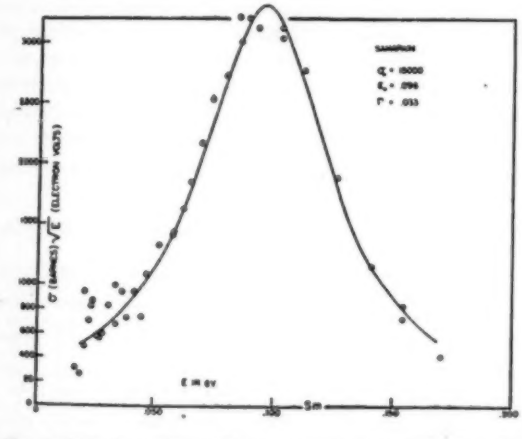

FIG. 1. Experimental results on the resonance scattering of neutrons on samarium. The solid line is the best fitting Breit-Wigner resonance curve.

TABLE I. Constants of neutron resonance levels.

Absorbing isotope	E_0	$\sigma_0 \times 10^{24}$	Γ	$\int \sigma E^{\frac{1}{2}} dE$
In^{115}	1.39	>15,000	<0.15	8300
Rh^{103}	1.30	>2,500	<0.13	1200
Sm^{149}	.096	93,000	0.035	3200
Eu^{151}	<.03	>3,000	?	
Eu^{153}	.54	20,000	0.075	3500
Gd^{157}	.044	190,000	0.05	6300

The resonance in gadolinium and the low lying resonance in europium fall in a region where the second order of the Maxwellian continuum interferes with exact measurement. The resonance energies in these cases are approximations only.

The isotopic assignments in the cases of samarium and gadolinium are based upon the work of Lapp.[2] The assignments for europium are based upon the activations in the spectrometer of europium samples with monoenergetic neutrons of the exact resonance energies and subsequent identification of the induced radioactivity. Neutrons of 0.03 ev produced a 9-hr. period (Eu^{152}, $T_{\frac{1}{2}}$=9.4 hr.) in an amount consistent with the measured flux and cross section. Neutrons of 0.54 ev produced a long-lived activity estimated from the flux and cross section to have a half-life of between 5 and 10 years (Eu^{154}, $T_{\frac{1}{2}}$=5–8 yr.).

The resonance integral $\int \sigma E^{\frac{1}{2}} dE$ appears to be a method of characterizing these neutron resonances in terms of relative importance. The range covered by these integrals is relatively large, so that the occurrence of three resonances (whose integrals differ only by a factor of two) in three isotopes differing by one proton and three neutrons is surprising. Further extension of this apparent series is prevented because of the instability of the nuclei involved.

[1] W. H. Zinn, Phys. Rev. 70, 102A (1946); W. J. Sturm and S. Turkel, Phys. Rev. 70, 103A (1946); E. Fermi and L. Marshall, Phys. Rev. 70, 103A (1946); L. B. Borst, A. J. Ulrich, C. L. Osborne, and B. Hasbrouck, Phys. Rev. 70, 108A (1946).
[2] R. E. Lapp, J. R. Van Horn, and A. J. Dempster, Phys. Rev. 70, 104A (1946).

The Liquid Drop Model for Nuclear Fission*

R. D. PRESENT** AND F. REINES***
New York University, New York, New York
AND J. K. KNIPP****
Purdue University, Lafayette, Indiana
September 9, 1946

THE first extensive calculations on nuclear fission using the liquid drop model were made by Bohr and Wheeler.[1] The principal problem was to determine the potential energy surface, i.e., the potential energy as a function of the deformation parameters, and in particular the location of the saddle point giving the activation energy for fission. The deformation parameters were taken to be the coefficients a_n in the expansion of the radius vector in zonal harmonics (the surface of the drop is the locus $r = R\Sigma a_n P_n(\cos\theta)$. Bohr and Wheeler calculated the surface and Coulomb energies of the deformed drop out to fourth-order terms in a_2, including the coupling terms with a_4. Even in the case of the uranium isotopes, however, large deformations are needed to reach the critical shape corresponding to the saddle point. The few terms considered

by Bohr and Wheeler are inadequate to treat such large deformations and while their activation energy curve is not justified by their calculations, it can be regarded as a reasonable interpolation between the computed results for small deformations and the experimental results for uranium. Further calculations were made by Present and Knipp[2] who extended the potential energy series to higher order terms in a_2 and a_4 and included the coupling terms between even and odd harmonics in order to see whether the observed asymmetry of fission could be explained in this way. The series was extended to terms as high as a_2^8, $a_2^4a_4$ and $a_2^3a_4^3$ without yielding satisfactory convergence for the large values of a_2 at which the saddle point of the energy surface is located in the case of uranium fission. The use of ellipsoidal coordinates was found to offer no appreciable advantage.

Since the values of a_2 alone are large in the initial stages of fission (because of an accurate representation of the deforming drop by $P_2(\cos\theta)$ alone), it was decided to carry out computations for fixed values of a_2 expanding in terms of a_4. Separate calculations were made for $a_2=0.3$ and 0.4 which are partly beyond the range of validity of the earlier power series calculation. The method broke down for larger values of a_2 because of convergence difficulties with the Coulomb series for the coefficient of a_4^3. The results for the deformation $a_2=0.4$ make possible a determination of the activation energy and the saddle point deformation parameters for a nucleus with $x=0.80$ (where x represents half the ratio of the electrostatic energy of the undeformed drop to its surface energy). It will be recalled that if $x\geqslant 1$ the drop is unstable against small second harmonic deformations and divides spontaneously. The new results which hold for $x\geqslant 0.80$ can be extrapolated to the uranium isotopes ($x\approx 0.75$) and indicate an activation energy of about 5 or 6 Mev in agreement with experiment. Coupling terms with the sixth harmonic were included in the calculation, and the effect of a_6 was sufficiently small that a_8 and higher even harmonics could be neglected.

The above calculations, with even harmonics only, correspond to a symmetric fission. The primary odd harmonics a_1 and a_3 were next introduced in all possible low coupling terms with a_2 up to fifth order (e.g., $a_2^3a_1^2$, $a_2^3a_1a_3$, $a_2^3a_3^2$). The introduction of these terms raises the energy and their positive contribution increases with increasing a_2. The series ceases to be accurate at about $a_2=0.3$ but the uncertainties do not become large enough to affect the sign of the energy until $a_2\geqq 0.4$. It is concluded that the critical shape of a nucleus with $x\geqq 0.80$ is symmetrical according to the liquid drop model. However, the possibility is not excluded that for some large deformation beyond the critical shape, the contribution of the odd harmonics may change sign and the fission path deviate from symmetry. Since the cases of uranium and plutonium fission lie so close to $x=0.80$, it is highly probable that the critical shape of these nuclei is symmetrical on the liquid drop model. This justifies the calculation of the preceding paragraph in which the activation energy is obtained from even harmonics alone.

An attempt has also been made to calculate the lifetime against spontaneous fission from the Gamow formula. The multiple integral over the coordinates of all nuclear particles is transformed into an integral with respect to the deformation parameters a_n. The Jacobian of this transformation is evaluated from the velocity potential for a streamline motion of the nuclear particles. The results are at variance with experiment in predicting too short a lifetime for U^{235}.

We hope to publish a fuller account of these calculations within the near future.

* This work was begun in 1940 and completed in 1943. It was voluntarily withheld from publication until the end of the war.
** Now at the University of Tennessee and Clinton Laboratories.
*** Now at the Los Alamos Laboratory.
**** Now at Iowa State College.
[1] N. Bohr and J. A. Wheeler, Phys. Rev. 56, 426 (1939).
[2] R. D. Present and J. K. Knipp, Phys. Rev. 57, 751, 1188 (1940).

Water Spectrum Near One-Centimeter Wave-Length

C. H. Townes and F. R. Merritt
Bell Telephone Laboratories, Murray Hill, New Jersey
September 10, 1946

Becker and Autler[1] and Kyhl, Dicke, and Beringer[2] have measured the H_2O $(5_{-1}\text{–}6_{-5})$ line at 1.35-cm wave-length for mixtures of water in air at atmospheric pressure. Under these conditions the line is many thousands of megacycles wide. Using a technique described earlier[3] of sweeping an oscillator in frequency across the line, this line has been detected and measured in pure water vapor at pressures near one-tenth mm Hg. It is a few megacycles wide at this pressure and its frequency may be measured with great accuracy.

Equal quantities of H_2O and D_2O were mixed in order to obtain a vapor with 50 percent HDO molecules, and to look for the several HDO lines predicted near 1-centimeter wave-length by Hainer, King, and Cross.[4] A search was made between 22,100 and 25,400 megacycles frequency. One line was found. Data on this and the H_2O line are given in Table I.

Becker and Autler did not measure the half-widths of the H_2O line in pure water vapor, but it may be deduced from their measurements in air at high and low water concentrations. Likewise the intensities quoted for them are not their actual measurements, but their intensities reduced to allow for the half-widths measured in pure vapor at low pressure. The half-widths and intensities given for HDO are for a mixture of 50 percent HDO, 25 percent D_2O, and 25 percent H_2O. Agreement between the data of Becker and Autler and measurements at low pressure ap-

Table I.

	Frequency (megacycles) Becker and Autler	Frequency (megacycles) Present measurement	Maximum intensity Becker and Autler	(nepers/cm) Present measurement
H_2O		22,237±5		$4\pm2\times10^{-4}$
HDO	22,320±150	22,309±5	5.7×10^{-4}	$15\pm7\times10^{-4}$

	Half-width at half-maximum (megacycles)	Pressure (mm Hg)	Half-width at half-maximum for 760 mm pressure (megacycles) Predicted from Becker and Autler	Predicted from present meas.
H_2O	1.45	0.103	11,600±6000	10,700±200
HDO	1.3	0.12		8,200±1500

pears to be within the combined experimental errors in all cases.

The agreement in frequency for the H_2O line at low and high pressures is surprisingly good. It means that at least for this case, the strong collision approximation of Van Vleck and Weisskopf[5] must be rather good, and there can be very little frequency shift due to pressure as would otherwise be expected.[6]

Further effort will be made to obtain more accurate values for intensities and half-widths of these lines.

[1] S. H. Autler, G. E. Becker, and J. M. B. Kellogg, Phys. Rev. **69**, 694 (1946); G. E. Becker and S. H. Autler, Phys. Rev. **70**, 300 (1946).
[2] R. L. Kyhl, R. H. Dicke, and R. Beringer, Phys. Rev. **69**, 694 (1946).
[3] C. H. Townes, Phys. Rev., to be published.
[4] R. M. Hainer, G. W. King and P. C. Cross, Phys. Rev. **70**, 108 (1946).
[5] J. H. Van Vleck and V. F. Weisskopf, Rev. Mod. Phys. **17**, 227 (1945).
[6] H. M. Foley, Phys. Rev. **69**, 616 (1946).

Effects of High Initial Energies on Mass Spectra

HAROLD W. WASHBURN AND CLIFFORD E. BERRY
Consolidated Engineering Corporation, Pasadena, California
August 30, 1946

IT has been pointed out that discrimination at the second slit of a mass spectrometer occurs as a result of initial thermal or dissociation energies.[1] We find that similar effects can also occur at the exit slit. The total effect of such discrimination is to reduce the number of ions of a given mass which are able to traverse the slit system. The efficiency of collection is found to be a function of V/V_T for any given geometry, where V is the accelerating voltage and V_T is the voltage equivalent corresponding to the apparent absolute temperature (including any dissociation energy) of the ion in question.

The fact that discrimination occurs provides a way of experimentally measuring rather small energies of dissociation. Figure 1 shows curves of relative abundance *vs.* ion

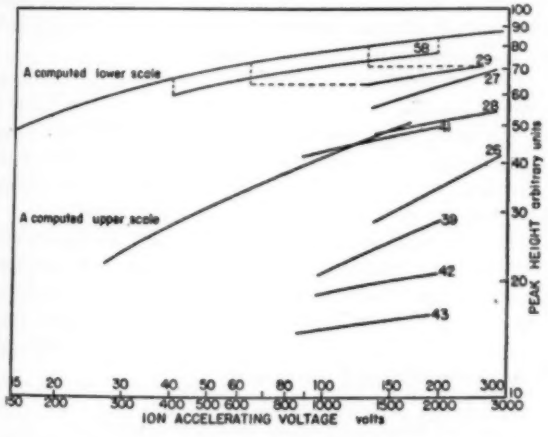

FIG. 1. Relative abundance of a number of ions from *n*-butane as a function of ion accelerating voltage.

TABLE I. Initial energies of several ions from *n*-butane.

Mass	Initial energy* ev	Abundance ratios: Magnetic scanning $V=1400$ v	Electric scanning $B=2200$ gauss	True abundance by extrapolation
26	2.4 ±0.7	36	42	134
27	0.36 ±0.6	235	267	367
28	0.12 ±0.3	199	225	238
29	0.08 ±0.01	270	303	302
39	0.83 ±0.06	102	98	243
41	0.11 ±0.01	192	200	378
42	0.085 ±0.04	83	88	90
43	0.045 ±0.005	660	699	665
58	0.041	100	100	100
58 sensitivity		81	73	100

* Includes thermal energy of 0.041 v corresponding to operating temperature of 475°K. Ionizing voltage = 50 v.

accelerating voltage for a number of ions obtained from *n*-butane. Curve *A* is a computed curve (derived in a manner similar to that of Coggeshall) which has been fitted to the experimental curve for the mass 58 ion, which we believe has only thermal energy. The computed curve is assumed to be a good extrapolation of the experimental curve both to low and to high voltages. To find the value of the initial energy of any ion, it is merely necessary to find the point on the voltage scale at which its curve fits the computed curve. The factor by which the voltage scale must be multiplied to accomplish this fit is the factor by which the temperature of the gas must be multiplied to give the apparent temperature of the ion. It should be noted that values obtained by this method do not take into account the true distribution of initial velocity, but rather assumes it to be Maxwellian. The amount of error from this source has not at this time been determined.

Table I shows the initial energies of several ions from *n*-butane. The spread of initial energy values indicated in Table I shows the range of values obtained in a single set of experiments. The spread could be reduced by using a greater range of voltages and by obtaining many experimental points on the curves. The absolute accuracy of the method was established for one case by obtaining the mass 58 curve at two temperatures. The two temperatures were 473°K and 550°K as measured by a thermocouple. The ratio of the temperatures as measured by the method described in this note was within ±2 percent of the ratio determined by the thermocouple readings.

In a properly designed ion source the effects of motion of the electron beam due to changing either the electric field or the magnetic field are found to be negligible compared with the effects of initial energies. As a result of initial energies, neither electric field scanning nor magnetic field scanning can produce true abundance ratios. This is clear from a study of the curves of Fig. 1, and from reference to the last three columns of Table I, which show the ratios obtained by each type of scanning, and the estimated true abundance ratios obtained by extrapolating the curves of Fig. 1 to very high voltages. From this standpoint, the choice of type of scanning seems to be one of convenience.

[1] N. D. Coggeshall, J. Chem. Phys. **12**, 19–27 (1944).

Resolution of a Rotational Line of the OCS Molecule and Its Stark Effect

T. W. DAKIN, W. E. GOOD, AND D. K. COLES
Westinghouse Research Laboratories, East Pittsburgh, Pennsylvania
October 1, 1946

WITH the method described by W. E. Good,[1] the absorption line due to the transition from the $J=1$ to the $J=2$ molecular rotational level has been resolved and shown on an oscilloscope. This line appears at the frequency of 24,320 megacycles or 0.8107 (cm^{-1}) wave numbers. The line was resolved at pressures of less than 10^{-1} mm of Hg. At pressures greater than this, the pressure broadening of the line was so great that the line was hardly observable by the oscilloscope method. The gas was introduced for the measurements, into a rectangular wave guide through which the microwaves were transmitted. Further details concerning the method can be found in the paper cited.

Carbon oxy-sulphide, OCS, is a linear molecule with the carbon atom between the oxygen and sulphur. Its moment of inertia calculated from the above frequency is 1.379×10^{-38} g cm^2.

The value (1.38×10^{-38} g cm^2) calculated using the interatomic distances observed by Cross and Brockway,[2] agrees well with this.

A linear molecule of this sort should show a Stark effect shift and splitting proportional to the square of the electric field strength and the square of the dipole moment.[3] When a d.c. electric field was applied to the carbon oxy-sulphide in the wave guide with the d.c. field parallel to the direction of the polarized electric vector of the traveling microwave, the rotational line split into two lines. One of these lines moved to a lower frequency than the unperturbed transition line and the other moved to a higher frequency. This effect was instantly (and to the authors, spectacularly) observed on the oscilloscope screen as the d.c. voltage was gradually increased. The single peak observed on the oscilloscope divided into two peaks, one of which was twice as high as the other. Figures 1–3.

The line which showed the least shift appeared twice as high (intense) as the other, in agreement with the theory. The energy level for the positive external (spatial) quantum number is the same as for the negative. Therefore, the $2(J+1)$ states become only $(J+1)$ levels. The frequency shift was found to be proportional to the square of the electric field strength, agreeing with the theory. Because the d.c. electric field is in the direction of the electric vector of the traveling microwave, no transition in the external quantum number occurs here when the rotational quantum number changes. Therefore, the frequency separation of the two lines from each other should be:

$$\Delta f=\left(\frac{3}{20}-\frac{1}{84}\right)\frac{8\pi^2 I}{\eta^2}\mu^2\cdot E^2 \text{ cycles/sec.},$$

where μ is the dipole moment and E the d.c. field strength. From the above equation the observed value of Δf and I, the moment of inertia, the dipole moment can be calculated. It was found to be 0.72×10^{-18} e.s.u. The principal uncertainty in the measurement is the separation of the electrodes (only 0.092 inch), which determines the field strength. Values of Δf as great as 5 megacycles were observed. Zahn and Miles[4] report a value of 0.65×10^{-18} for μ from dielectric constant data.

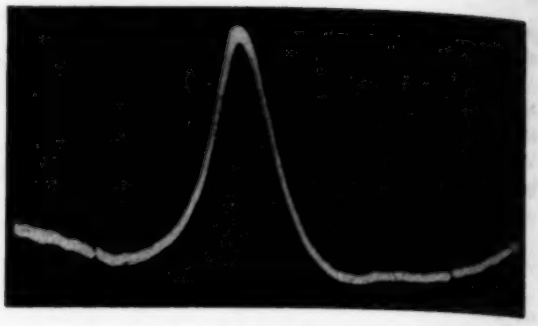

FIG. 1.

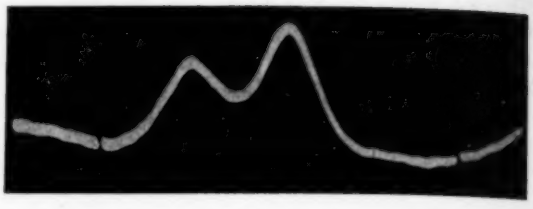

FIG. 2.

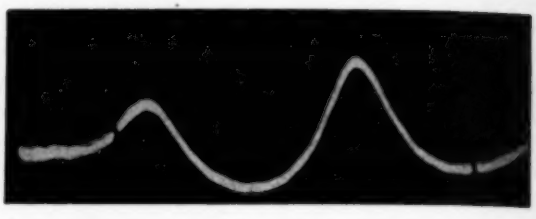

FIG. 3.

FIGS. 1–3. Oscilloscope pictures of absorption *versus* frequency for the OCS rotational line at 24,320 megacycles. The applied d.c. volts is 0 volt/cm in Fig. 1, 750 volts/cm in Fig. 2, 1070 volts/cm in Fig. 3. The frequency markers in the oscilloscope pictures are 6 megacycles apart in each case and appear as points of different intensity at each side of the oscilloscope trace. The base line is distorted so that the pictures give a somewhat inaccurate impression of the correct relative heights of the two peaks.

The d.c. field was applied by placing a thin strip of metal down the center of the wave guide and insulating it at the edges from the wave guide. This strip was in an equipotential plane with respect to the electric field of the traveling microwave. The d.c. field was then applied between this insulated strip and the wave guide.

Further measurements of the intensity of absorption, pressure broadening of the line, and more accurate measurements of the Stark effect are continuing. It is believed that this is the first time the Stark effect of a pure rotational line of a linear molecule has been observed, although it has been predicted theoretically.

[1] W. E. Good, Phys. Rev. 70, 213 (1946).
[2] Cross and Brockway, J. Chem. Phys. 3, 821 (1935).
[3] Cf. P. Debye, *Polar Molecules* (Chemical Catalog Company, New York, 1929).
[4] Zahn and Miles, Phys. Rev. 32, 497 (1928).

Absorption Curve of 31-Second $_8O^{19}$ Beta-Rays and Cross Section for Production by Thermal Neutrons*

LEO SEREN,** W. E. MOYER, AND W. STURM
Metallurgical Laboratory, University of Chicago, Chicago, Illinois
September 27, 1946

THE absorption of 31-second $_8O^{19}$ beta-rays has been measured by irradiating ordinary distilled water in the Argonne pile. The beta-rays were counted on a Duraluminum-walled Geiger counter. Aluminum absorbers up to 0.875 gram per cm² were used, and one point was taken with a 1.84 gram per cm² Pb absorber. (See the attached graph, Fig. 1.) From the absorption curve the range can be estimated as ~1.4 grams per cm² Al which corresponds to 3 Mev beta-rays. A further check on the energy is obtained by comparing the mass absorption coefficient of the $_8O^{19}$ beta-rays with that from $_{13}Al^{28}$ and $_{19}K^{42}$ beta-rays which we measured on the same geometry. For 31 sec. $_8O^{19}$ beta-rays, we got $\mu=2.56$ cm² per gram Al. For 2.4 min $_{13}Al^{28}$ beta-rays, we got $\mu=2.5$ cm² per gram Al, and a cloud-chamber measurement[1] of the energy of these beta-rays gave 3.4 Mev. For 12.4 hr. $_{19}K^{42}$ beta-rays, we got $\mu=2.56$ cm² per gram Al, and a cloud-chamber measurement[2] of the energy of these beta-rays gave 3.5 Mev.

From the range and absorption coefficient data, it would seem reasonable to conclude that the energy of the $_8O^{19}$ beta-rays is about 3.3 Mev. Gamma-rays also accompany the 31-sec. activity, as shown by the point on the absorption curve taken with the Pb absorber.

In addition to the 31-sec. beta-rays, we observed a half-life of ~4 minutes, probably caused by an impurity in the water. The saturation value of the ~4-minute activity was ~25 percent of the 31-sec. activity.

John Marshall[3] has measured the thermal neutron activation cross section[4] of $_8O^{18}$ assuming that $_8O^{19}$ beta-rays had the same absorption coefficient as UX_{II} beta-rays. On the same geometry that we used to measure the absorption coefficient of $_8O^{19}$ beta-rays, we obtained $\mu=4.88$ cm² per gram for UX_{II} beta-rays. Hence, Marshall's value of 3.5×10^{-4} barn[5] for the thermal neutron activation cross section of $_8O^{18}$ is high because he assumed $_8O^{19}$ beta-rays to be less penetrating than they actually are. A correction was made as follows: Counter wall used in Marshall's measurements was 0.050 gram per cm² Al, thickness of water layer used was 3 mm or 0.3 gram per cm². One-half of the water layer was the effective self-absorption thickness. Hence, the beta-ray absorption correction factor

$$\exp^{-(4.80-2.56)(0.050+0.150)}=\exp^{-0.464}=0.63$$

reduces the activation cross section of $_8O^{18}$ to 2.2×10^{-4} barn and the activation cross section for the normal oxygen atom is 4.4×10^{-7} barn. (The abundance of $_8O^{18}$ in normal oxygen is 0.20 percent.)

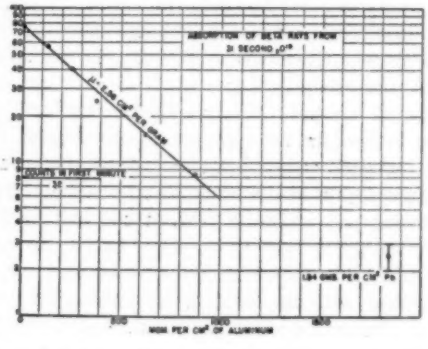
ABSORPTION OF BETA RAYS FROM
31 SECOND $_8O^{19}$
μ = 2.56 CM² PER GRAM
COUNTS IN FIRST MINUTE
= 50
184 GMS. PER CM² Pb
MGS PER CM² OF ALUMINUM

FIG. 1. Absorption of β-rays from O^{19}.

* This work was done under Manhattan Project sponsorship in October, 1943 and submitted for clearance June, 1946.
** Now with General Electric Research Laboratories, Schenectady, New York.
[1] J. M. Cork, J. R. Richardson, and F. N. D. Kurie, Phys. Rev. 49, 208 (1936).
[2] F. N. D. Kurie, J. R. Richardson, and H. C. Paxton, Phys. Rev. 49, 368 (1936).
[3] To be published in the Manhattan Project Technical Series.
[4] A survey of all thermal neutron activation cross sections measured at the Argonne Laboratory will be published shortly in *The Physical Review*.
[5] A barn equals 10^{-24} cm².

Proposal of a Method for the Separation of He^3 from He^4

JAMES FRANCK
Department of Chemistry, University of Chicago, Chicago, Illinois
September 24, 1946

THE isotope He^3 is present in helium according to Alvarez and Cornog in a concentration 10^{-7} to 10^{-8}. In a discussion with Earl Long about the problem of how to separate this rare He isotope from the bulk of He^4, it occurred to the present author that the superfluid state of liquid helium may offer an opportunity to carry out a separation process.

In London's theory the occurrence of superfluidity is explained as a quality acquired at very low temperatures by an atomic species obeying the Bose-Einstein statistic. He^4 having no spin is supposed to follow this statistic; but for He^3, which has odd nuclear spin, the rules of the Fermi statistic are valid and, correspondingly, no superfluid state is expected to occur for this isotope. Therefore, a great enrichment of He^3 in liquid He may be achieved by letting the bulk of He^4 run out of a container on account of its superfluidity, while He^3 is expected to remain in the residue.

If such an experiment should prove to be successful, it would not only have the practical value of producing a supply of He^3 to be used for experiments in nuclear physics, but would at the same time offer direct evidence in favor of London's theory.

The drawback of the proposed experiment is the fact that greater quantities of liquid helium (about 10 liters) are needed to carry it out. Since such amounts are usually not available, this proposal is published to bring it to the attention of those laboratories in which the special equipment for the production of greater quantities of liquid He is available.

Thresholds for Slow Neutron Induced Reactions

L. I. Schiff
Department of Physics, University of Pennsylvania, Philadelphia, Pennsylvania
October 2, 1946

THIS note discusses the possibility of determining the threshold energy of a particular mode of disintegration of a compound nucleus that can be formed from a stable nucleus by slow neutron capture. If ordinary slow neutron capture, characterized by the $1/v$ law, can produce the reaction, it is reasonable to believe that the energy of the newly formed compound nucleus is greater than that required for the mode of disintegration in question. Then if it were possible to introduce the neutron with a variable and measurable amount of negative kinetic energy, one could find the smallest excitation energy of the compound nucleus that would produce that disintegration. This can be accomplished by bombarding the original nucleus with deuterons, and selecting those reactions in which the outgoing proton carries off more energy than the incident deuteron minus the binding energy of the deuteron.

The selection of individual (d, p) processes of this type requires that coincidences be measured between one or more of the products of the nuclear reaction and outgoing protons of particular energies. An interesting case in which this could perhaps most readily be accomplished is the fission of one of the slow neutron fissionable heavy nuclei. The problem of detecting coincidences between fission fragments and protons in the presence of a strong deuteron beam, and at the same time measuring the proton energy, would present some experimental difficulties but does not seem to be insoluble.

The observations of Gant,[1] and of Jacobsen and Lassen,[2] on deuteron induced fissions in uranium and thorium, show a threshold at about 8 Mev. Since the normal isotopic mixture of uranium was used, any effect due to U^{235} of the type described above might well have escaped observation. It would be necessary to perform the coincidence experiment with enriched U^{235} or some other slow neutron fissionable isotope, and to use deuterons of energy not much above 8 Mev in order that the background due to fission following capture of the whole deuteron be minimized.

The reaction envisaged here would be expected to go according to the Oppenheimer-Phillips process. Volkoff's[3] expression for the energy transfer has been multiplied by the neutron sticking probability, which is assumed to be proportional to Bethe's[4] expression for the level density, to yield approximate energy distributions for the outgoing protons. These are shown in Fig. 1, for bombarding deuteron energies of 4, 6, and 8 Mev. Each curve is arbitrarily normalized to unit maximum; the total yields from all (d, p) processes are estimated from the transmutation function[5] to be in the ratio 1:1000:15,000 for the three bombarding energies. The curves of Fig. 1 must not of course be taken literally in the regions of relatively large proton energies, for then the large spacing of the levels of the compound nucleus will give the protons a group structure.

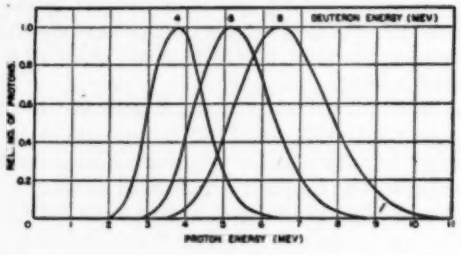

FIG. 1. Approximate energy distribution for outgoing protons.

The threshold energy for fission of the compound nucleus, such as U^{236}, is probably of the order of the photo-fission thresholds measured for U and Th by Haxby, Shoupp, Stephens, and Wells[5] and by Koch[6]; these are somewhat greater than 5 Mev. Thus one would expect fissions to occur for proton energies that are less than the incident deuteron energy by more than 1 Mev, if one assumes that the binding energy of a neutron in the compound nucleus is about 6 Mev. Thus if fission competes favorably with other modes of disintegration of the compound nucleus when it is energetically possible, Fig. 1 indicates that a substantial fraction of the outgoing protons will be accompanied by fissions, and that the threshold will appear near the maximum of the proton distribution.

[1] D. H. T. Gant, Nature **144**, 707 (1939).
[2] J. C. Jacobsen and N. O. Lassen, Phys. Rev. **58**, 867 (1940).
[3] G. M. Volkoff, Phys. Rev. **57**, 866 (1940).
[4] H. A. Bethe, Rev. Mod. Phys. **9**, 89 (1937).
[5] R. O. Haxby, W. E. Shoupp, W. E. Stephens, and W. H. Wells, Phys. Rev. **58**, 92 (1940).
[6] H. W. Koch, University of Illinois Thesis (1944).

A New Method for Displacing the Electron Beam in a Synchrotron*

J. S. Clark, I. A. Getting, and J. E. Thomas, Jr.
Massachusetts Institute of Technology, Cambridge, Massachusetts
September 18, 1946

A REQUIREMENT has been placed on the design of the 300-Mev synchrotron at M.I.T. that the electron beam strike the target during an interval of approximately one microsecond followed by a reduction of the beam to a minimal background level. The importance of this requirement stems from two important uses of the machine: (1) the identification of mesons through their characteristic half-life of two microseconds; and (2) the use of time-of-flight velocity analysis of mesons.

A method has been developed which makes it possible not only to displace the synchrotron orbit rapidly so as to strike an internal target, but also to force the beam out of the magnet always at the same point. The method consists of increasing the magnetic field on one half of the orbit and decreasing the field on the other half a corresponding amount. The two coils, whether in series or parallel, have zero coupling with the main magnet excitation coil. Two practical advantages acrue to this method of ejection: (1) the coils need not go into the gap; and (2) the total inductance (including mutual) is very low. This last point

makes it possible to force the beam entirely past the target in times of the order of two microseconds. The computed values for the 300-Mev M.I.T. machine are: ejection capacitor 2.7μf; capacitor voltage 12,000 v; time for total γ-ray pulse 2μ sec.; and peak current in the ejection coil 1400 amp.

The effect on the electrons in the beam is such that the equilibrium orbit is larger on one side of the magnet and smaller on the other side. The equilibrium orbit varies as $\Delta R/R=-\Delta B/[B(1-n)]$ where $\Delta B/B$ is the impressed fractional variation in the field at the orbit and n the usual exponent of radial dependence of the field. For $n\leqq\frac{3}{4}$, the natural period of the radial oscillation is twice the period of rotation in the orbit. Thus, the forced radial oscillations in the beam are similar to those developed in a linear harmonic oscillator driven by a square wave at twice the resonant frequency. Since the build-up time of the driving force is long compared with one period, only equilibrium oscillations need be considered. The resulting radial oscillation amplitude, A, is to the first order,

$$A/R=4\Delta B/\pi nB.$$

Direct integration of the electron's equations of motion gives the same result.

Thus, if $n\leqq\frac{3}{4}$, a one percent change in B produces oscillations of amplitude equal to 1.7 percent of the radius. These oscillations are 180° out of phase with the driving displacement and of the same frequency regardless of the value of n. The electrons reach maximum radius all at the same place, a fact which facilitates ejection of the entire beam.

* The research described in this letter was supported in part by Contract N5ori-78, U. S. Navy Department.

The Relative Probability of the (d, p) and the (d, n) Reactions in Bombarded Bismuth

J. M. Cork
Harrison M. Randall Laboratory of Physics, University of Michigan, Ann Arbor, Michigan
September 26, 1946

THE bombardment of bismuth (209) with high energy deuterons leads to the formation of both radium E and radium F (polonium). The latter is an alpha-emitter of half-life 140 days, while radium E emits beta-radiation with a half-life of 5 days, thereby converting into radium F. By noting the building-up of the alpha-emission from the target following bombardment, it is possible to determine the total number of each of the product atoms formed. Radium E (bismuth (210)) is formed by a (d, p) reaction while the formation of radium F follows from a (d, n) process. It is thus possible to observe the relative probability for the two competing processes.

Earlier investigations[1] have been made of this effect up to about 9.5 Mev. These results indicated that in this energy range the (d, p) reaction is much more probable. The ratio of the two yields was found to change from a value greater than 10 at 7 Mev down to about 5, at 9.5 Mev. This apparent anomaly that the proton can escape more easily than a neutron from an excited nucleus was reconciled by consideration of the Oppenheimer-Phillips process, according to which the deuteron need not enter the nucleus but dissociates outside into a scattered proton and a neutron that proceeds on into the nucleus. At higher energies it would appear reasonable to expect that the OP effect should greatly diminish and the above ratio fall to a value of one or even less.

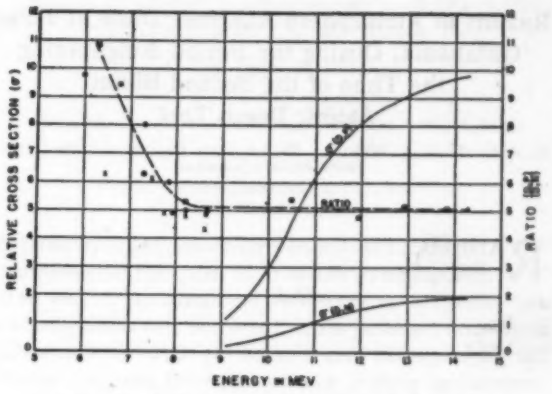

FIG. 1. Excitation curves and ratios obtained in this and other experiments.

Through the courtesy of Professor R. D. Evans and the kind assistance of Dr. Eric Clarke this phenomenon was studied up to 14.5 Mev by bombardment with the MIT cyclotron. Two types of bombardment were made. In one, a series of identical targets were exposed singly in turn to equal bombardments, each succeeding target being covered with an increasing thickness of aluminum foil so as to reduce the bombarding energy by the desired amount.

In another bombardment a stack of thin bismuth foils each of about 40 mg per cm^2 was exposed to a single bombardment. By using an alpha-counter with a thin window the growth of activity in each target was followed for many days, as in the previous investigations. From the growth curve the number of atoms of each kind produced could be readily determined. Since the exposure of each of the foils in the stack is identical it is possible to indicate an excitation curve for each process.

These excitation curves at the high energy together with the ratios obtained in this and previous experiments are shown in Fig. 1. The excitation curves seem to indicate an approach to saturation. The absolute cross sections can be determined only approximately since the effective geometry of the counter cannot be accurately determined. Within this limit the ordinate 10 may be regarded as 25×10^{-28} cm^2. The relative yields have no such uncertainty.

It is apparent that the ratio does not drop at higher energies to a value of one or less as had been expected but seems to remain within the experimental limit, at a value close to five.

Mr. R. W. Safford aided in this investigation, and the support of the Horace H. Rackham fund is gratefully acknowledged.

[1] J. M. Cork, J. Halpern, and H. Tatel, Phys. Rev. 57, 371 (1940); D. Hurst, R. Latham, and W. Lewis, Proc. Roy. Soc. A174, 126 (1940); H. Tatel and J. M. Cork, in press.

Results of Atmosphere Analyses Done at Tulsa, Oklahoma, During the Period Neighboring the Time of the Second Bikini Atomic Bomb Test

R. E. FEARSON, A. WENDELL ENGLE, JEAN THAYER, GILBERT SWIFT, AND IRVING JOHNSON
Tulsa, Oklahoma
September 23, 1946

RADIOACTIVE concentrates were prepared from the atmosphere by means to be described fully elsewhere, and subjected to inspection by means of various radioactive and chemical tests. The scope and thoroughness of the investigation was limited by lack of appropriate preparation, since it was not expected that any positive results at all would be obtained.

Concentrates were obtained from the atmosphere in sufficient strengths to enable definite indications to be had as to the nature of the substances recovered; chiefly by determination of the radioactive decay constants of the bodies studied. Five tests of the decay constants were performed, only three of which were thorough enough to elicit firm confidence. Of these three, one was based on beta-ray measurements alone, one was based on the concurrent use of beta-ray and alpha-ray measurement techniques, and the last was based on alpha-ray work only, the activity being too weak to permit beta-ray determinations. These three sets of data were obtained on July 26, July 28, and August 30, respectively. The data of July 26 and August 30 can be explained by saying that the substances obtained on these occasions were the active deposits of radon and of thoron; the data of July 28 cannot be so explained, and, apparently, correspond with a substance or substances unknown to us (see Fig. 1).

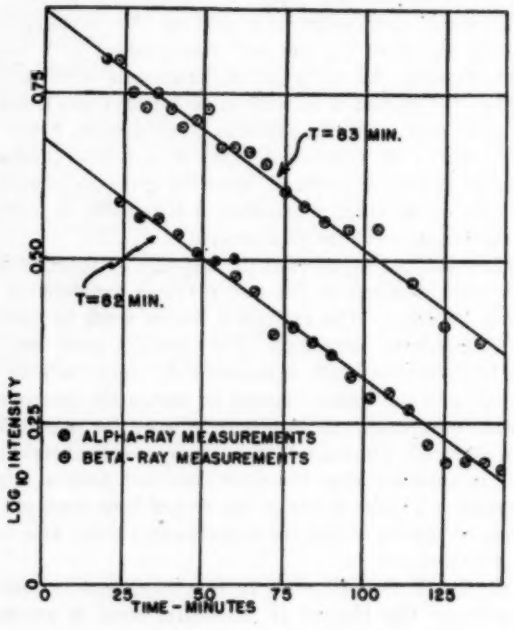

FIG. 1. Concurrent measurements of radioactivity made on two substantially identical atmosphere concentrate samples procured at Tulsa, Oklahoma on July 28, 1946, and having an initial intensity of approximately 5×10^{-10} curie.

A long-lived body was tentatively identified as lead, by co-precipitation methods. This was probably the active deposit of thoron, but further work must be done to make sure.

Our conclusions are:

(1) It seems plausible to explain the data of July 28 by assuming that the concentrate obtained by us is the active deposit of a new rare radioactive gas of atomic number 86, having an effective half-life of 82 minutes, and corresponding with at least two members of an unreported radioactive series.

(2) No general correlation of the total radioactive intensity with the explosion of the bomb was obtained, although our method of concentration was not well adapted to produce such a correlation, and it may be that a more suitable method would have.

The Ionization of the Atmosphere in the New York Area Before and After the Bikini Atom Bomb Test

VICTOR F. HESS
Fordham University, New York, New York
AND
PAUL LUGER, S.J.
Seattle College, Seattle, Washington
September 23, 1946

SINCE Herzog[1] reported a very marked increase of gamma-radiation from the air following the atomic bomb test at Bikini on July 1, 1946, it may be of interest to report some observations made in New York between June 29 and July 10. Herzog's measurements were made at Houston, Texas with a self-recording gamma-ray counter. It was not stated whether this apparatus was screened from below or on the sides.

We used an ionization meter devised by O. H. Gish and one of the authors[2] for field measurements. It consists of a cylindrical ionization chamber (volume 13 liters, filled with pure nitrogen at atmospheric pressure, brass walls, 2.5 mm thick) connected with a shielded Lindemann electrometer which is used here only as a null instrument. The readings are taken subjectively, in intervals of a few minutes, by means of a precision voltmeter which measures the compensating voltage necessary to bring the floating needle back to zero after known intervals of time.

The observations were taken on the flat roof of the Physics Building of Fordham University (140 ft. above sea level) near the Botanical Garden, New York.

Herzog observed an increase in the counting rate beginning on July 4, 8 P.M. (Houston time), and reaching a maximum of 77 percent above the normal counting rate on July 5, 3 A.M. The counting rate returned to normal 16 hours later.

Our observations were, naturally, not continuous, but

tests were made several times a day, for about one hour each time. A persistent increase of ionization extending over half a day or so could not have been missed.

The data observed at Fordham are given in Table I.

TABLE I. Total ionization on the roof of the Physics Building, Fordham University, New York, New York.

Time	Ionization	Time	Ionization
June 29 (mean)	6.28 *I*	July 7 11 A.M.	6.19 *I*
June 30 (mean)	6.07 *I*	July 7 8 P.M.	6.07 *I*
July 1 (mean)	6.07 *I*	July 8 8 A.M.	6.41 *I*
July 2 (mean)	6.32 *I*	July 8 10 A.M.	6.78 *I*
July 3 A.M.	5.96 *I*	July 8 11 A.M.	6.67 *I*
July 3 P.M.	6.08 *I*	July 8 noon	6.06 *I*
July 4 A.M.	6.26 *I*	July 8 1 P.M.	6.05 *I*
July 4 P.M.	5.93 *I*	July 8 7.30 P.M.	6.10 *I*
July 5 8 A.M.	5.95 *I*	July 9 8 A.M.	6.33 *I*
July 5 2 P.M.	6.20 *I*	July 9 3 P.M.	5.91 *I*
July 5 8 P.M.	6.47 *I*	July 10 10 A.M.	6.18 *I*
July 6 8 A.M.	6.24 *I*	July 10 8 P.M.	5.89 *I*
July 6 4 P.M.	6.00 *I*		

The total ionization I (in ion pairs produced per cc and sec. in pure nitrogen at N.P.T.) observed on the roof is, on the average, about 6 I, consisting of 2 I due to cosmic rays, 3 I local gamma-rays from the building, 0 to 0.5 I gamma-rays from the radioactive substances in the atmosphere and about 0.7 I residual ionization of the vessel itself.

The figures reported below are average values of from 30 to 60 min. continuous observation in each case. For the first few days mean values of the whole day are given.

Isolated higher values (as for instance on July 2 where a single value of 6.8 I was observed just for one hour) may be caused by cosmic-ray showers or bursts and are unimportant for judgment on any possible influence of the atom bomb cloud.

From the values shown in this table it is evident that no effect ascribable to the radioactive atom bomb cloud was noticed before July 8. On this date a slight increase of ionization (0.3 to 0.7 I) occurred and persisted for several hours. It is highly questionable, however, whether this effect was really produced by gamma-rays from the air, for two reasons: first, the general circulation in the United States, at levels of 7–12 km in the summer, is anticyclonic and in the eastern half of the country a northwesterly wind component would prohibit a radioactive air mass from reaching the New York area; second, from the weather maps (July 4 to July 8) the component wind velocity at 7 km, in the general direction from Houston to New York, was only 5 knots. Therefore the air mass present over Houston on July 5 would not have reached New York in much less than 200 hours. It is, of course, unfortunate that our observations were discontinued on July 10, but from the evidence presented here it is practically certain that no effects from the Bikini test were in evidence in the North Atlantic states, more than 7000 miles from the Bikini Islands.

We are indebted to Mr. Hormantas, Meteorological Office, LaGuardia Field for furnishing the meteorological data.

[1] G. Herzog, Phys. Rev. **70**, 227 (1946).
[2] See a forthcoming article of V. F. Hess, Trans. Am. Geophys. Union **27**, No. 5 (October, 1946).

Effort to Observe Anomalous Gamma-Rays Connected with Atomic Bomb Test of July 1, 1946

E. DOROTHY WEEKES
Petty Geophysical Engineering Company, San Antonio, Texas
AND
DONALD F. WEEKES
A & M College of Texas, College Station, Texas
September 17, 1946

A GAMMA-RAY anomaly associated with the atomic bomb test at Bikini Island on July 1, 1946, having been observed by Herzog[1] at Houston, Texas, on July 4 and 5, the absence of such an anomaly at College Station, 100 miles northwest of Houston, becomes a matter of interest.

Daily measurements of the background of stray radiation were made in a laboratory on the upper floor of a two-story brick building in College Station, during the following periods: June 25 to July 5; July 8 to 11; 16 to 19; and 23 to 26. The counting unit of an x-ray spectrometer which employs Geiger counter registration was used for the purpose. A rough indication of gamma-ray sensitivity was obtained by placing a four-ounce specimen of carnotite 15 inches from the longitudinal axis of the counter. This resulted in an increase of about 45 percent in the counting rate.

The observed background counting rates varied from 0.317 to 0.339 per sec., exceeding the average value of 0.329 by slightly more than the expected statistical fluctuation (0.0064 per sec.) on three dates, July 1, 2, and 18; but, even in these cases, the variations were too small to be regarded as significant.

Since the observations were all made at about the same time of day, it is unlikely that any local anomaly of as much as 24 hours duration occurred during the periods covered by the experiment. The observation of July 5 was concluded at 10:36 A.M., several hours after the maximum of the Houston anomaly but well before its expiration, and might have been expected to reveal the existence of this anomaly, had it been of regional extent.

[1] G. Herzog, Phys. Rev. **70**, 227 (1946).

Schwarzschild Interior Solution

NATHAN ROSEN AND BROWNIE NEWMAN
University of North Carolina, Chapel Hill, North Carolina
September 26, 1946

IN a recent paper,[1] Wyman gave an interesting discussion of the solution of the gravitational equations of general relativity for the case of a sphere of perfect fluid of constant density, using isotropic coordinates. He found that, for a given value of the density ρ, the mass m and the radius a were restricted by the conditions,

$$m \leqslant 0.4a, \quad a^2 \leqslant 0.27R^2, \tag{1}$$

with $R^2 = \frac{3}{8\pi\rho}$, instead of the conditions found for the Schwarzschild solution,[2]

$$m \leqslant 4a/9, \quad a^2 \leqslant 8R^2/9. \tag{2}$$

In the first place, it might be pointed out that the coordinate r as used in the Wyman solution is not the distance from the origin, and hence its value a at the boundary of the sphere is not the true radius. The latter, a_0, can be obtained by integrating the line element,

$$a_0=\int_0^a (g_{11})^{\frac{1}{2}}dr, \tag{3}$$

from which it follows that

$$2a_0/m=(1+x)^{\frac{1}{2}}x^{-\frac{1}{2}}\arctan x^{\frac{1}{2}}, \tag{4}$$

where $x=m/2a$. Similarly, in the Schwarzschild solution the corresponding radial variable, denoted by Wyman by $\bar{r}$ and obtained from r by means of the transformation equations given by Wyman, is not the distance from the origin. Let us denote the value of $\bar{r}$ at the boundary by $\bar{a}$. Then in the inequalities (2) a should really be replaced by $\bar{a}$. Corresponding to $\bar{a}$ we can again calculate the true radius of the sphere, a_0. Since the Wyman solution goes over into the Schwarzschild solution when one transforms r to $\bar{r}$, one would expect that a_0 (which is a scalar quantity) should be the same for both solutions.

It turns out, however, that this is not the case if one uses the limiting values as given by Wyman. The difficulty appears to lie in the criterion used by Wyman, namely, that x be a single-valued function of $y=a^2/R^2$, the two being related by Eq. (2.14) in Wyman's paper. In view of the fact that the quantity a (as distinguished from a_0) has no direct physical significance, the same is true of the variables x and y, and a criterion based on them is therefore questionable. If, instead of Eq. (2.14), one uses Wyman's Eq. (2.15) and asks that, for a given m, a be a single-valued function of ρ, one gets different limiting values.

A more satisfactory criterion appears to be the one based on the non-vanishing of $g_{44}=e^{\nu}$ (in Wyman's notation). If one uses this, one obtains, in place of (1), the conditions,

$$m\leqslant a, \quad a^2\leqslant 128R^2/729. \tag{5}$$

These are equivalent to the conditions (2) with $\bar{a}$ in place of a, on the basis of the relation between a and $\bar{a}$,

$$\bar{a}=(1+m/2a)^2a, \tag{6}$$

which follows from the transformation equations for $\bar{r}$ and r.

The true radius of the sphere a_0, from either form of the solution, is then found to satisfy the conditions,

$$\begin{aligned} m&\leqslant 2^{5/2}a_0/3^3\arctan 2^{-\frac{1}{2}}=0.3404a_0,\\ a_0^2&\leqslant 4(\arctan 2^{-\frac{1}{2}})^2R^2=1.5153R^2. \end{aligned} \tag{7}$$

In conclusion, it might be pointed out that, while the Wyman and Schwarzschild solutions are equivalent (since one can be obtained from the other by a coordinate transformation), the Wyman solution has the advantage in that all the components of the fundamental tensor and their normal derivatives are continuous at the boundary of the sphere, which is not the case for the Schwarzschild solution. This is associated with the fact that $\bar{r}$ as a function of r has a discontinuous second derivative at the boundary.

[1] Max Wyman, Phys. Rev. **70**, 74 (1946).
[2] A. S. Eddington, *Mathematical Theory of Relativity* (Cambridge, 1923), p. 170.

Decay Scheme for Te^{121}

S. B. Burson, P. T. Bittencourt,* R. B. Duffield, and M. Goldhaber
Department of Physics, University of Illinois, Urbana, Illinois
October 1, 1946

We have continued the investigation of the radiations emitted in the decay of Te^{121} ($125d^{\frac{1}{2}}$–$143d^{\frac{1}{2}}$) and have obtained a satisfactory explanation for the apparently anomalous x-ray coincidence previously observed.[1] Our results indicate that the metastable state of Te^{121} has an excitation energy of about 275 kev and that the transition to the ground state takes place in two steps.[4] The previously observed gamma-ray of 225 kev is preceded or followed by a strongly converted gamma-ray of about 50 kev within a mean time shorter than the resolving time of our coincidence circuit (0.8×10^{-8} sec.). The ground state of Te^{121} for which a half-life time of 17 days has been reported,[2] decays by K-electron capture to Sb^{121} which is usually left in an excited state of 610 kev.[3]

The following experiments led us to the suggested decay scheme:

(1) From x-ray crystal spectrometer studies[5] it is known that Sb and Te K x-rays are emitted by Te^{121} (125–$143d$) in equilibrium with its daughter product. With the help of matched Cd and In filters[5] we have established the existance of coincidences between Te K_α x-rays and the 225 kev gamma-rays. These coincidences could be understood if the 225 kev gamma-ray were preceded or followed by a hitherto overlooked internally converted gamma-ray transition.

(2) Since a previous search for soft electrons with the help of a Cellophane window counter had been unsuccessful[3] special counters were constructed containing samples of Te^{121} within the glass envelope. In one arrangement the electrons were bent into the sensitive volume of the counter by means of a variable magnetic field. Soft electrons were detected with an energy of about 17 kev and coincidences between these electrons and the 225 kev gamma-ray established.

(3) These soft electrons can be taken as evidence of a transition of about 50 kev. A search for an unconverted gamma-ray of this energy was made using a Xe-filled Geiger counter to emphasize this energy region. An absorption curve in Ag was taken and a gamma-ray component with an energy of about 48 kev was found.

(4) An isomeric chemical separation was performed, using the transition from telluric to tellurous acid.[1] The tellurous acid fraction, precipitated 7 days after synthesis of the telluric acid from Te^{121}, was found to show only the 610 kev gamma-ray component with a period of approximately 16 days.

The Te source used was produced by bombarding Sb with 10-Mev deuterons from the University of Illinois cyclotron. Our thanks are due to the cyclotron group for carrying out the bombardments.

* Rockefeller fellow of the University of São Paulo, São Paulo, Brazil.
[1] G. T. Seaborg, J. J. Livingood, and J. W. Kennedy, Phys. Rev. **57**, 363 (1940).
[2] J. E. Edwards and M. L. Pool, Phys. Rev. **69**, 140 (1946).
[3] R. S. Yalow and M. Goldhaber, Phys. Rev. **66**, 36(A) (1944) and **67**, 59(A) (1945).
[4] A similar case in Br^{80} has been studied in detail by A. Berthelot, Ann. de physique [11], **19**, 219 (1944).
[5] R. D. O'Neal and G. Scharff-Goldhaber, Phys. Rev. **62**, 83 (1942).

A Comparison of the Stopping Power of Lead and Aluminum For Cosmic-Ray Mesotrons

ELIHU FEIN
Department of Physics, University of Chicago, Chicago, Illinois
September 24, 1946

AN experiment was performed to compare the stopping power of lead and aluminum for mesotrons with energies between 2×10^8 ev and 4×10^8 ev. Two identical coincidence counter arrangements were constructed in order that the rate of mesotrons passing through absorbers interposed between the counters of the two coincidence arrangements could be determined simultaneously. (See Fig. 1.) In this way the effect of variations in the mesotron intensity with time was eliminated. In order to select only mesotrons in the vertical coincidences, a 11.7-cm lead filter was placed above each coincidence set covering the solid angle of the coincidence counters 1, 2, 3, 4 and 1, 2, 3, 5. The influence of air showers was very greatly reduced by anti-coincidence counters 6. Thicknesses of the absorbers of lead and aluminum which should have the same stopping power according to the range curves given by the ionization loss theory of Bethe-Bloch were chosen, and the rate of mesotrons passing through them was determined.

The data in column *D* and *E* of Table I are the averages taken from the sets of data obtained by interchanging the absorbers in the two counter arrangements and redetermining the mesotron counting rates. As can be seen from column *E* of the table, the ratio of the counting rates of mesotrons traversing the aluminum absorber and the lead absorber is not one-to-one as would be expected if the absorbers would have the same stopping power. The ratio of the number of mesotrons traversing the aluminum to those traversing the lead increased up to 1.11, indicating that the lead absorber stopped more mesotrons than the aluminum absorber, this excess increasing with the thicker absorbers.

TABLE I. Summary of data. Column *A*: Thickness (in centimeters) of absorbers having the same stopping power according to the Bethe-Bloch range curves; Column *B*: Minimum energy (in ev) required for mesotrons to traverse the absorbers (from Bethe-Bloch range curves); Column *C*: Counting-rates of coincidence telescopes without absorbers (no./min.); Column *D*: Counting-rates of coincidence telescopes with absorbers interposed (no./min.); Column *E*: Ratio of counting-rates in column *D*.

A		*B*	*C*	*D*		*E*
Al	Pb			Al	Pb	Al : Pb
36.0	13.0	1.94×10^8	2.52 ± 0.03	2.21 ± 0.02	2.15 ± 0.02	1.03 ± 0.02
60.6	20.8	2.90×10^8	2.48 ± 0.02	2.11 ± 0.02	2.02 ± 0.02	1.06 ± 0.02
75.7	26.0	3.60×10^8	2.53 ± 0.03	2.14 ± 0.02	1.97 ± 0.02	1.11 ± 0.02

The possibility of whether multiple scattering could account for this effect was investigated. In order to determine the magnitude of a possible scattering effect, the lead absorber was moved from position *a* to positions *b* and *c* (see Fig. 1); increases in the counting-rate of 1.3 and of 4.0 percent, respectively, were observed. These increases are explained by the presence of the filter. The maximum angle[1] for scattering (in the absorber) mesotrons passing through counters 1, 2 into counters 3, 4 increases in exactly the same way as the angle for scattering mesotrons out of the beam decreases. Since the angle for scattering mesotrons into counters 3, 4 by the absorber is considerably greater at position *c* than at position *a*, the scattering of mesotrons in the filter will be more pronounced for position *c* than for position *a*.[2] However, when both the lead and aluminum absorbers were at position *a*, the difference between the maximum angles for scattering (in the absorbers) mesotrons passing through counters 1, 2 into counters 3, 4 (or 3, 5) for the two different absorbers was considerably less than the difference between the maximum angles for such scattering for the lead absorber at positions *c* and *a*. Since in the latter case an increase in the counting-rate of only 4.0 percent was observed, the filter will have no significant effect upon the counting-rates when the absorbers are at position *a*.

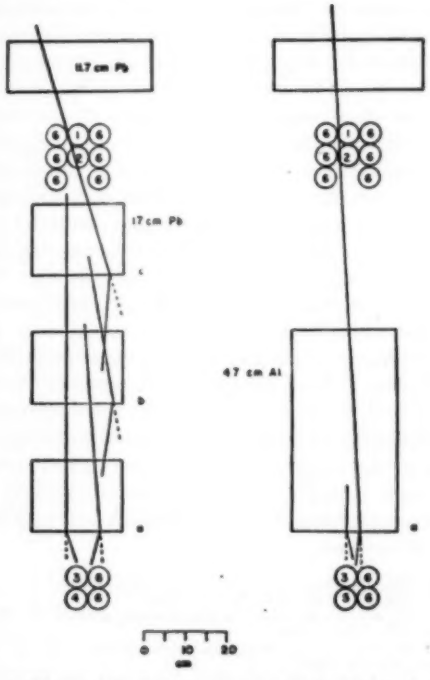

FIG. 1. Diagram of coincidence apparatus showing maximum scattering angles.

The possibility that a polarization effect might explain the anomaly observed in the stopping power of thicknesses of aluminum and lead which according to the Bethe-Bloch range curves should be equivalent is suggested.[3] Quantitative discussions on a possible polarization effect have been made by E. Fermi[4] and O. Halpern and H. Hall.[5] A comparison of the results of this experiment with theory will be given in a further publication.[6]

I wish to express my appreciation to Dr. Marcel Schein of the University of Chicago for suggesting the experiment and for his advice and encouragement in its pursuit.

[1] The mean angle of scattering for a particular absorber was calculated with the aid of the formula given for Coulomb scattering by B. Rossi and K. Greisen, Rev. Mod. Phys. 13, 241 (1941).
[2] The angles for scattering particles out of the beam are small, and the influence of the filter on scattered out particles is negligible.
[3] The possibility of a screening effect due to the polarization of the medium by the field of the particle traversing it was first suggested by W. F. G. Swan, J. Frank. Inst. 226, 598 (1938).
[4] E. Fermi, Phys. Rev. 56, 1242 (1939); Phys. Rev. 57, 485 (1940).
[5] O. Halpern and H. Hall, Phys. Rev. 57, 459 (1940).
[6] Reference may be made here to H. P. Koenig, Phys. Rev. 69, 590 (1946) in which the actual stopping power of both lead and aluminum also appears to be somewhat less than the theoretical stopping power of these two elements.

Persistent Currents in Frozen Metal-Ammonia Solutions

J. W. HODGINS
National Research Council of Canada, Ottawa, Ontario
September 21, 1946

R. A. OGG[1,2] has cited the persistence of currents in frozen rings of sodium solutions in liquid ammonia as support for the hypothesis of the Bose-Einstein condensation of trapped electron pairs.

However, Boorse *et al.*,[3] and Daunt and co-workers[4] have reported that under the conditions of their experiments there was no evidence of superconductivity. In this note, I wish to report a series of experiments in which corroboration was found for Dr. Ogg's observations.

The ring of metal-ammonia solution was formed in the trap C illustrated in Fig. 1. The bottom portion of the trap was constructed of especially thin glass to allow for rapid cooling. Freshly distilled sodium was cut under pure pentane, and transferred to a weighing tube which was immediately evacuated. The sodium was weighed by difference and transferred under pentane into trap *C*. The pentane was distilled from the sodium under reduced pressure and the trap pumped down to about 10^{-4} mm pressure, and then closed off from the system. Anhydrous ammonia was condensed into trap *B* which was surrounded by dry ice-acetone (−78°C). The volume of liquid ammonia necessary to give the required solution was measured in the graduated tube on the trap, and then distilled into trap *C*, now refrigerated in liquid air. With *C* immersed in liquid air, pumping was carried out for about an hour, to remove traces of permanent gases. The tap on *C* was then closed, and the trap was removed from the system, and allowed to warm up to either −34°C (boiling ammonia) or −78°C (dry ice). The familiar blue solution formed a ring in the trap which always contained 7.5–8.5 ml of solution.

As a source of magnetic flux, a solenoid coil was employed, containing a central hole large enough to accommodate a flask of liquid air. The flux density through the operating coil was found by calibration to be 1600 gauss.

The 3200-turn search coil had almost the same geometry as the ring of solution. A ballistic galvanometer was used in conjunction with the search coil, and the assembly was calibrated in terms of the current detectable in a 2-inch loop moved adjacent to the search coil. The sensitivity was found to be 0.1 ampere per scale division, corresponding to a field of strength 0.01 gauss for the ring concerned.

To make a test for persistent current, the ring of liquid solution was suspended in the center of the coil at the desired starting temperature, with the flux (1600 gauss) threading the coil. Liquid air was then allowed to just make contact with the ring of solution, care being taken not to allow the trap to dip into the liquid air more than ½ inch. This precaution was important in order to avoid "flashing" of the sodium solution from the ring to the sides of the trap. After two minutes' immersion in the liquid air, the frozen ring was withdrawn through the field, immediately placed above the search coil, and the galvanometer reading observed.

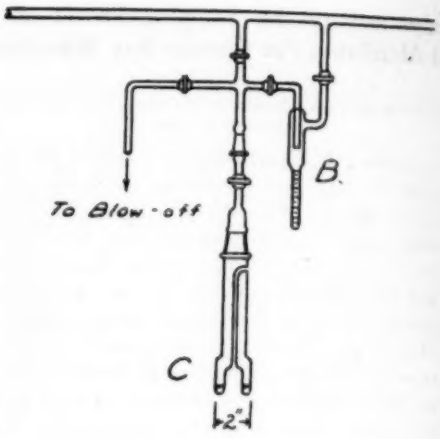

FIG. 1. Diagram of apparatus.

Some 115 experiments were carried out with solutions ranging in concentration from saturation to 0.90 molar. Four instances of persistent currents were observed in one series of 36 experiments on a solution where the mole ratio NH_3:Na was 43:1. It will be noted that this solution is in the concentration range where it exhibits liquid-liquid phase separation, and has an upper consolute temperature of −50°C.[5] This series was the only one yielding positive results. The first persistent current was observed on freezing from −70°C, at which temperature the two phases had already formed, while the other three results were obtained at a starting temperature of −34°C, where the solution was homogeneous. The galvanometer deflection indicated the expected polarity each time, and reversal of the direction of the solenoid field reversed the direction of the deflections caused by persistent currents in the frozen ring. This latter observation would seem to vitiate the possibility of the deflection being caused by paramagnetic regions in the solution. The largest of the persistent currents was 0.1 ampere, and its duration about one-half minute.

Twenty-four observations were also made by rapidly freezing lithium solutions in liquid air (mole-ratio NH_3:Li = 30:1) from above the consolute temperature. No persistent currents were observed, although liquid-liquid phase separation normally occurs at that concentration.

The resistance of the ring is indicated to be in the order of 10^{-12} ohm. It is suggested that the rapidity of freezing is not critical, for it is estimated that these solutions were not completely solid before a period of immersion of 15 seconds in the liquid air. The low incidence of successful experiments is attributed to the severe cracking of the samples on freezing. Lithium solutions were particularly bad in this respect.

[1] R. A. Ogg, Jr., Phys. Rev. **69**, 243 and 544 (1946).
[2] R. A. Ogg, Jr., Phys. Rev. **70**, 93 (1946).
[3] H. A. Boorse, D. B. Cook, R. B. Pontius, and M. W. Zemansky, Phys. Rev. **70**, 92–93 (1946).
[4] J. G. Daunt, M. Désirant, K. Mendelssohn, and A. J. Birch, Phys. Rev. **70**, 219 (1946).
[5] C. A. Kraus and W. W. Lucasse, J. Am. Chem. Soc. **44**, 1951 (1922).

A Metastable State of 22 Microseconds in Ta^{181}

S. DEBENEDETTI AND F. K. MCGOWAN
Clinton Laboratories, Oak Ridge, Tennessee
September 13, 1946

SHORT-LIVED metastable states can be detected by examining whether the β-rays from a radioactive source are followed, within a short but measurable time, by γ-rays or conversion elections. For this purpose a source deposited on a thin aluminum foil is introduced between the mica windows of two Geiger-Mueller counters A and B. The pulses of counter A are electronically delayed and fed into one channel of a coincidence circuit, while counter B is connected directly to the other channel. If we call T the delay time and τ the resolving time of the instrument, coincidences will be recorded only when a ray in counter B follows a ray in counter A after a time interval between $T-\tau$ and $T+\tau$. After each pulse in counter A the instrument is therefore sensitive during a time 2τ, which can be measured by counting random coincidences. The delay time T is measured by means of a calibrated oscilloscope.

The method fails for $T \lesssim 10^{-6}$ sec., because of the fluctuations in time lag between ionization and discharge in a G-M tube, and for $T \gtrsim 10^{-2}$ sec., because of competition from random coincidences.

Delayed coincidences well above the random coincidence background were detected with sources of Hf^{181}. In Fig. 1

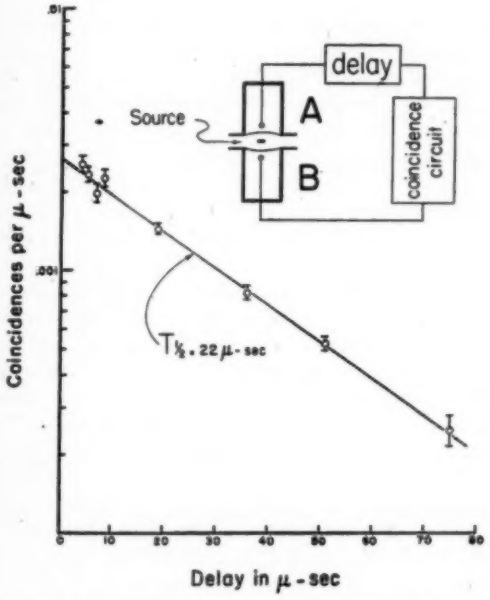

FIG. 1. Delayed coincidences as a function of delay time.

the number of delayed coincidences is plotted as a function of delay time. It appears from this curve that the disintegration of Hf^{181} leads to a metastable state Ta^{181*} which in turn decays to the ground state with a half-life of 22 microseconds.

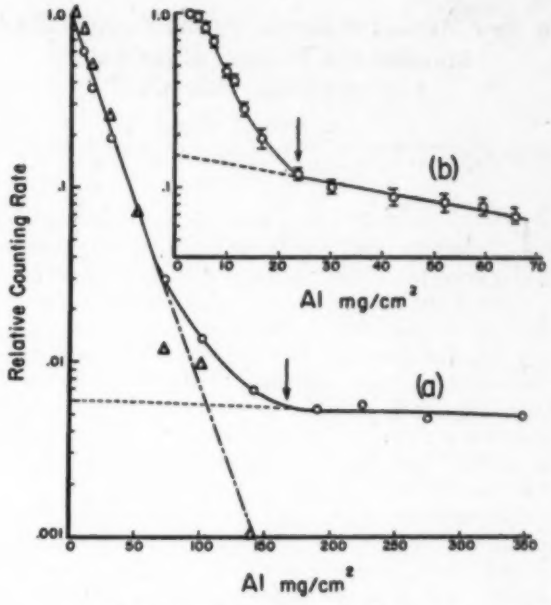

FIG. 2. Absorption of radiation from Hf^{181}.

Figure 2 shows the result of some absorption experiments, all performed under the geometrical conditions of Fig. 1. Such geometrical arrangement, obviously poor for energy determinations, was required for a sufficiently high counting rate. The circles of Fig. 2(a) were obtained by counting the single counts of counter A and represent the absorption of the radiation from Hf^{181}; this radiation seems to consist of a simple β-spectrum of maximum energy around 0.8 Mev, and of γ-rays of 0.5 Mev. The triangles in the same curve are obtained from delayed coincidence measurements when the absorber is located between the source and counter A, and represent the absorption of that part of the radiation which is followed by a delayed ray; it appears that the delayed rays follow the β-rays and not the γ-radiation. Finally Fig. 2(b) shows the result obtained from a measurement of delayed coincidences with the absorber between the source and counter B; this curve, which corresponds to the absorption of the delayed rays, can be interpreted by supposing that these consist mostly of electrons of 0.11 Mev. If such electrons are due to conversion in the K shell the excitation energy of the metastable level is about 0.18 Mev. As the result of a rough evaluation the number of conversion electrons per disintegration appears to be around 0.6.

From the half-life and the energy of the metastable state it seems probable that the transition involves a change of spin of 3 units. Since the spin of Ta^{181} is 7/2 the spin of the metastable level can be assumed to be $\frac{1}{2}$.

A search for short-lived isomers in the other isotopes of reported spin 7/2 and in more than 20 other nuclei has given negative results.

This work was done under the auspices of the Manhattan District.

A New Method of Measuring the Electric Dipole Moment and Moment of Inertia of Diatomic Polar Molecules*

HAROLD KENNETH HUGHES
Socony Vacuum Laboratories, Brooklyn 22, New York and Pupin Physics Laboratories, Columbia University, New York 27, New York
September 18, 1946

THIS paper will report on experiments in which the molecules of a molecular beam are caused to undergo a transition in a steady homogeneous electric field by an oscillating electric field at right angles to the d.c. component. This experiment is, therefore, closely analogous to the magnetic resonance method[1] which has been applied previously to atoms and molecules. The method to be described can be considered as an advance over previous methods in that a single rotational state of the molecule is studied even though it is present to only one part in ten thousand as a component of the beam.

The transition with which we are concerned is that in which the molecule, in this case CsF, goes from $R=1$, $p=0$ to $R=1$, $p=\pm 1$, where R is the rotational quantum number and p is the electric quantum number. This $\Delta R=0$ transition is ordinarily forbidden but the selection rule breaks down in the presence of the constant electric field, E.

Several persons[2] have calculated by perturbation methods the splitting of rotational energy levels in an electric field. As applied to the 1, 0→1, ±1 transition the frequency f, in cycles per second, is given by the expression

$$f=\frac{6\mu^2 IE^2}{20(9)10^4 hh^2}=4.529\times 10^{7}\mu IE^2, \qquad (1)$$

where μ is the permanent dipole moment in e.s.u., I is the moment of inertia in g cm², and E is the electric field strength in volts per cm. This method has been applied to cesium fluoride and a value of $9.89\times 10^{-78}\pm 1.2$ percent obtained for $\mu^2 I$.

For values of the parameter $\lambda=\mu E/cBh=2\mu EI/h^2$ which are $\ll 1$, it is seen that the energy difference between the states is proportional to $\mu^2 I$. At larger values, there is an important deviation from this functional relation which allows for an independent determination of both μ and I. Brouwer's second-order perturbation formula[3]

$$f=\frac{3\mu^2 E^2}{20h(h^2/2I)}-\frac{(0.00959)\mu^4 E^4}{h(h^2/2I)^3} \qquad (2)$$

is good to 0.1 percent up to $\lambda=1$, and was used in these experiments.

If we define two experimentally determined constants, α and β, by the equation

$$f/E^2=\alpha-\beta E^2, \qquad (3)$$

then it may be shown that

$$I=\beta\alpha^2(1.97\times 10^{-28}),\ \text{g cm}^2. \qquad (4)$$

Final values for the $R=1$ state of CsF are: $\alpha=448\pm 5.4$, $\beta=(1.91\pm 0.23)\times 10^{-5}$, $\mu=7.3\pm 0.5$ debye,[4] $I=(187\pm 22)\times 10^{-40}$ g cm² and $r=2.60\pm 0.16$ angstroms. It is to be noted that while $\mu^2 I$ is quite accurate, the values of μ and I separately are only approximate. This stems from the fact that μ and I can be determined separately only by a knowledge of β which is of the form of a correction term to α at high values of E. The present limitations on the accuracy of β are entirely instrumental and can be largely eliminated. The method is, therefore, inherently very accurate.

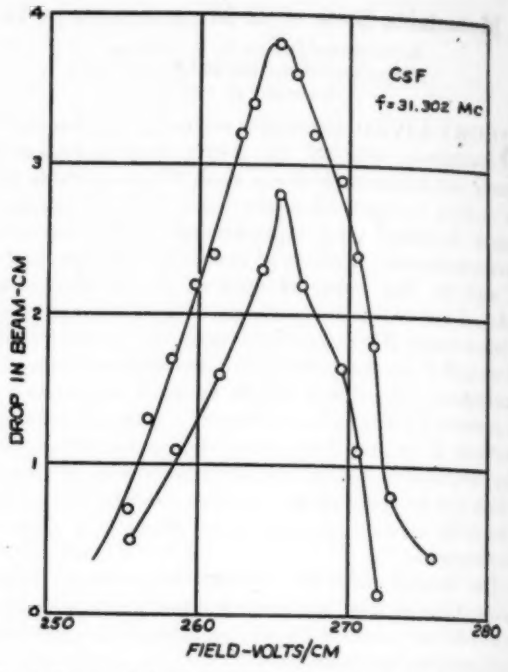

FIG. 1. Decrease in beam intensity as a function of the homogeneous electric field. The upper and lower curves are for relatively large and small amplitudes of the oscillating electric field.

A feature of the method, in common with the magnetic resonance method, is its extraordinary resolution of close energy levels which so far exceeds that of infra-red spectroscopy that moments of inertia may be obtained for heavy molecules which have previously been beyond reach. These experiments differ very markedly from earlier molecular beam deflection experiments which measured μ only, and with very limited accuracy.[5] In contrast to solution methods wherein the variation of permittivity is measured as a function of temperature, this procedure yields the electric moment entirely independent of mass interference effects.

The selection of the state for observation is accomplished as follows. The beam of molecules is produced and collimated in an evacuated apparatus in the usual way but instead of allowing it to fall upon the detector, a wire stop is interposed in the direct path. Only those molecules strike the detector which have been refocused around the stop in a sigmoid path by two inhomogeneous electric fields (named the A- and B-fields) which are transverse to the beam and pointed in the same direction.

The ability of the present method to isolate rotational states depends essentially on the fact that the effective electric moment of the molecule is a function of the electric field. The functional dependence of the moment on field

is itself dependent on the state so that, by a suitable choice of the A- and B-electric fields, it is possible to refocus a single electric state (quantized orientation of the angular momentum vector for a single rotational state). The effective induced moment of the 1, 0 state is positive at high fields (in the A-field) and negative at low fields (in the B-field). The states 0, 0 and 1, ± 1 do not have this property. Furthermore, the effective induced moment in a given electric field is inversely proportional to R^2 and the higher rotational states, therefore, have small effective moments relative to that for $R=1$. The function of the wire is to stop all molecules of small effective moment, the overwhelming fraction, which are not susceptible to refocusing operations. The relative population of the low rotational states is small and only 0.01 percent of the total beam is refocused at any one time. Relative electric moments for all orientations of the three lowest rotational states were obtained from a relationship derived by Lamb[6] which is good for all values of λ.

Between the refocusing A- and B-fields the beam passes through a homogeneous C-field wherein a superimposed radiofrequency electric field, normal to the d.c. component, induces transitions between electric levels. After this transition the molecules are in a new electric level with a different, indeed reversed effective electric moment in the B-field, and they are no longer refocused. This is observed by a decrease in the beam when the oscillator frequency equals the energy separation of the levels divided by Planck's constant. (Fig. 1.)

Further details will be discussed in a forthcoming article in *The Physical Review*.

This research was proposed to me by Professor I. I. Rabi and executed under his direction. I am also under obligation to several other members of the physics department. In particular, Professor P. Kusch gave me guidance during the last stage of the work and, with Dr. J. Trischka, assisted in the collection and evaluation of the data.

[*] Publication assisted by the Ernest Kempton Adams Fund for Physical Research of Columbia University.
[1] I. I. Rabi, S. Millman, P. Kusch, and J. R. Zacharias, Phys. Rev. 55, 526 (1939).
[2] See, for example, R. de L. Kronig, Proc. Nat. Acad. Wash. 12, 608 (1926).
[3] Brouwer, Dissertation, Amsterdam, 1930.
[4] 1 debye $=10^{-18}$ e.s.u.
[5] For literature references, consult Fraser, *Molecular Beams* (Chemical Publishing Corporation, New York, 1938), Chap. IV.
[6] Professor W. E. Lamb, private communication.

Secondary Emission from Germanium, Boron, and Silicon

L. R. Koller and J. S. Burgess
Research Laboratory, General Electric Company, Schenectady, New York
September 9, 1946

MEASUREMENTS of secondary emission were made on the semi-conductors germanium, boron, and silicon. No previous measurements on germanium or boron are given in the literature.

The silicon and germanium were cut from very pure vacuum melts which had been prepared in the laboratory for crystal rectifier studies. The boron was deposited on an iron disk by thermal decomposition of boron hydride.

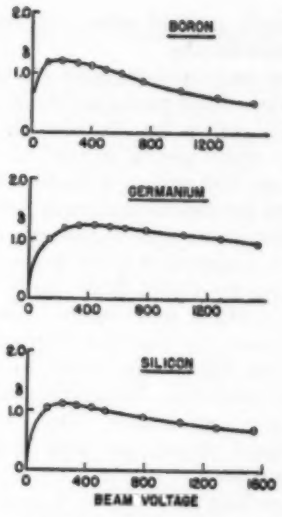

FIG. 1. Secondary emission from boron, germanium, and silicon.

The measurements were made in an electron gun type of tube. The electron beam was focused on the target through a hole in a cylindrical collector surrounding the target. The primary velocity was varied from 100 volts to 1500 volts. The beam current was 10^{-6} amp. and the spot diameter approximately 1 mm. The collector was held at +40 volts with respect to the target.

The measurements were made in tubes while on the pump at a pressure of 10^{-6} to 10^{-7} mm. The germanium and silicon were heated by high frequency to dull red before making measurements. The boron only received a 425°C bake out as at higher temperatures there was a possibility of interdiffusion of the iron and boron.

The maximum values of δ (the secondary to primary ratio) and the primary voltage at which they occur are as follows:

	S	V
Boron	1.2	150
Germanium	1.2	400
Silicon	1.1	250

The relation between δ and primary voltage for the three surfaces is given in Fig. 1.

Conductivity of Metal-Amine Solutions

S. I. Weissman
Department of Chemistry, Washington University, St. Louis, Missouri
September 20, 1946

IT has been reported recently by Ogg[1] that when a solution of sodium in liquid ammonia, in the concentration range which yields two liquid phases, is rapidly frozen, a large decrease in resistance occurs. The writer has observed this decrease in resistance by a current-potential method, and has found in agreement with the work of Daunt, Désirant, Mendelssohn, and Birch[2] that the small resistance of the frozen solution resided in the solid itself and not in the solid-electrode contact. It is still possible that this resistance is a property of the contacts between

the pieces of badly cracked solid, and that uncracked pieces are super-conducting.

The potassium methylamine system has been reported[2] to separate into two liquid phases at concentrations higher than 0.01N. The writer has observed this effect with methylamine to which several percent of ammonia has been added but not with pure methylamine. Rapid freezing of these solutions has yielded changes in resistance similar to those occurring in the sodium-ammonia system. When a 0.05N solution of potassium in ten to one methylamine-ammonia was rapidly chilled from 260°K to 90°K and then "healed" at 170°K (ten degrees below the melting point of the mixture), the resistance dropped from a value of 700 ohms at the highest temperature to a steady value of 0.3 ohm in the solid state. The solid possessed a lustrous, metallic, blue-gray appearance. When this solid was melted, two liquid phases, one blue and one bronze, resulted; the resistance of this mixture at a temperature just above the melting point was 2600 ohms.

Ogg has suggested an interpretation of the great decrease in resistance in the sodium-ammonia system in terms of a Bose-Einstein condensation of electron pairs. While the decrease for the above solutions occurs at a temperature well below the B-E condensation temperature for an ideal gas of density corresponding to the concentration of the solution, the discontinuity in resistance of the potassium methylamine-ammonia system occurs at a somewhat higher temperature than the corresponding B-E condensation temperature. For a solution 0.05N in potassium (0.025N in electron pairs) the corresponding condensation temperature would be about 90°K, while the decrease in resistance occurs at about 180°K.

[1] R. A. Ogg, Jr., Phys. Rev. 69, 243, and 544 (1946).
[2] J. G. Daunt, M. Désirant, K. Mendelssohn, and A. J. Birch, Phys. Rev. 70, 219 (1946).
[3] Gibson and Phipps, J. Am. Chem. Soc. 48, 312 (1926).

On the Level Scheme of Mg^{24} and the Mass of Na^{24}

R. G. SACHS
Argonne National Laboratory, P. O. Box 5207, Chicago 80, Illinois
September 25, 1946

SIEGBAHN has recently reported[1] the γ-ray spectrum associated with the disintegration of Na^{24} to consist of two lines, one at 1.38 Mev and the other at 2.76 Mev. In determining the corresponding level scheme of Mg^{24}, he assumes that these γ-transitions are in cascade. It has already been pointed out[2] that this assumption leads to a mass for Na^{24} which is undesirably high compared to the masses of similar nuclei in the same part of the periodic table. In particular, the mass of 23.99893 given by Siegbahn is about 1.5 Mev greater than that calculated by Barkas[3] for Na^{24}.

Although this is by no means certain evidence that the level assignment is wrong, it should be kept in mind that it is possible to construct a level scheme consistent with the data and giving a mass of Na^{24} which is in close agreement with the Barkas value. In this scheme,[2] it is assumed that the two levels of Mg^{24} are at 1.38 Mev and 2.76 Mev. Then the 1.38 γ-ray would actually consist of two cascading γ-rays of very nearly equal energy and the 2.76 radiation would be produced by a direct transition from the higher level to the ground state. This assumption is in good agreement with the results of Wilkins[4] and of Dicke and Marshall[5] on the inelastic scattering of protons by Mg. The level at 1.30 Mev obtained by Little, Long, and Mandeville[6] from the inelastic scattering of neutrons on Mg also agrees reasonably well with this scheme. The corresponding mass of Na^{24} would be 23.99745.

In this alternate scheme, the intensities of the radiations of different energies would not be expected to be equal so the application to the determination of the efficiency curve of G-M counters proposed by Siegbahn[1] would not be possible.

[1] K. Siegbahn, Phys. Rev. 70, 127 (1946).
[2] A. Guthrie and R. G. Sachs, Phys. Rev. 62, 8 (1942).
[3] W. H. Barkas, Phys. Rev. 55, 691 (1939).
[4] T. R. Wilkins, Phys. Rev. 60, 365 (1941).
[5] R. H. Dicke and J. Marshall, Jr., Phys. Rev. 63, 86 (1943).
[6] R. N. Little, R. W. Long, and C. E. Mandeville, Phys. Rev. 69, 414 (1946).

Expanding Universe and the Origin of Elements

G. GAMOW
The George Washington University, Washington, D. C.
September 13, 1946

IT is generally agreed at present that the relative abundances of various chemical elements were determined by physical conditions existing in the universe during the early stages of its expansion, when the temperature and density were sufficiently high to secure appreciable reaction-rates for the light as well as for the heavy nuclei.

In all the so-far published attempts in this direction the observed abundance-curve is supposed to represent some equilibrium state determined by nuclear binding energies at some very high temperature and density.[1–3] This point of view encounters, however, serious difficulties in the comparison with empirical facts. Indeed, since binding energy is, in a first approximation, a linear function of atomic weight, any such equilibrium theory would necessarily lead to a rapid exponential decrease of abundance through the entire natural sequence of elements. It is known, however, that whereas such a rapid decrease actually takes place for the first half of chemical elements, the abundance of heavier nuclei remains nearly constant.[4] Attempts have been made[3] to explain this discrepancy by the assumption that heavy elements were formed at higher temperatures, and that their abundances were already "frozen" when the adjustment of lighter elements was taking place. Such an explanation, however, can be easily ruled out if one remembers that at the temperatures and densities in question (about 10^{10}°K, and 10^{6} g/cm^3) nuclear transformations are mostly caused by the processes of absorption and re-evaporation of free neutrons so that their rates are essentially the same for the light and for the heavy elements. Thus it appears that the only way of explaining the observed abundance-curve lies in the assumption of some kind of unequilibrium process taking place during a limited interval of time.

The above conclusion finds a strong support in the study of the expansion process itself. According to the general theory of expanding universe,[5] the time dependence of any linear dimension l in it is given by the formula

$$\frac{dl}{dt}=\left(\frac{8\pi G}{3}\rho l^2-\frac{C^2}{R^2}\right)^{\frac{1}{2}}, \tag{1}$$

where G is the Newton constant, ρ the mean density, and R (real or imaginary) a constant describing the curvature of space. It may be noticed that the above expression represents a relativistic analog of the familiar classical formula

$$v=\left(2\cdot\frac{4\pi l^3}{3}\rho\cdot\frac{G}{l}-2E\right)^{\frac{1}{2}} \tag{2}$$

for the inertial expansion-velocity of a gravitating dust sphere with the total energy E per unit mass. The imaginary and real values of R correspond to an unlimited expansion (in case of superescape velocity), and to the expansion which will be ultimately turned into a contraction by the forces of gravity (subescape velocity). To use some definite numbers, let us consider in the present state of the universe (considered as quite uniform) a cube containing, say, 1 g of matter. Since the present mean density of the universe is $\rho_{present}\leqq 10^{-30}$ g/cm^3, the side of our cube will be: $l_{present}\leqq 10^{10}$ cm. According to Hubble,[6] the present expansion-rate of the universe is 1.8×10^{-17} cm/sec. per cm, so that $(dl/dt)_{present}\leqq 1.8\times 10^{-7}$ cm/sec. Substituting the numerical values in (1) we obtain

$$1.8\times 10^{-7}=(5.7\times 10^{-17}-C^2/R^2)^{\frac{1}{2}}, \tag{3}$$

showing that at the present stage of expansion the first term under the radical (corresponding to the potential energy of gravity) is negligibly small as compared with the second one. For the numerical value of the (constant) radius of curvature we get from (3): $R=1.7\times 10^{17}\sqrt{-1}$ cm or about 0.2 imaginary light year.

In the past history of the universe, when l was considerably smaller, and ρ correspondingly larger, the first term in (1) was playing an important role corresponding physically to the slowing-down effect of gravity on the original expansion. The transition from the slowed down to the free expansion took place at the epoch when the two terms were comparable, i.e., when l was about one thousandth of its present value. At this epoch the gravitational clustering of matter into stars, stellar clusters, and galaxies, probably must have taken place.[7]

Applying our formula (2) with $C^2/R^2=-3.3\times 10^{-14}$ to the earlier epoch when the average density of masses in the universe was of the order of 10^6 g/cm^3 (as required by the conditions for the formation of elements), we find that at that time $l\leqq 10^{-2}$ cm, and $dl/dt\leqq 0.01$ cm/sec. This means that *at the epoch when the mean density of the universe was of the order of 10^6 g/cm^3, the expansion must have been proceeding at such a high rate, that this high density was reduced by an order of magnitude in only about one second.* It goes without saying that one must be very careful in extrapolating the expansion formula to such an early epoch, but, on the other hand, this formula represents nothing more than the statement of the law of conservation of energy in the inertial expansion against the forces of gravity.

Returning to our problem of the formation of elements, we see that *the conditions necessary for rapid nuclear reactions were existing only for a very short time*, so that it may be quite dangerous to speak about an equilibrium-state which must have been established during this period. It is also interesting to notice that the calculated time-period during which rapid nuclear transformations could have taken place is considerably shorter than the β-decay period of free neutrons which is presumably of the order of magnitude of one hour. Thus if free neutrons were present in large quantities in the beginning of the expansion, the mean density and temperature of expanding matter must have dropped to comparatively low values *before* these neutrons had time to turn into protons. We can anticipate that neutrons forming this comparatively cold cloud were gradually coagulating into larger and larger neutral complexes which later turned into various atomic species by subsequent processes of β-emission. From this point of view the decrease of relative abundance along the natural sequence of elements must be understood as being caused by the longer time which was required for the formation of heavy neutronic complexes by the successive processes of radiative capture. The present high abundance of hydrogen must have resulted from the competition between the β-decay of original neutrons which was turning them into inactive protons, and the coagulation-process through which these neutrons were being incorporated into heavier nuclear units.

It is hoped that the further more detailed development of the ideas presented above will permit us to understand the observed abundance-curve of chemical elements giving at the same time valuable information concerning the early stages of the expanding universe.

[1] v. Weizsäcker, Physik. Zeits. 39, 633 (1938).
[2] Chandrasekhar and Henrich, Astrophys. J. 95, 288 (1942).
[3] G. Wataghin, Phys. Rev. 66, 149 (1944).
[4] Goldschmidt, *Verteilung der Elemente* (Oslo, 1938).
[5] R. Tolman, *Relativity, Thermodynamics and Cosmology* (Oxford Press, New York, 1934).
[6] Hubble, *The Realm of the Nebulae* (Yale University Press, New Haven, 1936).
[7] G. Gamow and E. Teller, Phys. Rev. 55, 654 (1939).

The Problem of Quantization of Higher Order Equations

GEORGE RAYSKI
Institute of Theoretical Mechanics, University of Warsaw, Warsaw, Poland
June 29, 1946

SUPPOSE there is given a function L depending on a field function $\psi(x)$ and its first and second derivatives:

$$L(\psi, \psi x_\mu, \psi x_\mu x_\nu). \tag{1}$$

This may be regarded as the generalized Lagrangian function. We may require, as usual

$$\delta\int L dx=0. \tag{2}$$

By introducing variations which vanish together with their derivatives on the surface S of the integration volume

$(\delta\psi_S=0,\ \delta\psi x_{\mu S}=0)$, we are led to the generalized Lagrangian equation

$$\frac{\partial L}{\partial\dot{\psi}}-\Sigma_\nu\frac{\partial}{\partial x_\nu}\frac{\partial L}{\partial\psi x_\nu}+\Sigma_{\mu\nu}\frac{\partial^2}{\partial x_\nu\partial x_\mu}\frac{\partial L}{\partial\psi x_\mu x_\nu}=0. \tag{3}$$

There exists an energy-impulse tensor

$$T_{\mu\nu}=\psi x_\mu\Sigma_\rho\frac{\partial}{\partial x_\rho}\frac{\partial L}{\partial\psi x_\nu x_\rho}+\psi x_\nu\Sigma_\rho\frac{\partial}{\partial x_\rho}\frac{\partial L}{\partial\psi x_\mu x_\rho}-\frac{\partial L}{\partial\psi x_\mu x_\nu}\cdot\Sigma_\rho\psi x_\rho x_\rho$$
$$-\Sigma_\rho\psi x_\rho\frac{\partial}{\partial x_\rho}\frac{\partial L}{\partial\psi x_\mu x_\nu}-\psi x_\nu\frac{\partial L}{\partial\psi x_\mu}+L\delta_{\mu\nu}, \tag{4}$$

which is symmetrical in case of asymmetrical function L and gives the continuity equation

$$\Sigma_\mu\frac{\partial}{\partial x_\mu}T_{\mu\nu}=0, \tag{5}$$

which guarantees the laws of conservation of energy, momentum, and angular momentum. If L is a gauge-invariant function of ψ and ψ^*, we may also introduce a current density vector

$$s_\mu=\left\{\frac{\partial L}{\partial\dot{\psi}}\cdot\dot{\psi}-\left(\Sigma_\nu\frac{\partial}{\partial x_\nu}\frac{\partial L}{\partial\psi x_\mu x_\nu}\right)\psi\right.$$
$$\left.+\Sigma_\nu\frac{\partial L}{\partial\psi x_\mu x_\nu}\cdot\psi x_\nu\right\}-\{\text{compl. conjug.}\}. \tag{6}$$

The simplest form of the generalized Lagrangian function (1) is

$$L=-\tfrac{1}{2}c^2(a^2\Sigma_{\mu\nu}\psi x_\mu{}^2x_\nu+\Sigma_\nu\psi x_\nu{}^2+\mu^2\psi^2). \tag{7}$$

The corresponding equation (3) becomes in this case

$$-a^2\Box\,\Box\psi+\Box\psi-\mu^2\psi=0, \tag{8}$$

which seems to be of some physical interest, in view of the papers of F. Bopp,[1] B. Podolsky,[2] and C. Kikuchi,[3] in case $\mu=0$.

Now the question arises whether there exists a possibility of direct quantization of such a field. From (4) and (7) we get rather a complicated expression for energy density $-T_{44}$ which may be somewhat simplified by adding a divergence $\Delta(\dot{\psi}\ \text{grad}\ \dot{\psi})-\Delta(\ddot{\psi}\ \text{grad}\ \psi)$. We thus obtain, if we put $\partial\psi/\partial t=\alpha$, $\partial^2\psi/\partial t^2=\beta$, $\partial^3\psi/\partial t^3=\gamma$

$$\epsilon=a^2\left(\frac{\alpha\gamma}{c^2}-\alpha\Delta\alpha-\tfrac{1}{2}\frac{\beta^2}{c^2}+\tfrac{1}{2}c^2\Sigma_{kl}\psi x_k{}^2x_l\right)$$
$$+\tfrac{1}{2}(\alpha^2+c^2\,\text{grad}^2\,\psi+\mu^2c^2\psi^2. \tag{9}$$

We may regard these time driviatives (α, β, γ) as independent variables, replace them by operators, and postulate some commutation relations between them to satisfy the usual quantum equation of motion

$$\dot{f}=[H,f],\qquad [a,b]=\frac{i}{h}(ab-ba) \tag{10}$$

(where $H=\int\kappa dx$ and $\kappa=\epsilon$). This is a natural generalization of the usual procedure in view of the fact that the conjugate momentum in the usual theory of a scalar field $(a=0)$ is $\pi=\dot{\psi}$. In order to simplify our formulas we shall introduce as independent field variables not α, β, γ, but some linear combinations of them, namely:

$$\begin{aligned}\pi&=a^2(\gamma/c^2-\Delta\alpha)+\alpha,\\ \rho&=-a^2\beta/c^2,\\ \sigma&=a^2\alpha/c^2\end{aligned} \tag{11}$$

(if, $a=0$, this becomes simply $\pi=\dot{\psi}$ and $\rho=\sigma=0$).

The commutation rules needed are

$$[\pi(x),\psi(x')]=\delta(x-x'),\quad [\rho(x'),\pi(x)]=a^2\Delta\delta(x-x'),$$
$$[\sigma(x'),\rho(x)]=-\frac{a^2}{c^2}\delta(x-x'), \tag{12}$$

while all other commutators vanish. It may be easily seen that in consequence of commutation relations (12) the Eq. (10) is satisfied if only the field function satisfies the Eq. (8). The equations

$$f_x=-[P_x,f]\qquad (x=x_1,x_2,x_3) \tag{13}$$

(where $P_x=-\int T_{4x}dx$ with α, β, γ replaced by π, ρ, σ) are also satisfied, which (together with (10)) reveals the relativistic invariance of the procedure.

In order to obtain the eigenvalues of the operators H, P_x, etc., we are obliged to replace the field functions by Fourier series:

$$\psi=\Sigma_k q_k e^{ikx},\quad \pi=\Sigma_k p_k e^{ikx},\quad \rho=\Sigma_k r_k e^{ikx},\quad \sigma=\Sigma_k s_k e^{ikx}$$

which splits the expression H, as usual, into independent terms H_k; then we may replace q_k, p_k, e_k, s_k by suitable differential operators and reduce the problem to an eigenvalue problem of a differential equation with partial derivatives.

Thus we have shown the possibility of quantization of the interesting fourth-order Eq. (8) by a generalization of the usual formalism.

[1] F. Bopp, Ann. d. Physik **38**, 345 (1940).
[2] B. Podolsky, Phys. Rev. **62**, 68 (1942).
[3] C. Kikuchi, Phys. Rev. **69**, 125 (1946).

Report of the 1946 Spring Meeting of the American Society for X-Ray and Electron Diffraction

THE 1946 spring meeting of the American Society for X-Ray and Electron Diffraction was held at Silver Bay, New York, June 10–15. The following papers were given:

E. W. Hughes, California Institute of Technology. **X-ray examinations of some synthetic oxygen-carrying chelate compounds.**

N. Davidson and J. Hillier, RCA Laboratories, Princeton, New Jersey. **Single crystal electron diffraction by microcrystalline materials.**

M. Schneider, and I. Fankuchen, Polytechnic Institute of Brooklyn. **Some D.D.T. analogues.**

R. Pepinsky, Alabama Polytechnic Institute. **Some aspects of electronic instrumentation in x-ray diffraction studies.**

A. de Bretteville, Jr., Laboratory for Insulation Research, Massachusetts Institute of Technology. **Oscillographic study of the dielectric properties of barium titanate.**

F. G. Chesley, Central Research Laboratories, Inc., Red Wing, Minnesota. **The design and construction of an electron diffraction camera and its application to the selenium rectifier problem.**

W. Parrish and E. Cisney, Philips Laboratories, Inc., Irvington-on-Hudson, New York. **Collimator systems and filter techniques for x-ray powder cameras.**

R. W. G. Wyckoff, National Institute of Health, Bethesda, Maryland. **Structure of macro molecular crystals by use of the electron microscope.**

M. A. Peacock, University of Toronto. **Structure of rickardite, $Cu_{4-x}Te_3$.**

E. W. Hughes and W. N. Lipscomb, Jr., California Institute of Technology. **The structure of methyl ammonium chloride.**

M. J. Buerger, G. Klein, and G. Hamburger, Massachusetts Institute of Technology. **The structure of nepheline.**

M. L. Huggins, Kodak Research Laboratories, Rochester, New York. **Equations for various types of summations.**

M. J. Buerger, Massachusetts Institute of Technology. **The interpretation of Harker syntheses.**

D. Wrinch, Department of Physics, Smith College. **Fourier transforms and complex organic crystals.**

D. Harker, General Electric Research Laboratory. **Microwaves (short wave radio) and scale models in determining crystal structures.**

R. Pepinsky, Alabama Polytechnic Institute. **Summation of two-dimensional Fourier series by electronic means.**

A. D. Booth, Birkbeck College, University of London. **Fourier methods and machines in England 1940–1946.**

E. W. Hughes, California Institute of Technology. **Punched card methods in x-ray and electron diffraction calculations.**

D. McLachlan, Jr., American Cyanamid Company, Stamford, Connecticut. **A new numbered strip method for summing Fourier series.**

M. J. Buerger, Massachusetts Institute of Technology. **Derivative crystal structures.**

F. N. Rhines, Carnegie Institute of Technology. **The thesis that order-disorder changes are ordinary phase changes.**

E. J. Armstrong, Bell Telephone Laboratories. **Application of the Barrett technique to some problems concerning non-metallic crystals.**

D. D'Eustachio, Collman Manufacturing Company, Erie, Pennsylvania. **Surface layers and mosaic structure in some valence crystals.**

L. Sturkey, Dow Chemical Company, Midland, Michigan. **Refraction and absorption effects in electron diffraction.**

J. Karle, Naval Research Laboratory, Washington, D.C. **Theory of electron scattering by oriented long chain molecules.**

J. W. Hickman, Westinghouse Research Laboratories, East Pittsburgh, Pennsylvania. **Electron diffraction studies of oxide film formation on W, Mo, and W, Mo, Ni and Cr alloys.**

E. A. Gulbransen, Westinghouse Research Laboratories, East Pittsburgh, Pennsylvania. **Deviation of lattice parameters of thin oxide films by electron diffraction analysis.**

E. I. Allessandrini, General Electric Research Laboratory. **Oxide films on chromium.**

Mimeographed abstracts of these papers are being mailed to the members of the society. Anyone wishing an abstract of any paper should write to the author of that paper.

ELIZABETH J. ARMSTRONG, *Acting Secretary,*
American Society for X-Ray and
Electron Diffraction